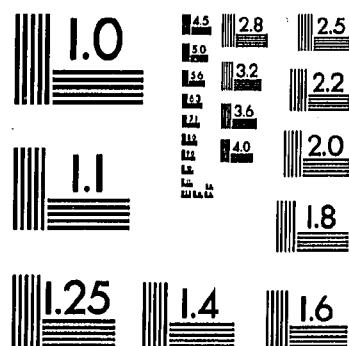
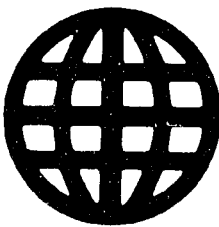


# UMI University Microfilms International



MICROCOPY RESOLUTION TEST CHART  
NATIONAL BUREAU OF STANDARDS  
STANDARD REFERENCE MATERIAL 1010a  
(ANSI and ISO TEST CHART No. 2)

**University Microfilms Inc.**

300 N. Zeeb Road, Ann Arbor, MI 48106



## INFORMATION TO USERS

This reproduction was made from a copy of a manuscript sent to us for publication and microfilming. While the most advanced technology has been used to photograph and reproduce this manuscript, the quality of the reproduction is heavily dependent upon the quality of the material submitted. Pages in any manuscript may have indistinct print. In all cases the best available copy has been filmed.

The following explanation of techniques is provided to help clarify notations which may appear on this reproduction.

1. Manuscripts may not always be complete. When it is not possible to obtain missing pages, a note appears to indicate this.
2. When copyrighted materials are removed from the manuscript, a note appears to indicate this.
3. Oversize materials (maps, drawings, and charts) are photographed by sectioning the original, beginning at the upper left hand corner and continuing from left to right in equal sections with small overlaps. Each oversize page is also filmed as one exposure and is available, for an additional charge, as a standard 35mm slide or in black and white paper format.\*
4. Most photographs reproduce acceptably on positive microfilm or microfiche but lack clarity on xerographic copies made from the microfilm. For an additional charge, all photographs are available in black and white standard 35mm slide format.\*

\*For more information about black and white slides or enlarged paper reproductions, please contact the Dissertations Customer Services Department.

**U·M·I** Dissertation  
Information Service

University Microfilms International  
A Bell & Howell Information Company  
300 N. Zeeb Road, Ann Arbor, Michigan 48106



1328200

**Rasmusson, Randall Lee**

A MODEL OF FROG ATRIAL AND SINUS ELECTRICAL ACTIVITY

*Rice University*

M.S. 1986

University  
Microfilms  
International 300 N. Zeeb Road, Ann Arbor, MI 48106



**PLEASE NOTE:**

In all cases this material has been filmed in the best possible way from the available copy. Problems encountered with this document have been identified here with a check mark ✓.

1. Glossy photographs or pages ✓
2. Colored illustrations, paper or print \_\_\_\_\_
3. Photographs with dark background ✓
4. Illustrations are poor copy \_\_\_\_\_
5. Pages with black marks, not original copy \_\_\_\_\_
6. Print shows through as there is text on both sides of page \_\_\_\_\_
7. Indistinct, broken or small print on several pages ✓
8. Print exceeds margin requirements \_\_\_\_\_
9. Tightly bound copy with print lost in spine \_\_\_\_\_
10. Computer printout pages with indistinct print \_\_\_\_\_
11. Page(s) \_\_\_\_\_ lacking when material received, and not available from school or author.
12. Page(s) \_\_\_\_\_ seem to be missing in numbering only as text follows.
13. Two pages numbered \_\_\_\_\_. Text follows.
14. Curling and wrinkled pages \_\_\_\_\_
15. Dissertation contains pages with print at a slant, filmed as received ✓
16. Other \_\_\_\_\_  
\_\_\_\_\_  
\_\_\_\_\_

University  
Microfilms  
International





RICE UNIVERSITY

A MODEL OF FROG ATRIAL AND SINUS ELECTRICAL ACTIVITY

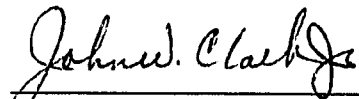
by

RANDALL LEE RASMUSSEN

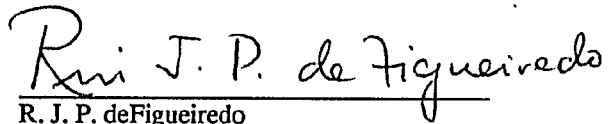
A THESIS SUBMITTED  
IN PARTIAL FULFILLMENT OF THE  
REQUIREMENTS FOR THE DEGREE

MASTER OF SCIENCE

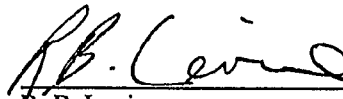
APPROVED, THESIS COMMITTEE:



J. W. Clark  
Professor of Electrical Engineering  
Chairman



R. J. P. deFigueiredo  
Professor of Electrical Engineering



R. B. Levine  
Assistant Professor of Biology

HOUSTON, TEXAS

APRIL, 1986

## **Abstract**

### **A Model of Frog Atrial and Sinus Electrical Activity**

**by**

**Randall Lee Rasmusson**

A mathematical model for the calculation of membrane action potential in bullfrog atrium and sinus-venosus is developed from relevant single-cell voltage clamp measurements. Ionic channels are combined with a  $Na^+/K^+$  pump, a  $Na^+/Ca^{++}$  exchanger and a  $Ca^{++}$  pump as mechanisms generating transmembrane currents. The concentration dependence of the pump and exchanger currents was addressed by incorporating a lumped three-compartment model of the cell and its immediate environment.

Repolarization of the action potential and the frequency dependence of its duration were found to be governed primarily by the activation of the delayed rectifier current ( $I_K$ ). On the other hand, pump and exchanger currents were found to contribute very little to the action potential shape, although they were of sufficient magnitude to influence diastolic depolarization in the sinus-venosus model. Accumulation/depletion phenomena were shown not to be important in either repolarization or pacing. The intracellular calcium homeostasis model produced sufficient binding to troponin to qualitatively mimic the "staircase effect" of mechanical contraction.

## **ACKNOWLEDGEMENTS**

I wish to express my sincere thanks to Dr. John Clark and Dr. Wayne Giles without whose patient instruction, guidance and support this work would never have been accomplished. A special thanks goes to Dr. Don Campbell and Mr. Keith Robinson, who helped with a lot of late hours when time was critical, as well as contributing invaluable criticism and advice. My thanks are also extended to the other members of Wayne Giles lab at the University of Calgary, in particular Dr. Robert Clark and Dr. Erwin Shibata, who were always ready to answer my questions and lend me their help. Thanks also to Dr. Denis Noble for providing free access to his program "Heart" which has been a source of information and background in this work. My thanks go to the professors, staff and students of the Rice University Electrical and Computer Engineering Department for their help, especially Dr. Nirmala Ganapathy and Ms. Keri Hicks who were there when I needed help.

I also wish to express my gratitude to Ms. Lenore Doell, and Ms. Anna Tyberg for a lot of typing. Most of all my heartfelt gratitude goes to my parents, Dr. and Mrs. Rasmusson (Mom and Dad) for all the love, patience, faith and encouragement they have always bestowed on me and for always being there when I needed them.

## TABLE OF CONTENTS

CHAPTER I:	<u>Introduction</u>	
I.0	Foreword	1
I.2	Hodgkin-Huxley Theory and Analysis of Experimental data	9
I.2.0	Squid Axon	9
I.2.1	Hodgkin-Huxley Assumptions	14
I.2.2	Hodgkin-Huxley Mathematical Description of Ionic Currents	16
I.2.2.1	Non-inactivating Ionic Currents	17
I.2.2.2	Activation of a Transient Ionic Current	28
I.2.2.3	Inactivation of a Transient Ionic Current	33
I.3	Mathematical Models of the Cardiac Action Potential	35
I.4	Data Recording and Analysis	37
I.5	The Single Cell Experimental Procedure	40
I.5.1	Equivalent Cell Circuit of a Bullfrog Atrial Cell	41
I.6	Specific Aims of This Thesis	47
CHAPTER II:	<u>Ionic Currents in Atrial Cells: A Mathematical Description</u>	
II.0	Introduction	49
II.1	Time-Independent or Background Ionic Currents	50
II.2	Time- and Voltage-dependent Ionic Currents	60
II.2.1	$I_{Na}$	61
II.2.2	$I_{Ca}$	68
II.2.3	$I_K$	78
II.3	Ionic Pump and Exchanger Currents:	85
II.3.1	$Na^+ / K^+$ Pump	86
II.3.2	$Na^+ / Ca^{++}$ Exchanger	92
II.3.3	The $Ca^{++}$ Pump	95

II.4 Compartmental Models of an Atrial Cell: $\text{Na}^+$ - $\text{K}^+$ Accumulation/Depletion Phenomena, and $\text{Ca}^{++}$ Buffering	99
II.4.0 Introduction	99
II.4.1 Description of the Restricted Extracellular Space(s)	99
II.4.2 Internal Concentration Model	110
II.5 Summary of the Atrial Model	130
II.6 Modifications for Modelling Bullfrog Sinus Venosus	133
CHAPTER III: <u>Computational Aspects and Initial Model Testing</u>	
III.0 Introduction	156
III.1 Methods of Integration	180
III.2 Testing the Atrial Model	183
III.2.1 Background Currents	200
III.2.2 The Transient Sodium Current	203
III.2.3 The Transient Calcium Current	203
III.2.4 The Delayed Rectifier Current	211
III.2.5 The Extracellular Compartment	215
III.2.6 The Intracellular Compartment	220
III.2.7 Summary of Initial Model Testing	223
III.3 Testing the Sinus Venosus Model	226
III.3.1 Background Currents	233
III.3.2 The Transient Calcium Current	233
III.3.3 The Delayed Rectifier Current	241
III.3.4 The Extracellular Compartment	241
III.4 Summary	247
CHAPTER IV: <u>Results</u>	
IV.0 Introduction	248
IV.1 The Mechanism of Repolarization in Atrium	252
IV.1.1 Interval-Duration Experiments	256

IV.1.2 All or None Repolarization	260
IV.1.3 Buffering, $\text{Na}^+ / \text{Ca}^{++}$ Exchange and Repolarization	268
IV.1.4 The Resting Potential and Late Repolarization	275
IV.2 Frequency Dependent Effects on $\text{Ca}^{++}$ in Atrium	287
IV.2.1 Intracellular Calcium and Frequency	287
IV.2.2 External Calcium Depletion	294
IV.3 Frequency and Intracellular $\text{Na}^+$	297
IV.4 Pacing in the Bullfrog Sinus-Venous	298
IV.4.1 Pacing in the Absence of Pump and Exchanger Currents	302
IV.4.2 Pacing in the Presence of Pump and Exchanger Currents	306
IV.4.3 Pacing in the Presence of a Restricted Extracellular Space	310
CHAPTER V: <u>Discussion</u>	
V.1 Previous Work	313
V.2 Usefulness of this model in determining the physiological role of ionic, pump, or exchanger currents in normal electrophysiological activity in the heart	315
V.3 The physiological significance of the sodium and potassium pump currents and sodium calcium exchange currents in bullfrog heart	320
V.4 Future development and uses of these mathematical models	322
Bibliography	324

## CHAPTER I

### I.1 Foreword

The ionic mechanisms underlying the spontaneous electrophysiological activity in the heart have intrigued and puzzled both biological and physical scientists for over a century. Gaskell (1884, 1887) first demonstrated that the spontaneous contractions of the heart were myogenic in origin--that is, they did not require any input from the nervous system. Approximately 45 years ago Bozler (1942) used extracellular recording techniques to demonstrate that a slow depolarization precedes the development of the action potential in the heart. Today, using presently available electrophysiological and computer modelling techniques, questions such as what produces the heart beat and what ion fluxes underlie the pacemaker potential and the action potential can be addressed quantitatively.

Conventional microelectrode recordings can be used as a starting point to define this problem. As an example, Panels (a) and (b) of Figure 1.0 show conventional microelectrode recordings made from two commonly used preparations: the frog sinus venosus or pacemaker tissue, and frog atrium. As can be seen from figure 1(b) the pacemaker potential (or the slow diastolic

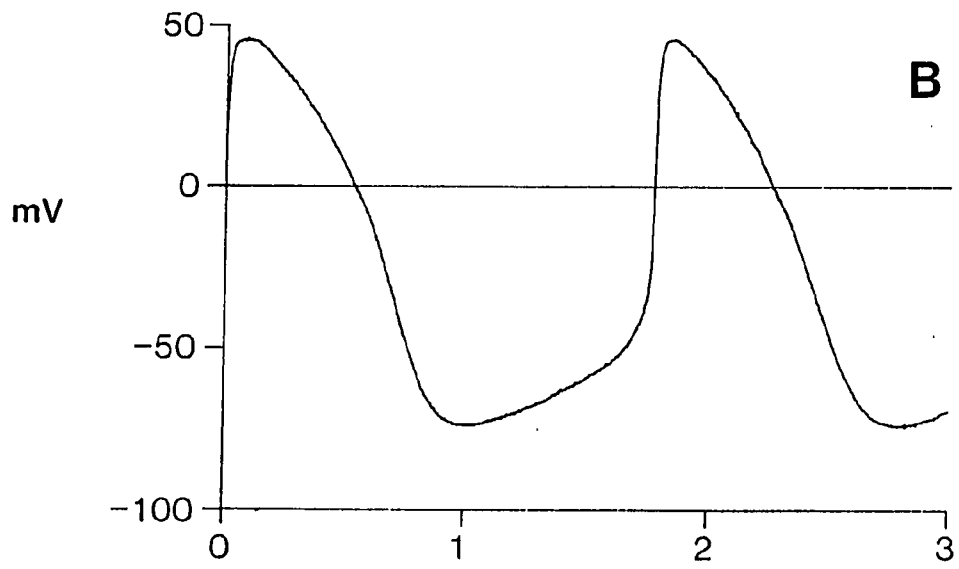
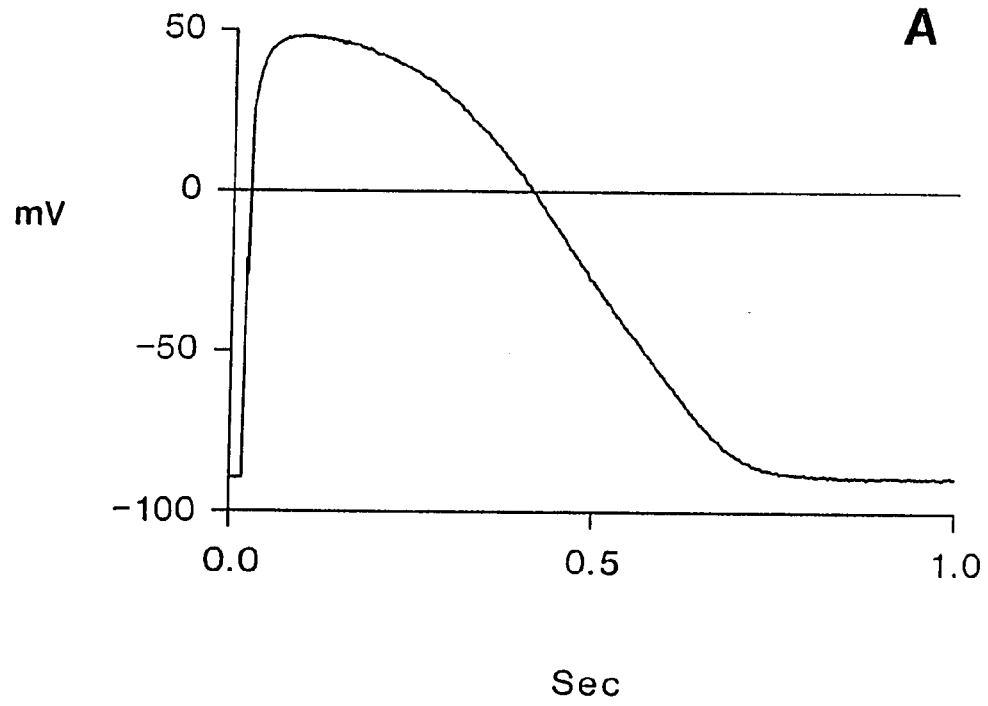
Figure 1.0Panel A

A "typical" atrial action potential recorded from an isolated bullfrog atrial myocyte.

Panel B

A "typical" sinus venosus waveform recorded from an isolated bullfrog sinus-venosus myocyte.





depolarization) spans the voltage range--approximately -65 mV to -45 mV; it is a gradual depolarization with a rate of change of transmembrane voltage ( $dV/dt$ ) varying between 0.02 and 0.05 V/sec in frog sinus venosus.

In contrast, the atrial cell is quiescent at a resting potential near -90 mV until it is excited by an externally applied stimulus. The leading edge of the atrial action potential (called the rapid upstroke) depolarizes the cell from 'rest' to approximately +35 mV at a maximum rate of approximately 40 V/sec. The plateau phase of the action potential lasts approximately 200 msec and usually, although not always, has a convex shape. Following the plateau, the action potential repolarizes at a much slower rate (5-10 V/sec) than during depolarization. A significant negative after-potential is never observed in the atrial action potential, but occasionally a positive after-potential is recorded.

The voltage clamp technique, developed in the late 1940's, is the principle method used to investigate the ionic basis of the action potential in cardiac tissue. Early investigators used cardiac tissue derived from the specialized conduction system of the heart; the Purkinje fibre. This tissue was chosen since Purkinje strands are very easily identified and isolated from the heart, and the individual cells comprising the strands are relatively large and only weakly contractile. Thus, single or double (for

voltage clamping) microelectrode impalements can be obtained with relative ease. The original data from this type of work (Vassalle, 1966; Noble and Tsien, 1968) showed that at a time corresponding to the development of the slow diastolic depolarization, there was a relaxation or decline in an outward current. In principle, this could produce the slow diastolic depolarization that is observed in pacing purkinje fibre preparations. Subsequently, Noble and Tsien (1969 a,b) identified the time- and voltage-dependent outward current(s) which initiate repolarization in the cardiac Purkinje fibre. Just previously, Reuter (1967) had obtained the first evidence for a transmembrane current carried by calcium ions. The characteristics of this calcium current seemed appropriate for maintaining or generating the plateau of the action potential.

Within the past three years both frog atrial and frog pacemaker tissue have been studied using isolated single cells and a suction microelectrode technique (Hume and Giles(1983)). Thus, for the first time, quantitative data describing many (or in some cases all) of the ionic currents which are relevant to the development of these membrane potential changes are available. In addition since the single cells have a relatively simple microanatomy, an electrically equivalent circuit can be developed which accurately describes both the passive and active electrical properties of these two types of cells.

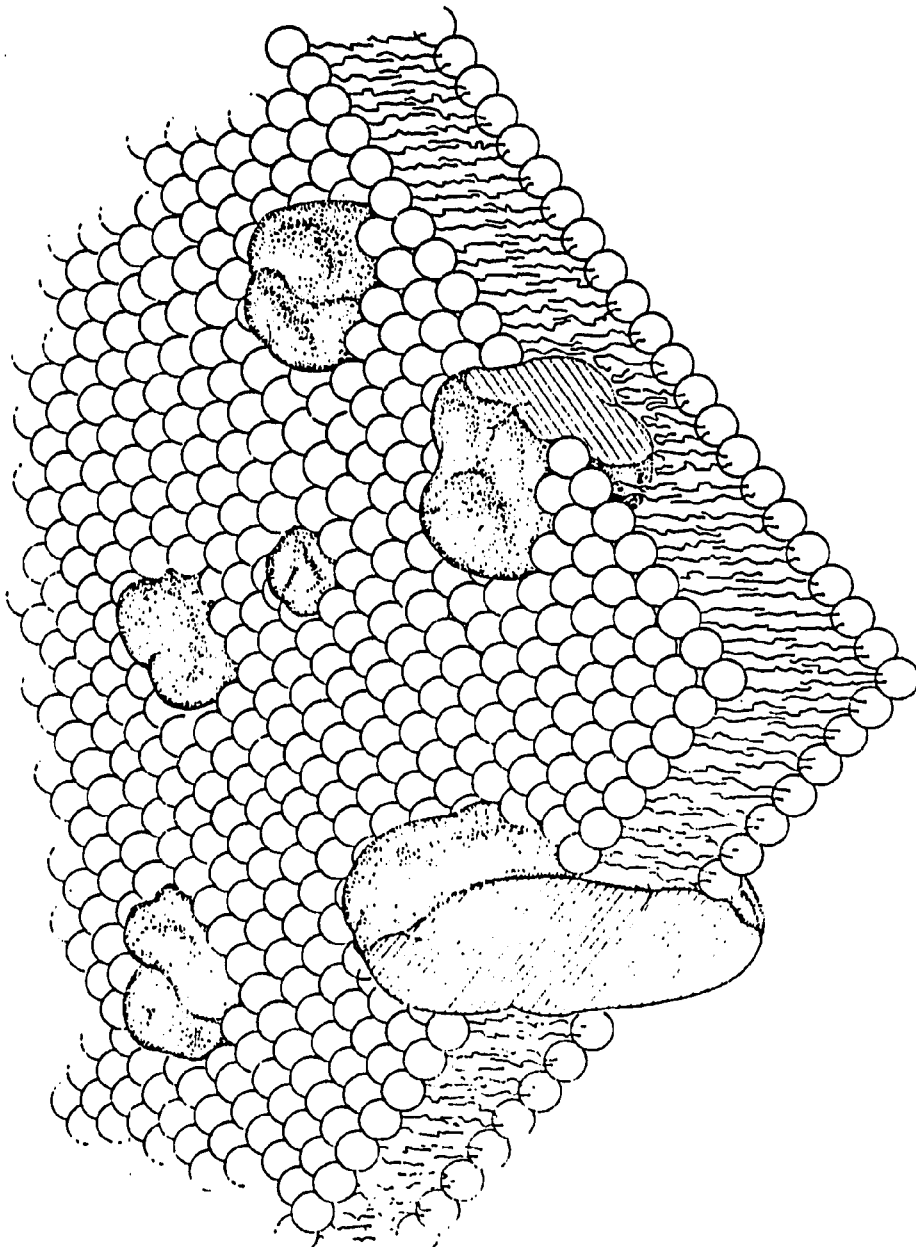
Biological membranes play a crucial role in almost all cellular phenomena, including transmembrane electrical phenomena.

The biological membrane is an extremely thin but quite stable film of lipid and protein molecules. The basic constituent of a cell membrane is a bimolecular sheet of lipid molecules. A lipid molecule has both hydrophilic and hydrophobic portions. The bulky head of a lipid molecule is hydrophilic and the two long tails of the molecule are hydrophobic. When placed in an aqueous environment these molecules tend to form a two-layer membrane, with the hydrophilic heads on the outside and the hydrophobic tails interacting with one another in the center of the bi-layer (Singer and Nicholson, 1972). Membrane proteins are densely interspersed among the lipid molecules (Figure 1.1). Some of these proteins completely traverse the membrane, and some of these proteins form channels or pumps, allowing specific ions or molecules to pass through the membrane or be pumped or driven across it against a concentration gradient.

Recent experimental and theoretical work has drawn attention to the very significant and functionally important effects of changes in ion concentration either inside the cell or in the small spaces between cells (cleft spaces). These spaces are restricted in the sense that diffusion from them is significantly slowed. In addition, it has been recognized that there are significant transmembrane ion movements that occur, not only through

Figure 1.1

A diagram of the structure of a typical cell membrane composed of a bi-layer of lipid molecules with larger proteins interspersed within the bi-layer. Note the bulky hydrophilic heads are oriented towards the aqueous environment while the hydrophobic tails are oriented towards each other within the membrane.



conventional time- and voltage-dependent channels, but also via energy ATP-requiring pump or ion exchanger mechanisms.

## I.2 HODGKIN-HUXLEY THEORY AND ANALYSIS OF EXPERIMENTAL DATA

### I.2.0 Squid Axon.

The pioneering work in mathematical reconstruction of action potentials in excitable tissue was published in 1952 by Hodgkin and Huxley. Earlier, they had adapted the voltage clamp technique developed by Cole(1949) and Marmot (1949) so that a particularly well-suited nerve axon, the squid giant axon, could be voltage clamped. These voltage clamp experiments showed conclusively that two time- and voltage-dependent currents, a sodium current ( $i_{Na}$ ) and a potassium current ( $i_K$ ) generated this simple nerve action potential (see Figure 1.2). Hodgkin and Huxley then developed kinetic expressions for the time- and voltage-dependence of the 'gating reactions' which control these currents. These were used in combination with expressions for the electrochemical driving force on each of these ions, the fully-activated current voltage relationships, and an equivalent circuit model of the cell (Figure 1.3) to mathematically reconstruct the squid axon action potential. They then determined the experiments that would yield the quantitative data necessary to validate their electrical equivalent model.

Figure 1.2

Numerical solution of the Hodgkin and Huxley (1952d) model of the squid action potential showing the components of membrane current during the action potential.

Panel A

The model generated squid axon action potential.

Panel B

The computed underlying currents that combine to generate the squid action potential.

Hodgkin and Huxley defined inward currents as positive, outward currents and the resting potential as 0mV.



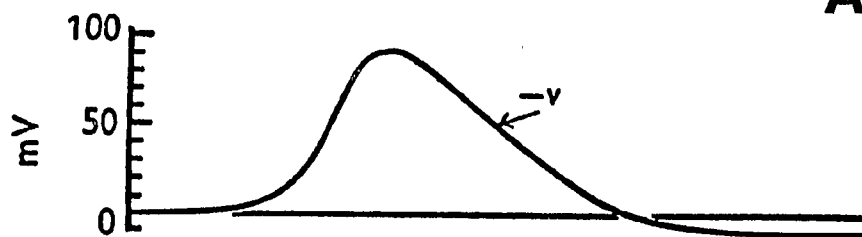
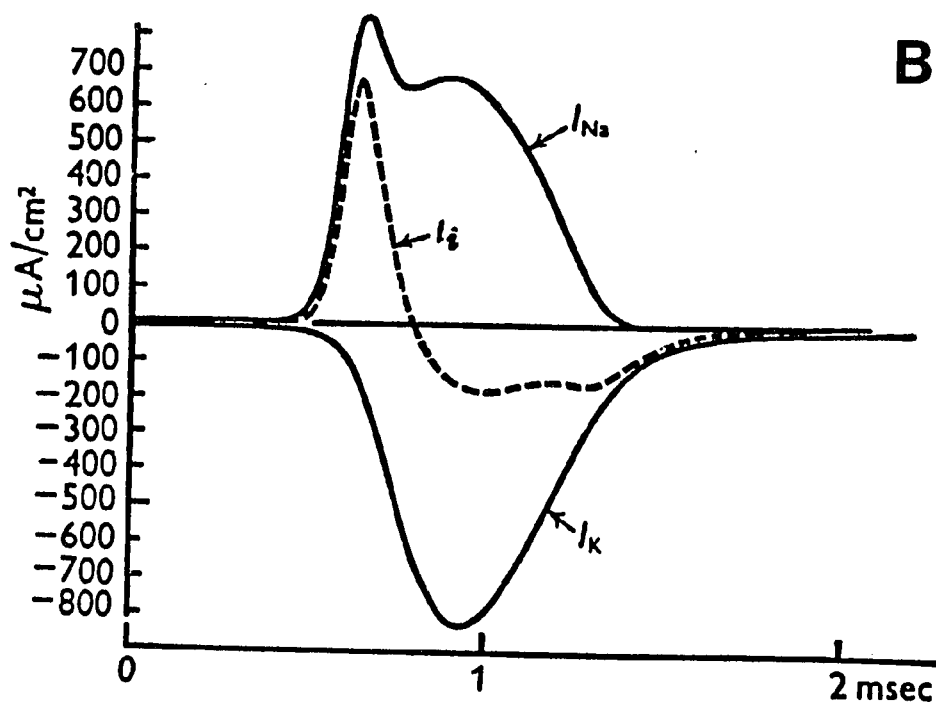
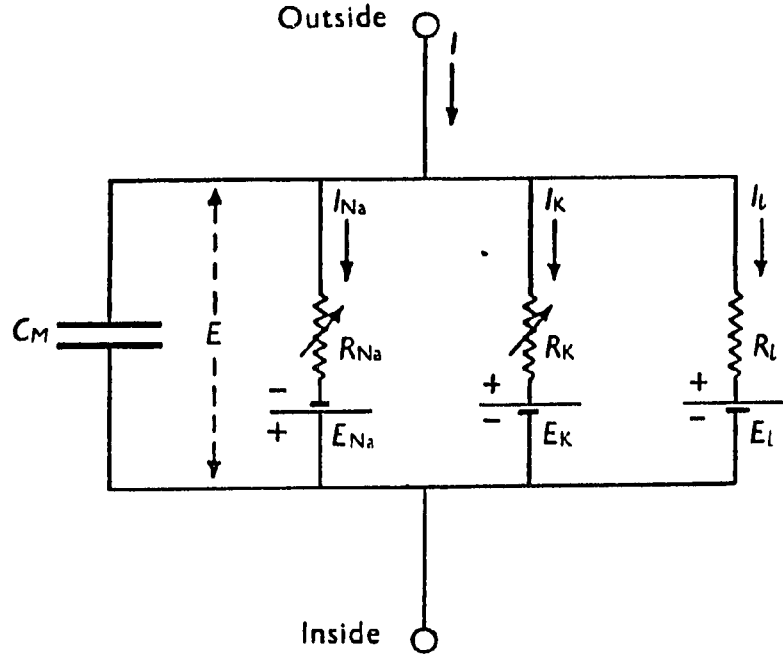
**A****B**

Figure 1.3

The electrical circuit representing the membrane and the equations which describe the behavior of the Hodgkin-Huxley (1952d) model of squid axon. The two resistive components  $R_{Na}=1/g_{Na}$  and  $R_K=1/g_K$  vary with time and potential as described by the equations while all other components are constant.

Potentials are given in mV, current density in  $\mu A/cm^2$ , conductances in mmho/cm<sup>2</sup>, capacity in  $\mu Fd/cm^2$  and time in msec. Note that Hodgkin and Huxley define inward currents as positive, outward currents as negative and the resting potential as 0mV.



$$I = C_M \frac{dV}{dt} + \bar{g}_K n^4 (V - V_K) + \bar{g}_{Na} m^3 h (V - V_{Na}) + \bar{g}_l (V - V_l),$$

$$dn/dt = \alpha_n(1 - n) - \beta_n n,$$

$$dm/dt = \alpha_m(1 - m) - \beta_m m,$$

$$dh/dt = \alpha_h(1 - h) - \beta_h h,$$

$$\alpha_n = 0.01 (V + 10) / \left( \exp \frac{V + 10}{10} - 1 \right),$$

$$\beta_n = 0.125 \exp (V/80),$$

$$\alpha_m = 0.1 (V + 25) / \left( \exp \frac{V + 25}{10} - 1 \right),$$

$$\beta_m = 4 \exp (V/18),$$

$$\alpha_h = 0.07 \exp (V/20),$$

$$\beta_h = 1 / \left( \exp \frac{V + 30}{10} + 1 \right).$$

### I.2.1 Hodgkin-Huxley Assumptions.

On the basis of previous electrophysiological and transmembrane impedance data, Hodgkin and Huxley (1952a-d) hypothesized that the squid giant axon action potential is generated by two voltage and time-dependent transmembrane currents, an inward  $\text{Na}^+$  current ( $i_{\text{Na}}$ ) and an outward  $\text{K}^+$  current ( $i_{\text{K}}$ ). Quantitative measurement of these currents requires control of the transmembrane voltage, and minimization or removal of capacitative current flow. To achieve this, Hodgkin and Huxley developed a number of voltage clamp protocols, consisting of single or paired rectangular clamp steps of variable durations and amplitudes. The following summarizes the basic assumptions upon which the Hodgkin-Huxley formalism is based; and describes the rationale behind some of the most commonly used protocols.

Voltage clamp data is nearly always interpreted in terms of and/or compared with, the Hodgkin-Huxley model of membrane excitation (Hodgkin and Huxley, 1952a-d). This model quantitatively describes the voltage- and time-dependent conductances which underlie the action potential in squid axon. The formulation of the Hodgkin-Huxley model was based upon a set of assumptions which were later verified by experimental results. However, the physical interpretation of the data at the molecular level is still somewhat uncertain. Six essential assumptions in the Hodgkin-Huxley formalism, are:

- (i) The ionic current is carried entirely by ions which are subject to electrical and diffusional forces only, i.e., their electrochemical gradient. Other possibilities, such as hydrostatic pressure or current generated by an electrogenic  $\text{Na}^+ - \text{K}^+$  pump, are assumed to be negligible.
- (ii)  $\text{Na}^+$  and  $\text{K}^+$  ions flow through separate channels in the membrane and there is no direct interaction between them. This means that the flux of any ion species is independent of the concentration of all other ions. This assumption was essential in the rationale for separating the total ionic current into two main components,  $i_{\text{Na}}$  and  $i_{\text{K}}$  (Hodgkin and Huxley, 1952a). The current flow through any channel is expressed as the product of the ionic conductance of the channel and the electrochemical driving force. Note therefore that the electrochemical driving force on the carrier ion must be constant; any accumulation or depletion of the carrier ion (e.g.,  $\text{K}^+$ ), will invalidate quantitative Hodgkin-Huxley analysis of that ( $\text{K}^+$ ) current.
- (iii) Each channel can be in only one of two conductance states, open or closed, and each channel opens and closes independently. Ions may pass through the channel only when it is in the open state.

- (iv) Each population of channels is homogeneous and is controlled by one or more independent 'gates'. Gates are hypothesized to be charged groups which move across the membrane in response to a change in membrane potential (Armstrong and Bezanilla, 1974). The voltage dependence of the gates can be modified by a variety of agents. Frankenhauser and Hodgkin (1957) first described the effects of changes in external calcium ions. Calcium ions were shown to act by modifying the fixed surface charge associated with the membrane, thus affecting the local field acting on the 'gates'. Other cations ( $H^+$  and  $Mg^{2+}$ ) and anions, as well as changes in total ionic strength can also affect the voltage dependence of the gating mechanism (Hille, Woodhull and Shapiro, 1975).
- (v) The condition for a channel to be in the closed state is that at least one of the gates is closed. The condition for a channel to be open is that all of the gates are open.
- (vi) The opening and closing of each gate obeys a first-order reaction with voltage-dependent rate coefficients,  $\alpha$  and  $\beta$ , respectively.

### I.2.2 Hodgkin-Huxley Mathematical Description of Ionic Currents.

#### I.2.2.0 Introduction

Hodgkin and Huxley (1952d) were the first to develop a complete quantitative description of the conductance mechanisms which underlie the action potential in an excitable cell. It is now almost universally accepted that the time- and voltage-dependent changes in ionic conductances in excitable cells are due to the opening and closing of membrane channels which are controlled by voltage- and time-dependent gating mechanisms. Transient currents, such as the fast inward sodium current ( $i_{Na}$ ), are controlled by both activation and inactivation processes. However, other maintained currents, such as some outward potassium current(s) ( $i_K$ ), may be controlled only by activation gates. If the ion transfer processes corresponding to the fully-activated channels are found experimentally to be linear functions of transmembrane potential as they are in squid axon, they are treated as ohmic conductances.

#### I.2.2.1 Non-inactivating Ionic Currents:

When the transmembrane potential is not equal to the equilibrium potential for the permeant ion(s), a net current will flow. Its magnitude and direction are determined by the electrochemical gradient, i.e., the difference between the membrane potential and the equilibrium potential of the ion(s). The equilibrium, reversal, or Nernst potential is a measure of the

electrochemical energy needed to move an ion of a particular species across the membrane due to the different concentrations of that ion. It is this potential difference due to the concentration difference that has been described as the Nernst "battery". It is described by the Nernst equation:

$$E = \frac{RT}{ZF} \ln \frac{[S]_o}{[S]_i} \quad (1.1)$$

where R is the universal gas constant ( $R=8314$ ), T is the temperature in  $^{\circ}\text{K}$ , Z is the valency of the ionic species involved, F is the Faraday constant ( $F=96500$  coulombes/Faraday) and  $[S]_o$  and  $[S]_i$  are the extracellular and intracellular ionic concentrations of species, S. For monovalent anions, at a temperature of  $25^{\circ}\text{C}$  (for frog heart), this equation becomes:

$$E = 58.6 \log \frac{[S]_o}{[S]_i} \quad (1.2)$$

where E is in millivolts. Ionic channels have important properties in addition to ionic selectivity. Two important ones are (i) voltage-dependent gating and (ii) ion transfer characteristics. The gating is the opening-closing mechanism of the channel. The ion transfer characteristic describes the voltage dependence of each individual channel in its open state.



Thus, the general expression for a voltage gated current carried by an ion ( $j$ ) crossing the membrane through a population of identical ion selective channels is given by:

$$i_j = g_j(V_m - E_j) \quad (1.3)$$

where  $i_j$  is the current carried by ion  $j$ ;  $g_j$  is the conductance of the membrane to ion  $j$ ;  $V_m$  is the membrane potential and  $E_j$  is the equilibrium (Nernst) potential for ion  $j$  ( $V_m$  and  $E_j$  are usually in millivolts while  $g_j$  and  $i_j$  are frequently specific conductances and currents. e.g.  $\text{mS}/\text{cm}^2$  and  $\text{micro Amps}/\text{cm}^2$ ). Equation 1.3 is obviously a modification of Ohm's law, ( $V_m - E_j = i_j r_j$ ) and if  $G$  is a constant linear conductance the equivalent circuit element is shown in Figure 1.4, Panel B (Figure 1.4 also shows several other commonly encountered equivalent circuit elements). Equation (1.1) does not imply that the channel has a constant conductance; it does, however, have a maximum conductance,  $\bar{g}_j$ , when it is fully activated. When a fraction,  $x$ , of the maximum conductance is activated, then the conductance is given as

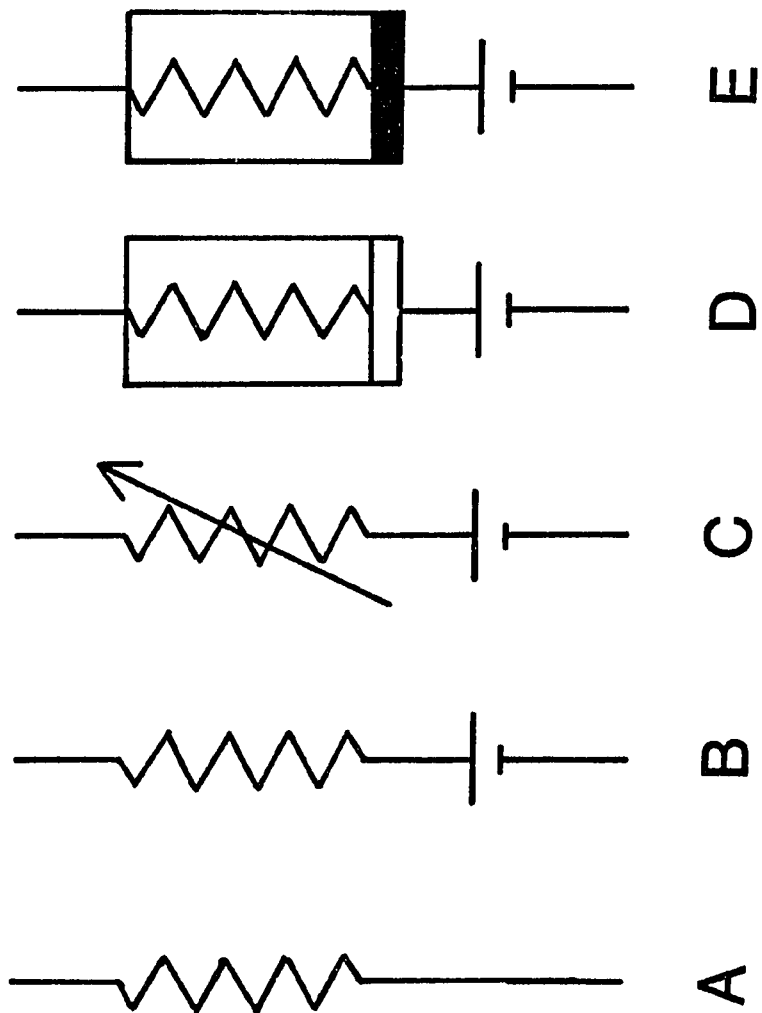
$$g_j = \bar{g}_j \cdot x \quad (1.4)$$

If more than one independent 'gate' with identical characteristics, controls the channel, the activation variable must be raised

Figure 1.4

Common symbols for lumped parameter Channel Models

- A) Linear Time Invariant with no Nernst battery, this characterization is used for non selective ionic leak channels.
- B) Linear Time Invariant with a Nernst battery, this characterization is used for ion selective channels, and due to the selectivity has a nernst potential associated with it.
- C) Linear Time Varying with a Nernst battery, this characterization is used for gated (i.e. time varying) channels showing ionic selectivity.
- D) Non-linear Time Invariant with a Nernst battery, this characterization implies no gating but a conductance that is not linear (e.g.  $I_{K1}$ ).
- E) Non-linear Time Varying with a Nernst battery, this characterization implies that the channel is gated but that its instantaneous current to voltage relationship is not described by a straight line.



to an integer power,  $g_j = g_j \cdot x^P$ . Therefore, the Hodgkin-Huxley equation for such an ionic current is of the form

$$i_j = g_j \cdot x^P \cdot (V_m - E_j) \quad (1.5)$$

This equation describes the passive flow of current,  $i_j$  down its electrochemical gradient ( $V_m - E_j$ ) through a membrane conductance set by the product  $g_j \cdot x^P$ . Equation (1.5) can be rewritten as

$$i_j = \bar{i}_j \cdot x^P \quad (1.6)$$

$i_j$  replaces  $g_j \cdot (V_m - E_j)$  and is an instantaneous function of voltage describing the process of ion movement. This process is called the ion transfer function or characteristic. The ion transfer characteristic is determined by measuring the ionic current when  $x$  or  $x^P$ , is made equal to one. The preparation is depolarized from a holding potential ( $V_{\text{hold}}$ ) to a conditioning potential ( $V_{\text{cond}}$ ) for a time interval long enough to ensure that  $x$  reaches its steady-state value ( $x_{\infty} = 1$ ). At this time the membrane is clamped to a constant test potential ( $V_{\text{test}}$ ) which may be set to any number of levels. The amplitude of the tail current is measured immediately after the capacitive transient associated with the voltage step has subsided and is plotted as a function of

$V_{\text{test}}$ . This voltage clamp protocol therefore measures the fully-activated instantaneous current-voltage relationship and hence describes the voltage-dependence of the ion transfer phenomenon. The potential at which the current reverses direction is the equilibrium potential. For a perfectly selective channel the reversal potential is given by the Nernst equation for the ion conducted by the channel.

As noted above, Hodgkin and Huxley (1952) showed that the ion transfer processes in squid giant axon are linear functions of the transmembrane potential, i.e., they each behave as a simple ohmic conductance. In most excitable cells however, the relationship between the fully-activated current and the membrane potential is nonlinear, indicating that the ion transfer reaction is potential dependent. Such nonlinearities are characterized according to the direction in which the membrane most easily passes current. Examples of both outward rectification [ $i_K$  in frog nerve fibres (Frankenhauser, 1962)] and inward rectification [ $i_{K_2}$  in sheep purkinje fibres (Noble and Tsien, 1968)] have been reported in the literature. Adrian (1969) gives a comprehensive review of rectification mechanisms in excitable membranes.

The function  $x^P$  in equation (1.5) controls the kinetic processes of a conventional Hodgkin-Huxley channel. It is independent of the magnitude and direction of current flow and is

called the gating variable. Hodgkin and Huxley (1952d) denoted the gating variable as a dimensionless, strongly voltage-dependent scalar, varying between zero and one. The fraction ( $x$ ) of the maximum conductance (i.e. all channels open) which is activated may be represented by a first-order reaction describing the transitions between the open state and a closed state

$$dx/dt = \alpha_x(1 - x) - \beta_x(x) \quad (1.7)$$

where  $\alpha_x$  and  $\beta_x$  are voltage dependent rate coefficients for the opening and closing of the particular channel under consideration.

In the steady-state,  $dx/dt = 0$  and the steady-state value ( $x_\infty$ ) may be obtained by setting equation (1.7) equal to zero. This gives the relationship

$$x_\infty = \frac{\alpha_x}{\alpha_x + \beta_x} \quad (1.8)$$

Furthermore, since equation (1.7) describes a first-order reaction, the time course of  $x$  after a step in voltage is a simple exponential function with a time constant given by

$$\tau_x = 1/(\alpha_x + \beta_x) \quad (1.9)$$

The gating variable response to a step increase in voltage is described by

$$X(t) = X_{\infty} - (X_0 - X_{\infty}) \exp(-t/\tau) \quad (1.10)$$

where  $X_0 = X(0)$  and  $\tau_x$  is given by (1.9) and  $X_{\infty}$  is given by (1.8). For the case where a channel is controlled by a single gating variable the channel current is, according to equation 1.5:

$$i_{\text{channel}}(V_m, t) = \bar{g}_{\text{channel}} X(V_m, t) [V_m - E_{\text{channel}}] \quad (1.11)$$

Generally where channels are controlled by only one gating variable (possibly raised to a power) this gating variable is called an activation variable. That is, a step increase in voltage results in a monotonic increase in membrane conductance as shown by the currents in Figure 1.5, Panel A. Some channels are governed by two types of gating processes, one that increases channel conductance (activation) and a second that decreases or turns off the conductance (inactivation). The activation gating variable in general has much faster kinetics than the inactivation variable. The time course of an ionic channel current having both activating and inactivating gating processes, shows an initial increase in conductance as activation occurs followed by a decrease in conductance as the inactivation process begins to dominate.

Figure 1.5

Example of typical currents measured in squid Axon.

Panel A

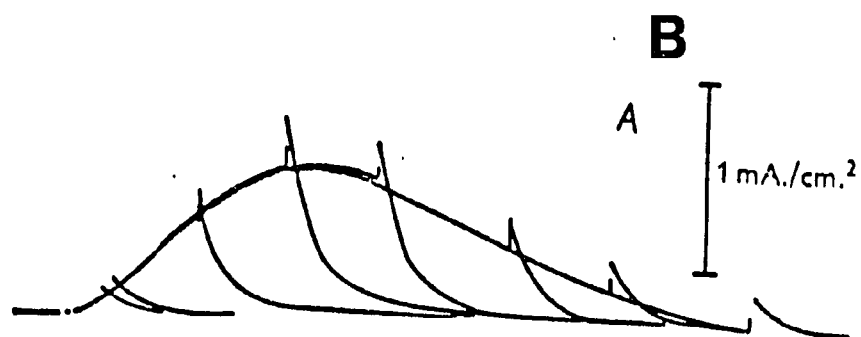
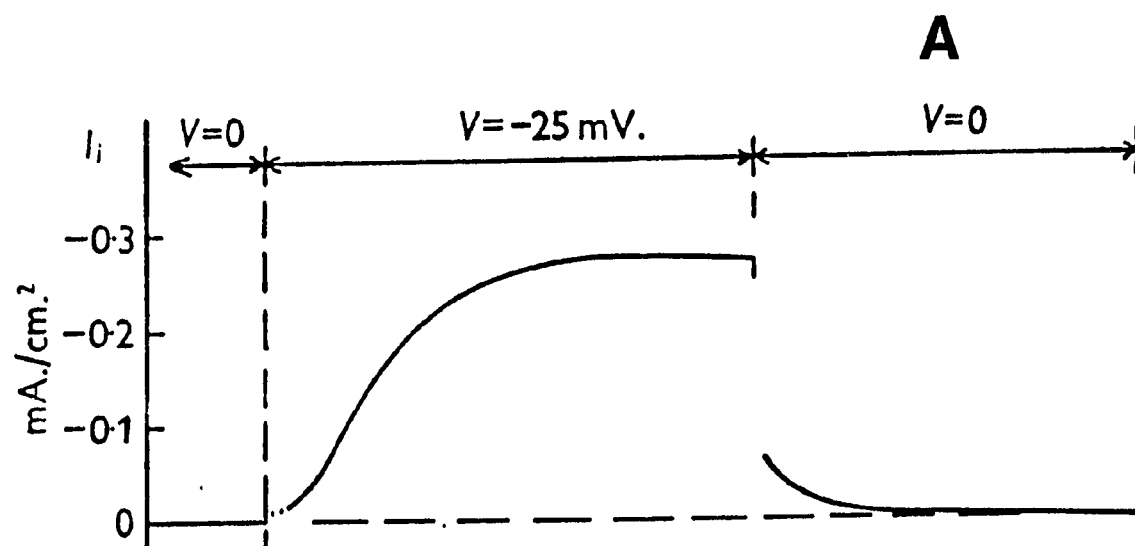
$I_K$  - a current displaying only activation by the expression  $n^4$ , note the sigmoid activation upon depolarization. On return to resting potential the current declines to zero in an exponential decay.

Panel B

$I_{Na}$  - a current displaying sigmoid activation due to the cubic nature of the  $m$  variable ( $m^3$ ) and a single exponential decline to zero (inactivation) due to the  $h$  variable, during a depolarizing pulse. The "spikes seen in this particular trace are the resulting currents from a return to the resting potential.

Hodgkin and Huxley defined positive currents as inward and negative currents as outward, the opposite of the convention used in most cardiac work and the opposite of the sign convention used in this thesis.





This is shown by the ionic currents in Figure 1.5(b) which are brief inward (negative) currents which start at zero peak and decline again to zero.

#### I.2.2.2 Activation of Transient Ionic Current:

The activation time-course of an ionic current can be fully described by the voltage dependent kinetic rate constants;  $\alpha_x$  and  $\beta_x$ , and the power term  $P$  (see Equation 1.5). A quantitative description of the steady-state voltage-dependence of the activation variable may be obtained by measuring the 'tails' of the current. To obtain the necessary experimental data, the preparation is depolarized from a fixed holding potential ( $V_{\text{hold}}$ ) to a test potential ( $V_{\text{test}}$ ) for a duration long enough to allow the activation process to reach its steady-state value. At the end of the test pulse the membrane is clamped back to the holding potential and the amplitude of the tail current at the beginning of this step is measured. Since the Hodgkin-Huxley variables do not change instantaneously, the peak values of the tail currents yield information concerning the values of the gating variable(s) reached at the end of the clamp to  $V_{\text{test}}$ . The magnitude of the tail current ( $i_t$ ) of ion described as:

$$i_t = \bar{g}_j(V_{\text{hold}}) \cdot (V_{\text{hold}} - E_j) \cdot [x_{\infty}(V_{\text{test}}) - x_{\infty}(V_{\text{hold}})] \quad (1.12)$$

Since the driving force  $e = (V_{\text{hold}} - E_j)$  and the maximum conductance  $\bar{g}_j(V_{\text{hold}})$  are held constant, the only variable determining  $i_t$  is the steady-state value of  $x_{\infty}^P$  at the test potential. If  $p$  is known, the steady-state value of the single activation gate may be obtained as the  $x^P$  of the data comprising the steady-state activation curve. The normalized plot of  $x_{\infty}$  as a function of potential is called a steady-state activation curve, and is in general a monotonic function of voltage which describes the voltage dependence of the activation gating mechanism.

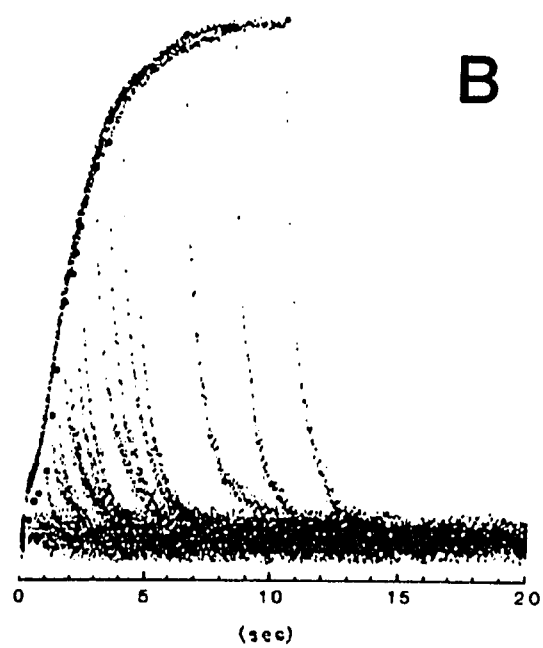
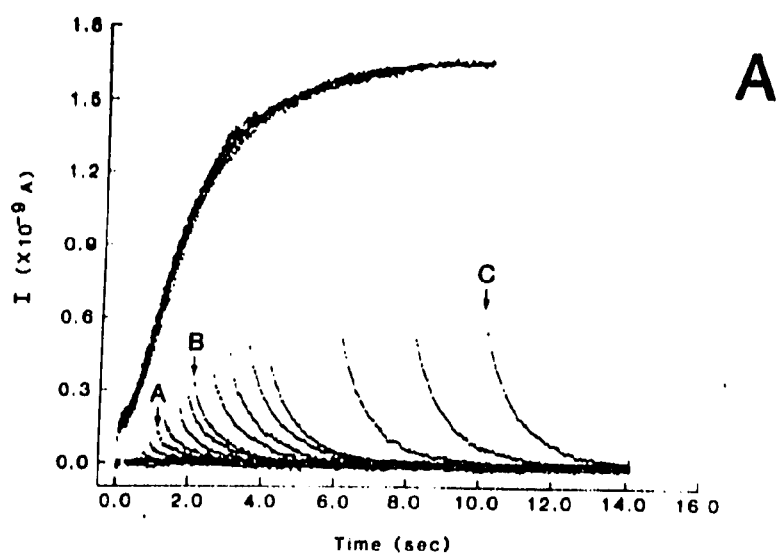
As mentioned above, it is assumed that the Hodgkin-Huxley gating variables do not change instantaneously. This is a very important assumption which must be experimentally tested and demonstrated. At the end of depolarizing rectangular voltage clamp pulses of variable durations, the current 'tail' decays or deactivates, as a simple exponential. The amplitude of these 'decay tails' may be used as a measure of the amount of current which has been activated by a preceding depolarization (Hodgkin and Huxley, 1952c). The time course of activation of the current should match the time course of the 'envelope' of decay tails for a given level of depolarization, if the gating variable in fact does not change its value instantaneously (see Fig. 1.6). Furthermore, the time constant of each decay tail should be a unique function of membrane potential. Since each depolarizing voltage clamp pulse returns to the same potential, each decay tail

Figure 1.6Panel A

An envelope of tails test for an activating current. This protocol involved repetitive application of rectangular depolarizing pulses of varying but fixed amplitude. The activation phases are superimposed and the resulting tails are shown as relaxations back to the baseline. Each tail shows a single exponential with a fixed time constant. (Shibata, 1983).

Panel B

Superimposed records of the onset of the current and of the scaled current tail record. Note that the time course of the envelope of tails and the time course of the onset of the current are very similar. The current tails may be used to measure the kinetics of the current.



should have the same time constant. A multi-exponential decay tail may suggest that another conductance process (ionic current), or a non-Hodgkin-Huxley current change (accumulation/depletion effect) is also involved.

The time-course of the activation process can also be obtained by depolarizing the membrane from a fixed holding potential ( $V_{\text{hold}}$ ) to a varied test potential ( $V_{\text{test}}$ ). The time constant,  $\tau_x$ , and value of  $p$  are obtained by fitting the time-dependent current in response to the test potential to the following equation  $i = A[1 - \exp(-t/\tau_x)]^p$ . The activation time course is sigmoid except when  $p = 1$ . Hodgkin and Huxley (1952) found that a value of  $p = 4$  provided the best fit for the potassium current activation gating variable  $n$  and  $p = 3$  for the activation gating variable  $m$  for the sodium current in squid axon. Their results suggest that there are four mutually independent voltage dependent 'gates' controlling each channel.

The above protocol provides time constant, or kinetic information for activation in only a limited range of potentials. In the range of potentials where the current is not activated (i.e. negative to its 'threshold'), determination of the time constant is obtained by measuring the time constant of deactivation. The cell is depolarized to a fixed conditioning level ( $V_0$ ) that activates the current, and is then clamped to potentials negative to the activation threshold. The time constant of the tail current

( $\tau_{\text{decay}}$ ) at these fixed, relatively negative potentials is measured. The time course of deactivation is proportional to  $[\exp -t/\tau_x]^p$ . From this expression, the measured time constant of decay is represented as

$$\tau_{\text{decay}} = \tau_x/p \quad (1.13)$$

and  $\tau_x$  may then be plotted as a function of potential.

#### I.2.2.3 Inactivation of Transient Ionic Current:

The inactivation process of a transient ionic current is described by the steady-state inactivation variable ( $y_\infty$ ), the number of gates ( $q$ ) controlling the inactivation process, and the time constant of inactivation ( $\tau_y$ ).

The steady-state inactivation relation is obtained in a similar fashion to the determination of the steady-state activation relation, in that its value is measured by allowing the inactivation variable to reach its steady state at a particular voltage level and measuring the resulting maximum current at some reference potential without allowing the inactivation variable to change significantly. In most potentials of interest the activation gating variable will not always be one (i.e. completely open) and will interfere with the measurement of the steady state inactivation relation. Voltage clamp protocols designed to minimise

the effects of the activation variable on the measurement of the steady state inactivation relation in all ranges of potential, through manipulation of the different time and voltage dependencies of the activation and inactivation process, are commonly used. (Meeves, 1978; Gillespie and Meeves, 1980).

The time constant of the inactivation process may be obtained directly, in a limited range of potentials, by depolarizing the membrane to variable potential levels ( $V_{\text{test}}$ ) and obtaining the best fit of the decay of the current to an exponential function. The time constant is then plotted as a function of the test potential ( $V_{\text{test}}$ ).

The recovery from inactivation may be studied using two identical clamp pulses at a fixed holding potential. The preparation is depolarized ( $P_I$ ) to a conditioning potential for a duration sufficiently long to produce inactivation. It is then repolarized to  $V_{\text{hold}}$  for a variable time ( $\Delta t$ ). During this period inactivation is removed. At pre-selected times ( $\Delta t$ ) a pulse  $P_{II}$ , which is identical to  $P_I$  is applied. This 'paired pulse' test is repeated at different  $\Delta t$ 's. The ratio of the peak currents is then plotted as a function of the interpulse duration. The relationship obtained by plotting the relative magnitude of the current,  $P_{II}$ , against the time between the pulses,  $\Delta t$ , is equal to the time course of removal of inactivation at  $V_{\text{hold}}$ . The time constant



( $\tau_y$ ) can be obtained as a function of potential by repeating the entire 'recovery' curve at a different holding potential.

### I.3 Mathematical models of the Cardiac Action Potential.

Noble (1962) made the first attempt to mathematically reconstruct the cardiac action potential. In this simulation, a simple modification of this Hodgkin-Huxley formulation was used. The decline, turn-off, or inactivation of the sodium current was simply made approx. 200 times slower. This resulted in a maintained inward current, and lengthened the 'squid' action potential from approximately 1-2 msec to 300-400 msec. In addition, Noble (1962) introduced the concept of rectification of a time-independent or background current. The result of both of these changes was a reduced  $K^+$  efflux (due to rectification) and a maintained  $Na^+$  influx during the plateau phase of the action potential; these have been retained as general characteristics of all more recent models of cardiac electrical activity. In the subsequent 15 years cardiac electrophysiologists have been able to obtain important new data concerning the mechanism of the cardiac action potential, mainly from Purkinje fibre preparations. In 1975 McAllister, Noble, and Tsien published a revised and much more complex model of the Purkinje fibre action potential. In this model there were nine currents; the action potential resulted from a very complex interaction of these current components. Two

years later Beeler and Reuter (1977) used a very similar approach to develop a mathematical model of the action potential in mammalian ventricle.

As noted earlier, within the last ten years it has become apparent that in addition to accurately determining the equivalent circuit of excitable cells and describing their time- and voltage-dependent ionic currents, both experimentalists and theoreticians must take careful account of the possibility that relatively large transmembrane fluxes into quite small intra- or extracellular spaces can have pronounced effects on the subsequent electrical activity of the cell. The most complete theoretical treatment of this type of problem has very recently been published by DiFrancesco and Noble (1985). In this recent model, the model of McAllister, Noble, and Tsien (1975) has been up-dated (and corrected based on multicellular data); in addition, mathematical equations for diffusion in restricted spaces and for current generated by an electrogenic sodium/potassium pump and a sodium/calcium exchange mechanism have been introduced.

Our goal was to use this type of approach to further study the plateau and repolarization phases of the action potential of the frog atrium, based on single cell data. A number of earlier attempts to mathematically reconstruct various action potential waveforms from bullfrog heart have been published. The first of these was that of Besseau (1971) who attempted to model the action

potential of frog atrium. Subsequently Goldman and Morad (1977) and Druhard and Roberge (1981) have attempted to mathematically reconstruct the repolarization phase of the frog ventricular action potential (The frog ventricle has current systems which are similar to frog atrium; Tung and Morad(1985)). However, in all of these studies, the current densities were estimated (as opposed to directly obtained from relevant single cell studies) and no attempt was made to account for the possible effects of changes in extracellular/intracellular ion concentrations. The major conclusions concerning the initiation of repolarization reached in the two more recent studies were significantly different. It is well recognized that repolarization and action potential duration are very important cardiac electrophysiological variables, both physiologically and pathophysiologically, and a mathematical model based on the relevant single cell data, should be very useful in the interpretation of these phenomena.

#### I.4 Data Recording and Analysis:

The size and kinetics of transmembrane ionic currents (e.g. Hume and Giles, 1983; Giles and Shibata, 1985) were quantitatively analyzed using a PDP 11/70 or VAX 11/750 computer. This was done as follows. The voltage clamp data were replayed from FM tape into a digital oscilloscope (Norland 3001, Fort Atkinson, WI), and digitized at rates ranging from 100 Hz to 10 kHz, depending upon

the approximate time-course of the process being analyzed. With the existing software, each trace is limited to 1024 points at 12 bits/point resolution. The digitized data were either sent directly to the PDP 11/70 or VAX 11/750 for processing and storage, or stored on a floppy diskette.

Two nonlinear least-squared analysis programs were used to obtain time constant data. A program called DISCRETE developed by Provencher (1976) (see Appendix I) was used for the majority of the data. This exponential fitting routine allows the user to set the zero time, first and last points, and the baseline value of each current record in the data file. The analysis then automatically yields an estimate of the number of exponential components and their magnitudes and time constants, without the user providing initial guesses of these values.

After this initial analysis had consistently determined the number of exponentials in each ionic current component, additional time constant analysis was carried out using the simpler and faster program EST2. Program EST2 was written by Mr. Keith Robinson and is based on a subroutine provided by Bevington (1969). This program is a nonlinear minimization of least-squares routine which may be used to fit exponential and other functions directly to experimental data. The accuracy of EST2 was tested and assessed by comparing the solutions it yielded with the time constant(s) and initial amplitude(s) from DISCRETE. The results

showed no significant differences in the fits generated by either DISCRETE or EST2. In the last stage of the kinetic analysis, the time constant(s) were then tabulated and averaged and the rate constants ( $R = 1/t$ ) were obtained and plotted as a function of potential.

The  $\alpha_n(V)$  and  $\beta_n(V)$  rate equations were obtained using one of two methods. One method was to make a table of values for  $\alpha_n(V)$  and  $\beta_n(V)$  rate constants by taking the ratio of the fraction of activation [ $n_\infty(V)$  or  $1-n_\infty(V)$ ; see eq. (2.8)] to the time constant [ $\tau_n(V)$ ] at the same potential level;  $\alpha_n = n_\infty/\tau_n$ ;  $\beta_n = (1-n_\infty)/\tau_n$ . Program ESTIMATE was then used to fit various forms of the rate equations to the  $\alpha$  and  $\beta$  data. ESTIMATE is a nonlinear least-squares routine similar to the program EST2. The second method for obtaining the equation for rate constant vs. potential data entailed use of a nonlinear least-square program ACTFIT, to fit both the steady-state activation [ $n_\infty(V)$ ] and the rate constant [ $R_n(V) = 1/\tau_n(V)$ ] values to a Hodgkin and Huxley type equation of the form

$$\alpha_n = \frac{\alpha_1(V-E)}{[(1-\exp(a_2(V-E)))]} \quad (1.14)$$

$$\beta_n = \beta_1 \exp(\beta_2(V-E)) \quad (1.15)$$

The current-voltage relations, reversal potential determinations and steady-state inactivation data were obtained by replaying data from FM tape onto a Gould chart recorder (Hume and Giles, 1983). The playback tape speed was reduced to 0.25 of the recording speed, to achieve a frequency response at the recorder of approximately 400 Hz. This frequency response did not distort any of the ionic current measurements, since in this preparation their kinetics are relatively slow.

#### 1.5 The Single Cell Experimental Procedure.

The frog heart has been a major focus for study of cardiac electrophysiology within the last 30 years. Originally the reason for this was convenience and ease. The heart can easily be obtained and can be maintained at room temperature for periods of many hours when it is placed in a Ringer's solution. More recently, it has been possible to use enzymatic dispersion techniques to isolate single cells from various regions of the frog heart (Hume and Giles, 1981; Hume and Giles, 1983). These cells provide a good model system for the study of atrial electrophysiology and are particularly attractive for voltage clamp work since they have no extensive intracellular membrane system (no transverse tubule system and very little SR) and since the isolated cells can be impaled and recorded with relative ease. The surface of these long spindle-shaped cells (see Fig. 2.18) is

not perfectly smooth; it is fenestrated with caveolae (small in-pocketings or infoldings approx.  $300 \text{ \AA}$  in diameter). These caveolae significantly increase the surface area of the cell (approx. 50%) and might restrict the diffusion of ions moving either into or out of the cell. In a typical action potential recording, or in a voltage clamp experiment, these cells are superfused with a normal Ringer's solution having the following constituents:

All solutions were made with glass-distilled water and were kept saturated with 95%  $\text{O}_2$ /5%  $\text{CO}_2$ . Standard Ringer's solution contained: NaCl, 90.6 mM;  $\text{NaHCO}_3$ , 20 mM; KCl, 2.5 mM;  $\text{MgCl}_2$ , 50.0 mM;  $\text{CaCl}_2$ , 2.5 mM; and glucose, 10 mM. The measured osmolarity of this solution was 241 mOsm. All electrophysiological experiments were carried out in standard Ringer's solution. Calcium-free Ringer's solution was identical to standard Ringer's solution, except that  $\text{CaCl}_2$  was omitted. In experiments in which the concentration of KCl was varied, the osmolarity was held constant by removal or addition of NaCl.

#### 1.5.1 Equivalent Circuit of a Bullfrog Atrial Cell:

In 1981 Hume and Giles described the passive electrical properties of this cell-type. From these it is possible to formulate an appropriate equivalent circuit. The passive electrical

properties of the cell from that work are shown in Tables 1 and 2. Figure 1.7 shows the appropriate equivalent circuit from the data.

These electrophysiological measurements and more recent ones by Moore, Shibata, Clark and Giles (1985) strongly suggest that the resting atrial cell can be represented by a very simple equivalent circuit: a parallel combination of a capacitance and a resistance. However, it must be remembered that the technique used in recording from these cells requires placement of a suction microelectrode into the cell. This microelectrode typically has a resistance of 1-10 megohms and this resistance often increases substantially (doubles) during an experiment. Therefore, the access resistance or series resistance of the pipette is a significant factor and must be accounted for when studying either the passive or the active ionic currents in this cell-type. Moreover, it is important to remember that although the suction pipette method gives very high seal resistances--resistances between the edge of the pipette and the ruptured membrane--these resistances are not infinite and are in the range of  $10^9$  ohms (Gigohms). As will be noted later in this thesis, under some circumstances--particularly when studying the quantitative properties of background currents--this seal resistance or possible changes in it must be considered.



Figure 1.7

A simplified schematic of the passive properties of the sarcolemma of a bullfrog atrial cell within a single micro electrode impalement.  $R_m$  is the passive membrane resistance,  $C_m$  is the membrane capacitance.  $R_{Seal}$  is the resistance due to the membrane - electrode interface, and  $R_{Electrode}$  is the series resistance of the measurement electrode.

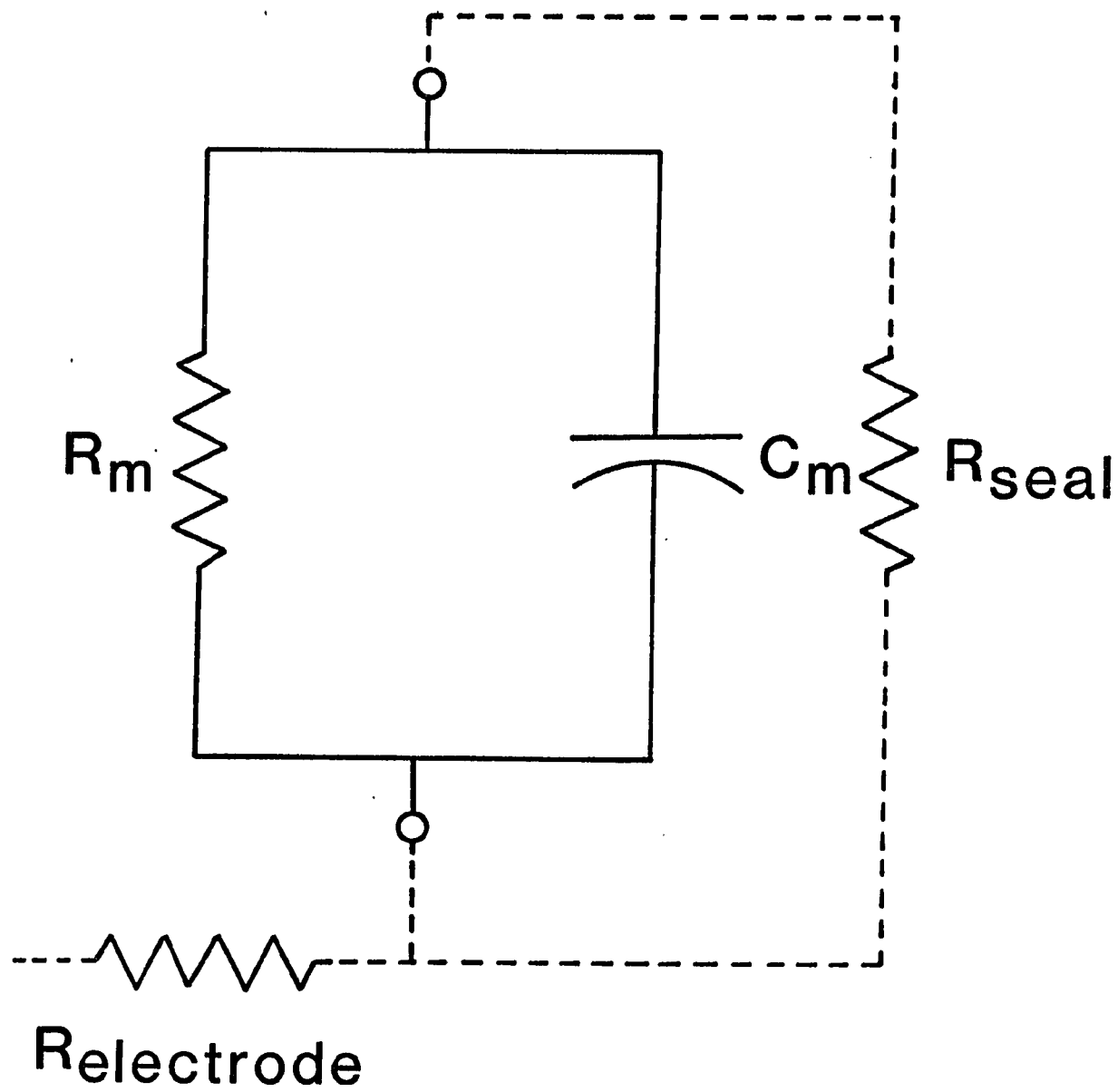


TABLE 1.1  
SUMMARY OF ELECTRICAL PARAMETERS OF FROG ATRIAL CELLS (n = 12)

	Mean $\pm$ SD
Resting membrane potential	-88.6 mV $\pm$ 1.7
Action potential amplitude	124.4 mV $\pm$ 8.1
Action potential overshoot	35.8 mV $\pm$ 7.1
Action potential duration	722.5 ms $\pm$ 106.3
Upstroke velocity ( $V_{\text{Max}}$ )	42.2 V/s $\pm$ 11.8
Input resistance ( $R_{\text{in}}$ )	219.8 M $\Omega$ $\pm$ 77.4
Membrane time constant ( $\tau_{\text{m}}$ )	19.7 ms $\pm$ 7.3
Cell length	204.0 $\mu\text{m}$ $\pm$ 34.8
Cell diameter (measured at the widest region of the cell near the nucleus)	7.1 $\mu\text{m}$ $\pm$ 0.8

TABLE 1.2  
ELECTRICAL CONSTANTS OF SINGLE FROG ATRIAL CELLS

Cell	$V_r$	Cell length	$R_{in}$	$\tau_m$	$\lambda$	$R_i$	$R_m$	$r_i$	$r_m$	$C_m$
	mV	$\mu m$	M $\Omega$	ms	$\mu m$	$\Omega cm$	k $\Omega cm^2$	$\times 10^8 \Omega cm^{-1}$	$\times 10^6 \mu cm$	$\mu F cm^{-2}$
1	-88	225	300	31.8	838	187.4	10.4	9.4	6.6	3.1
2	-87	270	224	14.9	977	121.3	9.3	6.2	5.9	1.6
3	-85	125	106	15.1						
4	-88	333	133	14.5	936	95.2	6.7	4.9	4.3	2.2
5	-84	350	400	33.4						
6	-87	325	101	9.5	934	71.1	5.0	3.5	3.2	1.9
Mean	-86.5	271	210.7	19.9	921.3	118.1	7.9	6.0	5.0	2.2
$\pm$ SEM	0.7	34.8	49.3	4.1	29.5	24.5	1.2	1.2	0.8	0.3

## 1.6 SPECIFIC AIMS OF THIS THESIS

- (i) To mathematically reconstruct the action potential of an atrial cell from the bullfrog heart using Hodgkin-Huxley descriptions of the background and the time- and voltage-dependent ionic currents.
- (ii) To examine in detail the mechanism of the repolarization phase of the action potential.
- (iii) To include in the above model (1) a mathematical expression for an energy-requiring electrogenic sodium/potassium pump; and in addition, (2) model the diffusional processes in the restricted extracellular space immediately outside of a single atrial cell within the multicellular atrial trabeculum.
- (iv) To use existing biochemical information concerning the amounts, the distribution, and the kinetics of the relevant calcium-buffering mechanisms themselves and to model the major calcium-buffering reactions occurring within the heart.
- (v) Formulate mathematical expressions for an electrogenic sodium/calcium exchange mechanism so that the possible influences of sodium/calcium exchange on the size and

duration of the action potential could be simulated both with and in the absence of intracellular calcium-buffering mechanisms.

- (vi) To assess the extent to which physiological changes in heart rate will produce significant changes in the intracellular activity of sodium, the extracellular activity of potassium, and the intra and extracellular activities of calcium.
- (vii) To mathematically reconstruct the pacemaker and action potential of a sinus-venosus cell from the bullfrog heart using Hodgkin-Huxley descriptions of the background and the time- and voltage-dependent ionic currents.
- (viii) To assess the possible physiologic role which ionic pump and exchanger currents as well as accumulation/depletion phenomena in the development of the pacemaker potential.

## CHAPTER II

### Ionic Currents in Single Atrial Cells: A Mathematical Description

#### II.0 Introduction:

Figure 1.0 in the previous Chapter shows a typical action potential recorded from frog atrium. The major aim of this Chapter is to provide the background information necessary for developing a mathematical (Hodgkin-Huxley) description of each of the ionic currents which underlie the resting potential and the action potential in this cardiac tissue.

Within the past five years Giles and his colleagues have studied bullfrog atrial cells extensively and have shown that the following time- and voltage-dependent ionic currents are present:

- (1) A relatively large (6 nanoamps) fast transient inward sodium current.
- (2) A much smaller and slower transient inward calcium current.
- (3) A relatively slow but quite large time- and voltage-dependent outward potassium current or delayed rectifier.

In addition, the resting potential is maintained by a significant potassium flux. This potassium current system exhibits very

strong inward rectification and is therefore similar to the background potassium current  $I_{K_1}$  present in most other cardiac cell types and in a wide variety of other excitable and inexcitable tissues. The ion concentration gradients are maintained in this cell and most other cells by an energy-requiring (ATP-requiring)  $\text{Na}^+/\text{K}^+$  pump and a  $\text{Na}^+/\text{Ca}^{++}$  exchanger mechanism. In addition, in frog heart and most other cardiac tissues there is clear evidence for the presence of an ATP-requiring  $\text{Ca}^{++}$  pump. We have used the Hodgkin-Huxley theory to formulate mathematical equations describing the kinetics and the ion transfer processes of each of these current components based either upon our own experimental measurements or the best available data from the literature.

## II.1 Time-independent or Background Ionic Currents:

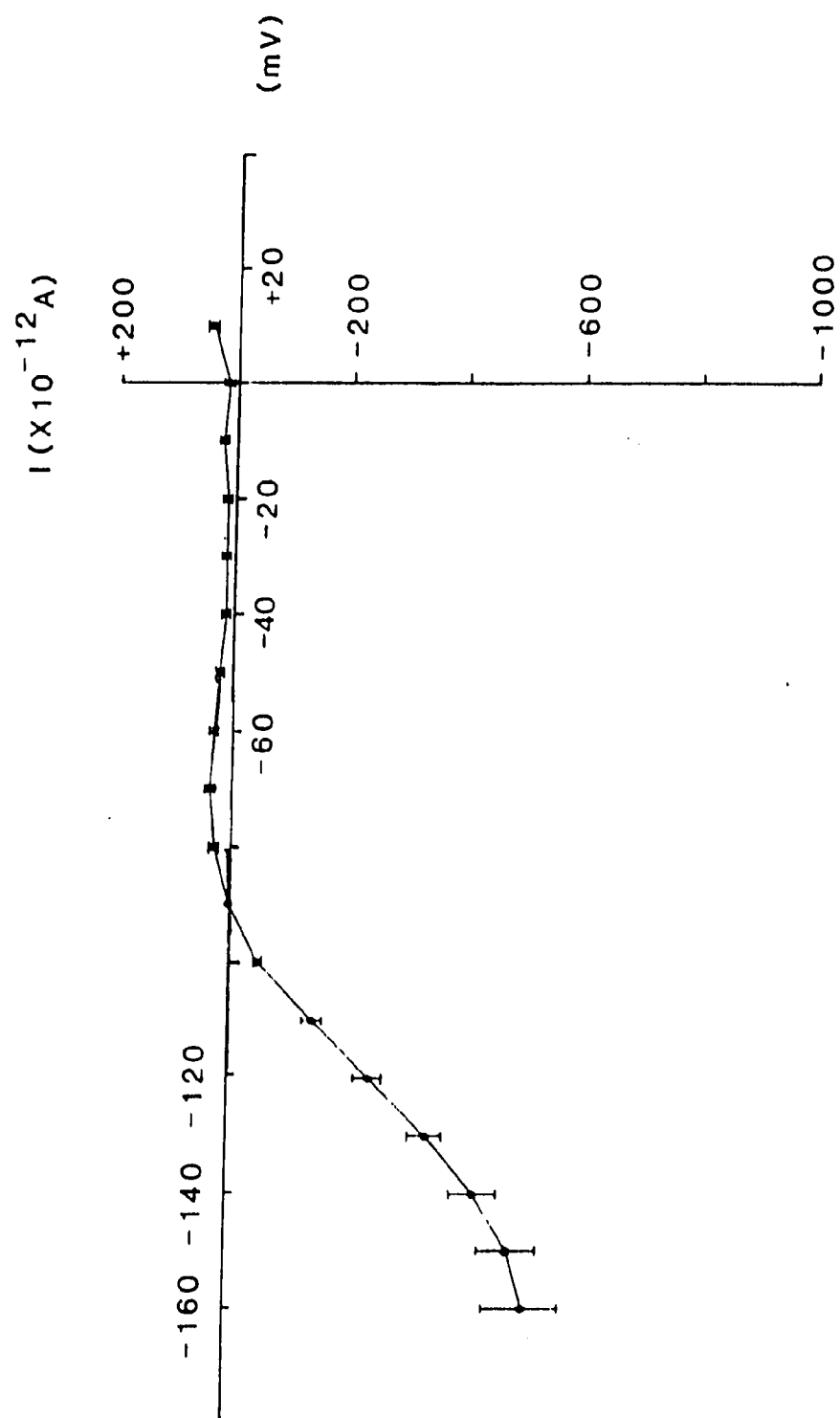
Background ionic currents, by definition, are the ionic currents which show no measureable time-dependence. In general, they are very important in determining the resting membrane potential, but often they play no role in the time-course of the action potential. This however may not be true with respect to the final phase of repolarization of the action potential, and is not true in considerations of development of the pacemaker potential.

In the present model of electrophysiological activity in the atrial cell there are two important time-independent background ionic currents: (1) an inwardly rectifying potassium current, and



Figure 2.1

Measurement of the time-independent background current ( $I_K$ ) in an isolated atrial cell. The cell was superfused in TTX ( $3 \times 10^{-6}$  M) and  $\text{LaCl}_3$  ( $10^{-5}$  M) containing Ringers. The holding potential and short (100 msec) command pulses were applied. Maximum inward or minimum outward ionic currents were measured. Note the significant inward rectification.

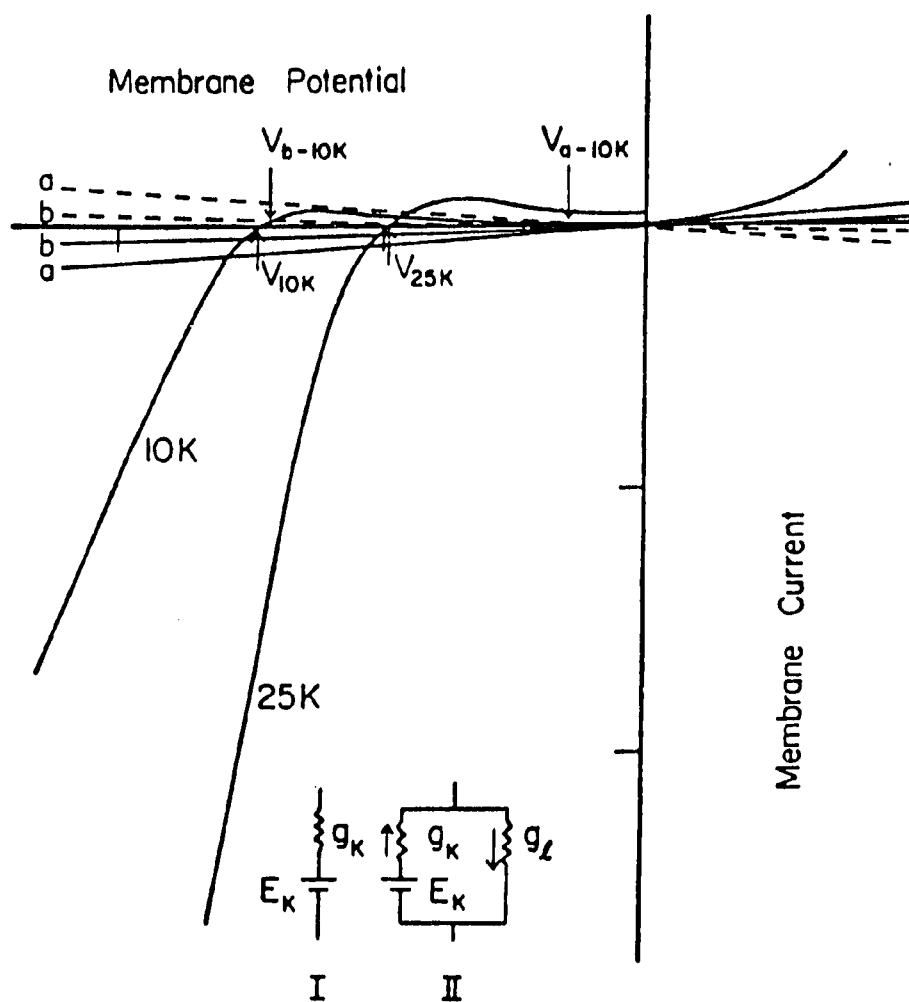


(2) a linear inward current system presumed to be carried mainly by sodium ions.

The inwardly rectifying background potassium current has been identified and studied in some detail in frog atrial cells (Hume and Giles, 1983).  $I_{K_1}$  in this cell type displays strong inward-going rectification and may exhibit negative slope in the range of potentials positive to approximately -70 mV (see Figure 2.1). The  $I_{K_1}$  current-voltage (I-V) relationship is measured by blocking all other time- and voltage-dependent currents and measuring the current in response to short depolarizing or hyperpolarizing voltage-clamp pulses following the decay of the capacitative transient. It is obvious from the data in Fig. 2.1 that this current system generates very little current in the outward direction. Therefore, it is very important to consider the possible contributions of other currents in this I-V curve. In particular the electrode seal resistance is not infinite and the exact value of the seal resistance could influence the size and the shape of  $I_{K_1}$  in the range of potentials positive to -60 mV. Hagiwara and Jaffe, (1979) have drawn attention to the way in which this may occur and the significance of seal resistance or changes in seal resistance for proper measurement of resting potential. The main point of their argument is illustrated by Figure 2.2 taken from their paper.

Figure 2.2

Illustration of the interaction of the inwardly rectifying current, " $I_{K1}$ " and the leakage conductance introduced by electrode impalement in accurately measuring  $I_{K1}$ . The figure shows a schematic current-voltage relationship of the inward rectifier current (in 10mM  $[K^+]$  and 25 mM  $[K^+]$  bath concentrations) and two different hypothetical linear background leakage currents. (indicated by solid lines a and b) which must constitute a portion of this current measurement. To obtain the amount of current due to  $I_{K1}$  alone a correction factor must be added to the measured current (a and b broken lines represent the appropriate correction factors).



In our experiments the seal resistance was estimated and the experimentally observed  $I_{K_1}$  was adjusted correspondingly. As can be seen from Figure 2.2 subtracting a positive (leak) conductance from the nearly flat experimental I-V (figure 2.1) will make the region of negative slope much more prominent. Attempts to explain the anomalous (inward) rectification in terms of the underlying long-pore effects (e.g. Hille and Schwarz (1978)) involve models which are themselves very complicated and computationally involved. DiFrancesco and Noble (1985) have used a simple, but purely empirical formulation first suggested by Hagiwara and Takahashi (1974). The atrial model uses this formulation with the conductance adjusted to match data obtained from single frog atrial cells:

$$I_{K_1} = G_{K_1} \frac{[K_o]}{([K_o] + K_m)} \frac{E - E_k}{1 + \exp((V_m - E_k - 20)2F/RT)} \quad (2.1)$$

This formulation is empirical; however, an important physiological variable, relatively large changes of potassium in the small clefts surrounding the cells and/or in the caveolae can be adequately described by using the modified DiFrancesco and Noble formulation.

The second background current in frog atrium is a steady inward current thought to be carried mainly by sodium ions (Keenan

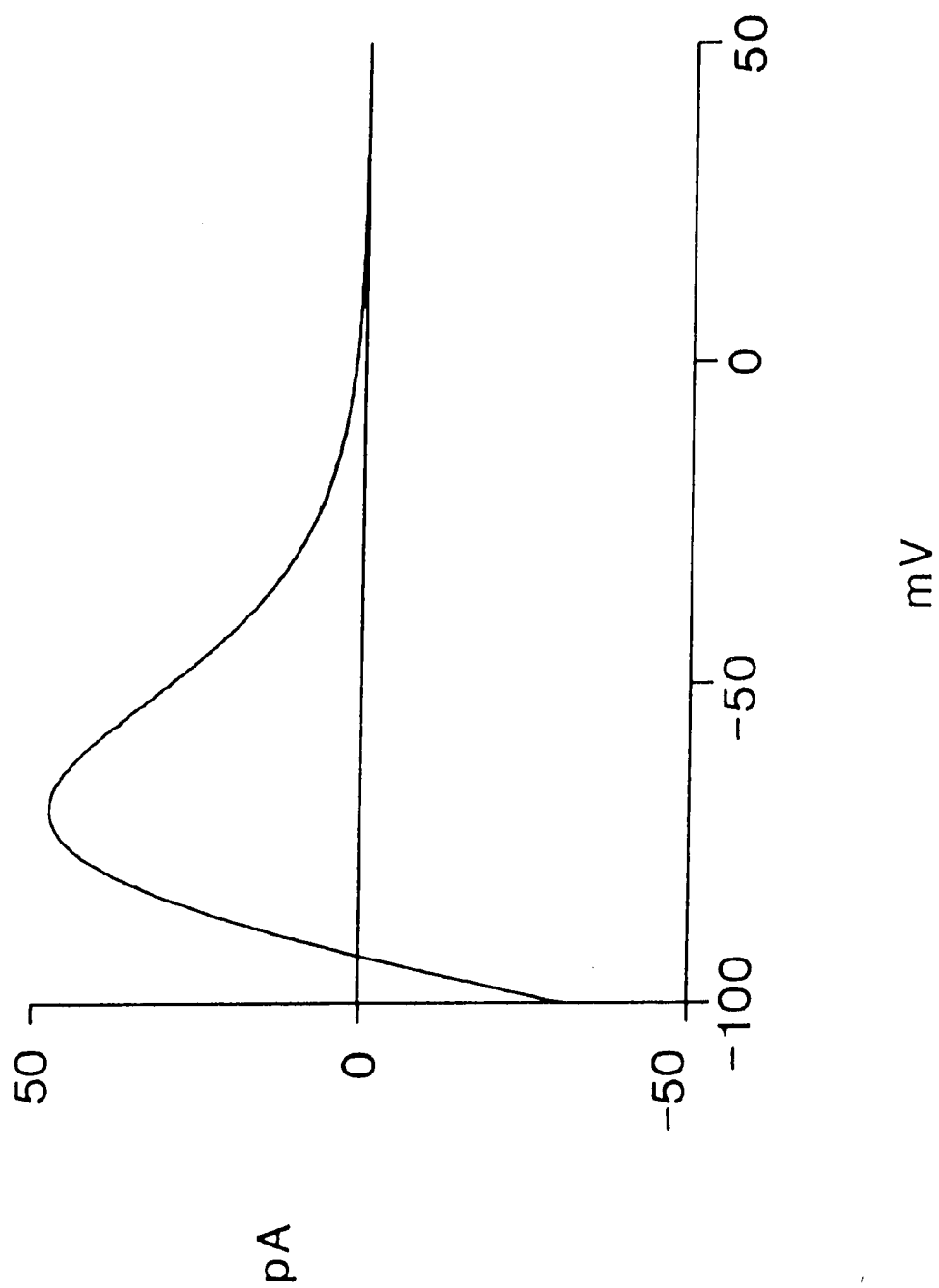
and Neidergerke, 1967). The principal determinants of this current therefore are the reversal potential for sodium ions (approx. +55 mV, R. Clark and W.R. Giles, 1985 in preparation) and the size of the conductance at any potential. The reversal potential for this current system (54 millivolts) was chosen to be a constant value that is considerably lower than the reversal potential calculated for a "pure" sodium current using model ionic concentrations (closer to 70 millivolts). This choice of a formulation for the background inward current reflects the great deal of uncertainty concerning this current. The 54 mV reversal potential was "borrowed" from reversal potential measurements of the sodium inward current (the only measurable sodium specific current in frog atrium). We have estimated the size of the inward leak current indirectly by measuring the current required to hyperpolarize the cell to the potassium equilibrium potential. The resulting current voltage relationship is shown in Figure 2.3 and has a slope conductance of  $1.5 \times 10^{-10}$  siemens. This current is thought to be responsible for maintaining or holding the resting potential positive to the Nernst potential for potassium (approx. -95 mV, Walker and Ladle, 1971). The mathematical description of this background sodium current is therefore very simple. It is given in Equation 2.2:

$$I_{\text{Back}} = I_{\text{NaBack}} + I_{\text{CaBack}} \quad (2.2)$$

Figure 2.3

The model current-voltage relation for  $I_{K1}$  in 2.5 mM external  $[K^+]$  and 95 mM internal  $[K^+]$ . Remember that the magnitude and shape of the current are sensitive to concentration changes as well as the reversal potential.





$$I_{\text{NaBack}} = G_{\text{Na}} (V_m - 54) \quad (2.3)$$

$$G_{\text{Na}} = 1.5 \times 10^{-4} \text{ } \mu\text{siemens}$$

The magnitude and ionic composition of the background inward current system is derived from resting ionic flux measurements, resting membrane potential, and values of resting ionic concentrations. A very small portion, less than 1%, of this current attributed to calcium influx was added in order to reproduce the resting passive calcium influx levels recorded by Niedegerke (1963), Niedegerke, Page, and Talbot (1969a,b) and Chapman (1979) and to keep resting internal calcium concentrations from reaching sub-nanomolar values.

$$I_{\text{CaBack}} = G_{\text{CaBack}} (V_m - 54) \quad (2.4)$$

$$G_{\text{Ca}} = 5 \times 10^{-7} \text{ } \mu\text{siemens}$$

## II.2 Time- and Voltage-dependent Ionic Currents:

As noted in the previous Chapter, there are three important time- and voltage-dependent ionic currents underlying the action potential in bullfrog atrium. In this section the major characteristics of each of these currents will be briefly reviewed and the mathematical descriptions used in this computer simulation will be given.

#### II.2.1 $I_{Na}$ :

The TTX-sensitive fast transient inward current was first studied quantitatively in squid axon (Hodgkin and Huxley, 1952,a-d). Subsequent investigations in heart muscle were begun by Beeler and Reuter (1970). However, these and most other studies in multicellular cardiac tissue suffered from inconsistency and lack of precision in measurement of both the size and the kinetics of the current due in large part to series resistance artifacts. Within the last five years, the size and the kinetics of this sodium current have been measured in a variety of single cardiac cell preparations (e.g. Brown, Lee, and Powell, 1980; Ebihara and Johnson, 1980; for review see Fozzard, et al., 1985). This current, as noted previously, is responsible for the initial rapid depolarization of the action potential.

Although sodium current in frog atrium was studied using multicellular trabeculae and a double sucrose gap approach nearly 20 years ago; for reasons given above quantitative data was not available until very recently. Hume and Giles (1983) identified

this current, and estimated its size relative to  $I_{Ca}$ , (see below). More complete and quantitative studies are now underway (Clark and Giles, in preparation). The mathematical description given below is based upon very recent experimental data and also upon theoretical work in which the extent of spatial uniformity during the relevant voltage-clamp experiments and the effects of the cable structure of the cell on sodium current have been included. A typical family of sodium currents is shown in Figure 2.4. The equations for a full description of the time- and voltage-dependence of this current and its ion transfer characteristics are:

$$I_{Na} = m^3 h \quad \overline{I_{Na}} \quad (2.5)$$

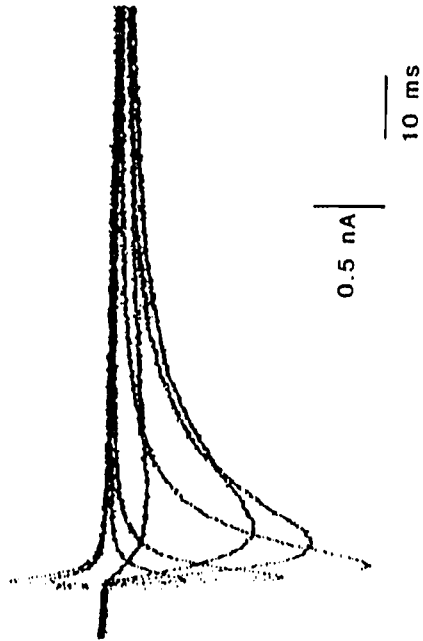
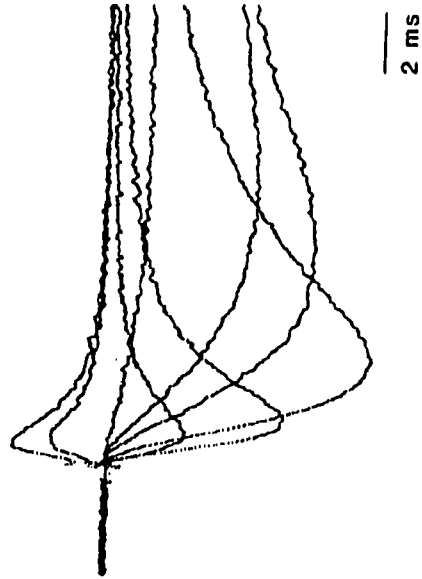
$$\overline{I_{Na}} = \frac{\overline{G_{Na}} [Na]_i \cdot \frac{F^2}{RT} \cdot V_m \cdot (\exp(\frac{F}{RT}(V_m - E_{Na})) - 1)}{\exp(V_m \cdot \frac{F}{RT}) - 1.0} \quad (2.6)$$

$$\overline{G_{Na}} = 132 \quad (2.7)$$

$$\frac{dm}{dt} = (1 - m) \alpha_m - m \beta_m \quad (2.8)$$

Figure 2.4

A typical "family" of sodium currents measured in frog Atrium for various steps in potential at 10°C. Note that the currents transients are over within 20 to 30 milliseconds even in cold temperatures which slow down their kinetics.



$$\alpha_m = \frac{0.0757 (V_m - 31.2)}{1 - \exp(-0.0617(V_m - 31.2))} \quad (2.9)$$

$$\beta_m = 2.26 (\exp(-0.042 (V_m + 28.46))) \quad (2.10)$$

$$\frac{dh}{dt} = (1-h) \alpha_h - h \beta_h \quad (2.11)$$

$$\alpha_h = 0.051 \exp(-0.124 (V_m + 85.45)) \quad (2.12)$$

$$\beta_h = \frac{1.2707}{1 + \exp(-0.0764 (V_m + 2.91))} \quad (2.13)$$

See Figure 2.5 for plots of  $m_\infty$ ,  $h_\infty$ ,  $\tau_m^{-1}$  and  $\tau_h^{-1}$ . As shown in the Result Section of this thesis, this description of currents provides a reasonable, albeit semiquantitative, match of the electrophysiological data themselves and also of the upstroke of the action potential. At present it is not fruitful to further

Figure 2.5

Plots of the voltage dependence of the gating variables controlling the Fast inward current ( $I_{Na}$ ) in the atrial model.

Panel A

The steady state ( $\infty$ ) values for the gating variables  $m$  and  $h$ .

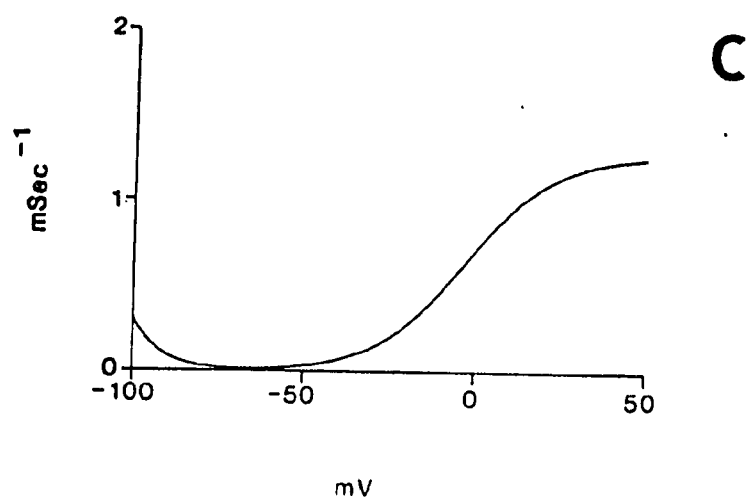
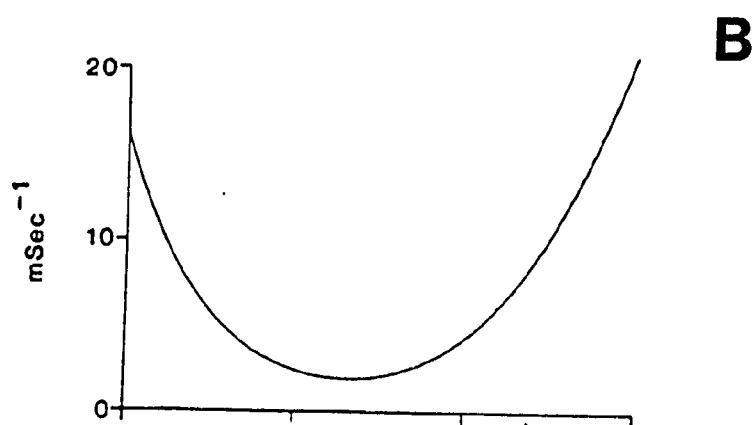
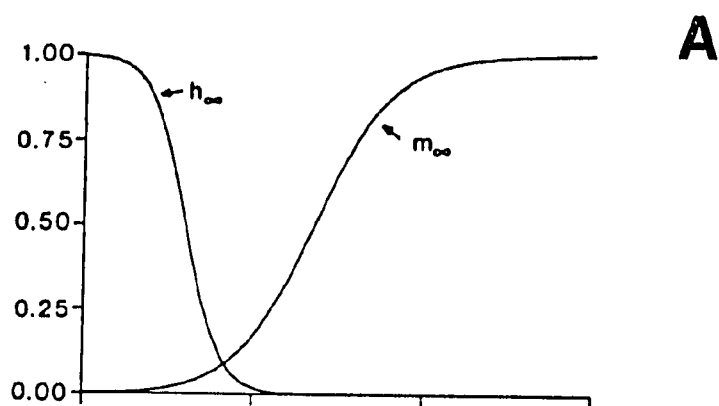
PANEL B

The rate constant ( $1/\tau$ ) for the  $m$  gating variable as a function of transmembrane potential.

Panel C

The rate constant ( $1/\tau$ ) for the  $h$  gating variable as a function of transmembrane potential.





pursue a different or more exact description of the current because the relevant experimental data have not been obtained with sufficient accuracy or reproducibility to merit this.

The information generated with the Hodgkin-Huxely model may still be correct in specific instances. Experimental evidence aimed at determining in great detail the behavior of  $\text{Na}^+$  currents in the heart in order to develop more precise models of excitation have led to measurements indicating deviations from the  $m^3h$  formulation. As in nerve inactivation, recovery from inactivation may occur with a time lag, and two or more time constants of inactivation are often observed. (Fozzard, January and Makielski(1985))

### 2.2.2 $I_{\text{Ca}}$ :

As noted previously the calcium current is both smaller and slower than  $I_{\text{Na}}$ . Therefore  $I_{\text{Ca}}$  is easier to study quantitatively using the single microelectrode voltage-clamp technique; however, a number of technical difficulties remain. For example, in some ranges of potential the activation of the calcium current is sufficiently fast that problems of overlap of the activation of  $I_{\text{Ca}}$  with the capacitive transient remain; these are particularly important in attempts to measure peak tail currents in order to obtain, for example, fully-activated current

voltage relationships. The mathematical model of the calcium current is therefore based on somewhat incomplete data. The peak I-V relationship can be obtained quite accurately but the steady-state inactivation curve can be obtained reliably only negative to 0 mV. Formulation of the model of the inactivation process was a straightforward interpretation of the experimental data. The steady-state inactivation relation has been experimentally determined accurately over the majority of the physiological range of voltages found in the frog atrial action potential and semi-quantitatively in the ranges positive to 0 mV (Figure 2.6(a)). Unlike most inactivation relations the measured inactivation relation for the calcium current in frog atrium is not monotonic, it appears to be an ordinary inactivation relation negative to 0 mV but positive to 0 mV the inactivation relation increases, that is the gating variable begins to reopen at positive potentials. By matching this steady-state curve to two Boltzman relations (One for inactivation in negative potentials and one for "reactivation" at positive potentials Figure 2.6(b)) the steady-state relation can be well-described. Similarly the time constants of inactivation have been measured over a limited range of potentials (Figure 2.6(c)) and the corresponding rate constants can be well described by a gaussian curve (Figure 2.6(d)).

Figure 2.6

Plots of the observed and modelled kinetics of calcium current inactivation (the "f" gating variable) as a function of transmembrane potential.

Panel A

Observed  $f_{\infty}$  relation Campbell (1985).

Panel B

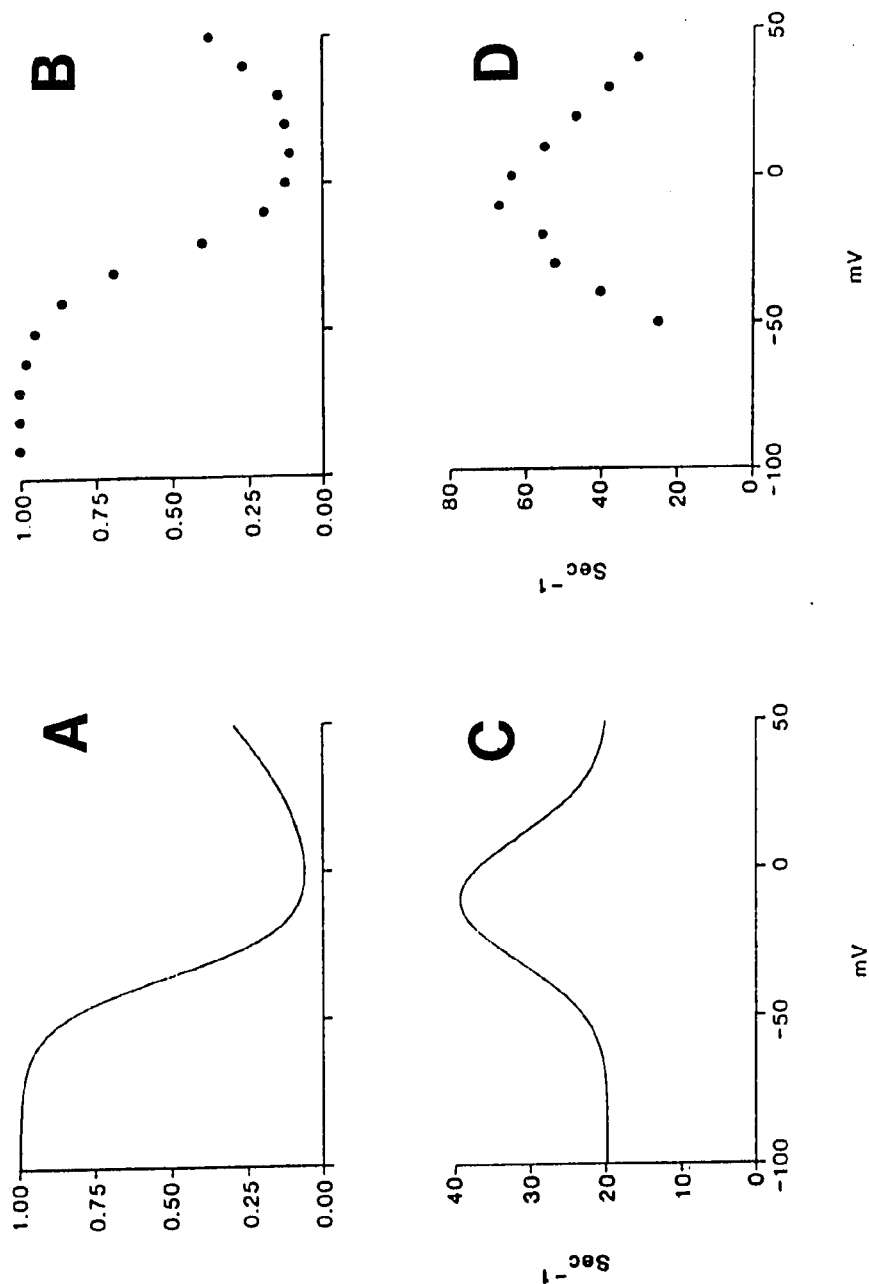
Model  $f_{\infty}$  relation.

Panel C

Observed  $\gamma^{-1}$  relationship for the f gating variable  
Campbell (1985)

Panel D

Model  $\gamma^{-1}$  relationship for the f gating variable



Having characterized both the time constant as well as the steady-state voltage-dependence of the gating variable, the model description of the inactivation gating variable  $f$  is complete.

$$\frac{df}{dt} = f_{\infty} \tau_f^{-1} - f \tau_f^{-1} \quad (2.14)$$

$$\tau_f^{-1} = 0.001(19.7 \exp(-(0.034 ((V_m + 10))^2) + 19.8) \quad (2.15)$$

$$f_{\infty} = \frac{1.0}{1.0 + \exp((35.1 + V_m)/8.6)} + \frac{0.6}{1.0 + \exp((50 - V_m)/20.0)} \quad (2.16)$$

The steady-state activation curve can be estimated as follows from the peak I-V relation: Assume that positive to +10 mV the current is fully-activated and that the activation process is complete before any substantial inactivation has had time to occur. Further assume that the I-V relation of the fully-activated channel is linear in the range of +10 mV to the reversal potential. Based upon these assumptions the voltage-dependence of the steady-state activation variable relation may be arrived at as follows:

- 1) Pass a line through the points between +10 mV and the reversal potential,
- 2) call the line  $I_{\text{fully-act}}$ , and
- 3) take the ratio of the measured peak currents ( $I_{\text{Peak}}$ ) to the estimated fully-activated currents ( $I_{\text{fully-act}}$ ) at various voltages (see Figure 2.7). This gives us an estimate of the steady-state activation variable  $d$  as a function of membrane potential.

$$d_{\infty} = \frac{I_{\text{Peak}}}{I_{\text{fully-act}}} \quad (2.17)$$

Although some experimental results indicate that the activation of  $I_{\text{Ca}}$  is a very complex process, we have chosen to use only a single gating variable ( $d$ ) raised to the first power. The steady-state voltage dependence of  $d$  was assumed to obey a simple Boltzmann relation while the time-dependent characteristics were obtained by assuming symmetric  $\alpha$  and  $\beta$ -rate constants which reproduced the desired Boltzmann relationships and provided at least a qualitative fit to the time-course of the onset of the calcium current. The equations describing the  $d$  gating variable are:

$$\frac{dd}{dt} = d_{\infty} \tau_d^{-1} - d \tau_d^{-1} \quad (2.18)$$

$$d_{\infty} = \frac{1.0}{1.0 + \exp(-(10.0 + V_m)/6.24)} \quad (2.19)$$

$$\tau_d^{-1} = \frac{0.035(V_m + 10.0)}{d_{\infty} (1 - \exp(-(V_m + 10.0)/6.24))} \quad (2.20)$$

Figure 2.8 shows plots of  $d_{\infty}$  and  $\tau_d^{-1}$ . The fully activated current voltage relationship for  $I_{\text{Ca}}$  was assumed to obey the

Figure 2.7

The current to voltage relationship for  $I_{Ca}$  as measured in bullfrog sinus-venosus cells (Shibata (1983)). The line bracketed by standard error bars represents the observed peak inward current measured. The straight line through the points positive to 0 mV represents an estimate of what the current would be if it were completely activated. By taking the ratio of this estimate ( $I_{fully\ Act.}$ ) to the measured peak current ( $I_{peak}$ ) an estimate of how activated the channel is (i.e.  $d_{\infty}$ ) may be obtained. This value is then used as a starting point and is then "tuned" within the model program.



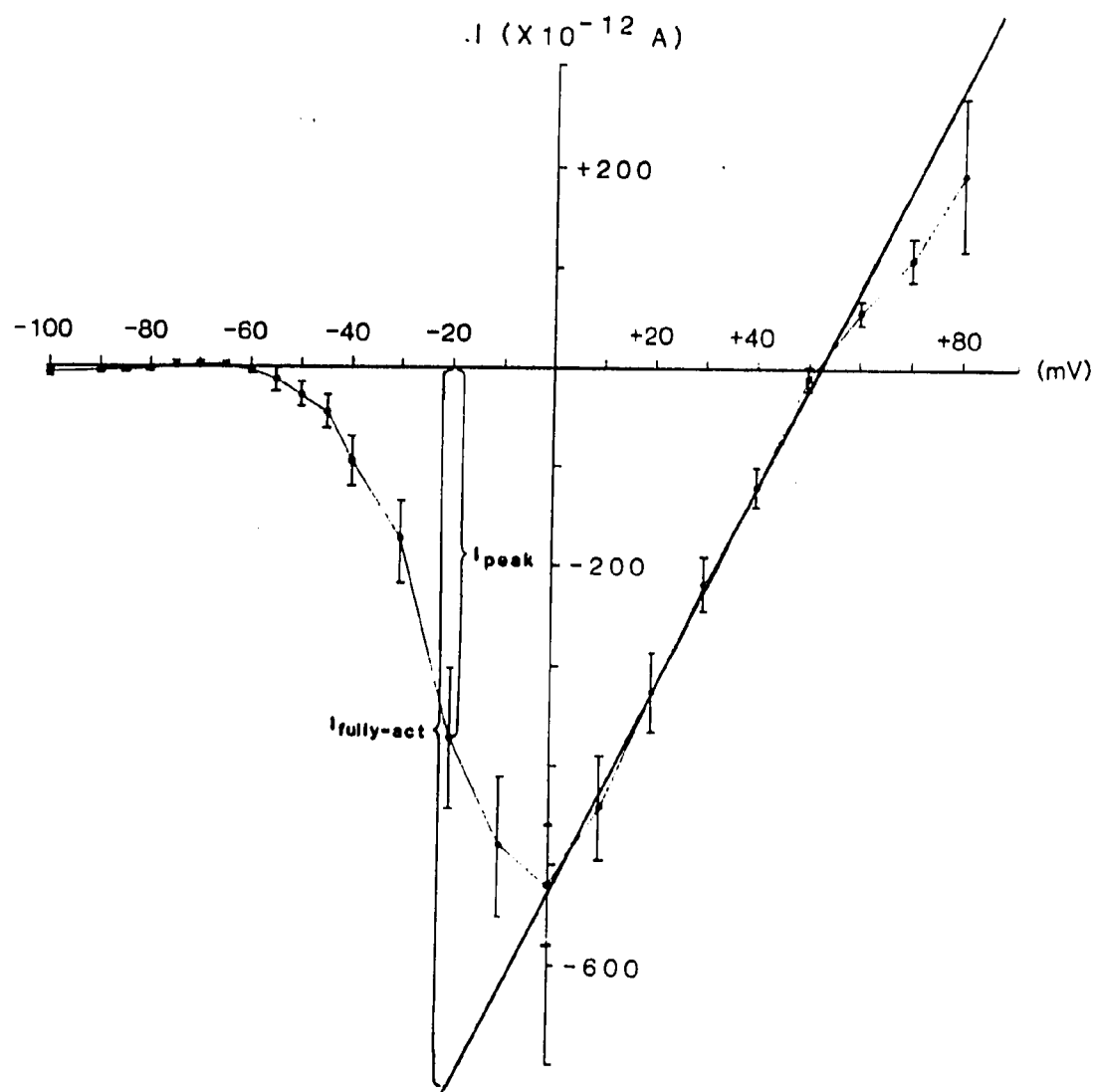


Figure 2.8

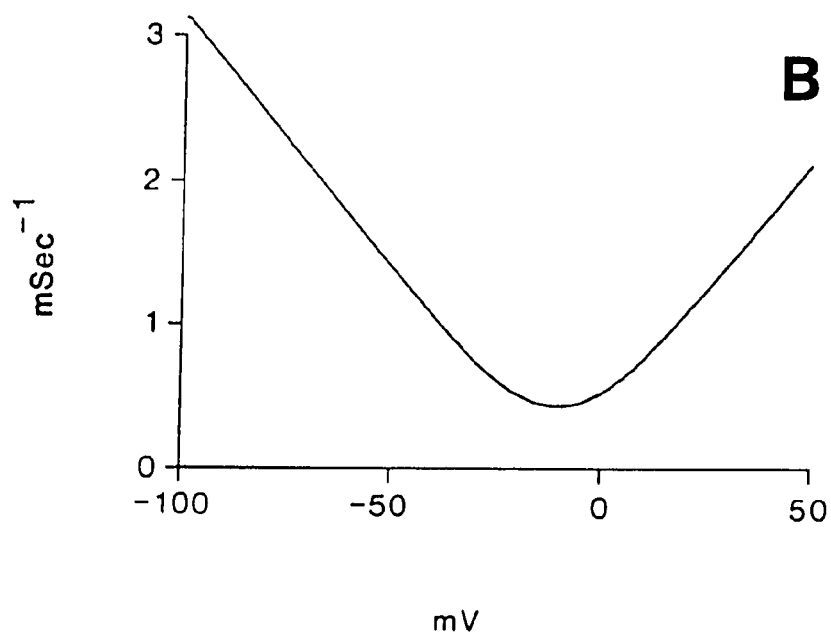
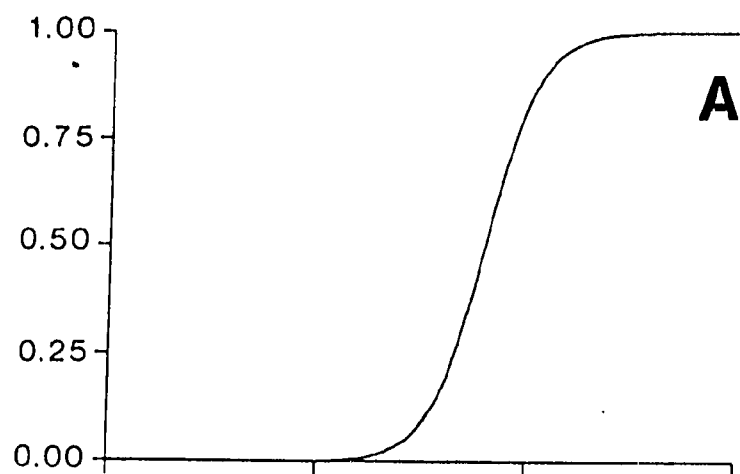
Plots of the voltage dependence of the d gating variable controlling the activation of the second inward current ( $I_{Ca}$ ) in the atrial model.

Panel A

The steady state ( $\infty$ ) values for the d gating variable

Panel B

The rate constant ( $1/\tau$ ) for the d gating variable as a function of transmembrane potential.



Goldman-Hodgkin-Katz constant field equation for a single divalent ionic species. The experimental evidence for this particular formulation is lacking however. It is clear that a linear current voltage relationship for this type of channel is inappropriate due to the marked inward rectification positive to the reversal potential (see Figure 2.7). The expression for the fully-activated current-voltage relationship of  $I_{Ca}$  is:

$$\overline{I_{Ca}} = \frac{G_{Ca} V_m F^2/RT ([Ca]_i (\exp((2V_m F/RT))) - [Ca]_i)}{\exp(2V_m F/RT) - 1.0} \quad (2.19)$$

### II.2.3 $I_K$ :

The time- and voltage-dependent potassium current or the delayed rectifier,  $I_K$ , is the most completely characterized transmembrane current system in single isolated bullfrog atrial cells (Hume and Giles, 1983; Hume, Giles, Robinson, Nathan, Shibata and Rasmusson, in press). This current is thought to be functionally important: it initiates repolarization in atrial muscle. The experimental data strongly suggest that  $I_K$  can be described as a classical Hodgkin-Huxley channel. The ion transfer mechanism is highly selective for potassium ions and the kinetics are well-described by a single time- and voltage-dependent gating variable. However, there is significant sigmoidicity in the onset kinetics.

Mathematically this can be accounted for by raising the single exponential function describing the activation characteristics to the second power. The mathematical equations describing the kinetics and the fully activated current voltage relationship are:

$$I_K = \overline{I_K} n^2 \quad (2.22)$$

$$\frac{dn}{dt} = (1-n) \alpha_n - n\beta_n \quad (2.23)$$

$$\alpha_n = \frac{0.000014 (V_m + 26.5)}{1 - \exp(-0.128 (V_m + 26.5))} \quad (2.24)$$

$$\beta_n = 0.000285 \exp(-0.0381 (V_m + 26.5)) \quad (2.25)$$

A comparison of experimental results and model  $n_\infty$  and  $\tau_n^{-1}$  reveals that the very strict Hodgkin-Huxley gating model matches the experimental data with a high degree of agreement (see Figure 2.9). The ion transfer characteristics of  $I_K$  which can be obtained from the fully-activated current-voltage relationship indicate that this can be described reasonably well by an ohmic conductance. However, positive to about -10 mV some inward rectification is observed in both frog atrium and frog sinus venosus (see Figure 2.10, Panel A). This inward rectification is also present in single cardiac cells derived from the mammalian S-A

Figure 2.9

Plots of the model and observed values describing the kinetics of  $I_K$  activation (the "N" gating variable) as a function of transmembrane potential.

Panel A

Observed  $N_\infty$  relation (Robinson (1983))

Panel B

Model  $N_\infty$  relation

Panel C

Observed  $T_N^{-1}$  relation (Robinson (1983))

Panel D

Model  $T_N^{-1}$  relation

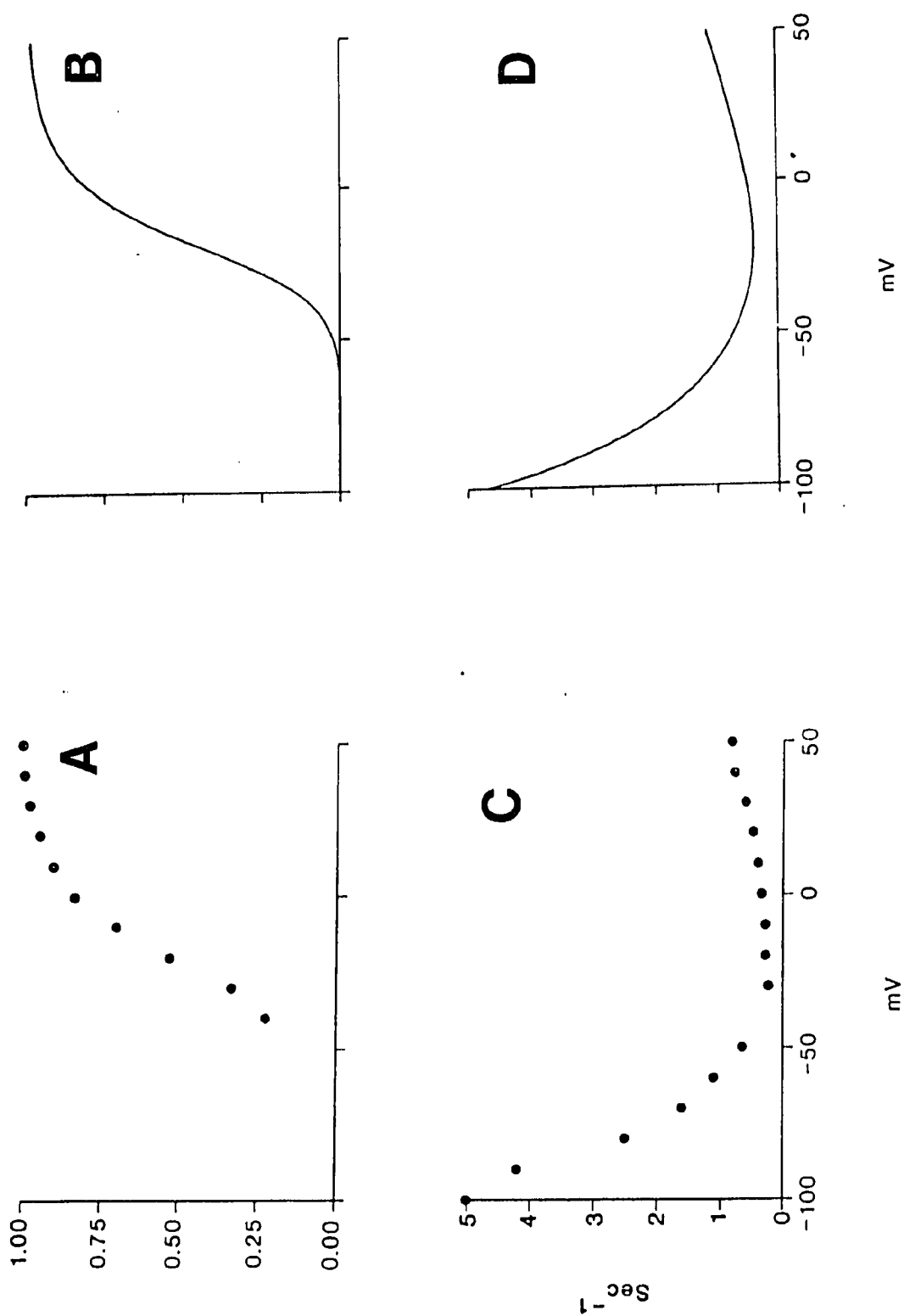


Figure 2.10

The fully activated current-voltage relation for the  $I_K$  current.

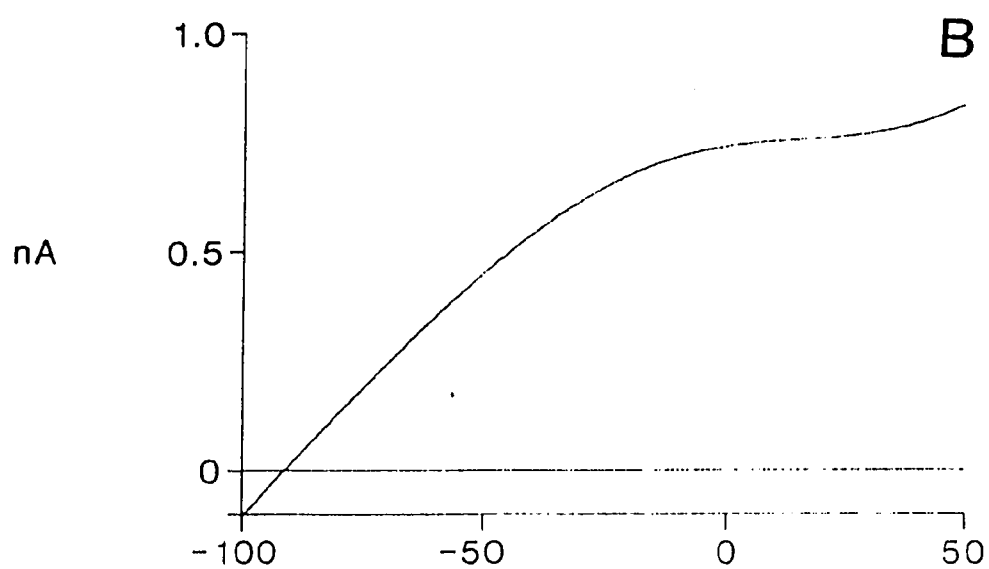
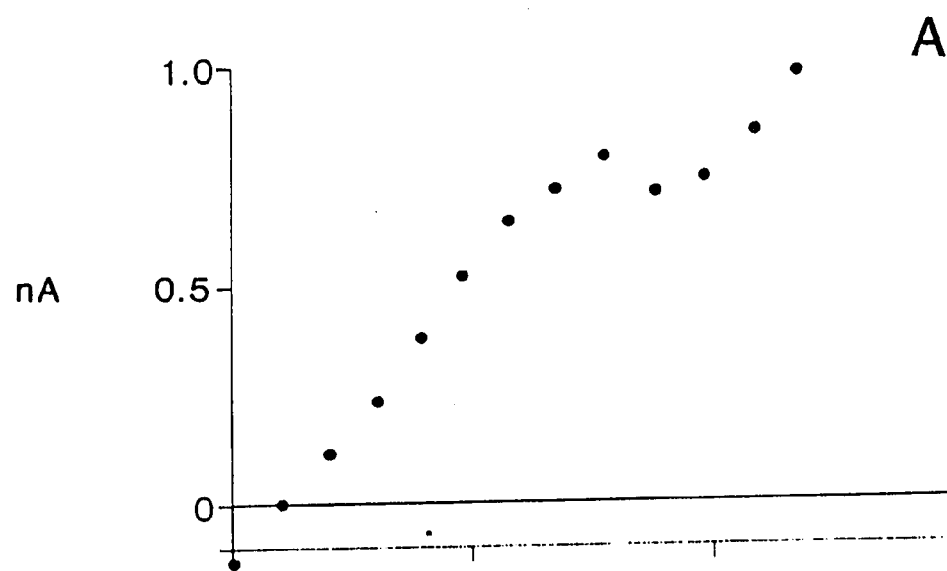
Panel A

The measured instantaneous fully activated current to voltage relation for  $I_K$  current for Bullfrog sinus-venosus, note that the current is very linear over its lower range but rectifies positive to -30 mV.

Panel B

Model values of the ion transfer relation for the  $I_K$  current in Frog atrium in 2.5 mM external  $[K^+]$  and 95 mM internal  $[K^+]$ .





node (Nakayama et al., 1984). In order to mathematically simulate the amount of inward rectification which was observed, a formulation was used in which a Boltzmann distribution activated at relatively large positive potentials was subtracted from the linear ohmic conductance (see Figure 2.10, Panel B).

$$\bar{I}_K = G_K ((V_m - E_K) + \text{Rectification}) \quad (2.26)$$

$$\text{Rectification} = \frac{95.0}{1 + \exp((V_m - E_K - 78)/25)} - 95.0 \quad (2.27)$$

$$G_K = 0.0125 \text{ microsiemens}$$

This mathematical formulation is entirely empirical. DiFrancesco and Noble (1985) have used a different formulation derived from rate theory, which postulates that the major energy barrier for ion movement within the transmembrane electrical field is situated at the inner surface of the membrane (Noble, 1972; Jack, Noble and Tsien, 1975). A single energy barrier model of this sort predicts a form of rectification which is a single exponential term and is not linear over any portion of its range. The formulation of DiFrancesco and Noble, (1985) was modelled by such a single exponential term. Equation 2.26 allows the model to accurately

describe the observed linearity of the I-V characteristic over a broad range of potentials in frog atrium.

### II.3 Ionic Pumps and Exchanger Currents:

In the heart, atrial and ventricular tissue are normally quiescent, showing no spontaneous activity. Their resting potential is between -80 and -90 mV. This potential is about 10 mV positive to the Nernst potential for potassium ions and approximately 140-150 mV negative to the Nernst potential for sodium ions. Although the membrane resistance in the diastole, quiescent period between contractions is very high; nevertheless it is finite, and the sodium and potassium concentration gradients would very quickly 'run down' unless there existed a system for maintaining the low intracellular sodium and extracellular potassium levels. An energy-requiring  $\text{Na}^+/\text{K}^+$  pump plays this role in virtually every excitable tissue and most inexcitable tissues where transmembrane concentration gradients exist. Since the arrangement of this pump is such that it transports three sodium ions for every two potassium ions it generates a small current--the so-called electrogenic  $\text{Na}^+/\text{K}^+$  pump current. Although such pump currents may be expected to be relatively small compared to the currents considered previously, under conditions where the membrane resistance is very high, or the rate of change of voltage

( $dV/dt$ ) is very low, or both, they can in principle exert a considerable electrophysiological effect. In atrium and ventricle, this is thought to occur following periods of rapid stimulation.

### II.3.1 $Na^+/K^+$ Pump:

Much of the detailed mechanistic information concerning the physical chemistry and the energy requirements of the  $Na^+/K^+$  pump mechanism have come from studies on red blood cells and red cell 'ghosts' where ion concentrations can be established on both sides of the functional membrane and where ATP levels can be varied. However, electrophysiological methods have also been used to identify the electrogenic current arising from turn-over of the pump. As noted previously, this is possible because three sodium ions are pumped out of the cell for every two potassium ions which are pumped in; thus the pump generates an outward current in heart (Gadsby, 1984). Although the recent experiments of Hasuo and Koketsu (1985) in isolated trabeculae from bullfrog heart suggest that this pump is voltage-dependent much of the other experimental evidence indicates that it is only weakly modulated by potential (for a review see Gadsby, 1984). Recently, Shibata, Momose and Giles have measured the maximally activated  $Na^+/K^+$  pump current in single atrial cells. So far, however, they do not have reliable data concerning its voltage-dependence.

As noted previously, quantitative models that characterize the physical-chemical reaction cycles of the  $Na^+/K^+$  pump are

available. Chapman, et al. (1983) have developed a very complex model of the sodium pump dynamics. In this model detailed formulations for concentration dependence, voltage dependence, time dependence, and ATPase activity are provided. However, the experimental data available from Gadsby et al. (1985) indicate that there is very little voltage-dependence in the physiological range of potentials. We have therefore chosen to model the  $\text{Na}^+/\text{K}^+$  pump in a relatively simple way following the work of DiFrancesco and Noble (1985) on the calf Purkinje fibre. The DiFrancesco and Noble formulation for the  $\text{Na}^+/\text{K}^+$  electrogenic pump current is:

$$i_p = \overline{i_p} \frac{[\text{K}]_o}{(K_{mK} + [\text{K}]_o)} \frac{[\text{Na}]_i}{(K_{mNa} + [\text{Na}]_i)} \quad (2.28)$$

The equation we have used is:

$$i_{\text{NaK}} = \overline{i_{\text{NaK}}} \frac{[\text{K}]_o^2}{(K_{mK} + [\text{K}]_o)} \frac{[\text{Na}]_i^3}{(K_{mNa} + [\text{Na}]_i)} \quad (2.29)$$

where

$\overline{i_{\text{NaK}}} = 0.0772$  nanoamps, the fully activated current

$K_{mK}$ : apparent half-maximal activation at 1.5 mM

$K_{mNa}$ : apparent half-maximal activation at 21 mM

The DiFrancesco and Noble mathematical formulation given in (2.25) is simply a product of two Michaelis-Menton kinetic models. It implies that the ion transport process is governed by two independent first order binding reactions; one for potassium on the external side of the membrane and one for sodium on the internal membrane surface.

Most experimental data on the  $Na^+/K^+$  pump do not exhibit standard Michaelis-Menton kinetics. A sigmoidal activation has been reported by Mullins and Frumento, (1963) and Keynes and Swan, (1959) in frog skeletal muscle; Sachs, (1970) and Sachs and Welt, (1967) in human red blood cell; and Kracke and DeWeer (1982) in squid giant axons. Sigmoidal activation of the  $Na^+/K^+$  pump was reported to have a cubic dependence on  $(Na^+)_i$  by Mullins and Frumento (1963) and Keynes and Swan (1959). Sachs (1970) reported that a squared relation was sufficient to explain the sigmoidicity while noting that a cubic relation could not be ruled out given accuracy of the data. Mullins and Frumento (1963) described their results as:

$$M_o = \frac{1}{1 + \frac{K}{[Na]_i}} \quad (2.30)$$

where  $M_o$  is a scalar proportional to the sodium efflux due to the  $\text{Na}^+/\text{K}^+$  pump as a function of the particular ionic species under consideration.

Sachs described his results as:

$$M_o = \frac{1}{1 + \frac{b}{[\text{Na}]_i} + \frac{c}{[\text{Na}]_i^2}} \quad (2.31)$$

In measuring the concentration dependence of the  $\text{Na}^+/\text{K}^+$  pump on  $[\text{K}^+]_o$ , Sachs and Welt, (1967) found sigmoidal behaviour also. They reported that the data was well-described by an equation of the form:

$$M_o = \frac{1}{1 + \frac{b}{[\text{K}]_o} + \frac{c}{[\text{K}]_o^2}} \quad (2.32)$$

and presented a simple two-site model from which this equation was derived.

The  $\text{K}^+$  activation term in Equation 2.29 is just a special case of the more general expression given in Sachs and Welt (1967). The  $\text{Na}^+$  activation term is an extension of Sachs model for  $(\text{Na}^+)_i$  dependence; it implies that three sodium ions must be bound for pump transfer to occur. The two activation expressions are multiplied together as in the DiFrancesco and Noble model and

in accordance with the multiplicative dependence suggested by Keynes and Swan, (1959). The term  $\bar{I}_p$  in Equation (2.29) represents the maximally activated current as experimentally determined (Shibata, Momose, and Giles, 1984).

The original pump current formulation used in the atrial model was identical to the formulation in the DiFrancesco-Noble model (1985). The differences between the two formulations seems slight given the uncertainty in half maximal activation (See Table 2.1) and peak capacity (Gadsby, 1984), and indeed this is the case over most of the concentration range. However an internal sodium concentration of approximately 7.5 millimolar (Keenan and Niedergerke, 1967) is well below the 15 to 30 millimolar half-maximal activation concentration.



Table 2.1

Reference	Preparation	Experiment	$K_m$ due to $[Na]_i$	$K_m$ due to $[K]_c$	Sigmoidicity observed?
Sachs & Welt (1967)	Human Red Blood Cells	Radioactive Tracer	---	2mM	Yes
Sachs (1970)	Human Red Blood Cells	Radioactive Tracer	20mM	---	Yes
Mullins & Frumento (1963)	Frog Sartorius Muscle	Radioactive Tracer	17mM	---	Yes
Kracke & DeWeer (1982)	Squid Axon	Radioactive Tracer	27mM	---	Yes
Gadsby (1980)	Canine Purkinje	Voltage Clamp	---	1mM	No
Nelson & Blaustein (1980)	Barnacle Muscle fibres	Radioactive Tracer	20mM	---	Yes
Average $K_m$ Values			21mM	1.5mM	

### II.3.2 Na<sup>+</sup>/Ca<sup>2+</sup> Exchanger:

As noted previously, there is a significant calcium influx into atrial cells and all other cardiac cells with each heart beat. Calcium plays a variety of very important intracellular roles including triggering and controlling contraction. However, abnormally high intracellular levels of calcium are known to be extremely toxic to cardiac and most other cells; if maintained, abnormally high levels of calcium will quickly result in cell death. In atrial cells from the bullfrog, it is thought that most of the calcium which triggers and controls contraction is derived from the influx corresponding to the calcium current,  $I_{Ca}$ . This is in contrast to the mammalian ventricle where it is thought that only a relatively small amount of calcium enters the cell with each heart beat and that much of the calcium needed for the mechanical functioning of the cell is released from the sarcoplasmic reticulum and subsequently sequestered back into this extensive intracellular compartment (Fabiato, 1982). One of the most important processes thought to be able to extrude the intracellular calcium 'load' is the so-called  $Na^+/Ca^{2+}$  exchanger. This exchanger, as its name implies, extrudes calcium while bringing about sodium entry into the cell. This process does not depend directly on energy or ATP breakdown, but is critically dependent upon the normal maintenance of the sodium gradient. It therefore is secondarily dependent upon the proper functioning of

the  $\text{Na}^+/\text{K}^+$  pump (Reuter and Seitz, 1968; Mullins, 1981). Within the last five years a considerable amount of evidence has accumulated suggesting that the  $\text{Na}^+/\text{Ca}^{2+}$  exchange process is not electroneutral; rather, it is thought to be able to generate current as a consequence of transporting three or four sodium ions for each calcium ion (for review see Chapman, 1979; Eisner and Lederer, 1984).

Thus, since this exchanger mechanism is electrogenic it can be important not only in extruding intracellular calcium, but also in generating a net transmembrane current. This current, although relatively small, may be important in various parts of the action potential. For example, in the recent model of DiFrancesco and Noble (1985) it generates a significant inward current which helps to maintain the plateau of the Purkinje fibre action potential.

The mathematical formulation for the  $\text{Na}^+/\text{Ca}^{2+}$  exchanger was derived from thermodynamic considerations by Mullins (1977, 1981). In our mathematical formulation of the  $\text{Na}^+/\text{Ca}^{2+}$  exchanger process, equations similar to those of Mullins, and identical to those of DiFrancesco and Noble (1985), employing a 3  $\text{Na}^+$  to 1  $\text{Ca}^{2+}$  stoichiometry were used. The resulting expression for the  $\text{Na}^+/\text{Ca}^{2+}$  exchanger current is:

$$I_{NaCa} = \frac{1.5 \times 10^{-6} ([Na]_i^3 [Ca]_o \cdot e^{\frac{.5VmF}{RT}} - [Na]_o^3 [Ca]_i e^{\frac{.5VmF}{RT}})}{1 + 0.0001 ([Ca]_i [Na]_o^3 + [Ca]_o [Na]_i^3)} \quad (2.33)$$

This equation results from a simplification of the model proposed by Mullins (1977) in which the following assumptions are made:

- 1) a 3 to 1 Na to Ca stoichiometry
- 2) dependence upon only the  $Na^+$  electrochemical gradient for energy
- 3) translocation rather than carrier loading is the rate limiting step
- 4) the energy barrier in the transmembrane electrical field is symmetrical (0.5 in the exponential term).

Furthermore there are two constants in the Equation 2.33. These two numbers constitute an 'aggregation' of several parameters in the actual exchanger process. The denominator constant (0.0001) is a product of all the rate constants for Na and Ca binding divided by the summation of affinity terms for sodium binding. Since most of these parameters have not been measured and the concentration dependence of the current voltage relation is unknown, this constant is somewhat arbitrary. The value 0.0001 for the denominator is the value used in DiFrancesco and Noble (1985); the

results of model simulations seem to be relatively insensitive to this parameter.

The numerator constant term puts the current into the proper units and scales the current magnitude. Since the magnitude of the Na/Ca exchange process is not known in frog atrium, this term is estimated by selecting a value for this constant which will maintain an expected resting internal calcium concentration during stimulation at physiologic rates (2 to 4 seconds per beat) and during rest. In this model cellular  $\text{Ca}^{2+}$  homeostasis was maintained by this  $\text{Na}^+/\text{Ca}^{2+}$  exchanger operating in parallel with a calcium pump.

### II.3.3 The Calcium Pump:

The properties of the Na/Ca exchange process allow it to extrude a large amount of  $\text{Ca}^{2+}$  when the internal calcium concentration is relatively high. Operating in parallel with the exchange process is a low capacity but high affinity ATP-dependent  $\text{Ca}^{2+}$  pump. Consequently, this extrusion mechanism is important in setting and maintaining the very low resting calcium levels found in most electrically active cells. The best evidence for this in frog heart comes from the data of Morcos (1981). In these experiments sarcolemmal vesicles from frog ventricle were pre-loaded with radioactively labelled  $\text{Ca}^{2+}$  via  $\text{Na}^+ - \text{Ca}^{2+}$  exchange. The

cells subsequently lost 92% of their  $\text{Ca}^{2+}$  when ATP was present and only 60% in the absence of ATP.

The ATP dependent pumping of calcium ions in heart is a very complicated process, modulated in a variety of ways by a number of factors (eg. by calmodulin, Mg concentrations, ATP concentration, pH, and calcium concentration). For a recent review of the properties of sodium insensitive, ATP dependent calcium pumps in a variety of membranes see Schatzmann (1983), DiPolo and Beauge (1983), and Hasselbach and Oetliker (1983). The calcium pump has a definite dependence upon internal calcium with a half maximal pumping capacity around 1 mM. Whether or not this reaction is coupled (i.e. whether or not some other ion is pumped in when calcium is pumped) is still unknown; it has however been found to be electrogenic in vesicles prepared from rat pancreatic acinar cell membranes (Bayerdörfer et al, 1985). If the pump current is electrogenic then we might expect some voltage dependence to be shown and indeed Bayerdörfer et al (1985) have found that the pump current may be modified by as much as 39% by the application of substantial potential gradients.

After considering the available data on the calcium pumping process, we have adopted the formula used by Cannel and Allen (1984) in their model of calcium movements during activation of the sarcomere of frog skeletal muscle.

$$I_{\text{Capump}} = \overline{I}_{\text{Capump}} \cdot \frac{[\text{Ca}]_i}{[\text{Ca}]_i + K_m} \quad (2.34)$$

$$K_m = 1 \text{ mM}$$

$$\overline{I}_{\text{Capump}} = 0.00135 \text{ nanoAmps}$$

It is obvious that this expression omits the potential dependence of the calcium pump. However, this omission is probably not significant in most situations that might arise in frog atrial cells. Thus:

- 1) The Ca pump is presumed to be important only during periods of rest.
- 2) The very small Ca pump current would be insignificant in comparison to the uncertainties concerning the magnitude of the calcium current, and the Na/Ca exchange process at the depolarized voltage levels.
- 3) In the absence of even semi-quantitative data on the voltage dependence of the calcium pump, introduction of a voltage-dependent formulation may result in a less accurate description.

The magnitude of the calcium pump current was determined by taking the estimate of  $5 \times 10^{-8}$  mg of sarcolemmal protein per

bullfrog atrial cell (Campbell, 1985) and the estimate of Caroni et al (1983) of 0.3% of sarcolemmal protein containing the required Ca-ATPase activity. This means that there is  $1.5 \times 10^{-10}$  mg of pumping protein. The pumping capacity represented by  $1.5 \times 10^{-10}$  mg of pumping protein can be estimated from the data of Caroni et al (1983) who measured a  $V_{\max}$  of .8 mMoles ATP/mg protein minute and a stoichiometry of 1 ATP:1Ca<sup>++</sup>:

$$I_{\max} = 1.5 \times 10^{-10} \text{ mg Protein} \frac{8 \times 10^{-6} \text{ mATP}}{\text{mg Protein min}} \frac{1 \text{ min}}{60 \text{ sec}} \frac{1 \text{ Ca}^{++}}{1 \text{ ATP}} \frac{2.96500 \text{ C}}{\text{F}}$$

(2.35)

$$\overline{I}_{\text{Capump}} < I_{\max} = 3.86 \times 10^{-12} \text{ Amps} \sim 4 \text{ picoAmps}$$

Thus, the maximal pumping capacity in our model is estimated from the amount of sarcolemmal protein, rather than a voltage clamp data. The model of Ca<sup>++</sup> pump activity is formulated only to depend on internal Ca<sup>++</sup> activity and not ATPase activity so the maximal pump activity used in the expression (1.3 pico-amps) is a smaller value to account for the less than maximal activation by the levels of ATP in isolated bullfrog atrial cells.



## II.4 Compartmental Models of an Atrial Cell: $\text{Na}^+ - \text{K}^+$ Accumulation/Depletion Phenomena, and $\text{Ca}^{2+}$ Buffering.

### II.4.0 Introduction:

The cell membrane or sarcolemma is an essential component of a healthy atrial cell. However, this membrane and its ionic transport processes do not function in isolation; they are dependent upon their environments both intra- and extracellular. Chapter I describes the transmembrane ionic currents in a cell; but each important current system is also dependent on internal and external ionic concentrations. Ionic concentrations may vary under a variety of physiologic, pathologic and experimental conditions. Therefore in order to characterize the function of the single atrial cell more than a single cell membrane model is needed. Hence, the membrane model of Chapter I has been coupled to a compartmental model including some important effects of ionic concentrations in the immediate environment of the atrial cell.

### II.4.1 Description of the Restricted Extracellular Space(s)

As previously mentioned the single frog atrial cell is a long and thin ~ 200 - 300  $\mu\text{m}$  long and ~ 5  $\mu\text{m}$  in diameter. In frog heart muscle these cells are arranged parallel to one another in long thin cylindrical bundles called trabeculae, each of which has a diameter of 20 - 100  $\mu\text{m}$ . Each trabeculum is surrounded by a

thin layer of endothelial cells that form the trabecular sheath (see Figure 2.11). Within the trabeculum a mode of signal transmission is required for propagation of the electrical impulse. It is generally accepted that this cell-to-cell electrical coupling is performed by nexuses, which are specialized structures randomly distributed like 'spot welds' throughout the cell membrane. These form low resistance intercellular pathways between single cells. It is these gap junctions, which provide the tight electrical coupling which allows atrial trabeculae to act as an electrically functional syncytium. Consequently when an action potential or other electrical event is initiated in a particular cell, it can propagate to other nearby cells.

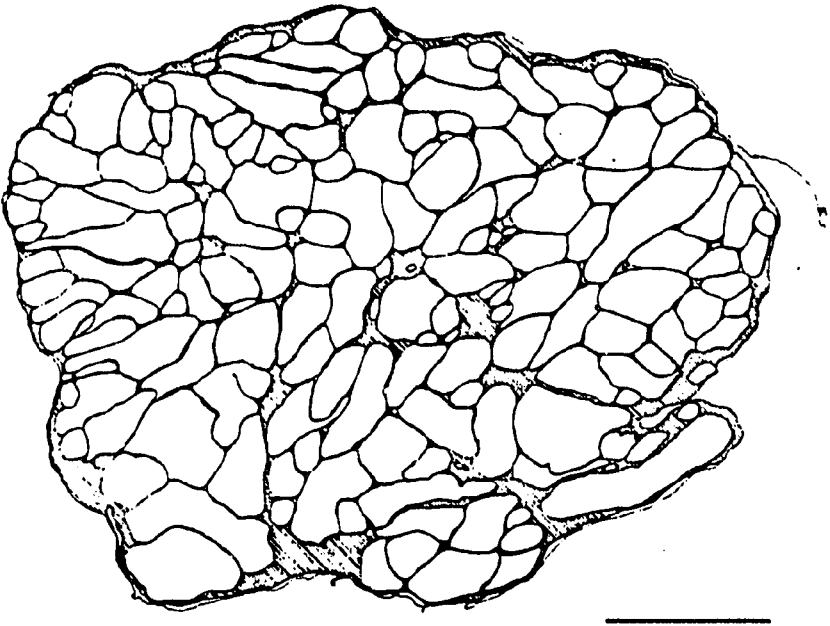
It is important to note that the cells within the trabeculum are certainly 'nearby'; they are packed very tightly. Haas et al (1983) found that within an atrial trabeculum cells occupied an average of 88% of trabecular space while only 12% was found to be extracellular space. Even if 50% of the intracellular space is occupied by various organelles (mitochondria, nucleus, etc.) and is thus not available as space for the diffusion of free ions entering or exiting the cell via the cell membrane, the extracellular space is still only approximately 27% of the available cell volume.

The volume of extracellular space within a trabeculum might not be a significant consideration in characterization of ionic

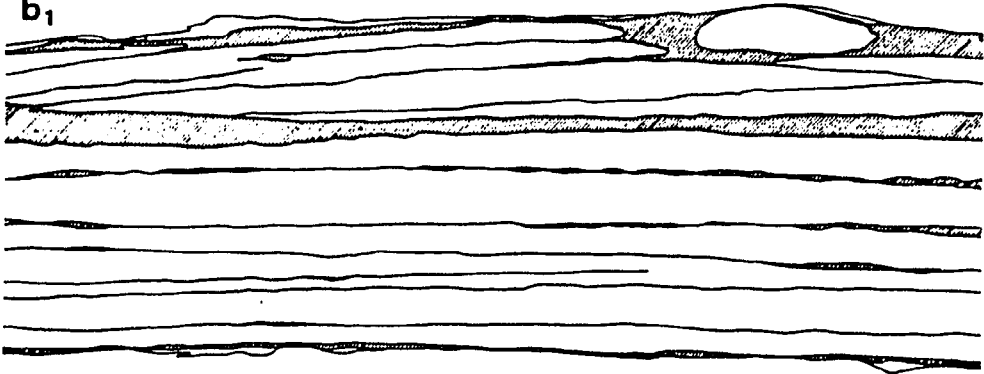
Figure 2.11

Drawings of cross-sectioned (a) and longitudinal-sectioned ( $b_1$ ,  $b_2$ ) bullfrog atrial trabeculae demonstrating the expanse of the extracellular space (shaded areas) and single myocardial cells (white areas); ( $b_1$ ) and ( $b_2$ ) represent successive pictures taken from the same longitudinal section. Scales: 10 $\mu$ m. (Haas et al. 1971).

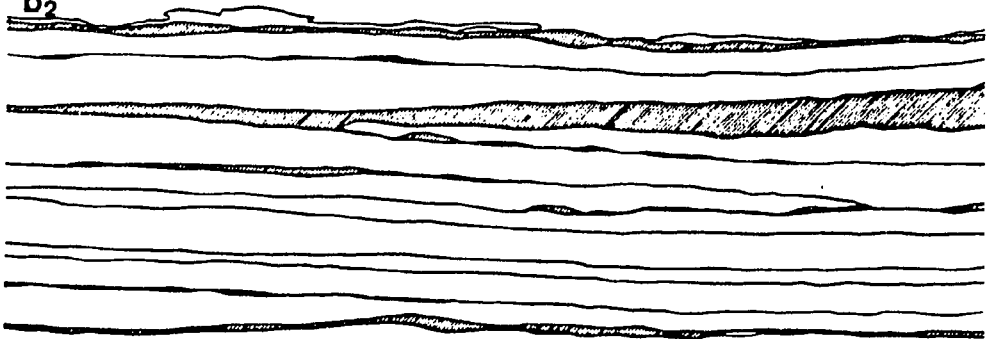
a



b<sub>1</sub>



b<sub>2</sub>



currents and/or concentration changes immediately adjacent to the cell membrane if the extracellular spaces within a trabeculum were always well-perfused. Unfortunately this is not the case. Each frog heart fibre is surrounded by a trabecular sheath and this sheath constitutes a significant barrier to ionic diffusion into the extracellular space. The trabecular sheath consists of a layer of endothelial cells. Ions pass through this barrier by means of simple diffusion within the aqueous spaces of the narrow clefts separating the adjacent cells. The approximate width of these clefts is  $12.5\text{ }\mu\text{m}$  (Page and Niedergierke, 1972). Using transmission electron microscope data measurements (Page and Niedergierke, 1972) estimated the time constant of diffusion across the endothelial sheath for 17 ventricular bundles. They found that the time constant across the endothelial sheath was approximately 3.32 seconds for bundles with a cross-sectional area of 980 to  $28600\text{ }\mu\text{m}^2$  which comprises 98% of the total bundle population. For bundles of much small cross-sectional area the time constant of perfusion is smaller.

When measuring the changes in resting potential of frog atrial trabeculae that occur with step changes in the potassium concentration of the bathing solution, S. Noble, (1976) measured a time constant which was seldom less than 5 sec and usually more of the order of 10 seconds. While the difference in time constants

of perfusion might be explained due to the difference in preparation and experimental methods between Page and Neidergerke (1972) and S. Noble (1976) another likely explanation lies with the physical arrangement of cells within the trabeculae. Atrial cells are arranged physically very close to one another. This close physical proximity can also be a barrier to free ionic diffusion, allowing different ionic concentrations at different levels (or depths) within a preparation. Morad (1980) has published data using  $K^+$  sensitive microelectrodes on frog ventricular strips which show a correlation of electrode depth and potassium accumulation (depletion) during rapid stimulation (hyperpolarization). Unfortunately, the diameter of this preparation was about 1 mm which is much larger than atrial trabeculae which average only approx 100  $\mu m$ . Hence, quantitative details concerning the role axial diffusion in single trabeculae remains unclear.

In previous sections of this chapter a model characterizing the electrical properties of an isolated patch of membrane were described. This model is based upon measurements made on single isolated bullfrog atrial cells. It is of interest to incorporate it into a model of a multicellular preparation with a restricted extracellular space. This is the first time that a cardiac model based upon single cell measurements has been incorporated into a multicellular simulation including a restricted extracellular

space. Previous simulations have included effects of extracellular accumulation/depletion (DiFrancesco and Noble, 1985; Coulombe and Corabouef, 1983; Cohen and Kline, 1982). However, the data were either estimated or taken from measurements on multicellular properties. The important difference is that, as has long been known, the restricted extracellular space can strongly affect the kinetics, magnitude and perceived number of currents which are recorded (for a review see Attwell, Eisner, and Cohen, 1979). Thus, such experimental results from multicellular preparations must themselves be re-evaluated in light of the effects of accumulation and depletion.

A second source of error in multicellular preparations arises from the possibility of a non-uniform voltage distribution within the entire preparation. This is due to the finite resistance of the intracellular medium. This resistance "inserts" what might be best described as a resistance of unknown size between the experimental control signal and various parts of the preparation to be controlled (i.e. the membrane). This is a technical difficulty associated with multicellular preparations and unfortunately it is impossible to tell from the usual records of potential or current versus time alone whether an experimental record is characteristic of the membrane or an artifact of the method (Kootsey, 1975).

If the single cell membrane model is to be re-incorporated into a multicellular preparation model, a mathematical description of that preparation must be selected. To that end we must first ask what problems can be addressed and what experimental data are available. Certainly addressing the problem of non-uniformity of voltage clamp of multicellular preparations is interesting, but the problem of coupling, propagation, and conduction in multicellular preparations lies beyond the scope of this work. However, the effects of a restricted extracellular space, is also an interesting area, and as mentioned earlier in this chapter experimental data and measurements are available on most aspects of the problem. S. Noble (1976) has shown that, under changes in stimulation rate, shifts in the resting potential may occur in frog atrium. Also, Morad (1980) had indicated that external potassium accumulation plays an important role in the repolarization of the action potential. A model formulation should be useful for further analysis of these experimental results.

Selection of a model for the extracellular space of atrial trabeculae becomes a choice between two alternatives: 1) a distributed parameter model, or 2) a compartmental model. The compartmental model was chosen over the distributed parameter model for the following four reasons:

- 1) The compartmental model is indicated by the presence of an endothelial sheath.



The presence of a lumped diffusional barrier such as the endothelial sheath is an indicator for a lumped parameter model (i.e. a compartmental). While such discrete barriers may be included within the framework of a distributed parameter model, as they were in the case of Cohen and Kline (1982), the appropriateness of distributed parameter process can be questioned on the ground that it fails to account for the strongly contractile nature of atrial tissue. The phasic contraction-relaxation cycles will provide a considerable stirring action within the trabeculum.

- 2) There are more quantitative measurements appropriate to a compartmental model.

Time constants of wash-out are measured as single exponentials in most published multicellular preparation experiments (S. Noble, 1976; Morad, 1980; Kline and Morad, 1976; Cleeman et al, 1984; Kline and Cohen, 1984) and these measurements may be used directly in a compartmental model (Attwell, Eisner and Cohen, 1979). These same single time constants have been used by Kline and Cohen (1984) to help estimate parameters in distributed modelling but this method involves detailed assumptions about the diffusional process and the trabecular morphology.

- 3) Previous modelling indicates the results will be similar.

Coulombe and Coraboeuf (1983) performed a direct comparison of these two diffusional models in their study of accumulation in the clefts of Purkinje fibres using a modified version of the

model of McAllister, Noble and Tsien (1975). They noted that these two models, 'namely the radial diffusion model and the simplified three compartmental model give essential similar results' (Coulombe and Coraboeuf, 1983). DiFrancesco and Noble (1985) have reached the very similar conclusion that for many purposes, their results are little affected by assuming a homogeneous  $K^+$  concentration in the three compartmental models in their study of Purkinje fibre.

4) There is an enormous reduction in computer time.

Since the solution to a distributed parameter model requires a complete set of membrane equations be solved for each spatial step in a radial diffusion problem the increase in computer time can be enormous, and indeed Coulombe and Coraboeuf (1983) found that the time saving of approximately a factor of 10 by using the compartmental model.

Given these four considerations, a three compartmental model of the cleft or restricted extracellular space was adopted. The three compartmental models adopted for this study mathematically simulate the variation in the restricted extracellular space was completely isolated from the bulk medium, that is, if there were no ionic diffusion to or from the bulk medium then changes in ion concentration of the cleft compartment would only be due to currents from the intracellular compartment i.e. only by the membrane currents.

$$\frac{d[S]}{dt} = \frac{i_s/F}{Vol_c} \quad (2.36)$$

where  $i_s$  is the sum of the currents of ionic species  $S$  crossing the membrane.  $F$  is the faraday and  $Vol_c$  is the cleft volume. The currents generated by the membrane model are in nanoamps per cell. Therefore the  $Vol_c$  represents the average amount of trabecular space per cell. That is if 10% of the trabeculum is free space and the remainder is intracellular space  $Vol_c$  equals 10% of one cell volume.

On the other hand, if transmembrane ion movements make no contribution the concentration in the extracellular compartment; then all changes in cleft concentration must be due to diffusion to or from the bulk medium. This is modelled as

$$\frac{d[S]}{dt} = \frac{[S]_b - [S]_c}{\tau_p} \quad (2.37)$$

where  $\tau_p$  is the time constant of perfusion measured experimentally. Combining these two effects yields the equations describing the concentrations in the restricted extracellular space immediately adjacent to a cell located within an atrial trabeculum. The equations describing this cleft concentrations for the three major ions under consideration are:

$$\frac{d[Na]_c}{dt} = \frac{[Na]_b - [Na]_c}{\tau_p} + \frac{3 I_{NaK} + 3 I_{NaCa} + I_{Na} + I_{NaBack}}{F Vol_c} \quad (2.38)$$

$$\frac{d[K]_c}{dt} = \frac{[K]_b - [K]_c}{\tau_p} + \frac{-2 I_{NaK} + I_{K1} + I_{KR}}{F Vol_c} \quad (2.39)$$

$$\frac{d[Ca]_c}{dt} = \frac{[Ca]_b - [Ca]_c}{\tau_p} + \frac{-I_{NaCa} + I_{Ca} + I_{Cap} + I_{CaBack}}{F Vol_c} \quad (2.40)$$

where  $[S]_c$  is the cleft concentration of ionic species S

$[S]_b$  is the bulk perfusion concentration of ionic species S

$\tau_p$  is the time constant of equilibration between the bulk medium and cleft (restricted extracellular) space = 10 sec (S. Noble, 1976)

$I_*$  is the membrane ionic current of type \* that was described in the previous section. (e.g.  $I_{NaK}$ ,  $I_{Ca}$ , etc)

$Vol_c$  is the 'half cleft' volume immediately facing each cell  
=  $4 \times 10^{-13}$  l or 10% of cell volume

F is the faraday.

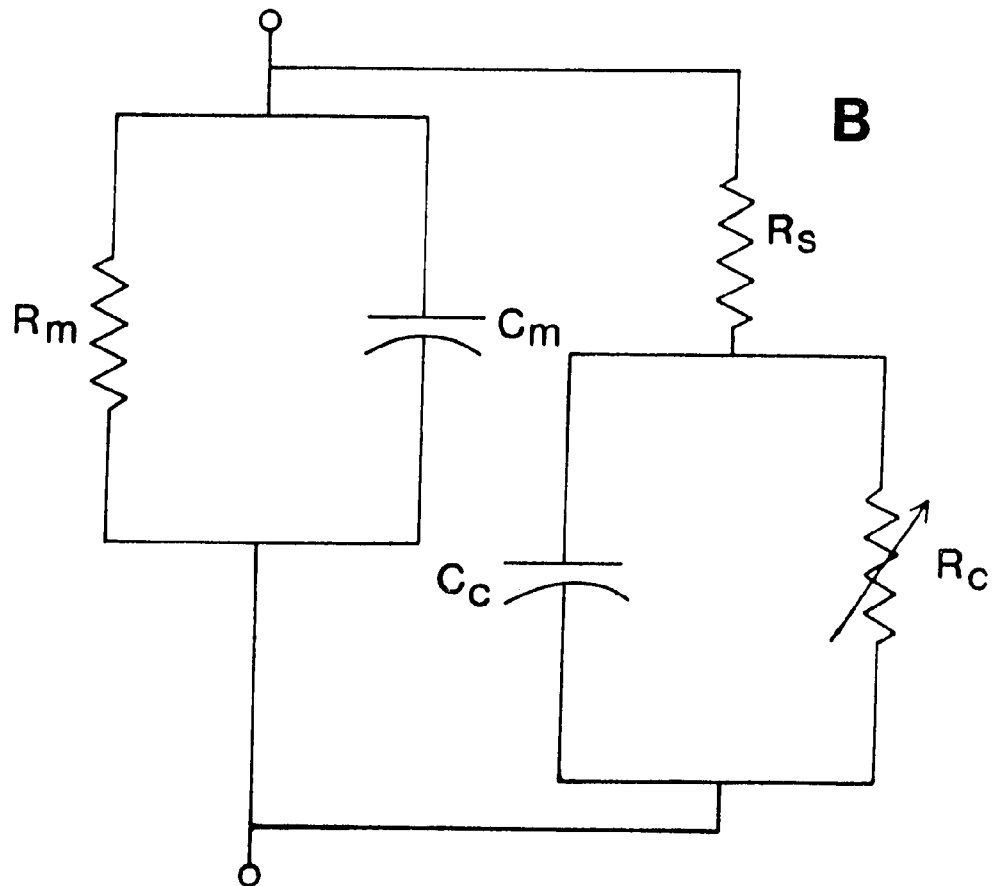
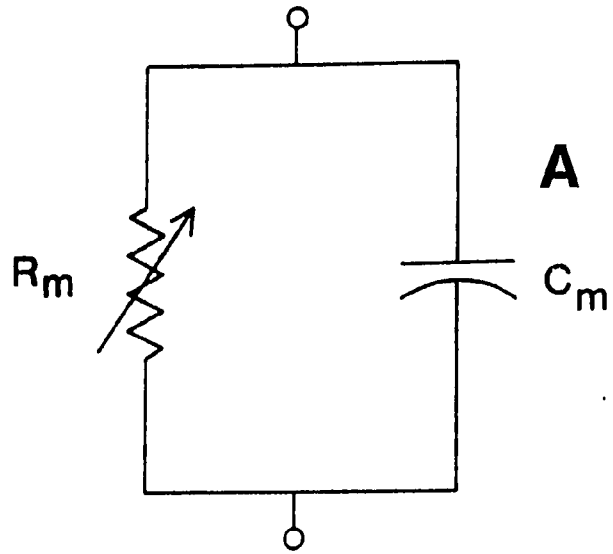
#### II.4.2 Internal Concentration Model.

It is important to assess the implications of changes in the intracellular concentrations of the major intracellular ions on

the function of the cell membrane in both physiological and experimental situations. Beeler and Reuter (1977) attempted to do this as an integral part of their electrophysiological model. They computed changes in the reversal potential for  $I_{Ca}$  as a function of  $Ca^{2+}$  entry. A recent and much more complete attempt to model such changes has been published by DiFrancesco and Noble (1985) for Purkinje fibre. Microscopic examination of frog atrium indicates no transverse tubule system and only a very limited sarcoplasmic reticulum (cf. Hume and Giles, 1981). In support of this, the admittance studies of Moore et al (1985) indicate that a simple first order equivalent circuit well describes the passive equivalent circuit of an atrial cell. It therefore seems appropriate to assume that all  $Na^+$ ,  $K^+$ , and  $Ca^{2+}$  fluxes into and out of the myoplasm of an isolated bullfrog atrial cell occur across the sarcolemma. That is, there are no other significant ionic pathways such as the transverse tubule system in connection with the internal membrane system (i.e. sarcoplasmic reticulum) as exists in mammalian ventricle (Page and Niedergerke, 1972). Figure 2.12 shows the equivalent circuit of a mammalian ventricular cell, compared with that of a bullfrog atrial cell. Note the parallel pathway represented by the transverse tubule system and sarcoplasmic reticulum. In the absence of any other means of transmembrane ionic fluxes the intracellular space constitutes a well-defined compartment for the modelling of local ionic concentrations.

Figure 2.12

A schematic representation of the passive electrical properties of frog Atrial and rabbit ventricular cells. Note the additional RC network representing the T-system and Saroplasmic Reticulum that is in parallel with the cell membrane. (Moore et al. 1984)). Figure A is the equivalent circuit for the passive frog atrial cell it consists of a parallel combination of a resistance and a capacitance due to the sarcolemma. The circuit in figure B contains additional elements due to the internal membrane system and the access resistance.



Since the physical structure underlying the compartmental model is well-defined the next question pertinent to the modelling of the intracellular space is: Does the intracellular space constitute a 'well-mixed' compartment or do we need to consider the radial diffusional processes that occur within the cell? This question is similar to the one considered in modelling diffusion within the extracellular space. Should a distributed parameter diffusion model be used or should a lumped parameter (compartmental) model be used? If the intracellular medium is well-mixed, that is to say if the intracellular diffusional process occurs so quickly that they can be considered instantaneous, then a simple compartmental model is appropriate.

To evaluate this, consider first the geometry of an isolated single atrial cell which at its very widest, (in the region of the nucleus) is about 7 mM wide (Hume and Giles, 1981). If the current densities in the cell membrane are uniform then in order to achieve mixing the ions must be able to diffuse evenly through a radial distance of at most 3.5 mM. This leaves the question of how fast do ions diffuse within medium such as myoplasm? The answer is not the same as the answer for diffusion of ions in a saline solution. It has been long known that the mobility of  $\text{Ca}^{++}$  in squid axons (Hodgkin and Keynes, 1957) and skeletal muscle (Kushmerick and Podolsky, 1969) is greatly reduced compared to the expected values in a saline solution. Two factors are known to



alter the mobility of ions in a cell body. One is the viscosity of cytoplasm and the physical impediment or tortuosity imposed by immobile structures (eg. organelles, cytoskeleton), the other is the intracellular mechanisms responsible for regulating the internal concentrations of free ions.

It is particularly important to consider the intracellular mechanisms regulating the free-Ca concentrations in the intracellular compartment. Calcium plays an important role in any contractile tissue and in order for the contractile proteins of a cell to relax an overall intracellular calcium concentration must be less than 1 micromolar. Since the resting concentration of free calcium in cardiac muscle is on the order of  $10^{-7}$  molar (Noble, 1979) very significant changes in total ionic concentration could occur via the calcium channel current in the absence of these regulatory mechanisms. Because internal sodium and potassium ion concentrations are at least 4 orders of magnitude higher than calcium, abrupt ionic changes which would affect the concentrations of these ions and consequently any internal regulatory mechanisms governing will not happen as quickly, with respect to internal diffusion time, due to the limited magnitude of bullfrog atrial membrane currents. For example if enough ions enter to cause a 10 mM change in a resting calcium concentration of  $10^{-7}$  molar calcium concentration has changed by 2 orders of magnitude while the same number of  $\text{Na}^+$  ions crossing the membrane will

change the internal  $\text{Na}^+$  concentration by 10 mMolar--less than 0.1% change in internal sodium concentration. The internal compartment is 'well-mixed' for sodium and potassium if it is well-mixed' for calcium since calcium represents a 'worst case'.

The time course of diffusion of intracellular calcium is further slowed by the intracellular mechanism regulating the free  $\text{Ca}^{++}$  concentration in the intracellular compartment. It can be shown that the presence of a distributed high capacity population of immobile binding sites that react rapidly with the diffusing ions would effect a diffusion process by reducing the effective diffusion process by reducing the effective diffusion coefficient (Crank, 1975). Consequently, data needs to be considered from cells that experience and regulate large calcium influxes. Such cells may have faster and more abundant intracellular calcium regulation mechanisms than cells which experience only a small  $\text{Ca}^{++}$  influx. Nasi and Tillotson (1985) have measured the time course of spherical diffusion in *Aplysia* nerve cell bodies using optical techniques. They were unable to measure any time delay in the diffusional process for  $\text{Ca}^{++}$  for distances up to 12  $\mu\text{M}$ . This indicates that even in the presence of substantial calcium buffering radial diffusion occurs almost instantaneously within the less than 3.5  $\mu\text{M}$  distance of the cell wall in atrial cells. Therefore a well-stirred compartment is a good approximation to

the physical situation and a lumped compartmental model is appropriate.

The compartmental model for  $\text{Na}^+$  and  $\text{K}^+$  is described by:

$$\frac{d[\text{Na}]_i}{dt} = \frac{-I_{\text{Na}} - I_{\text{NaLeak}} - 3 I_{\text{NaCa}} - 3 I_{\text{NaK}}}{F \text{Vol}_i} \quad (2.41)$$

$$\frac{d[\text{K}]_i}{dt} = \frac{-I_{\text{K}} - I_{\text{K1}} + 2 I_{\text{NaK}}}{F \text{Vol}_i} \quad (2.42)$$

where  $\text{Vol}_i$  = the available intracellular volume in M liters = 2 picolitres or 50% of cell volume

$F$  = the faraday

$[\text{S}]_i$  = the internal concentration in millimolar

$I_*$  is the membrane ionic current named "\*" that was described in the previous sections, in nanoamps.

The available cell volume is half of the total cell volume of 3.9 picolitres, since 50% of the total cell volume is considered to be occupied by internal organelles. The simple formula used for describing concentration of internal  $\text{Na}^+$  and  $\text{K}^+$  assumes that all  $\text{Na}^+$  and  $\text{K}^+$  entering the cell remain as free ions. Unfortunately this is not the case for calcium, the same calcium regulation mechanisms which inhibit free  $\text{Ca}^{++}$  diffusion also

significantly affect free  $\text{Ca}^{++}$  concentration. In order to properly assess the effects of calcium concentration these mechanisms must be included in the model of local membrane environment.

The internal regulatory mechanisms for calcium do considerably more than just affect rate of diffusion of free calcium ions within the intracellular medium. They also buffer the free  $\text{Ca}^{2+}$  ion concentration immediately adjacent to the cell membrane. As a result of the intracellular buffering of rapid changes in internal calcium, the internal calcium concentration cannot be accurately described by a simple integral of the transmembrane calcium fluxes.

The question is what are the major factors affecting internal calcium concentration within the cell and how may these processes be mathematically described? Here the relative anatomical simplicity of the bullfrog atrial cell may again be appreciated. In preparations with an extensive transverse tubule (T-system) and sarcoplasmic reticulum, calcium uptake and release within the cell may be dominated by properties of these non-sarcolemmal structures. In frog cardiac cells, there is strong evidence that all calcium entry takes place from the external bathing medium (Chapman, 1979; Morad, Goldman and Trentham, 1983). This is not the case in skeletal muscle nor in the mammalian

ventricle (for review see Chapman, 1979; Hasselbach and Oetliker, 1983).

The development of tension in muscle is regulated by free myoplasmic calcium concentration. In skeletal muscle about 90% of this activator calcium is contained in the terminal cisternae of the sarcoplasmic reticulum (Hasselbach and Oetliker, 1983). The precise release mechanism for this calcium store remains obscure. Re-uptake of  $\text{Ca}^{2+}$  occurs largely via an ATP requiring calcium pumping mechanism. Further complicating the analysis of excitation-contraction coupling in mammalian heart is the fact that the internal membrane system may be electrically coupled to the sarcolemma (Moore et al, 1984) and that significant accumulation/depletion phenomena may occur within this system (Barry and Adrian, 1973). In mammalian cardiac tissue it is also the case that  $\text{Ca}^{++}$  release from internal stores provides  $\text{Ca}^{++}$  directly to the intracellular medium (Bassingthwaighe and Reuter, 1972; Morad and Goldman, 1973).

Previous models describing calcium movements in mammalian skeletal muscle (Wallinga de Jonge et al, 1981) and in frog skeletal muscle (Cannell and Allen, 1984) address two important aspects of these phenomena. First they describe uptake and release of calcium from and to the sarcoplasm by the sarcoplasmic reticulum and terminal cisternae. Second they consider the interaction of important internal calcium-binding proteins within the sarcoplasm.

The original Beeler and Reuter (1977) simple description of the extrusion of calcium from the cell has been much expanded in the DiFrancesco and Noble (1985) model of mammalian Purkinje fibre. The DiFrancesco and Noble (1985) model of internal calcium movements differs from the earlier models of skeletal muscle activity in one important respect: it considers only the effects of uptake and release of calcium by the sarcoplasmic reticulum as an internal regulation mechanism of calcium activity. The omission of internal binding proteins from the DiFrancesco and Noble (1985) model is curious since both skeletal muscle models (Wallinga de Jonge, 1981; Cannell and Allen, 1984) conclude that the internal binding proteins represent a significant binding capacity for  $\text{Ca}^{2+}$ . Just as these binding proteins may slow the diffusion of calcium through the cell, they can also slow the time course and reduce the predicted amplitude of calcium concentration within the cell. Indeed, according to Cannell and Allen (1984) the predicted effects of calcium binding were still present 150 msec after a 'twitch'.

The situation in frog cardiac cells is almost exactly the opposite of that for mammalian Purkinje fibres as modelled by DiFrancesco and Noble (1985). As mentioned earlier the frog atrial cell contains no transverse tubule system and only a very limited sarcoplasmic reticulum (cf. Hume and Giles, 1981). In frog ventricular cells the SR makes up only 0.5% of the total cell

column (Page and Niedergerke, 1972) while in frog skeletal muscle the SR has been found to be 9% of total cell volume. Besides there being nearly 20 times less sarcoplasmic reticulum in frog heart the density of calcium pumping sites in the sarcoplasmic reticulum, as indicated by maximal rates of calcium uptake in isolated sarcoplasmic reticulum vesicles, is roughly twice as great for skeletal muscle SR as for cardiac SR (Chapman, 1979; Borle, 1981). Based on these estimates we might expect the calcium regulatory contribution of the sarcoplasmic reticulum in frog cardiac cells to be 40 times smaller than in frog skeletal muscle.

A variety of experimental results also indicate a minimal role for the release of calcium from the SR in a 'twitch' response in amphibian cardiac fibres. Thus, in normal Ringers solution pharmacological agents which promote calcium release from the SR produce either no or only very small contractions, and changes in resting tension when applied to amphibian heart (Chapman and Miller, 1974a; Chapman, 1979). This indicates that internal calcium release plays no important role in contraction, a result consistent with the data of Fabiato and Fabiato (1978). They found no evidence for a Ca-induced Ca-release mechanism in chemically skinned frog ventricular cells. In a sucrose gap study of frog ventricle Klitzner and Morad (1983) also concluded that in frog ventricular muscle  $\text{Ca}^{++}$  for activation of tension is transported primarily from the extracellular space.

Because of the consistency of morphological and experimental data showing a lack of functional importance of the sarcoplasmic reticulum in frog cells, the sarcoplasmic reticulum is not considered in this model (either as a calcium regulator or as part of the equivalent circuit of the frog atrial cell). The model used to describe the internal calcium regulatory mechanisms of frog atrial cells is taken from Campbell (1985). The compartmental model of Campbell (1985) is based upon the work of Robertson, Johnson, and Potter (1981) appropriately modified for single frog atrial cells. This model includes the following components:

A. Myosin binding sites are not included. This is because the Robertson, Johnson and Potter (1981) paper demonstrated that cardiac myosin is almost completely saturated by  $Mg^{++}$  and that internal  $Mg^{++}$  would have to be reduced from 1 - 3 mM to  $1 \times 10^{-5}$  M or less before any significant calcium binding to myosin would occur. Since free internal  $Mg^{++}$  is normally in the millimolar range, physiologic conditions make this an irrelevant variable in modelling internal  $Ca^{2+}$  concentration changes.

B. Mitochondria uptake of calcium is not considered. It has been shown that at a free  $Ca^{++}$  concentration of 1 mM a concentration of 5 mM  $Mg^{++}$  completely inhibits  $Ca^{++}$  uptake in isolated rabbit heart



mitochondria (Sordahl, 1974). Since free internal  $Mg^{++}$  concentrations are in the millimolar range this mechanism of calcium uptake will be insignificant. Further, Borle (1981) has summarized the available literature and reported a sigmoid dependence of mitochondrial  $Ca^{2+}$  sequestration upon  $(Ca^{2+})_i$  with a half maximal capacity of  $5 \times 10^{-6}$  M for frog cardiac mitochondria. The relatively high half maximal capacity when considered in conjunction with the sigmoid turn-on would tend to minimize the effects of mitochondrial sequestration of calcium even in the absence of  $Mg^{++}$  inhibition.

C. Parvalbumin  $Ca^{2+}$  binding/buffering are not included since this type of  $Ca^{2+}$  buffering protein is apparently absent in the myoplasm of cardiac muscle (Robertson, Johnson, and Potter; 1981).

This leaves only the  $Ca^{++}$  binding proteins troponin and calmodulin for consideration in models of  $(Ca^{2+})_i$  homeostasis.

#### Troponin

There are two types of calcium binding sites on cardiac troponin. One is very specific for calcium the other exhibits competition between  $Ca^{++}$  and  $Mg^{++}$  (Holroyde, Robertson, Johnson, Solaro, and Potter, 1980; and Johnson, Collins, Robertson, and Potter, 1980). The two different binding sites will be designated Troponin-Ca for the calcium specific sites and Troponin-Mg for the

sites for which  $\text{Ca}^{++}$  and  $\text{Mg}^{++}$  compete. There are two Troponin-Mg sites and one troponin-Ca site per molecule. Under physiologic conditions there appears to be no cooperativity between these sites (Holroyde, Robertson, Johnson, Solaro, and Potter, 1980).

#### Calmodulin

Calmodulin also contains  $\text{Ca}^{++}$ -specific binding sites. There are four of these calcium specific sites per molecule; however Wollf, Poirier, et al (1977) report that, in the presence of 1 mM  $\text{Mg}^{++}$ , calmodulin only binds three  $\text{Ca}^{++}$  ions per molecule. It is assumed that there is no cooperativity between binding sites (Campbell, 1985).

In order to update the Robertson, Johnson, Potter (1981) model to coincide with new results in the literature (Potter and Zott, 1982) as well as to obtain values appropriate to single bullfrog atrial cells Campbell (1985) made the following modifications:

"Buffers: The concentrations and specific binding rate constants that were used for calmodulin and troponin were taken from Robertson, Johnson, and Potter (1981). The cellular content of both calmodulin and troponin were estimated in the following way (cf. Baylor, Chandler, and Marshall, 1983). From the data presented in Desmedt (1953) for frog skeletal (sartorium) muscle the conversion factor

for moles/kg whole muscle to moles/kg fibre  $H_2O$  (SR and mitochondria included) is  $1/0.662$ . It was assumed that this conversion factor is also applicable to frog atrial muscle. According to Page and Niedergengerke (1972) the SR and mitochondria occupy only 1.5% of the total cell volume in the frog ventricle. Therefore, multiplying the above conversion factor by  $1/0.985$  gives  $1/0.652$  as the appropriate conversion factor for converting moles/kg whole muscle to moles/kg myoplasmic  $H_2O$ . Using the values of concentration reported in Robertson, Johnson, and Potter (1981) for calmodulin and cardiac troponin one obtains a value for frog atrium of  $[calmodulin]_i = (5 \text{ mM/kg wet wt})/0.652 = 7.67 \times 10^{-6} \text{ M}$  and  $[troponin]_i = (28 \text{ mM/kg wet wt})/0.652 = 4.29 \times 10^{-5} \text{ M}$ . (This estimates of  $[troponin]_i$  for frog atrium is roughly 2.8 times less than the estimate of  $[troponin]_i$  for frog striated muscle of 0.12 mM made by Baylor, Chandler, and Marshall (1983)). It should also be noted that Potter and Zot (1982), studying skeletal troponin reconstituted to actin, have recently reported a  $K_A$  value 10 x less than that originally reported by Robertson, Johnson, and Potter (1981)--i.e. actin appears to reduce the calcium affinity of skeletal troponin by ten-fold. As pointed out by Baylor, Chandler, and Marshall (1983) two extreme ways of

producing such a ten-fold decrease in  $K_A$  are by 126  
either increasing  $K_{off}$  10X or decreasing  $K_{on}$  10X.  
Therefore, it was assumed that such a reduction of  
 $K_A$  may also occur for cardiac troponin in the  
presence of actin, and thus simulations were also  
carried out with either a 10X decrease in  $K_{on}$  or a  
10X increase in  $K_{off}$  for the various binding sites  
of cardiac troponin." (Campbell, 1985).

The decision on how to modify the  $K_{on}$   $K_{off}$  variables in the  
present modelling study was handled by increasing  $K_{off}$  for all  
sites troponin binding sites by a factor of ten. The basis for  
this modelling choice is that increases  $K_{off}$  has beneficial conse-  
quences in the sinus model where calcium influx is estimated to be  
three times as large. The parameters as used in the model are  
summarized in Table 2.2.

Table 2.2  
Estimated Concentrations and Rate Constants for Internal  $\text{Ca}^{++}$  Buffers

Protein	Cellular Concentration (moles/l)	Moles/ Cell	Number of Sites	Ion	$K_A$ (M)	$K_{on}$ ( $\text{mM}^{-1}\text{sec}^{-1}$ )	$K_{off}$ ( $\text{sec}^{-1}$ )
Calmodulin	$7.67 \times 10^{-6}$	$15 \times 10^{-18}$	3	$\text{Ca}^{2+}$	$4.2 \times 10^{-5}$	$1 \times 10^5$	238
Troponin	$4.29 \times 10^{-5}$	$84 \times 10^{-18}$	1	$\text{Ca}^{2+}$	$2 \times 10^{-6}$	$3.9 \times 10^4$	196.0
Sites:	"troponin-Ca"		1	$\text{Ca}^{2+}$	$3 \times 10^{-8}$	$1 \times 10^5$	3.3
	"troponin-Mg"		2	$\text{Mg}^{2+}$	$3 \times 10^{-3}$	$1 \times 10^2$	333.0

Adapted from Campbell (1985).

Given a knowledge of both the total amount of the internal buffering proteins and the binding rate constants for each protein to calcium it is a very straightforward process to write the equations describing the internal buffering of calcium. The state of each type of binding site is expressed as a fractional occupancy of the total amount of binding sites of that type by the ions capable of binding to that site.

$$\frac{dO_c}{dt} = 100.0 [Ca]_i (1.0 - O_c) - 0.238 O_c \quad (2.43)$$

$$\frac{dO_{Tc}}{dt} = 39.0 [Ca]_i (1.0 - O_{Tc}) - 0.196 O_{Tc} \quad (2.44)$$

$$\frac{dO_{TMgC}}{dt} = 100.0 [Ca]_i (1.0 - O_{TMgC} - O_{TMgM}) - 0.0033 O_{TMgC} \quad (2.45)$$

$$\frac{dO_{TMgm}}{dt} = 0.1 [Ca]_i (1.0 - O_{TMgC} - O_{TMgm}) - 0.333 O_{TMgm} \quad (2.46)$$

where:

$O_c$  is the fractional occupancy of calmodulin

$O_{Tc}$  is the fractional occupancy by  $Ca^{++}$  of calcium specific sites on troponin

$O_{TMgC}$  is the occupancy of the  $Ca^{++}-Mg^{++}$  competitive binding sites by calcium on troponin

$O_{TMgm}$  is the fractional occupancy of  $Ca^{++}-Mg^{++}$  competitive binding sites by magnesium on troponin.

The  $Ca^{2+}$  flux onto the buffers may now be calculated as:

$$O_b = K_1 \frac{dO_c}{dt} + K_2 \cdot \frac{dO_{Tc}}{dt} + K_3 \cdot \frac{dO_{TMgC}}{dt} \quad (2.47)$$

where:

$K_1 = 3 \times 15.0 \times 10^{-6}$  picomoles =  $45.0 \times 10^{-6}$  picomoles the # of moles of available calmodulin sites per cell.

$K_2 = 1 \times 84.0 \times 10^{-6}$  picomoles =  $84.0 \times 10^{-6}$  picomoles the # of moles of troponin Ca specific sites per cell

$K_3 = 2 \times 84 \times 10^{-6}$  picomoles =  $168.0 \times 10^{-6}$  picomoles the number of nanomoles of Ca-Mg competitive troponin sites per cell

$O_b$  = flux onto the buffers in nanomoles/second of picomoles/millisecond.

Now the model equation describing internal calcium concentration may be written:

$$\frac{d[Ca]_i}{dt} = \frac{2I_{NaCa} - I_{Ca} - I_{Cap} - I_{CaBackground}}{F} - O_b \quad (2.48)$$

$Vol_1$

### II.5 Summary of the Atrial Model

This model of the electrophysiological activity in an atrial cell is composed of two coupled subcomponents: (i) a cell membrane model consisting of the gated ionic currents, membrane capacitance, and electrogenic pump and exchanger mechanisms; and (ii) a compartmental model which combines the ionic currents in the membrane model with mathematical representations of the intracellular and extracellular structures, in addition to the sequestration and release of  $(Ca^{2+})_i$ . This combination or 'compartmental model' is diagrammed in Figure 2.13, Panel A. Our mathematical representation of this compartmentalization is a simplification of what really occurs. As shown in the Figure there are three relevant spaces, the concentrations of the major permeant ions,  $Ca^{2+}$ ,  $K^+$ , and  $Na^+$  define the 'state' of these spaces. In the intracellular space there are three different groups of  $Ca^{2+}$ -binding sites. The only way in which ions can move from the internal to the external or cleft spaces is via a transmembrane ionic current pump or exchanger mechanism. Time-dependent fluxes from the external cleft space to the bulk medium are approximated by a first-order process, instead of the more complex distributed parameter process which has been used in recent models (DiFrancesco and Noble, 1985; Coulombe and Corabouef, 1983).



Figure 2.13

A diagram of Atrial membrane model showing the various components. Panel A shows the compartmental model surrounding the membrane environment while Panel B gives a schematic description of the circuit elements used in the membrane model.

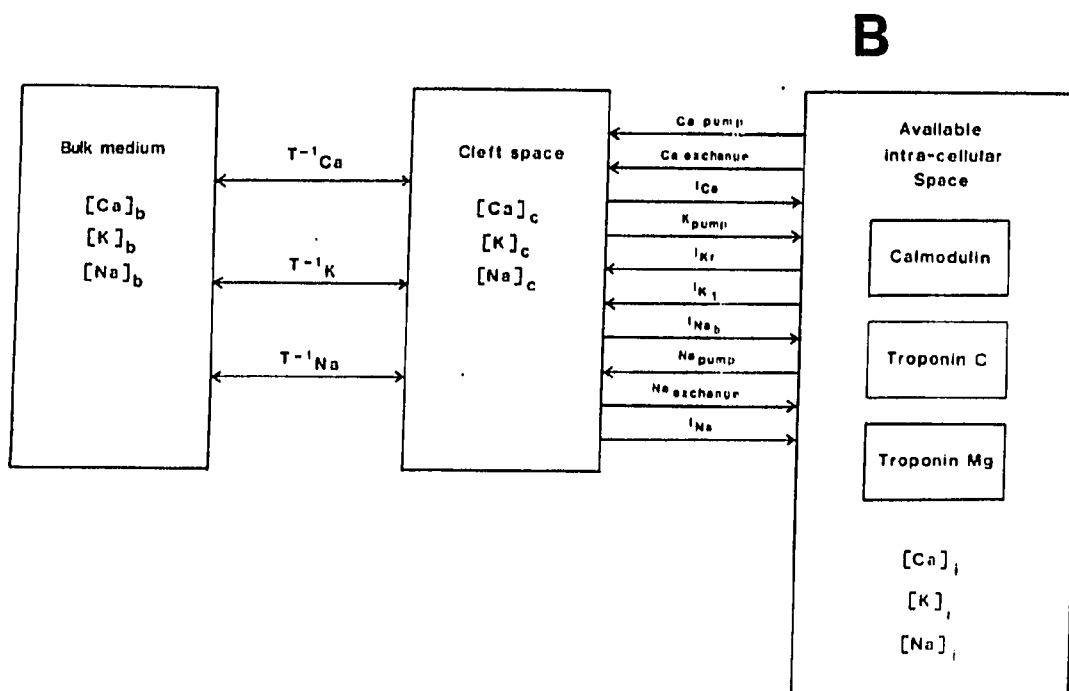
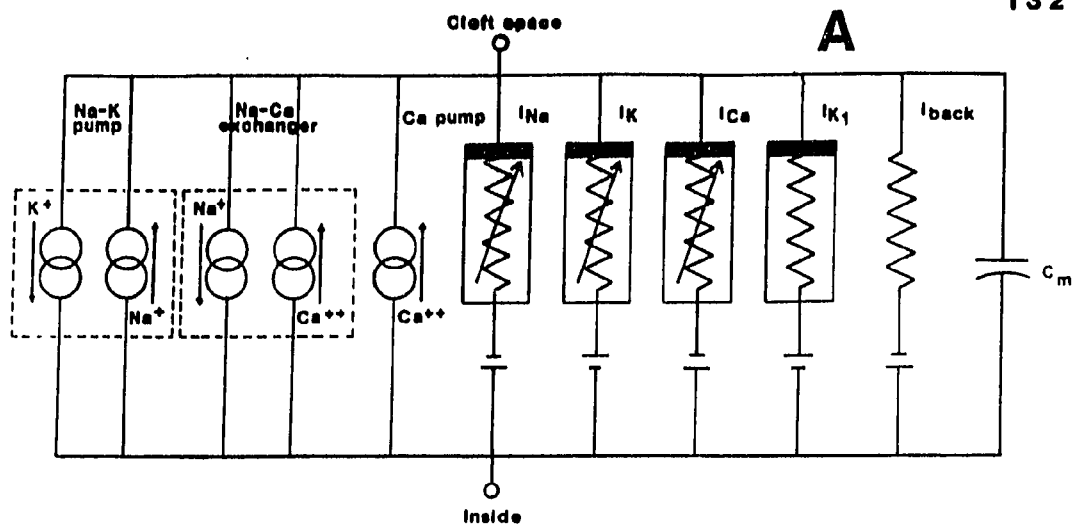


Figure 2.13, Panel B shows the equivalent circuit of an atrial cell, including each of the time- and voltage-dependent conductances and the pump and exchanger mechanisms described in the previous sections.

## II.6 Modifications for Modelling Bullfrog Sinus Venosus

The previous sections in this Chapter have described a model of electrophysiological responses in single cells from frog atrium. It addresses issues involved with the currents underlying a normally quiescent cell. Can this model be modified to reproduce the results of spontaneously active pacemaker cells particularly the frog sinus venosus?

It has become a common practice in the field of cardiac electrophysiology to take models of a particular cell type and to modify and adapt them to describe results in another cell type. Noble's 1962 model of cardiac electrical activity is a direct adaptation of the Hodgkin-Huxley model for squid axon electrical activity; this represents a large difference in cell type indeed. However, this pioneering work provided a number of very useful insights--even though it arose from an extreme paucity of data. In general, modelling work has preceded experimental activity in the field of cardiac electrophysiology. Progressively more specific models of cardiac tissue have been developed as more reliable data became available. With the introduction of the

sucrose gap technique (Rougier, Vassort and Stämpfli, 1968) near the end of the 1960's, cardiac electrophysiologists had a practical method of voltage clamping the multicellular cardiac preparations. In the mid-1970's McAllister, Noble and Tsien (1975) developed models based upon available data from cardiac muscle. These models in turn were modified to reproduce electrical activity in other portions of the heart e.g. Bristow and Clark (1982) changing the McAllister, Noble, and Tsien (1975) model of Purkinje fibre into sinoatrial nodal activity or to reproduce electrical activity in some other species e.g. Drouhard and Roberge (1982) who combined and adapted the mammalian models of both Beeler and Reuter (1977) and McAllister, Noble and Tsien (1975) for a model of frog ventricular activity.

The models of McAllister, Noble and Tsien (1975) and Beeler and Reuter (1977) served not only as attempts to describe the ionic currents underlying a particular action potential but also as reference point for investigators in the field. That is, these models represented a summary of current thinking on a very large number of ionic processes since the equations that make up the model are concise, and precise descriptions of the underlying electrophysiological activity. As illustrated in these papers when there is a paucity or a complete absence of data on particular underlying current it is possible to use the equations in a model of a related cell type, as a starting point. In order for

modelling to be useful it should be adaptable and be continually updated to take into account of the available reliable experimental data. As an example, DiFrancesco and Noble (1985) recently have published an updated and extended version of the McAllister, Noble and Tsien (1975) model for the Purkinje fibres. Subsequently, this model has been adapted by Noble and Noble (1984) in an attempt to reproduce mammalian pacemaker activity.

As mentioned earlier, the work in this thesis arises from recent progress in the experimental field. Unlike previously published models, most of the membrane current formulations are based on single cell measurements. Recently substantial experimental work has been done on single isolated sinus venosus, as well as the atrial cells of the bullfrog. The results on both cell types will provide the basis for the conversion of the atrial model into a related mathematical model for sinus pacing (cf. Giles and Shibata, 1985).

If we are going to modify a model of atrial activity so that it will simulate activity in the sinus venosus, where can we begin? What currents should be eliminated, added, or modified? An obvious first step is to examine how this can be accomplished experimentally.

In frog atrial muscle Brown and Noble (1969a) showed that pacing developed after depolarization produced by applying a steady depolarizing current. At that time they concluded that the

current which controlled pacing was a gated potassium current which deactivated upon repolarization and whose deactivation modulated the time course of diastolic depolarization. The currents underlying this 'induced pacing' were studied in more detail by Brown, Clark and Noble (1975). These experiments were performed in a double sucrose gap apparatus and were likely to have been 'contaminated' by potassium accumulation artifacts, making a quantitative analysis difficult (Brown and Noble, 1969b; and Brown, Clark and Noble, 1975). In spite of these experimental limitations the major conclusions reached are applicable and a year later Brown, Giles and Noble (1977) published a study on the frog sinus venosus which put forth the hypothesis that the generation of pacemaker activity involved both the decay of outward current and the activation of an inward  $\text{Ca}^{2+}$  current.

Since the addition of a depolarizing current to atrial preparations leads to (induces) pacing, an interesting question is: Is pacing due to this extra inward current or to the absence of an outward current in sinus tissue? Insights into possible 'pacemaker currents' can also be obtained from pharmacological blocker experiments. In the model of frog atrium there are only three significant currents in the diastolic range of potentials (-70 to -90 mV), the inward rectifier, the  $\text{Na}^+/\text{K}^+$  pump current and the background inward current. Since inhibition of the inward background current cannot depolarize the cell and lead to

pacemaker activity, let us consider the effects of blocking either of the two outward currents.

Relatively high doses ( $10^{-4}$ ) of ouabain can inhibit the sodium potassium pump. In a comparative study of the effects of ouabain on both Purkinje fibres and ventricular muscle of dog (Vassalle, Karis and Hoffman, 1962) found that application of ouabain resulted in spontaneous activity in Purkinje fibres but not in ventricular muscle. This result suggests that the current generated by the  $\text{Na}^+/\text{K}^+$  pump is sufficient to influence pacing activity; although it may not be sufficient to explain spontaneous activity in working myocardium.

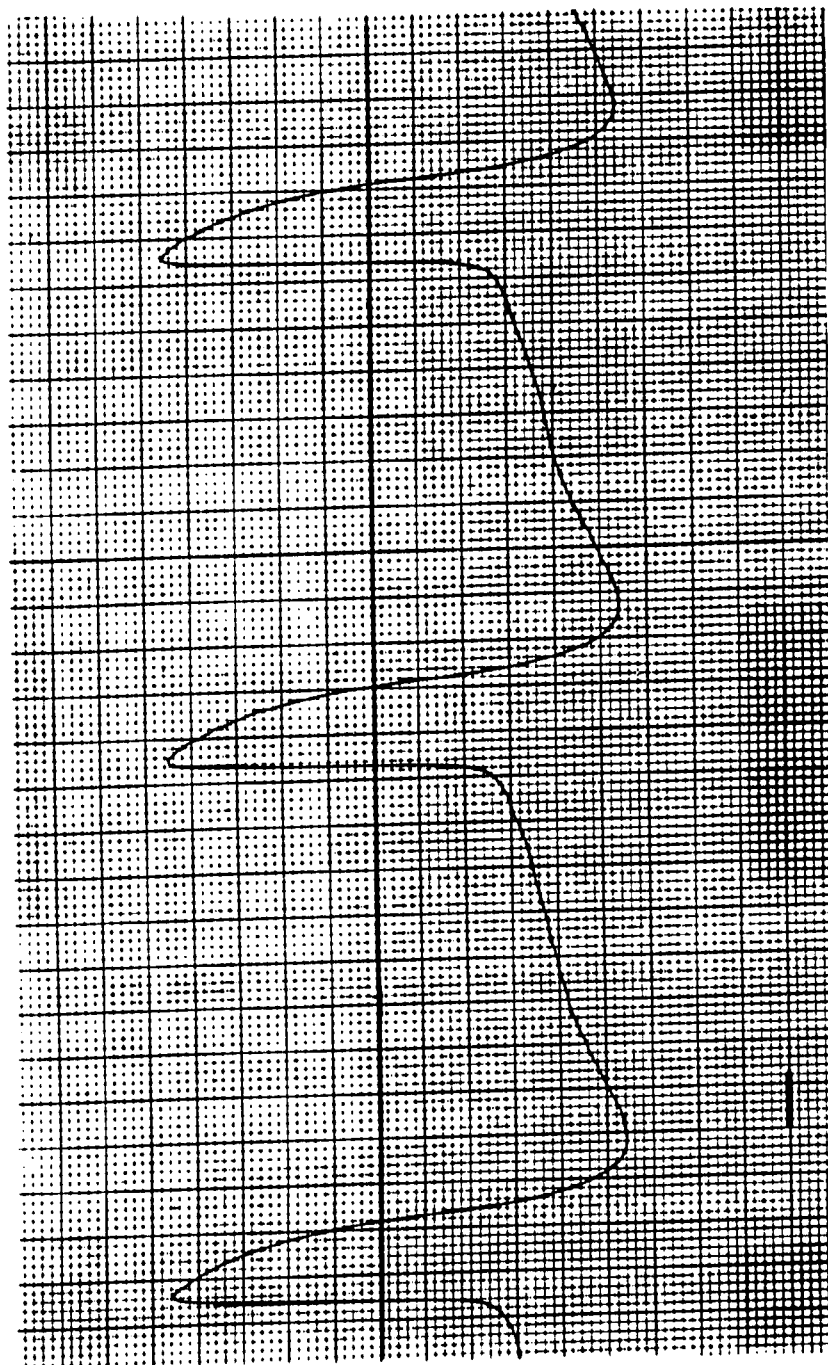
Small concentrations of  $\text{Ba}^{++}$  ions are known to block the resting permeability to potassium in a variety of cardiac preparations (eg. Hermsmeyer and Sperelakis, 1970) in frog ventricle, (Reid and Hecht, 1967) in dog ventricle, (Tournier, Mitra, and Morad, 1984) in guinea pig atrium and ventricle, Shibata and Giles (1984) and Argibay, Ildefonse, Ojeda, Rougier, and Tourneur (1983) in frog atrium. This inhibition of the inward rectifier is also found to induce automaticity in dog ventricle as well as in frog. This automaticity persists for very long times (Cranefield, 1975).

Since sustained pacing can be elicited from atrial muscle by the addition of barium we can now ask if the resulting action potentials resemble those of healthy sinus tissue. Fortunately  $\text{Ba}^{++}$  induced pacing appears very similar (see Figure 2.14) to sinus

Figure 2.14

Barium induced pacing in a bullfrog atrial cell. 500  $\mu\text{M}$   $\text{Ba}^{++}$  containing Ringer's solution was applied to an isolated bullfrog atrial cell resulting in spontaneous depolarization and pacing. Note the similarity in shape to the sinus-venosus pacing (figure 1.0). Scale mark is 250 m seconds.





pacing. The differences between the action potential of an isolated sinus venosus cell and one of an atrial cell after application of barium are almost indistinguishable.

The detailed comparison of atrial and sinus venosus experimental data and the necessary changes for mathematically simulating the sinus venosus activity can now be summarized:

$\bar{I}_{K_1}$  - The inward rectifier appears to be completely absent from sinus venosus cells. This has been reported in Shibata (1983), Shibata and Giles (1984) and Giles and Shibata (1985). Figure 2.15, Panel A shows the measured background current from sinus cells. Note the absence of inward rectification in sinus cells. Panel B shows the current voltage relation for an atrial cell before and after application of  $Ba^{++}$ . Consequently the sinus model has no  $I_{K_1}$  component. Due in part to the lack of a sustained resting efflux of  $K^+$  via this channel the value of  $[K]_i$  should be approximately 130 mM as opposed to 95 mM in the atrial model.

$\bar{I}_K$  - The gating kinetics of the delayed rectifier  $K^+$  current in both sinus and atrial cells appear to be identical within the accuracy of experimental measurements. Figure 2.16 shows the rate constant curves for sinus and atrium (Panels A and B) and the steady-state voltage-dependence for the

Figure 2.15

Measurement of the time independent background current in isolated sinus venosus pacemaker cell in isolated atrial cell before and after application of  $50 \mu\text{M Ba}^{++}$ .

Panel A

A maximum inward or minimum outward current measured upon a command pulse of 100 msec for a sinus-venosus cell superfused in TTX ( $3 \times 10^{-5} \text{ M}$ ) and  $\text{LaCl}_3$  ( $10^{-5} \text{ M}$ ) Ringer's Solution containing hepes buffer.

Panel B

The same procedure applied to an atrial cell under the same conditions before application of  $50 \mu\text{M Ba}^{++}$  (closed circles) and after (open circles).

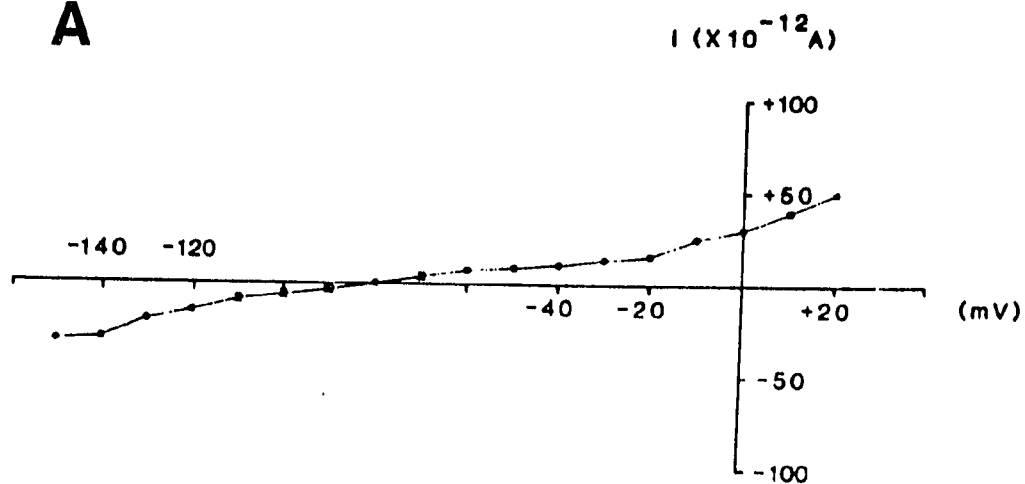
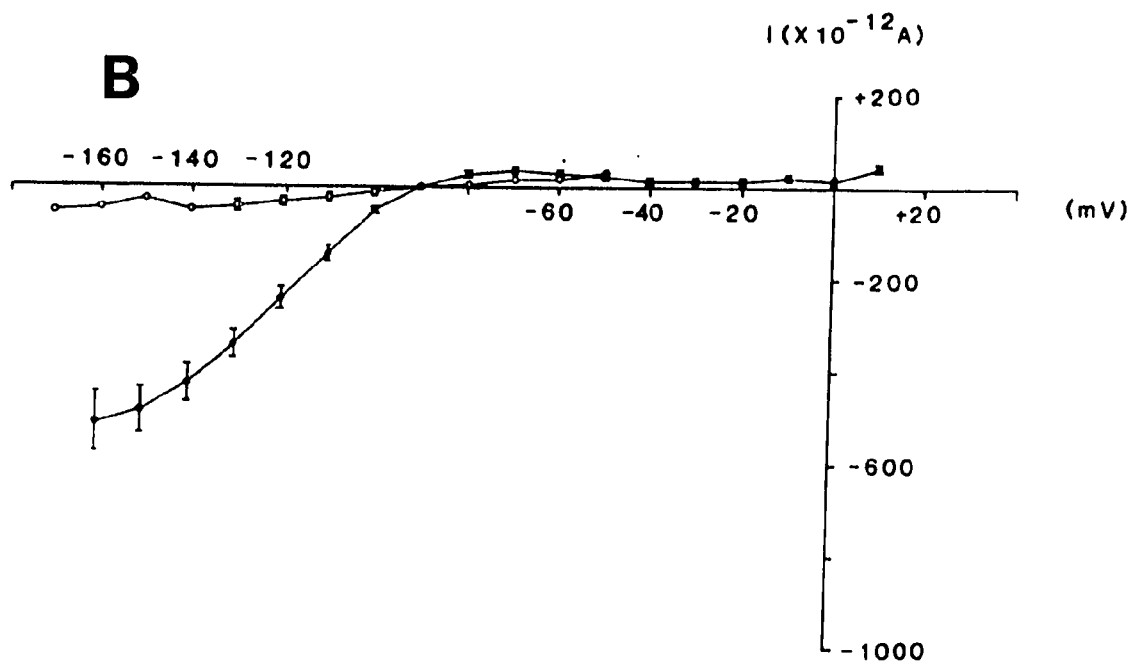
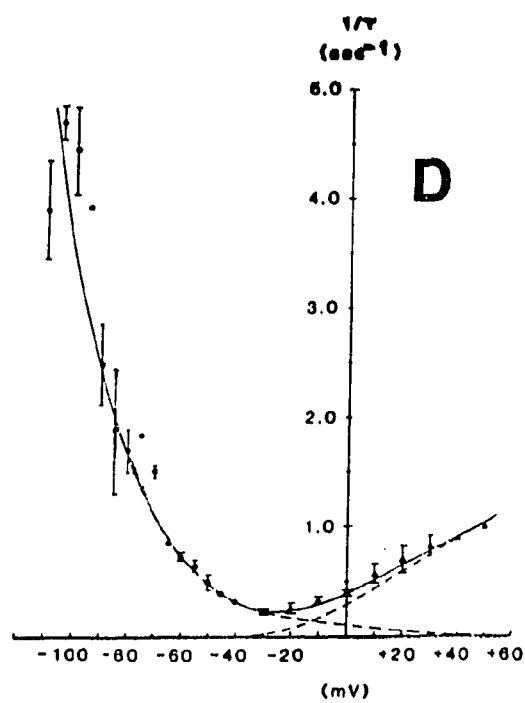
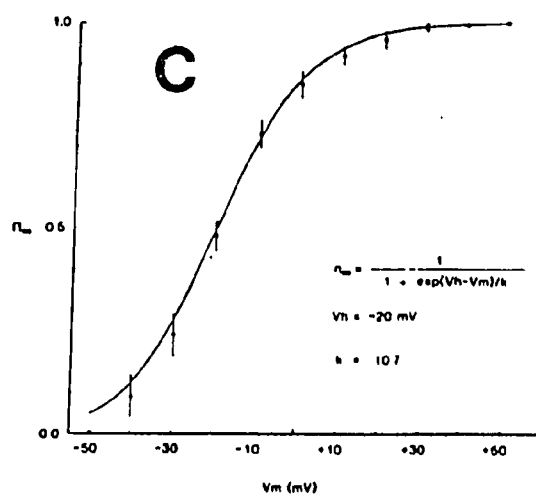
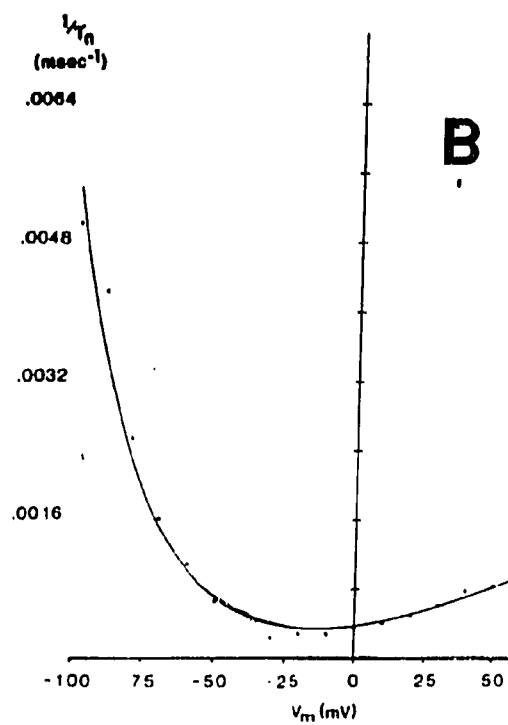
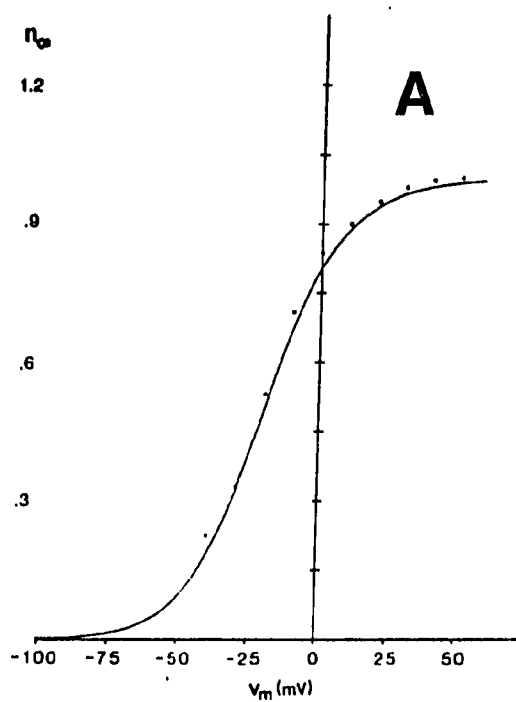
**A****B**

Figure 2.16

A comparison of the measured properties of the n gating variable for atrium and sinus venosus.

- A)  $N_{\infty}$  measured in Atrium Robinson (1983).
- B)  $N_{\infty}$  measured in sinus-venosus Shibata (1983).
- C)  $T_n^{-1}$  measured in Atrium Robinson (1983).
- D)  $T_n^{-1}$  measured in sinus venosus Shibata (1983).

Note the large degree of similarity.



gating variable (Figure 2.16, Panels C and D). Since these data are not significantly different, the potassium gating kinetics are considered to be identical in both the sinus and atrial models. The fully-activated current-voltage relation in the atrial model is based on the data of Giles and Shibata (1985) which is sinus venosus data. The entire formulation for  $I_K$  is the same in both models except that  $I_K$  is 8% smaller in the sinus model.

$I_{Na}$  - The fast TTX-sensitive inward current is not found in frog sinus venosus (Brown, Giles and Noble, 1977; Giles and Shibata, 1985). It therefore is not included in the sinus model.

$I_{Ca}$  - The inactivation of  $I_{Ca}$  in both sinus and atrium appears to be very similar. Figure 2.17, Panels A and B shows the measured steady-state characteristics of the f gating variable for both sinus and atrium. Panels C and D show the time constants of inactivation. These show the same peculiar shape for both sinus and atrium. The plots of peak I-V curves show a very similar shape indicating similar activation kinetics; note, however that the magnitudes of  $I_{Ca}$  are different by more than a factor of two (see Figure 2.18, Panels A and B). Therefore the calcium channel description is the same in both models except that the sinus model current is 2.3 times larger than that in the atrial model. In

Figure 2.17

A comparison of the measured properties of the  $f$  gating variable for atrium and sinus venosus.

- A)  $F_\infty$  measured in Atrium Campbell (1985).
- B)  $F_\infty$  measured in sinus-venosus Shibata (1983).
- C)  $T_f^{-1}$  measured in Atrium Campbell (1985).
- D)  $T_f^{-1}$  measured in sinus venosus Shibata (1983).

Note the large degree of similarity.



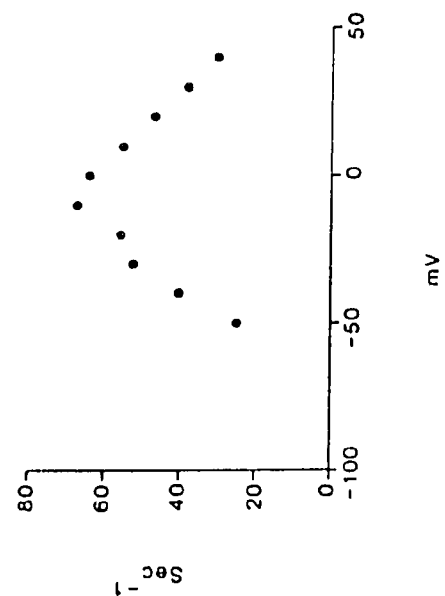
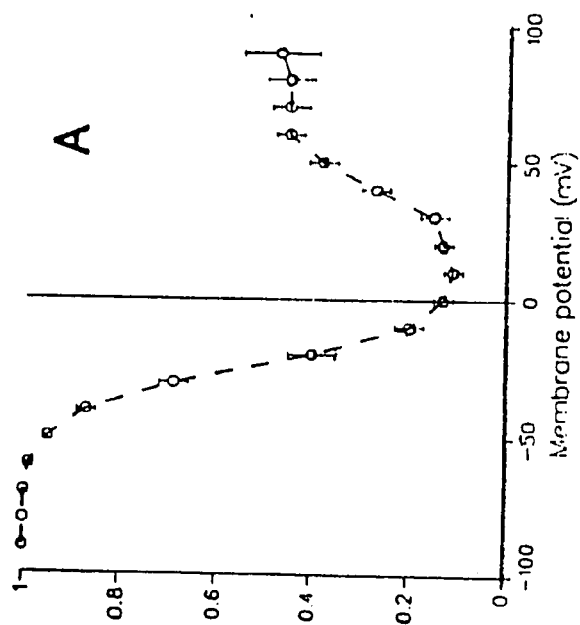
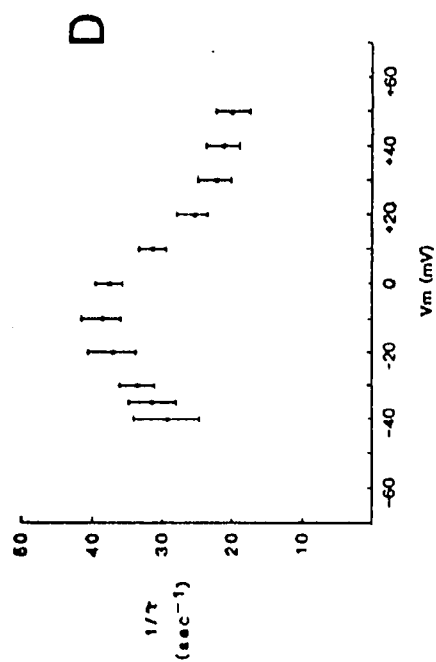
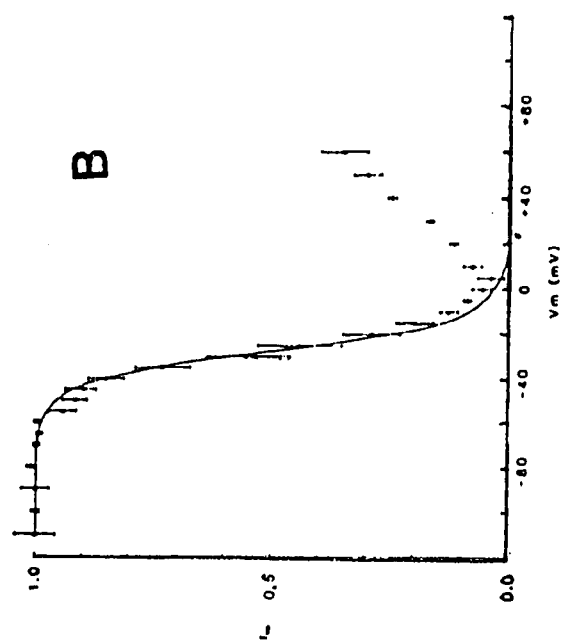
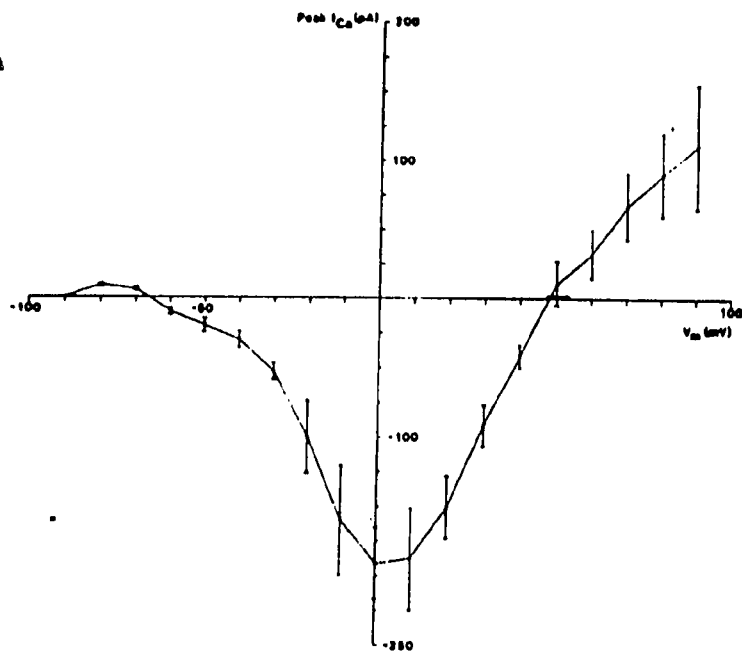
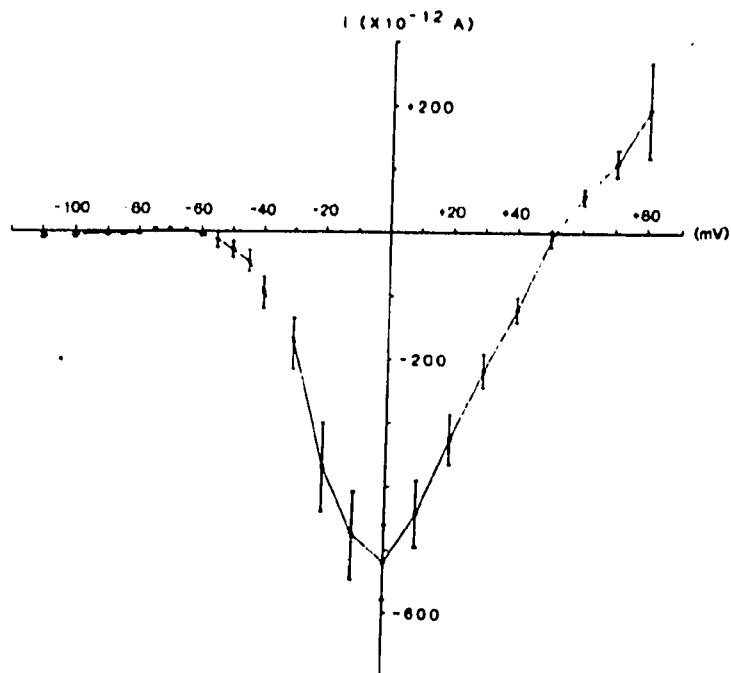


Figure 2.18

Peak calcium current to voltage relations measured for Atrium and sinus-venosus. Note that in the lower potential ranges  $I_{K2}$  interferes with the measurement of this current in Atrium (Panel A). The sinus-venosus (Panel B) calcium current is much larger than the same current in Atrium but otherwise seems very similar.

**A****B**

addition the reactivation or "tip up" of the inactivation variable has been increased by 33%.

$I_{\text{Nab}}$  and  $I_{\text{Cab}}$  - The inward background conductance has been scaled to reproduce the experimentally observed rate of diastolic depolarization heart-rate. The sinus model conductance is 77% of the atrial background conductance.

$I_{\text{NaK}}$  - In the absence of any quantitative data in sinus this pump current is identical in both sinus and atrium.

$I_{\text{Na-Ca}}$  - Since the influx of calcium has been greatly increased due to the increased magnitude of  $I_{\text{Ca}}$ , the magnitude of this calcium extrusion mechanism has also been increased. The magnitude of the Na-Ca exchanger is 2.67 times larger in the sinus model than in the atrium model.

$I_{\text{Cap}}$  - The calcium pump in sinus cells has been increased by a factor of five. It has been increased by a larger amount than the  $\text{Na}^+/\text{Ca}^{++}$  exchange process since, at the relatively depolarized levels of pacemaker cells, the  $\text{Na}^+/\text{Ca}^{++}$  is not operating in its most efficient range. Therefore the calcium pump must play a far more important role in calcium extrusion than in the corresponding atrial cell simulations.

$C_m$  - The membrane capacitance in single sinus venosus cells is taken to be 75 pfd (Giles and Shibata, 1985) as opposed to 100 pfd in atrial cells (Hume and Giles, 1981).

Vol - Since the two cells are visually indistinguishable (Shibata, personal communication; see Figure 2.19 comparing the two cells) it is assumed the cell and cleft volumes are the same in both atrial and sinus cells.

Calcium buffers - Since the cells have the same volume they are assumed to contain the same amount and types of buffer proteins.

In summary the modifications to reproduce sinus activity were:

1. Deletion of  $I_{K_1}$  and  $I_{Na}$
2. Increase of  $I_{Ca}$
3. Increase of calcium extrusion mechanisms
4. Adjustment of cell capacitance
5. Tuning of  $I_K$  and  $I_{Background}$  current magnitudes

These are straightforward modifications well-supported by the experimental data and the modified equations are listed in Table 3.1.

Figure 2.19

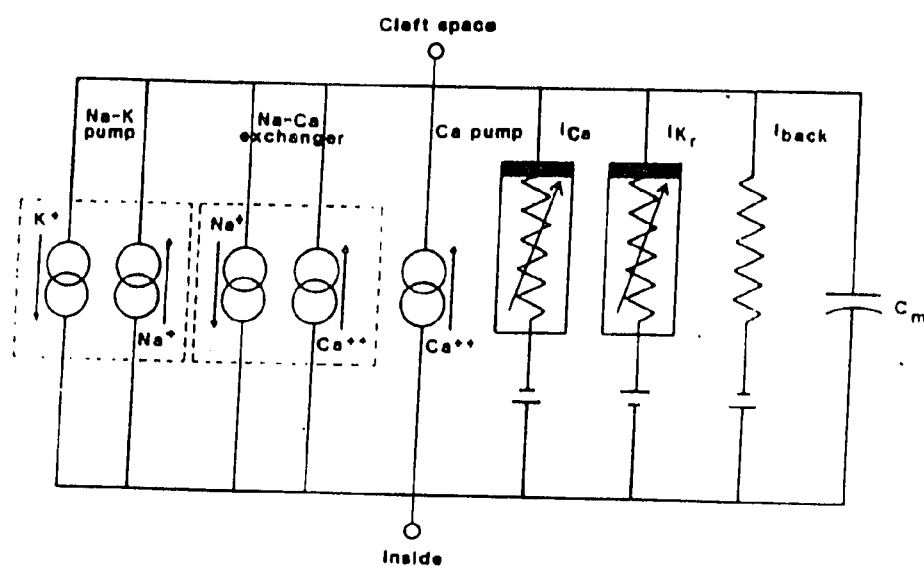
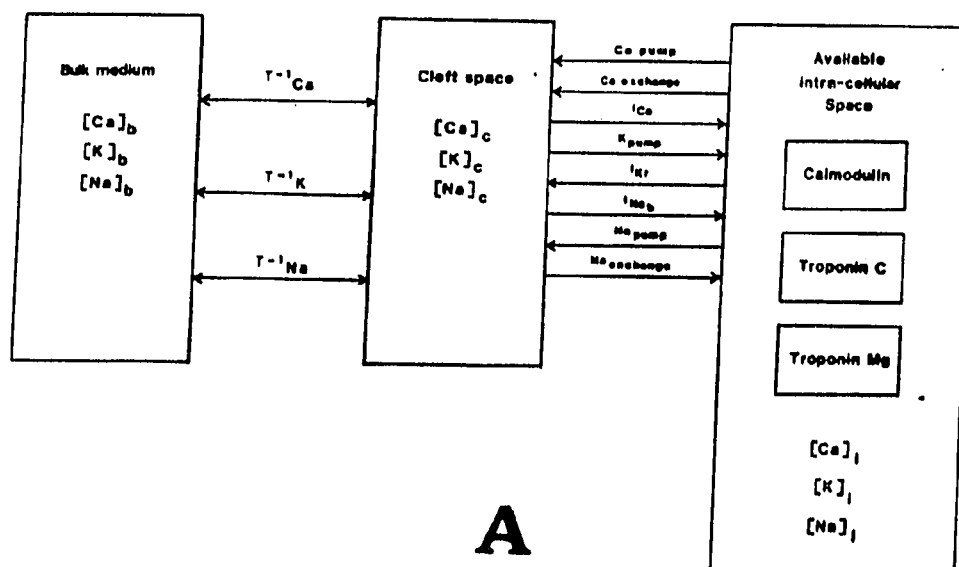
Pictures of an isolated bullfrog atrial cell (top panel) and an isolated bullfrog sinus-venosus cell.



Figure 2.20

A diagram of the Sinus-venosus membrane model showing the various components. Panel A shows the compartmental model surrounding the membrane environment while Panel B gives a schematic description of the circuit elements used in the membrane model.





CHAPTER III  
COMPUTATIONAL ASPECTS AND INITIAL MODEL TESTING

III.0     Introduction.

The preceding chapter presented the equations describing a model of cardiac electrical activity and summarized the experimental evidence used to formulate it. The equations and numerical values of the constants used are in Table 3.0 for the atrium and Table 3.1 for the sinus-venosus.

This chapter will first present the numerical method for solution(s) of this system of equations, and briefly describe the program structure. Secondly this chapter will present basic model results and provide a detailed comparison of these simulations with the relevant experimental findings.

Table 3.0Atrial Model Equations and ValuesSection A: Main Membrane Equation and Units

$$\frac{dV}{dt} = \frac{I_{stim} - I_{Na} - I_{Ca} - I_K - I_{K1} - I_{Background} - I_{NaK} - I_{NaCa} - I_{Cap}}{C_m} \quad (3.1)$$

$$C_m = 0.1 \text{ nanofds}$$

$[ ]_i$  = intracellular concentration in millimolar

$[ ]_c$  = cleft concentration in millimolar

$[ ]_b$  = bulk concentration in millimolar

$Vol_i$  = available intracellular volume in nanolitres

$Vol_c$  = cleft volume in nanolitres

$O_*$  = Occupancy (scalar)

$I_*$  = current in nanoamps

$d[ ]$  millimolar  
 $\frac{d[ ]}{dt}$  =  $\frac{\text{millimolar}}{\text{millisecond}}$

$V_m$  = membrane voltage in millivolts

$$\frac{dV_m}{dt} = \text{millivolts/millisecond}$$

$$E_* = \text{reversal potential in millivolts}$$

$$\tau^{-1} = \text{rate constant in msec}^{-1}$$

$$C_m = \text{capacitance in nanofds}$$

Table 3.0Section B: Background Current Systems

$$I_{\text{Background}} = I_{\text{NaBack}} + I_{\text{CaBack}} \quad (3.2)$$

$$I_{\text{NaBack}} = 0.00015 (V_m - 54.0) \quad (3.3)$$

$$I_{\text{CaBack}} = 0.0000005 (V_m - 54.0) \quad (3.4)$$

$$I_{K_1} = \frac{0.4 [K]_c (V_m - E_k)}{([K]_c + 210.0) (1 + \text{Exp}((V_m - E_k - 20.0) * 2.0 * 0.039))} \quad (3.5)$$

$$E_k = 58.6 \log_{10} \frac{[K]_c}{[K]_i} \quad (3.6)$$

Table 3.0

Section C: The Transient Inward Sodium Current System

$$I_{Na} = M^3 H \bar{I}_{Na} \quad (3.7)$$

$$\bar{I}_{Na} = \frac{0.132 \times 10^{-3} [Na]_i 96500 \exp(0.039(V_m - E_{Na})) - 1}{\exp(0.039 V_m) - 1} \quad (3.8)$$

$$[Na]_i \sim 7.5 \text{ millimolar}$$

$$E_{Na} = 59 \log \frac{[Na]_c}{[Na]_i} \quad (3.9)$$

$$\frac{dM}{dt} = (1 - M) \alpha_n - H \beta_m \quad (3.10)$$

$$\alpha_m = \frac{0.757 (V_m - 31.2)}{1 - \exp(-0.0617(V_m - 31.2))} \quad (3.11)$$

$$\beta_m = 2.26 \exp(-0.042(V_m + 28.46)) \quad (3.12)$$

$$\frac{dH}{dt} = (1 - H) \alpha_h - H \beta_h \quad (3.13)$$

$$\alpha_h = 0.051 \exp(-0.124(V_m + 85.45)) \quad (3.14)$$

$$\beta_h = \frac{1.27}{1 + \exp(-0.0764(V_m + 2.91))} \quad (3.15)$$

Table 3.0Section D: The Transient Calcium Current System

$$I_{Ca} = \overline{I_{Ca}} \cdot f \cdot d \quad (3.16)$$

$$\frac{df}{dt} = f_{\infty} \tau_f^{-1} - f \tau_f^{-1} \quad (3.17)$$

$$\tau_f^{-1} = 0.0197 \exp(-(0.0337(V_m + 10))^2) + 0.02 \quad (3.18)$$

$$f_{\infty} = \frac{1}{1 + \exp((35.1 + V_m)/8.6)} + \text{Reactivation} \quad (3.19)$$

$$\text{Reactivation} = \frac{0.6}{1 + \exp((50 - V_m)/20)} \quad (3.20)$$

$$\tau_d^{-1} = \frac{0.035(V_m + 10)}{(1 - \exp(-(V_m + 10)/6.24)) d_{\infty}} \quad (3.21)$$

$$d_{\infty} = \frac{1.0}{1 + \exp(-(10 + V_m)/6.24)} \quad (3.22)$$

$$\overline{I_{Ca}} = \frac{0.78 \times 10^{-6} \times 4 \times 96500 \times 0.039 V_m ([Ca]_i \exp(2 V_m 0.039) - [Ca]_c)}{\exp(2 V_m 0.039) - 1} \quad (3.23)$$

Table 3.0

Section E:The delayed rectifier current system:

$$I_K = n^2 \overline{I_K} \quad (3.24)$$

$$\frac{dn}{dt} = (1-n)\alpha_n - n\beta_n \quad (3.25)$$

$$\alpha_n = \frac{0.0000144 (V_m + 26.5)}{1 - \exp(-0.128 (V_m + 26.5))} \quad (3.26)$$

$$\beta_n = 0.000286 \exp(-0.038 (V_m + 26.462)) \quad (3.27)$$

$$\overline{I_K} = 0.0125 \cdot ((V_m - E_k) + \text{Rectification}) \quad (3.28)$$

$$\text{Rectification} = \frac{95.0}{1 + \exp((V_m - E_K - 78)/25)} - 95.0 \quad (3.29)$$

$$E_k = 59 \log_{10} \frac{[K]_c}{[K]_i} \quad (3.30)$$



Table 3.0Section F: Pump and exchange current systems

$$I_{NaK} = \overline{I_{NaK}} \frac{[Na]_i^3}{[Na]_i + 5.46} \frac{[K]_c^2}{[K]_c + 0.621} \quad (3.31)$$

$$\overline{I_{NaK}} = 0.0772 \text{ nanoamps}$$

$$I_{Cap} = \overline{I_{Cap}} \cdot \frac{[Ca]_i}{[Ca]_i + 0.001} \quad (3.32)$$

$$\overline{I_{Cap}} = 0.00135$$

$$I_{NaCa} = \frac{1.5 \times 10^{-6} ([Na]_i^3 [Ca]_c \exp(.0195 V_m) - [Na]_c^3 [Ca]_i \exp(-.0195 V_m))}{1 + .0001 ([Ca]_i [Na]_c^3 + [Ca]_c [Na]_i^3)} \quad (3.33)$$

Table 3.0Section G: External 'Cleft' Concentration System

$$\frac{d[Na]_c}{dt} = \frac{[Na]_b - [Na]_c}{\tau_p} + \frac{3I_{NaK} + 3I_{NaCa} + I_{Na} + I_{NaBack}}{F Vol_c} \quad (3.34)$$

$$\frac{d[K]_c}{dt} = \frac{[K]_b - [K]_c}{\tau_p} + \frac{-2I_{NaK} + I_{K1} + I_K}{F Vol_c} \quad (3.35)$$

$$\frac{d[Ca]_c}{dt} = \frac{[Ca]_b - [Ca]_c}{\tau_p} + \frac{-2I_{NaCa} + I_{Ca} + I_{Cap} + I_{CaBack}}{2F Vol_c} \quad (3.36)$$

$$F = 96500$$

$$\tau_p = 10000.0 \text{ milliseconds}$$

$$Vol_c = 0.0004 \text{ nanoliters}$$

Table 3.0

Section H: Internal Sodium and Potassium Concentration Systems

$$\frac{d[\text{Na}]_i}{dt} = \frac{-I_{\text{Na}} - I_{\text{NaBack}} - 3I_{\text{NaCa}} - 3I_{\text{NaK}}}{F \text{ Vol}_i} \quad (3.37)$$

$$\frac{d[\text{K}]_i}{dt} = \frac{-I_{\text{K}} - I_{\text{K1}} + 2I_{\text{NaK}}}{F \text{ Vol}_i} \quad (3.38)$$

$$F = 96500$$

$$\text{Vol}_i = 2.5 \times 10^{-3} \text{ nanolitres}$$

Table 3.0Section I: Internal Calcium Concentration System

$$\frac{dO_c}{dt} = 100.0 [Ca]_i (1.0 - O_c) - 0.238 O_c \quad (3.39)$$

$$\frac{dO_{Tc}}{dt} = 39.0 [Ca]_i (1.0 - O_{Tc}) - 0.196 O_{Tc} \quad (3.40)$$

$$\frac{dO_{TMgC}}{dt} = 100.0 [Ca]_i (1 - O_{TMgC} - O_{TMgM}) - 0.0033 O_{TMgC} \quad (3.41)$$

$$\frac{dO_{TMgM}}{dt} = 0.1 [Mg]_i (1 - O_{TMgC} - O_{TMgM}) - 0.333 O_{TMgM} \quad (3.42)$$

$$O_b = 15 \times 10^{-6} \frac{dO_c}{dt} + 84 \times 10^{-6} \frac{dO_{Tc}}{dt} + 168 \times 10^{-6} \frac{dO_{TMgC}}{dt} \quad (3.43)$$

$$\frac{d[Ca]_i}{dt} = \frac{2}{2 Vol_i} \frac{I_{NaCa} - I_{Ca} - I_{CaP}}{96500} + \frac{O_b}{Vol_i} \quad (3.44)$$

$$\text{Vol}_1 = 2.5 \times 10^{-3} \text{ nanolitres}$$

Table 3.1Sinus-Venosus Equations and ValuesSection A: Main Membrane Equation and Units

$$\frac{dV}{dt} = \frac{I_{stim} - I_{Ca} - I_K - I_{Background} - I_{NaK} - I_{NaCa} - I_{Cap}}{C_m} \quad (3.45)$$

$$C_m = 0.075 \text{ nanofds}$$

$[ ]_i$  = intracellular concentration in millimolar

$[ ]_c$  = cleft concentration in millimolar

$[ ]_b$  = bulk concentration in millimolar

$Vol_i$  = available intracellular volume in nanolitres

$Vol_c$  = cleft volume in nanolitres

$O_*$  = Occupancy (scalar)

$I_*$  = current in nanoamps

$\frac{d[ ]}{dt}$  =  $\frac{\text{millimolar}}{\text{millisecond}}$

$V_m$  = membrane voltage in millivolts

$$\frac{dV_m}{dt} = \text{millivolts/millisecond}$$

$$E_{*} = \text{reversal potential in millivolts}$$

$$\tau^{-1} = \text{rate constant in msec}^{-1}$$

$$C_m = \text{capacitance in nanofds}$$

Table 3.1Section B: Background Current System

$$I_{\text{Background}} = I_{\text{NaBack}} + I_{\text{CaBack}} \quad (3.46)$$

$$I_{\text{NaBack}} = 0.000115 (V_m - 54.0) \quad (3.47)$$

$$I_{\text{CaBack}} = 0.0000003 (V_m - 54.0) \quad (3.48)$$



Table 3.1Section C: The Transient Calcium Current System

$$I_{Ca} = \overline{I_{Ca}} \cdot f \cdot d \quad (3.49)$$

$$\frac{df}{dt} = f_{\infty}^{-1} \tau_f^{-1} - f \tau_f^{-1} \quad (3.50)$$

$$\tau_f^{-1} = 0.0197 \exp(-(0.0337(V_m + 10))^2) + 0.02 \quad (3.51)$$

$$f_{\infty} = \frac{1}{1 + \exp((35.1 + V_m)/8.6)} + \text{Reactivation} \quad (3.52)$$

$$\text{Reactivation} = \frac{0.8}{1 + \exp((50 - V_m)/20)} \quad (3.53)$$

$$\tau_d^{-1} = \frac{0.035 (V_m + 10)}{(1 - \exp(-(V_m + 10)/6.24))} d\infty \quad (3.54)$$

$$d_{\infty} = \frac{1.0}{1 + \exp(-(10 + V_m)/6.24)} \quad (3.55)$$

$$\overline{I_{Ca}} = \frac{1.82 \times 10^{-6} \times 4 \times 96500 \times 0.039 \ V_m ([Ca]_i \exp(2 V_m / 0.039) - [Ca]_o)}{\exp(2 V_m / 0.039) - 1} \quad (3.56)$$

Table 3.1

Section D: The delayed rectifier current system:

$$I_K = n^2 \overline{I_K} \quad (3.57)$$

$$\frac{dn}{dt} = (1-n)\alpha_n - n\beta_n \quad (3.58)$$

$$\alpha_n = \frac{0.0000144 (V_m + 26.5)}{1 - \exp(-0.128 (V_m + 26.5))} \quad (3.59)$$

$$\beta_n = 0.000286 \exp(-0.038 (V_m + 26.462)) \quad (3.60)$$

$$\overline{I_K} = 0.0115 \cdot ((V_m - E_K) + \text{Rectification}) \quad (3.61)$$

$$\text{Rectification} = \frac{95.0}{1 + \exp((V_m - E_K - 78)/25)} - 95.0 \quad (3.62)$$

$$E_k = 59 \log_{10} \frac{[K]_c}{[K]_1} \quad (3.63)$$

Table 3.1Section E: Pump and exchange current systems

$$I_{NaK} = \overline{I_{NaK}} \frac{[Na]_i^3}{[Na]_i + 5.46} \frac{[K]_o^2}{[K]_o + 0.621} \quad (3.64)$$

$$\overline{I_{NaK}} = 0.0772 \text{ nanoamps}$$

$$I_{Cap} = \overline{I_{Cap}} \cdot \frac{[Ca]_i}{[Ca]_i + 0.001} \quad (3.65)$$

$$\overline{I_{Cap}} = 0.00675 \text{ nanoamps}$$

$$I_{NaCa} = \frac{4 \times 10^{-6} ([Na]_i^3 [Ca]_o \exp(.0195 V_m) - [Na]_o^3 [Ca]_i \exp(-.0195 V_m))}{1 + .0001 ([Ca]_i [Na]_o^3 + [Ca]_o [Na]_i^3)} \quad (3.66)$$

Table 3.1Section F: External 'Cleft' Concentration System

$$\frac{d[Na]_c}{dt} = \frac{[Na]_b - [Na]_c}{\tau_p} + \frac{3I_{NaK} + 3I_{NaCa} + I_{NaBack}}{F Vol_c} \quad (3.67)$$

$$\frac{d[K]_c}{dt} = \frac{[K]_b - [K]_c}{\tau_p} + \frac{-2I_{NaK} + I_K}{F Vol_c} \quad (3.68)$$

$$\frac{d[Ca]_c}{dt} = \frac{[Ca]_b - [Ca]_c}{\tau_p} + \frac{-2I_{NaCa} + I_{Ca} + I_{Cap} + I_{CaBack}}{2F Vol_c} \quad (3.69)$$

$$F = 96500$$

$$\tau_p = 10000.0 \text{ milliseconds}$$

$$Vol_c = 0.0004 \text{ nanoliters}$$

Table 3.1Section G: Internal Sodium and Potassium Concentration Systems

$$\frac{d[Na]_i}{dt} = \frac{-I_{NaB} - 3I_{NaCa} - 3I_{NaK}}{F Vol_i} \quad (3.70)$$

$$\frac{d[K]_i}{dt} = \frac{-I_K + 2I_{NaK}}{F Vol_i} \quad (3.71)$$

$$F = 96500$$

$$Vol_i = 2.5 \times 10^{-3} \text{ nanolitres}$$

Table 3.1Section H: Internal Calcium Concentration System

$$\frac{dO_c}{dt} = 100.0 [Ca]_i (1.0 - O_c) - 0.238 O_c \quad (3.72)$$

$$\frac{dO_{Tc}}{dt} = 39.0 [Ca]_i (1.0 - O_{Tc}) - 0.196 O_{Tc} \quad (3.73)$$

$$\frac{dO_{TMgC}}{dt} = 100.0 [Ca]_i (1 - O_{TMgC} - O_{TMgM}) - 0.0033 O_{TMgC} \quad (3.74)$$

$$\frac{dO_{TMgM}}{dt} = .1 [Mg]_i (1 - O_{TMgC} - O_{TMgM}) - 0.333 O_{TMgM} \quad (3.75)$$

$$O_b = 15 \times 10^{-6} \frac{dO_c}{dt} + 84 \times 10^{-6} \frac{dO_{Tc}}{dt} + 168 \times 10^{-6} \frac{dO_{TMgC}}{dt} \quad (3.76)$$

$$\frac{d[Ca]_i}{dt} = \frac{2}{2 Vol_i} \frac{I_{NaCa} - I_{Ca} - I_{CaP}}{96500} + \frac{O_b}{Vol_i} \quad (3.77)$$



$$\text{Vol}_1 = 2.5 \times 10^{-3} \text{ nanolitres}$$

### III.1 Methods of Integration.

The complete model of the electrophysiological activity a unit patch of atrial cell membrane requires the solution of a 16th order differential equation, while the sinus venosus model requires the solution of a 14th order differential equation. In the atrial model the time constants involved can vary from 10's of useconds (sodium activation kinetics) to 10 seconds (perfusion time constant). As a result of this range of time constants (6 orders of magnitude), double precision arithmetic was used in all calculations, so that numerical errors resulting from truncation due to finite precision arithmetic could be minimized. A sufficiently small step in the calculation procedure was taken to ensure that the finite difference equation was an adequate approximation to the solution of the most quickly changing variable, without corrupting the solution of the most slowly changing variable by repeatedly adding zero due to truncation effects of finite precision arithmetic.

To cut down on computation time and to insure accurate numerical integration of the system of equations, a variable step-size algorithm was adopted. The change in each of the gating variables, the change in each fractional occupancy and the change in membrane potential were all monitored by the integration routine. The amount that each of these monitored variables was allowed to change per step was limited as follows:

$$\frac{dV}{dT} < 0.15 \text{ mV/sec} \quad (3.78)$$

$$\frac{d\text{Occupancy}}{dT} < 0.02 \text{ msec}^{-1} \quad (3.79)$$

and

$$\frac{d \text{ Gating Variable}}{dT} < 0.02 \text{ msec}^{-1} \quad (3.80)$$

This is how the stepsize was adjusted to ensure the correct numerical integration of the most quickly changing gating variable as suggested in Moore and Ramon (1974). The "correctness" of numerical integration was checked by adjusting the stepsize algorithm and testing for insensitivity of solution to stepsize (Burden and Faires, 1985). A limit on the length of a step was set at 0.1 msec (Bristow and Clark, 1982).

A fourth order Runge-Kutta method was used in conjunction with the variable stepsize algorithm to accomplish numerical integration. Runge-Kutta is a single step method, it depends only upon the current state of the system and has been found to be a highly reliable method for Hodgkin-Huxley equations (Moore and Ramon, 1974). A single step method was chosen over a multi-step method because it depends only on the current state of the system to take the next step, while a multi-step method requires that a recent history of the system be recorded so that a higher order approximation to the function to be solved may be used.

Unfortunately whenever a nonanalytic input is injected into the system, such as a voltage clamp or current stimulus, the higher order approximation is no longer valid and the history needs to be restarted using a single step method. In the interest of producing simple, easily readable and adaptable code the single step method was chosen.

The present simulation program was implemented in Fortran and was written with modification and transportability in mind. Various versions of the model program have been run on a VAX 11-750 using VMS, a VAX 11-750 using Unix, a Hewlett-Packard 9000 using Unix, and a Cyber 205 using NOS. The modifications of the code necessary for running on these computers involved only minor adjustment of input and output statements. The same program can be used to simulate atrial or sinus behavior, either considering only the single cell or including restricted extracellular spaces; it can also reproduce some pharmacological blocker phenomena.

### III.2 Testing the Atrial Model.

Having an atrial model based on voltage clamp results and computer program to implement it, the important question becomes: Does it function acceptably? This can be assessed by determining which experimental results it can successfully reproduce.

The first test for any such model involves simulation of a membrane (non-propagated) action potential. Do the characteristics of this action potential fall within the range of experimentally observed action potentials with regard to resting potential, amplitude, and duration and is the detailed shape of the action model something that closely resembles observed action potentials?

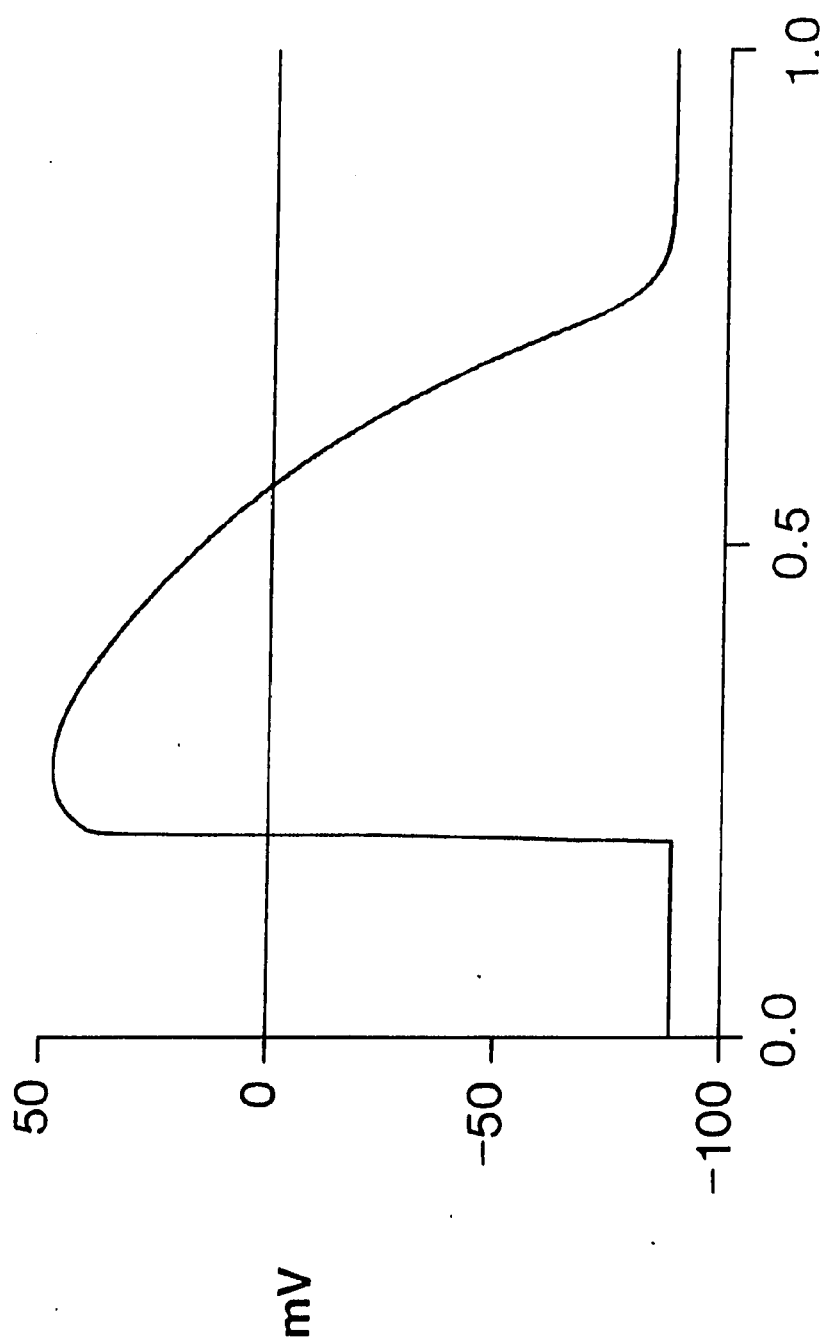
Figure 3.0 shows that this model produces an acceptable atrial action potential. When the parameters describing the model action potential are compared to the average parameters of the experimentally observed action potentials, the model succeeds in reproducing the results (listed in table 3.2) closely, considering the standard error of measurement associated with each of the experimental findings. The model action potential duration (480 msec) is somewhat less than the experimental action potential duration ( $722.5 \pm 106.3$  msec) (Table 3.2). Here it is important to note that a model based upon the average of several voltage clamp results may not produce a completely average action

Table 3.2  
Atrium  
 A Comparison of Experimental and Model Action Potential Characteristics

	Hume and Giles (1981) n=12	Hume and Giles (1983) n=9	Model
Resting Potential	-88.6 mV	-89.6 mV	-89 mV
Amplitude	124.4 mV	131.6 mV	137 mV
Duration	722.5 mSec	772.5 mSec	43.4 480 mSec
Upstroke Velocity	42.2 V/Sec	-----	40 V/sec
Overshoot	35.1 mV	42 mV	48 mV

Figure 3.0

The Atrial Model Action Potential. This is the model generated atrial action potential.





potential. The model however, should be able to characterise action potentials within the range of experimental observations. In analyzing available data, one observes considerable variability in measured conductances, as well as in the waveshape or experimental action potentials, particularly in single cells (W. Giles personal communication). Three different frequently observed action potentials are shown in Figure 3.1. Taking the longest duration action potential of these and overlaying it on the model action potential (Figure 3.2) we can see both similarities and discrepancies. These discrepancies can be minimized by scaling the conductances of the channels. Figure 3.3 shows the results of changing the magnitude of various channels to obtain a reasonably good fit to the experimental action potential. In this case five conductances were changed:

$I_{Ca}$  increased by 30% .

$I_K$  decreased by 20%.

$I_{K_1}$  decreased by 20%.

$I_{Nab}$  decreased by 33%.

$I_{Na}$  decreased by 35%.

None of these modifications seems unreasonable given the cell to cell variability indicated by the standard deviation (Standard error  $\times N$ ) in the measurements. In previous modelling studies it has not been standard practice to show a model fit to

Figure 3.1

Three different observed action potentials. Note that they all differ in amplitude duration and shape.

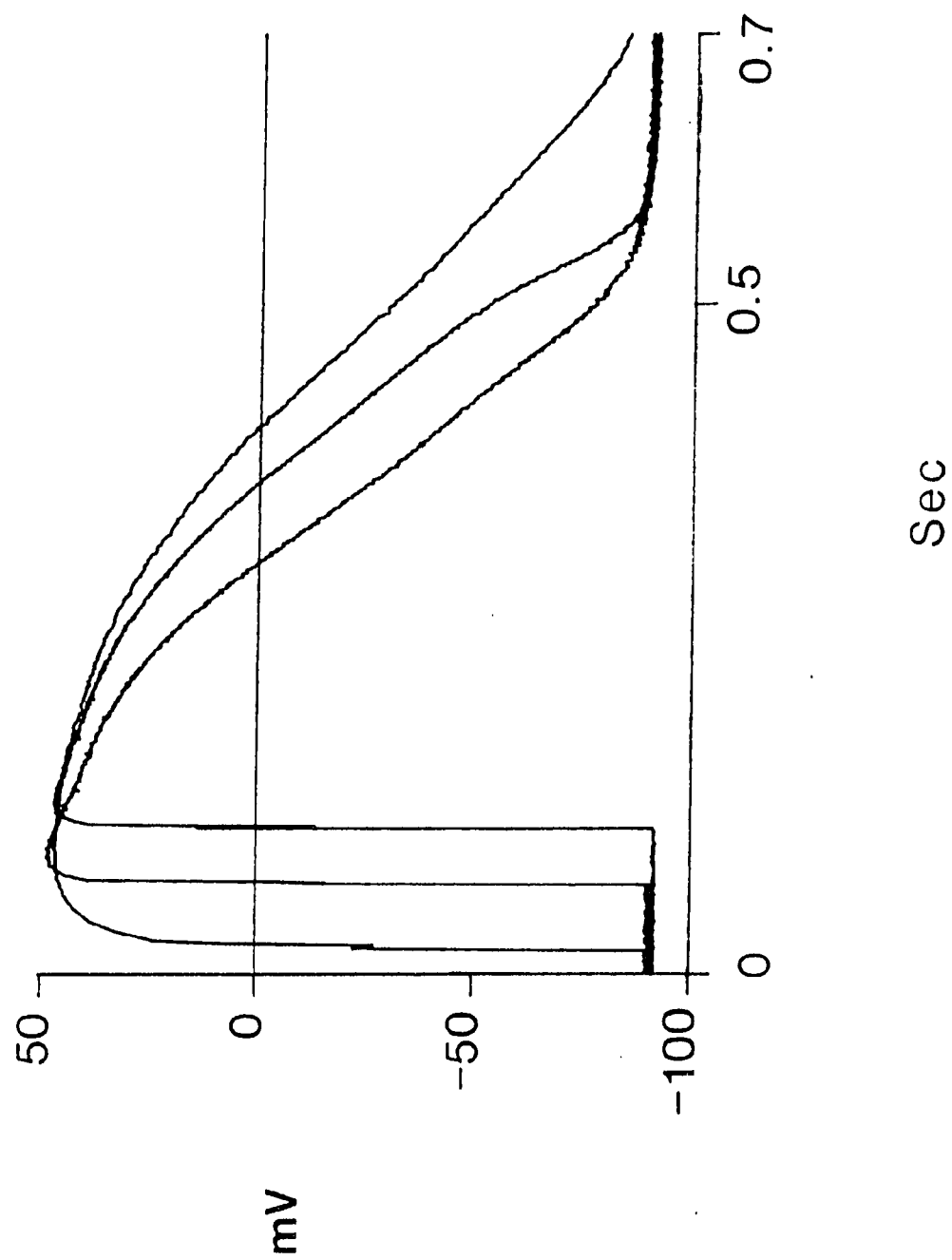


Figure 3.2

The overlay of the model action potential with the longest duration action potential from figure 3.1. Note that although the model action potential seems appropriately shaped it does not have the duration of the experimentally observed active potential.

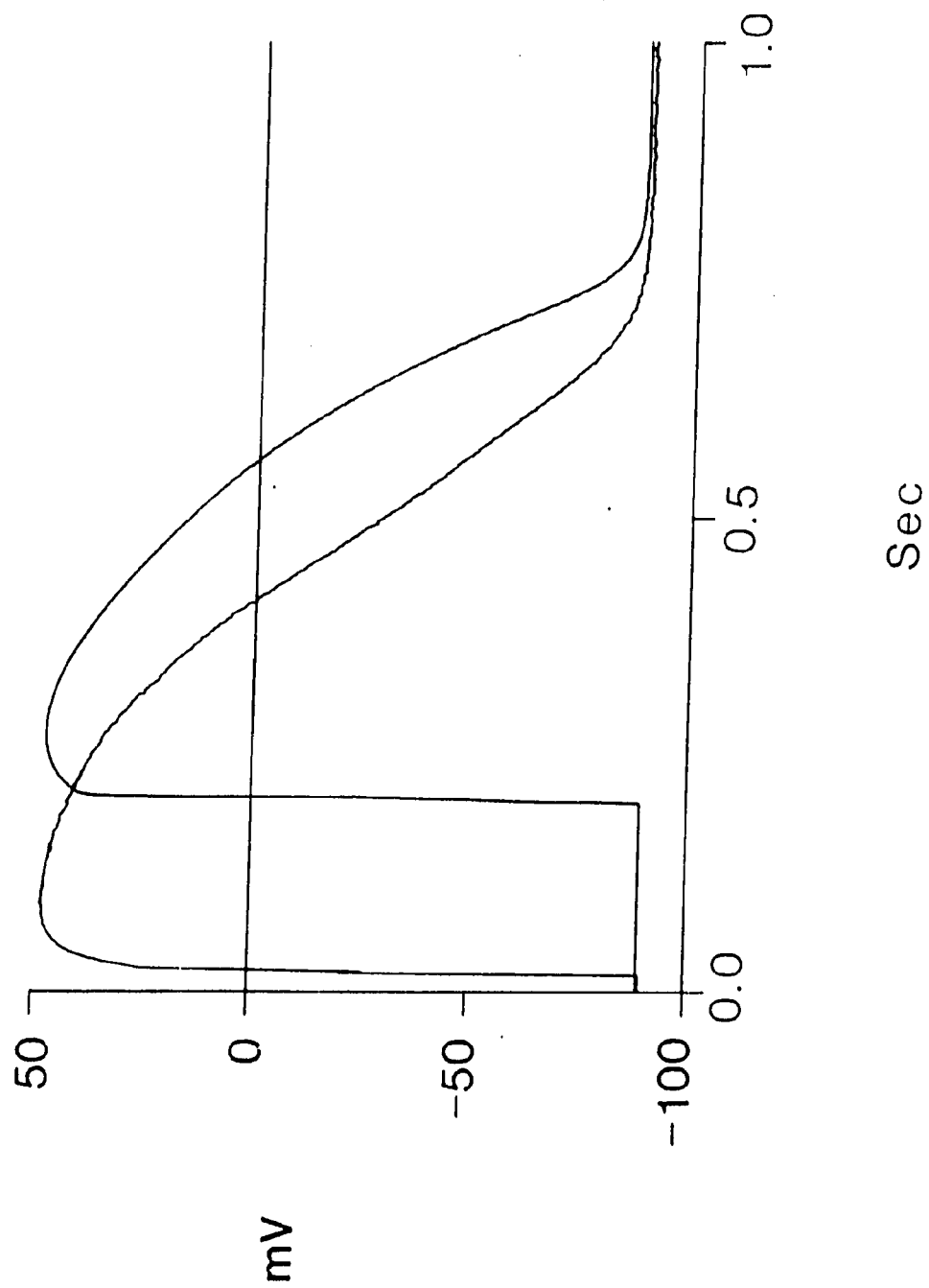
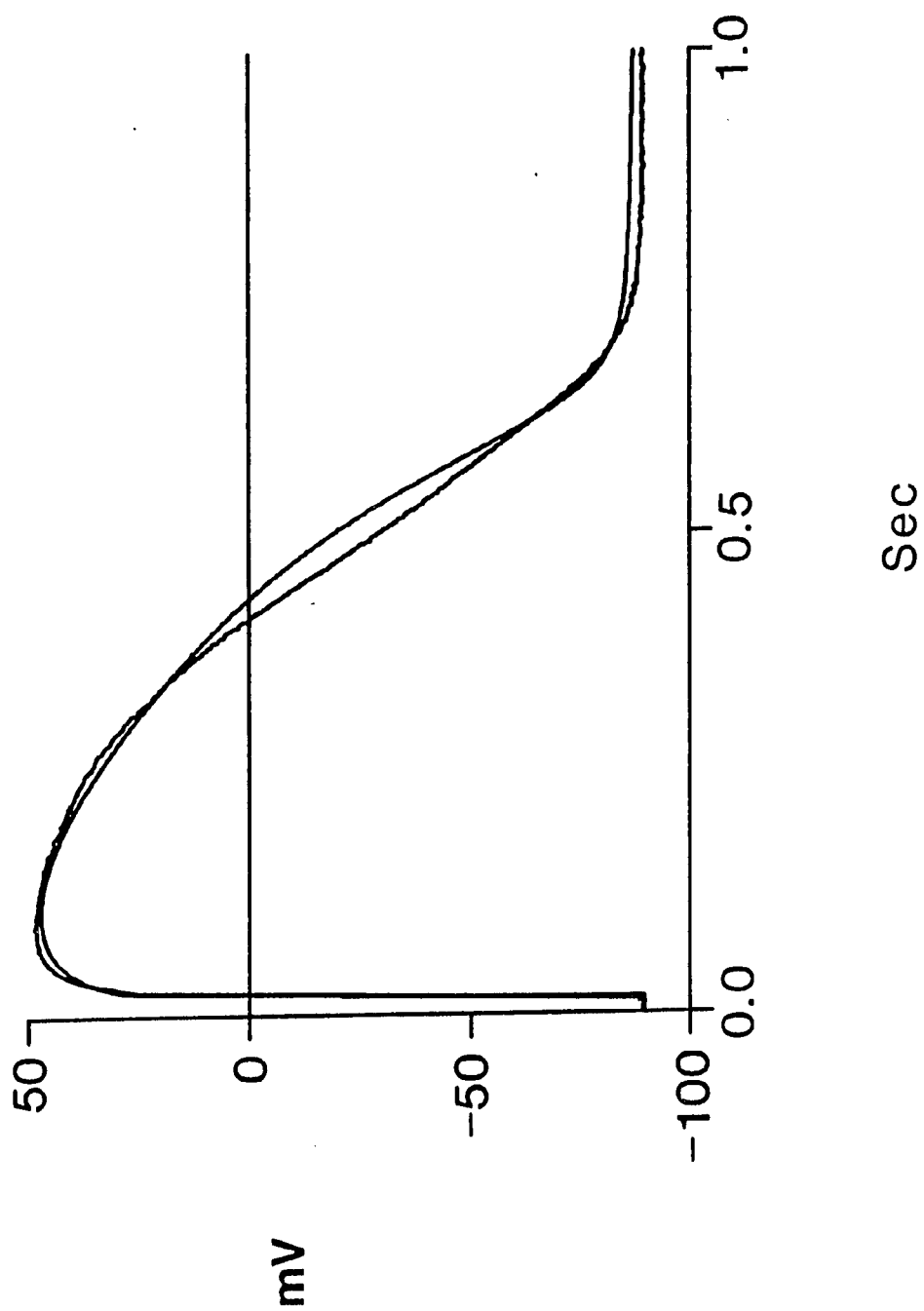


Figure 3.3

A match of the model atrial action potential to an experimentally observed action potential by changing the model conductances.



an adopted 'standard' action potential (eg. McAllister, Noble and Tsien (1975); Beeler and Reuter (1977); Yangihara, Noma, Irisawa (1980); DiFrancesco and Noble (1985)). The ability to reproduce experimentally observed action potentials is certainly one measure of the adequacy of such a model. In matching the waveshape of an action potential in Figure 3.3 by reasonable adjustment of the magnitudes of underlying currents one may also show that the time dependence of the current systems are appropriate. The current densities of the original formulation (based on average voltage clamp data) still represent a "best guess" as to actual current densities, so they will be used in all further simulations, especially in simulations concerning concentrations.

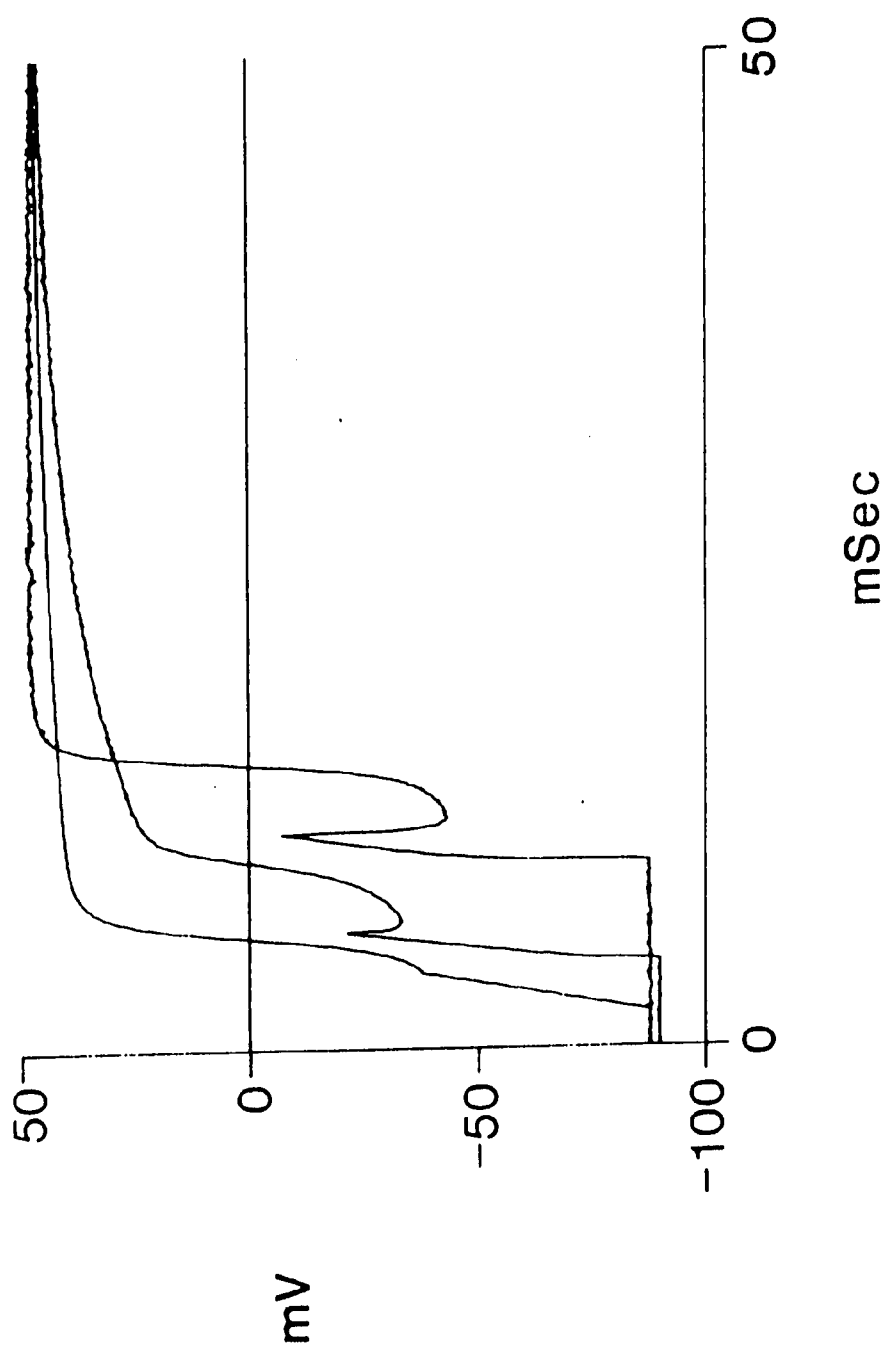
The leading edge or rapid upstroke of the atrial action potential also varies from cell-to-cell. Figure 3.4 shows two such experimental results, along with the model generated result. Note that the model action potential 'takes off' at a very similar potential to the experimental action potentials. The maximum rate of rise is similar. The slow, secondary depolarization begins near 35 mV ; i.e. within the same ranges of potential and with a similar time-course.

However, there are two significant discrepancies between the model and experimental results. First is the lack of a 'spike' on the leading edge of the model action potential. This spike is a result of the non-zero series resistance of the single



Figure 3.4

The leading edge of the atrial action potential. The two experimental action potentials may be identified by the "spike" artifact due to the series resistance of the stimulation electrode.



microelectrode. Since both stimulus current is injected and potential is measured through this electrode a potential difference is measured as a result of the stimulus current pulse. This manifests itself as an upward voltage step at the beginning of the stimulus current pulse and an equal negative voltage step at the end of the current pulse. Hence the 'spike' is merely an artifact of the measuring apparatus.

Secondly, the sigmoidicity of turn on, i.e. the delay following stimulation prior to the rapid upstroke phase is more pronounced in the experimental action potentials. Very likely a portion of the delay of the rapid upstroke is due to the cable properties of single atrial cells (W. Giles, and R. Clark, personal communication). The model assumptions are of a uniform patch of membrane and are not intended to reproduce effects due to the non-uniformities arising from the cable properties of single bullfrog atrial cells.

A series of two model action potentials stimulated at a frequency of 0.5 Hz until any initial condition consequences are minimized in Figure 3.5. The stimulus was 1.2 nanoamps in the depolarizing direction for 4 milliseconds. The relative magnitudes of the underlying membrane currents are displayed in Panel B. The transient sodium current is much larger than the other membrane currents and thus cannot be fully illustrated on the side

Figure 3.5

The action potential and underlying currents.

Panel A

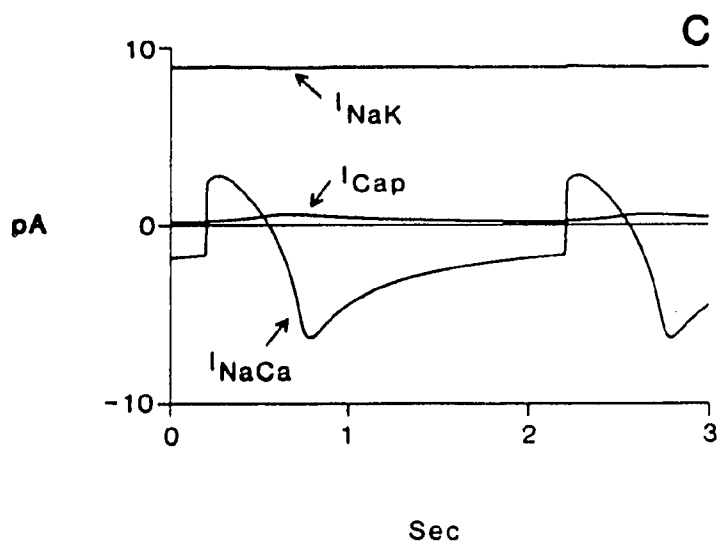
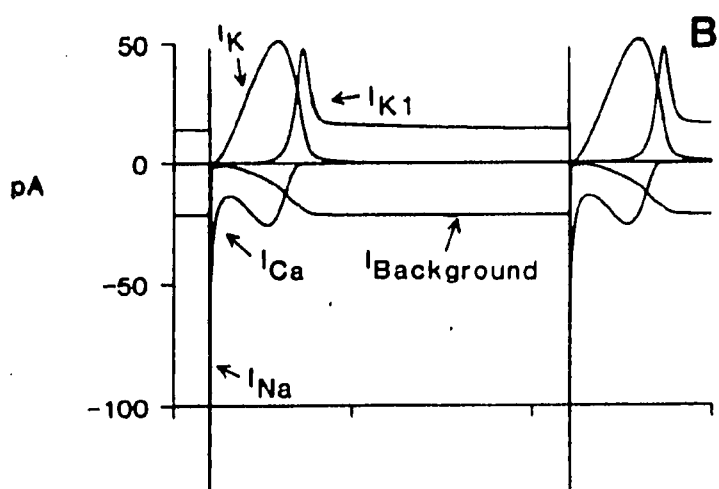
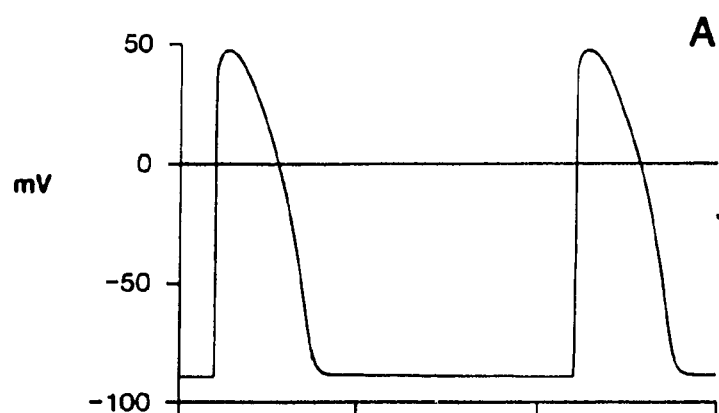
Two atrial action potentials elicited at a frequency of  
.5 hz.

Panel B

The underlying channel currents.

Panel C

The underlying pump and Exchange currents.



of this plot window. Panel C shows the underlying pump and exchanger currents for the model which are relatively smaller in amplitude but much slower in time course.

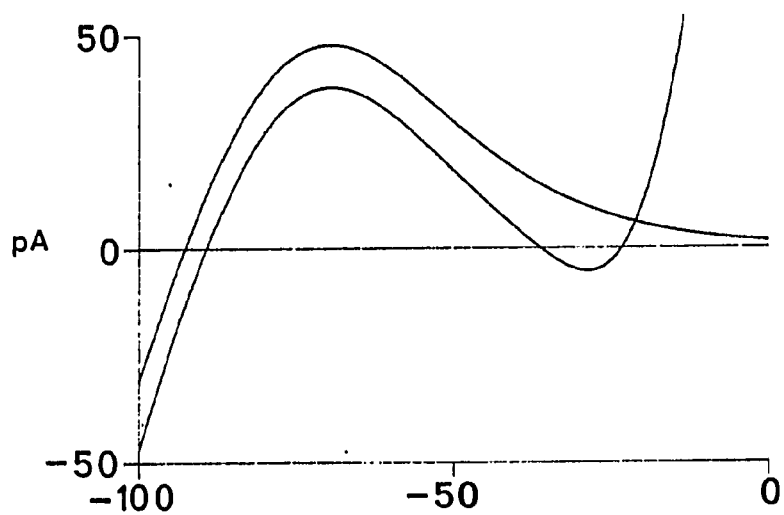
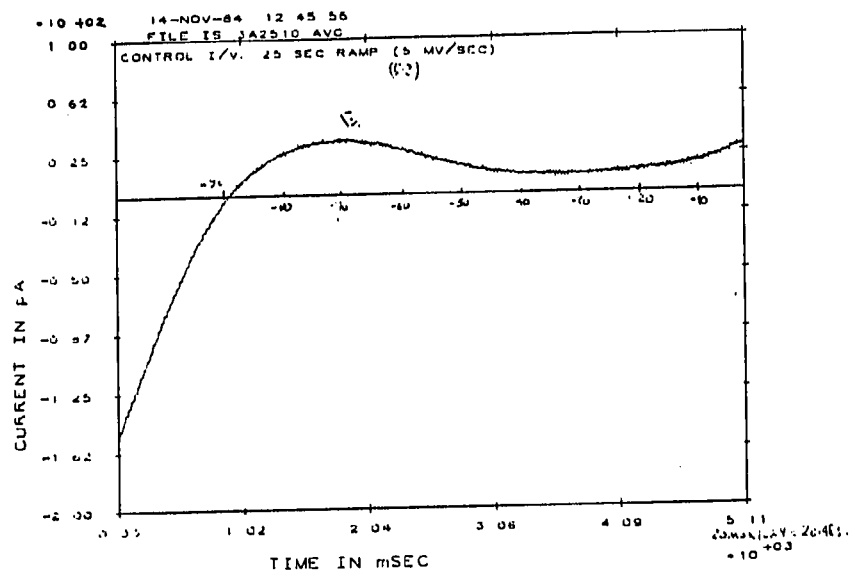
Thus, the model produces reasonable, repeatable action potentials. The next sections examine the ability of the model to reproduce the experimental voltage clamp results upon which it is based.

### III.2.1 Background Currents.

Figure 3.6, Panel A shows the results of an experimental protocol designed to identify the background (time-independent) currents in the range of potentials negative to -30 millivolts. These experimental results were generated as follows: The cell was clamped negative to its resting potential and a slow ramp input was applied (5 mV/sec) which allowed the membrane current to reach steady-state at all potentials. Note that positive to -30 mV the delayed rectifier begins to be activated. This experimental protocol was reproduced with the atrial model (Figure 3.6, Panel B). In the range negative to -30 the results match well; both have a peak in outward current at -70 mV and reverse near -90 mV. The current in the model generated result is slightly larger in magnitude than the experimental result. This can be attributed to the fact that the experimental result was obtained in the cold (6° C). This temperature difference would be expected to slow the experimental delayed rectifier gating kinetics, which may account

Figure 3.6

A measurement of the background currents generated by a slow ramping potential (5mV/sec). Panel A is the experimental measurement and panel B is the model generated result with the actual  $I_{K1}$  superimposed.





for the differences in outward current at the potentials positive to -30 mV.

### III.2.2 The Transient Sodium Current.

Figure 3.7 shows peak current values for an experimentally observed TTX-sensitive transient inward current (Panel A) and a model generated result (Panel B).  $I_{Na}$  peaks near the same (-10 mV) and also has a similar threshold of activation. However, the peak current in the model generated result is larger than the experimentally observed current. This is due to two experimental manipulations used to reduce the experimentally observed  $Na^+$  current. For the purpose of establishing adequate voltage clamp control: (i)  $I_{Na}$  was reduced by recording at  $6 - 10^{\circ}C$  and (ii)  $I_{Na}$  was reduced via partial inactivation by using a depolarized holding potential (-70 mV).

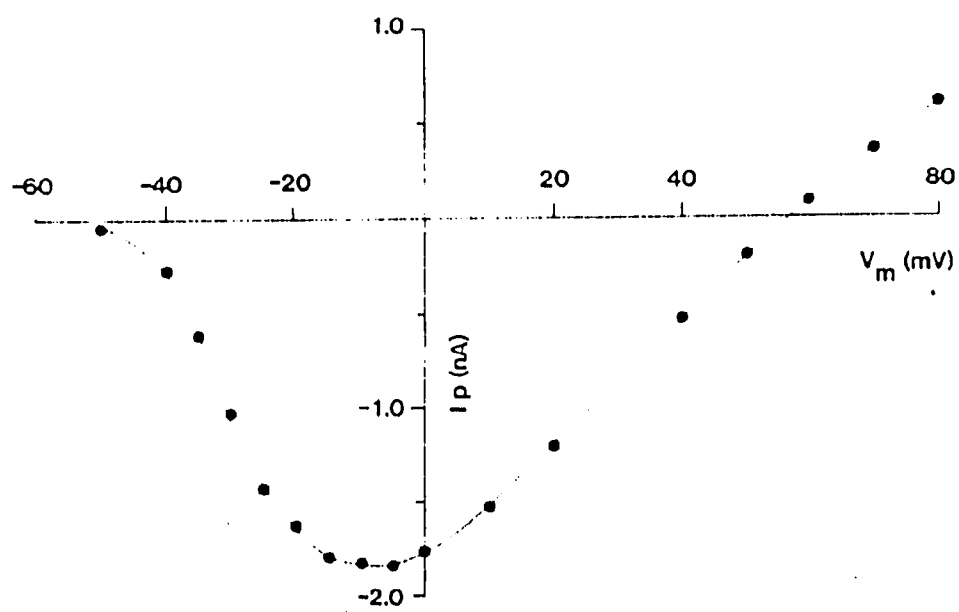
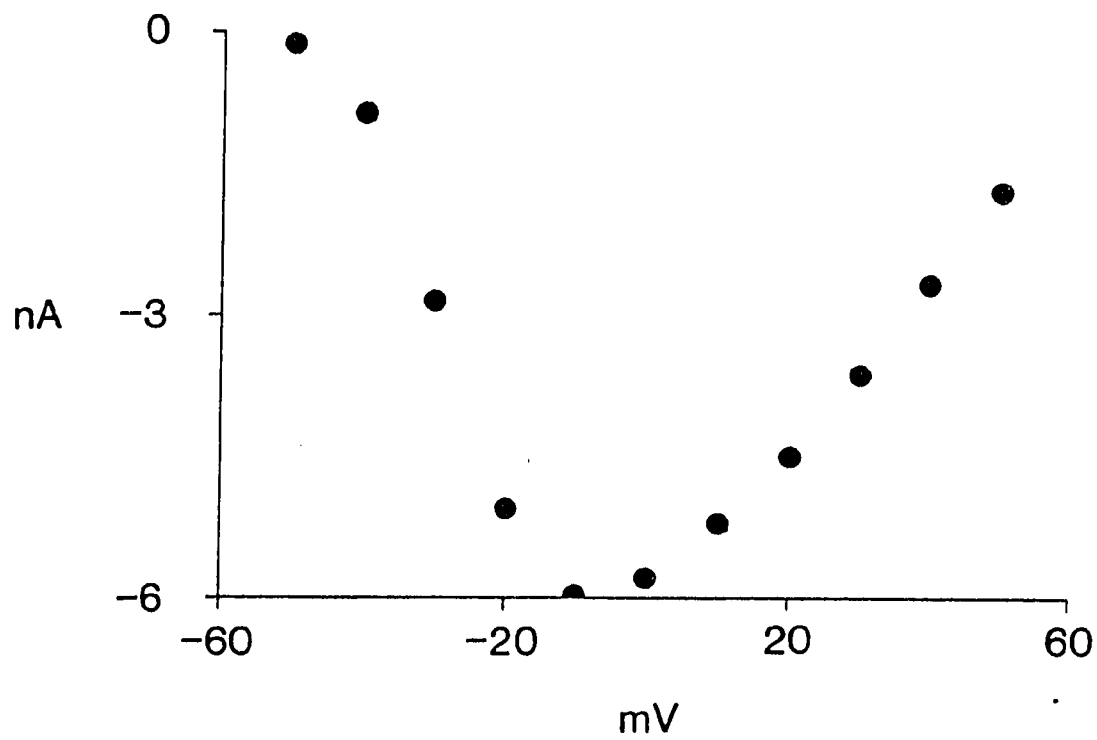
### III.2.3 Transient $Ca^{++}$ Current.

The transient calcium current,  $I_{Ca}$ , is TTX-insensitive, and is measured by blocking the much larger  $I_{Na}$  current with TTX. Representative experimental records are shown in Figure 3.8 (Panel A, from Hume and Giles, 1983). Analogous model generated currents are shown in Panel B. Due to the non-ideal clamp apparatus the experimental calcium measurements contain noticeable capacitive transients but are otherwise similar to the model current traces.

Figure 3.9 shows more quantitative check in which the experimental results of peak inward  $I_{Ca}$  recorded during a voltage

Figure 3.7

Peak current clamp potential for the fast inward ( $I_{Na}$ ) current. Panel B experimental result. Panel A model result.



clamp protocol superimposed upon the model generated results. Over a large portion of the physiologic range (-30 mV to +50 mV) the agreement is quite good; the values usually falling within or near the standard error of measurement of the experimental data.

Positive to +50 mV the model results diverge from the experimental data. This is due to the calcium channel being modelled assuming that it is impermeant to all other ions. The simulation provides agreement over the physiologic range (negative to +50 mV); however, positive to this potential the effects of eg. outward flux of  $K^+$  may dominate (Campbell, 1985; Hess and Tsien, 1984). Since these effects are important only at very depolarized potentials, they have not been included in this present model.

Negative to -30 mV the model results also diverge from the experimental data. This difference occurs in a range in which the inward rectifier ( $I_{K_1}$ ) is generating substantial current, and represents an experimental limitation. This is related to the determination of the zero membrane current level (resting potential) during voltage clamp simulations. The zero current level in this experimental protocol was established by clamping to the resting potential and defining the resulting current level as zero current. The membrane voltage can only be measured and hence 'clamped' with an accuracy of around 5 mV (W. Giles, personal

Figure 3.8

A series of voltage clamp records designed to measure the second inward current in frog Atrium ( $I_{Ca}$ ). Panel A shows typical experimental results. Panel B shows model generated results from the same voltage clamp protocol.

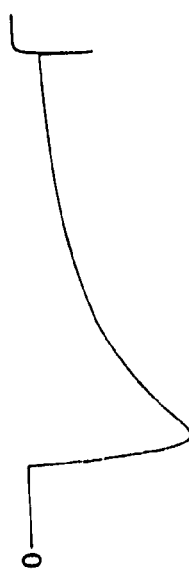
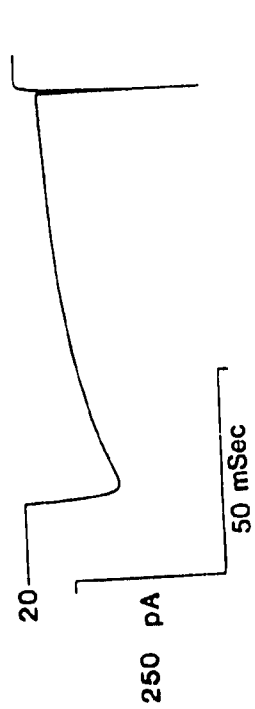
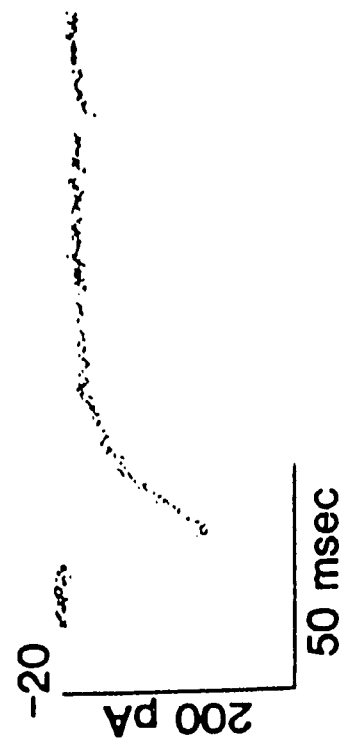
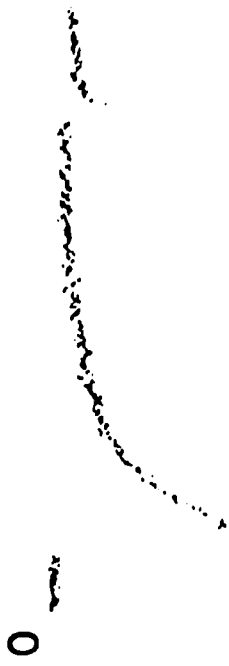
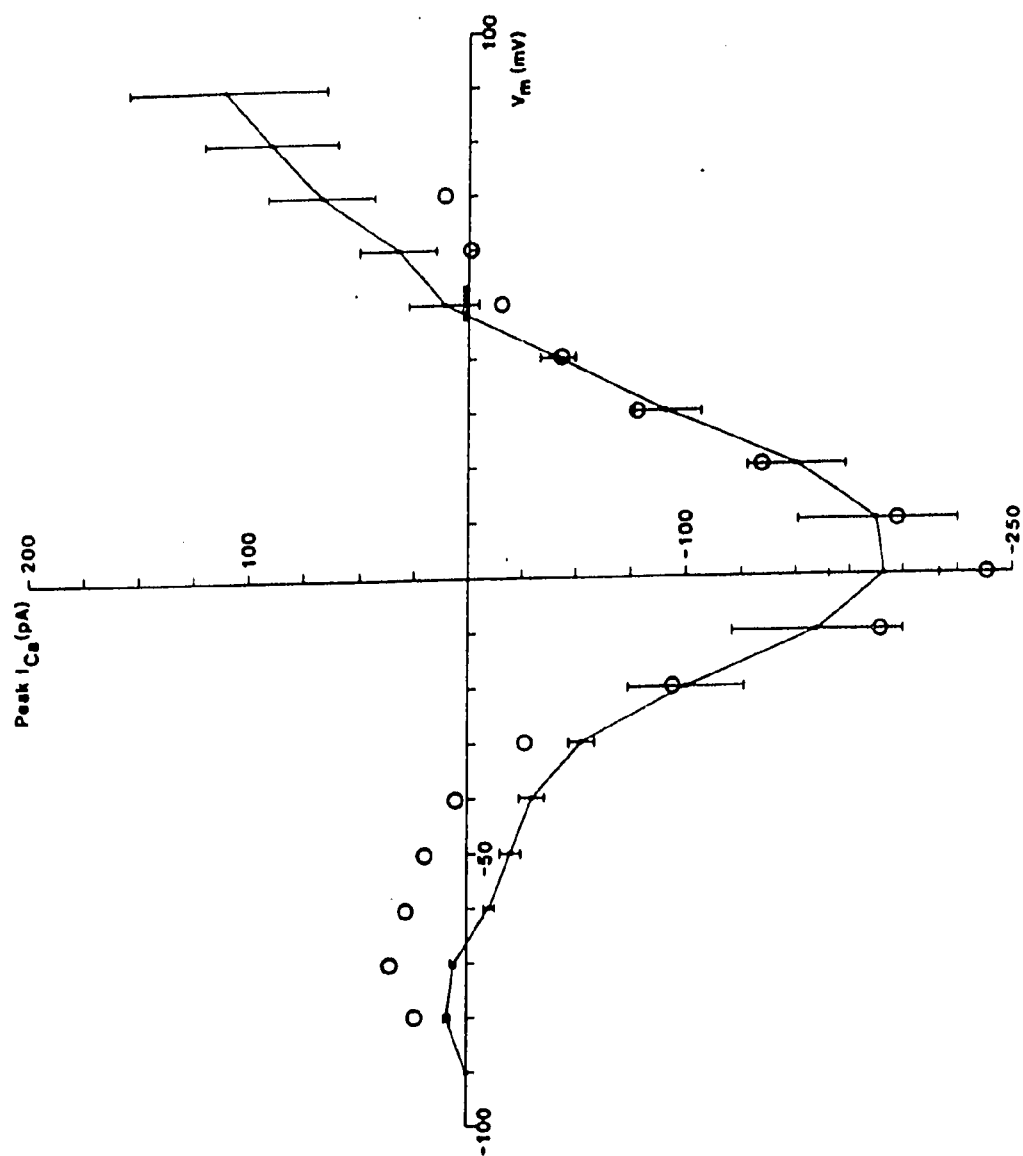


Figure 3.9

A comparison of peak currents for voltage clamp protocols designed to measure  $I_{Ca}$ . dots with standard error bars represent experimental measurements, while o's represent model generated peak currents.





communication) due to effects such as electrode tip potential. Consequently, the membrane may be clamped some 5 mV off of the true resting potential. Since the slope of  $I_{K_1}$  near resting potential is substantial (see background current section) significant errors in the zero current level can occur when the measured current is small (W. Giles, personal communication). The measurements in this range of potentials seem inconsistent with the results concerning the instantaneous rectifier shown previously. The calcium current in the healthy atrial cell in these potential ranges (-90 to -30 mV) is much smaller than and hence dominated by the  $I_{K_1}$  and  $I_{Na}$ . It is perhaps more appropriate to compare in the  $I_{Ca}$  sinus venosus since this tissue lacks both  $I_{K_1}$  and  $I_{Ca}$ . The agreement for the sinus model, in which only the current magnitude has been changed, is much better (see Figure 3.19).

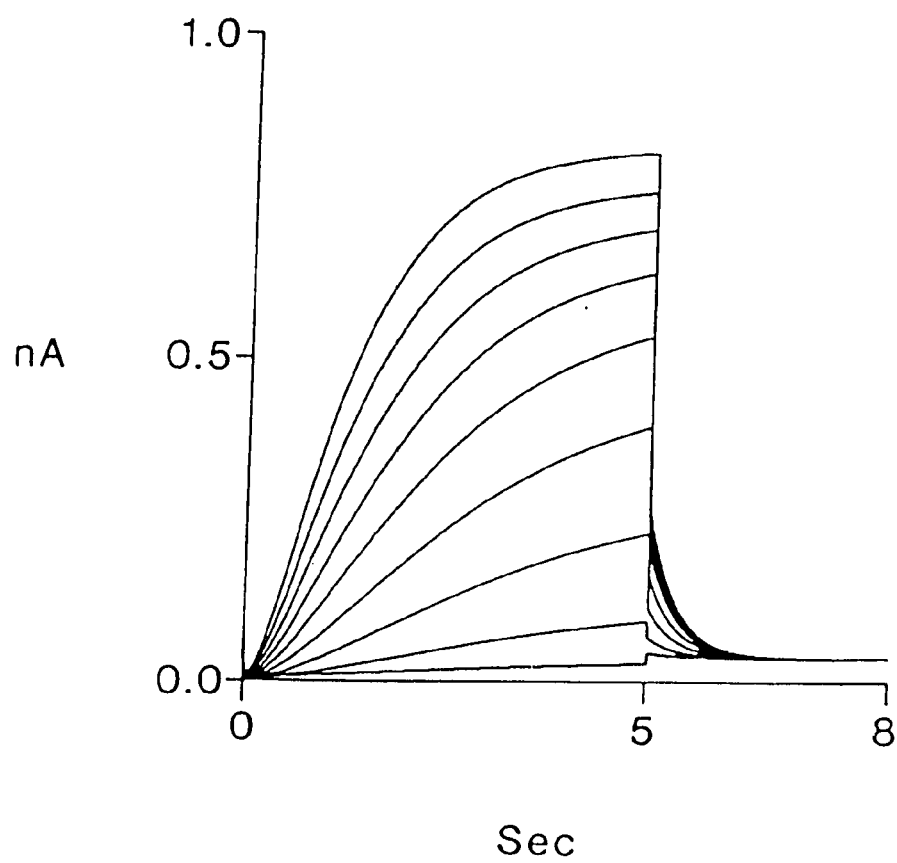
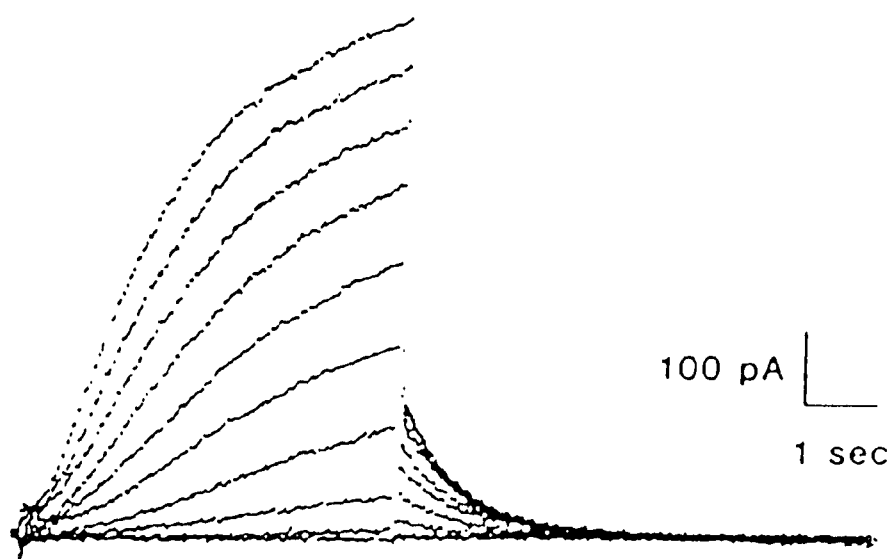
#### III.2.4 The Delayed Rectifier.

Figure 3.10 shows a comparison of experimental observations (Panel A) of the delayed rectifier current,  $I_K$ , and the analagous model results (Panel B). These match very well. In these simulations internal potassium concentration was held constant and internal calcium concentration was held constant.

The internal potassium concentration was fixed in this simulation because no change in internal potassium concentration is can be measured during these protocols. However the integrated

Figure 3.10

Measurement of the delayed rectifier. Panel A shows a set of experimental results from a voltage clamp protocol designed to measure  $I_K$  and Panel B shows the results of the same protocol on the atrial model. The clamp protocol was to hold at -90 mV step to the test potential (-40 mV in the bottom trace by 10 mV increments). The internal concentrations of  $Ca^{++}$  and  $K^+$  were held constant in the model simulation and the  $I_{Na}$  and  $I_{Ca}$  currents were blocked in order to reduce computation time.



K-efflux elicited during a long, large depolarizing pulse in this protocol is a significant fraction of total cell potassium. The reason for this apparent paradox is that potassium ions enter the cell from the electrode and maintain a nearly constant level of  $(K^+)_{\text{i}}$ . The internal calcium concentration was also held constant during this protocol. This was necessary since following the long depolarization the presence of a considerable  $Na^+/Ca^{++}$  exchange current upon a return to resting levels (i.e. during the 'tails') could obscure  $I_K$  tails.

Obviously the internal calcium concentration varies during these experiments; however a 10-second depolarization is a substantially non-physiologic situation. Important reservations arise concerning the modelling of calcium regulatory mechanisms in this situation. The voltage-dependence of the calcium pump is completely unknown, and its role in calcium regulation might be considerably enhanced during depolarization. This might mean that internal calcium concentration during depolarizing pulses is considerably over estimated. The calcium channel current has not had its kinetics studied during such a long depolarizing pulse, which might mean that some very slow form of inactivation of the calcium channel has been overlooked and hence not modelled. Reduction of calcium entry via the calcium channel current may not be entirely sufficient to eliminate calcium influx into the cell. Calcium may

enter the cell via the mechanism of the  $\text{Na}^+/\text{Ca}^{++}$  exchanger running 'backwards' (i.e. outward) during depolarization.

### III.2.5 Extracellular Compartment.

To test the extracellular compartment model formulation the membrane model was stimulated at a rate of 0.5 Hz for a 'long time' (i.e. 60 seconds) and an action potential was recorded for the model in the absence of the restricted extracellular space and displayed in Figure 3.12, Panel A. Note that the action potential is nearly identical in shape to the action potential generated in the absence of a restricted extracellular space. The time course of the changes in extracellular potassium and calcium concentration are shown in Panel B. The change in  $\text{K}^+$  concentration is similar in time course to that observed by Morad (1980) in bullfrog ventricle (3.12 Panel A) using  $\text{K}^+$ -sensitive microelectrodes, but is significantly smaller in magnitude. It has been noted that the experimental observations of  $\text{K}^+$  accumulation may contain significant artifacts, due to physical difficulty placing a microelectrode into contractile tissue (Coulombe and Corabouef, 1983) without injuring adjacent cells.

Optical measurements of the calcium depletion occurring during the course of a single beat in frog ventricles (3.12 Panel D Cleeman, Pizarro, and Morad, 1984) are similar in time-course;

Figure 3.11

Accumulation/Depletion in the restricted extracellular space during an action potential.

Panel A

A model action potential elicited after repetitive stimulation for a period of 60 seconds.

Panel B

The time course of cleft  $K^+$  and  $Ca^{++}$  concentration during the single action potential.

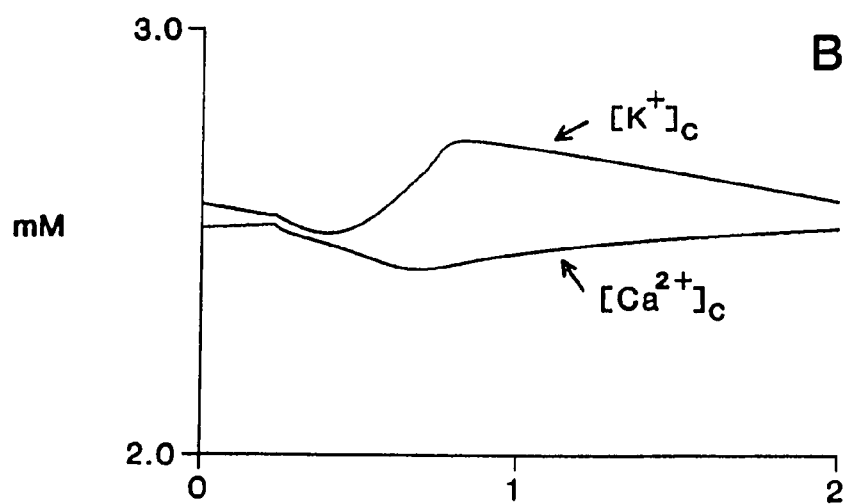
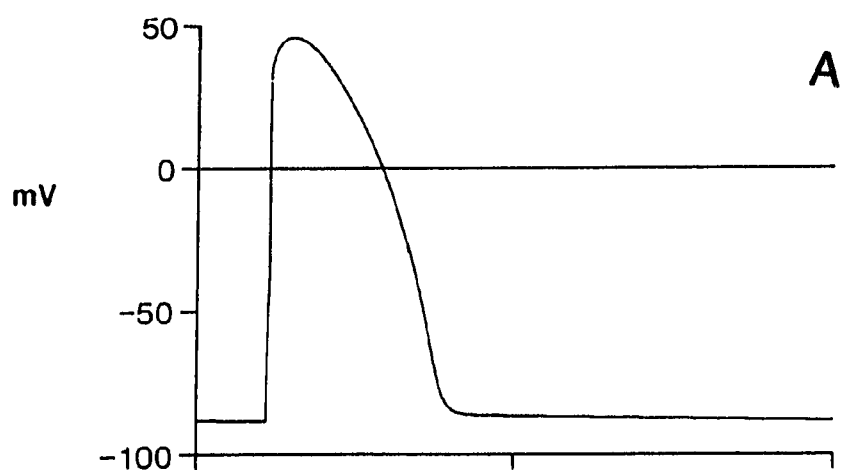


Figure 3.12

Accumulation/Depletion in the restricted extracellular space during an action potential.

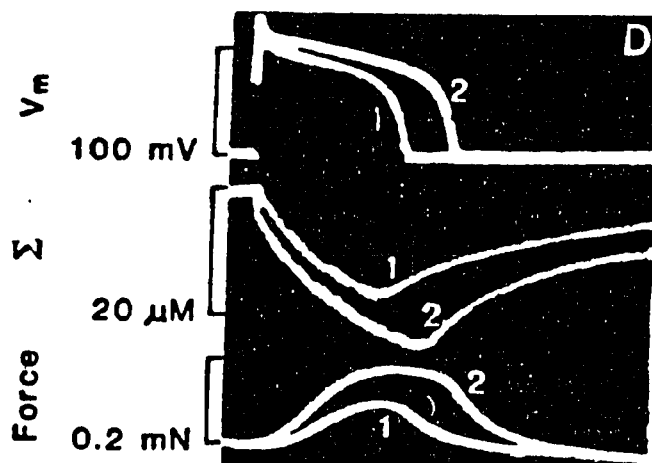
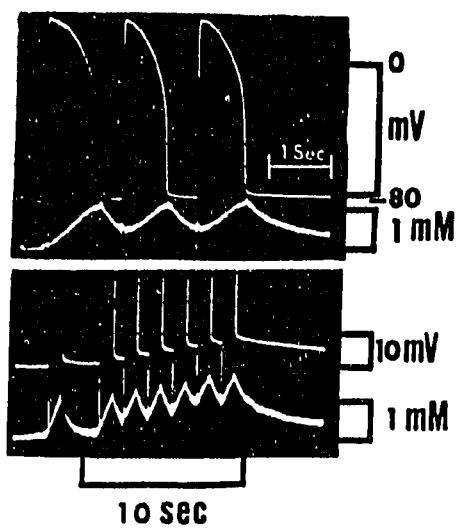
Top

The  $K^+$  sensitive micro-electrode measurements of Morad (1980) in the restricted extracellular space of Bullfrog Ventricle.

Bottom

The optical measurements of Cleeman, Pizarro and Morad (1984) of the time course of  $Ca^{++}$  concentration in the extracellular spaces of Bullfrog ventricle.





although the magnitude of this  $\text{Ca}^{2+}$  depletion effect is again different possibly due to the relatively low calcium concentration in these experiments. The time-course of calcium depletion in the extracellular space is similar in measurements indicate that there is a fairly steady calcium influx into the cell over most of the action potential, while most of the calcium extrusion occurs subsequent to repolarization in both experiment and model.

### III.2.6 Intracellular Compartment.

The internal concentrations of three major ionic species can be monitored continuously during the atrial simulation. Of these it is generally accepted that  $[\text{K}^+]_i$  remains fairly constant in a normally beating cell and  $[\text{Na}]_i$  does not shift substantially, even after repeated rapid stimulation, in frog atrium (Wayne Giles personal communication). As expected, calcium undergoes substantial variation during an action potential. Figure 3.13, Panel A shows the same two action potentials shown in Figure 3.13 earlier. Panel B shows the model predictions of internal sodium and potassium concentrations during these two beats, and demonstrates that they do not change significantly during a normal action potential.

Internal calcium concentration on the other hand, changes. Figure 3.13, Panel C shows the time-course of internal calcium concentration during the two action potentials in Panel A. The range of variation in internal calcium concentration is within the range of generally accepted values ( $10^{-7}$  M to  $10^{-6}$  M, Noble,

Figure 3.13

The time course of internal concentrations and occupancies during repetitive stimulation at .5 hz.

Panel A

The membrane action potential.

Panel B

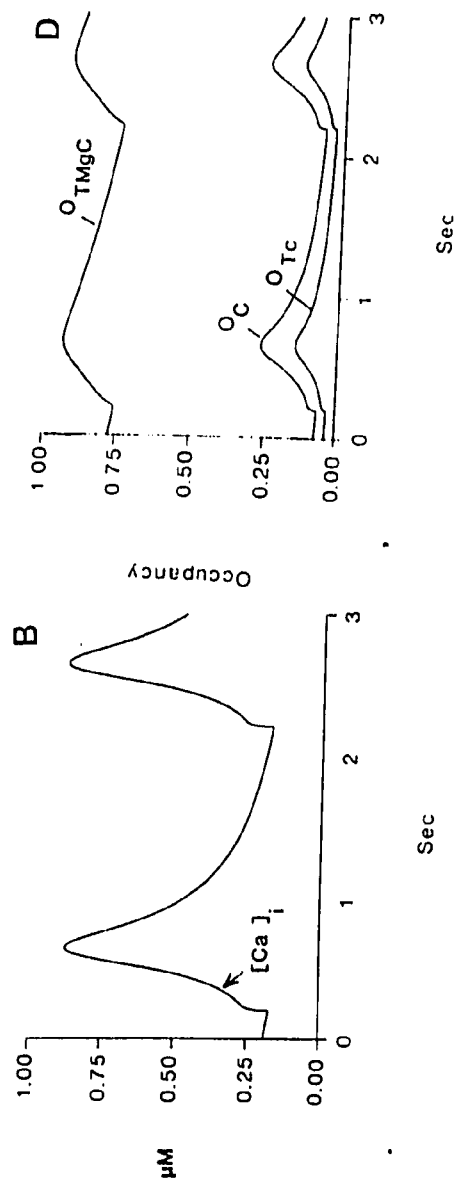
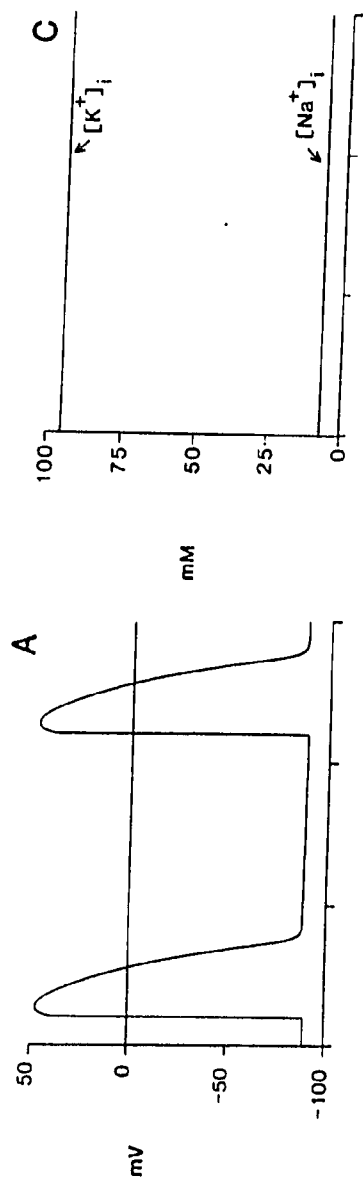
The internal concentrations of  $\text{Na}^+$  and  $\text{K}^+$  during the course of the two model action potentials.

Panel C

The time course of the internal activity of  $\text{Ca}^{++}$  during the two model action potentials.

Panel D

The time course of occupancy of the three different types of sites during the two model action potentials.



1979). Internal calcium also binds to internal proteins. The time-course of occupancy of these binding sites by calcium is given in Figure 3.13, Panel D. Of the binding sites the one of most interest is the calcium specific sites on troponin. Occupancy of these sites is associated with the physical contraction of the fibre. It is therefore important to ensure that enough calcium binds to this site to account for the tension observed in intact tissue. The occupancy developed during model simulations (15% of the total number of Calcium specific troponin sites) seems to be sufficient to account for the tension developed 10% to 30% of maximal tension observed by Fabiato (1982).

#### III.2.7 Summary of Initial Atrial Model Testing.

The preceding sections demonstrate that the atrial model is capable of reproducing many of the basic electrophysiological characteristics of atrial cell. Importantly it shows that an action potential with reasonable characteristics can be produced and that with simple manipulations of the relative magnitudes of the underlying currents a range of experimentally observed action potentials may be simulated quite closely. The model also reproduces voltage clamp results designed to reveal each of the different underlying current systems (i.e. we can get back out the results upon which the model is based). The buffering system offers an independent check of the total calcium influx during an action potential and the compartmental systems, both internal and

external, ensure that the  $\text{Na}^+/\text{K}^+$  pump and exchanger mechanisms are sufficient for maintaining the potential gradients. The next section will present a similar consistency check for the sinus venosus model.

Table 3.3  
Sinus-Venosus  
A Comparison of Experimental and Model Action Potential Characteristics

	Shibata 1983	Model
Max. Diastolic potential	-76 mV 1.05	-75 mV
Overshoot	47.4 mV 1.6	41 mV
Duration	530 msec 33.7	555 msec
Upstroke Velocity	4.6 V/sec 0.37	2.8 V/sec
Frequency	0.54 hz 0.02	0.5 hz

### III.3 Testing the Sinus Venosus Model.

The sinus venosus pacemaker model may also be compared to representative experimental data. Important properties of any primary pacemaker model involve the ability to show spontaneous pacing at the experimentally observed rate and the resemblance of the model generated waveform to the observed action potential

Figure 3.14, Panel A shows that the sinus venosus model does produce spontaneous pacing at a physiologically observed rate (0.5 Hz, Shibata, 1983). When the relevant parameters describing the sinus venosus model are compared to the average of the parameters of several experimentally observed waveforms from different cells, the model acceptably reproduces the results (listed in Table 3.3), especially considering the standard error of measurement associated with each of the experimental findings. The ionic currents underlying the sinus venosus waveform are shown in Figure 3.14, Panel B, while the pump and exchanger currents are shown in Panel C. The three panels demonstrate the interaction of the various currents that produce the diastolic depolarization and action potential.

A typical action potential is shown in Figure 3.15. It is apparent that the observed and model action potentials are very similar. Using the procedure of changing the relative magnitudes of the various currents, we can obtain a reasonably good fit to this experimental data. Figure 3.16 shows the results of changing



Figure 3.14

The sinus-venosus model action and underlying currents.

Panel A

The membrane action potential showing spontaneous pacing.

Panel B

The ionic channel currents underlying the membrane action potential  $I_{Ca}$ ,  $I_K$ ,  $I_{background}$ .

Panel C

The pump and exchanger currents underlying the membrane action potential  $I_{NaK}$ ,  $I_{Na/Ca}$  and  $I_{CaPump}$ .

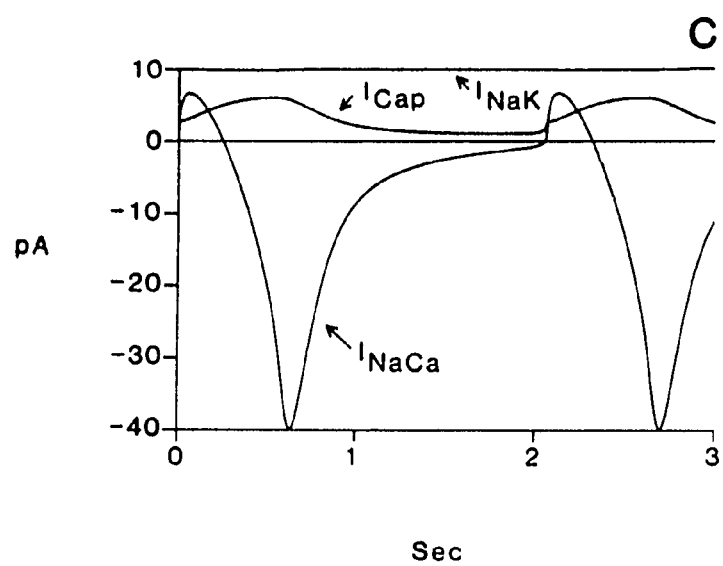
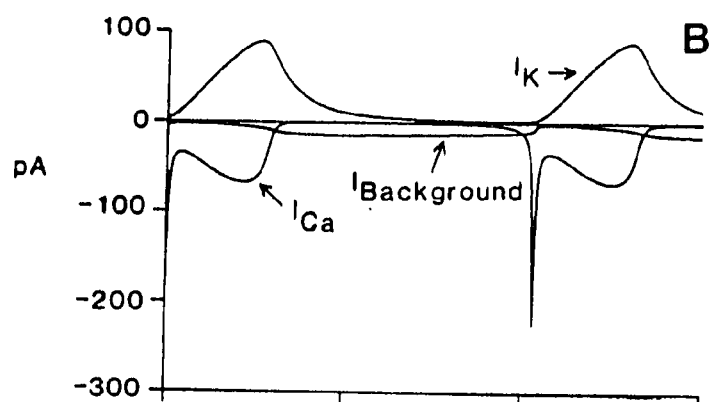
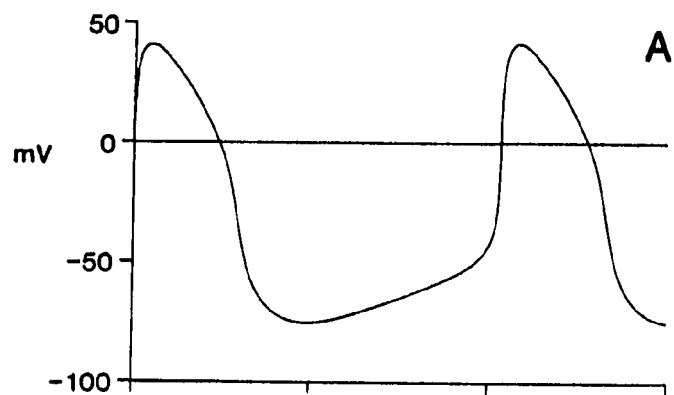
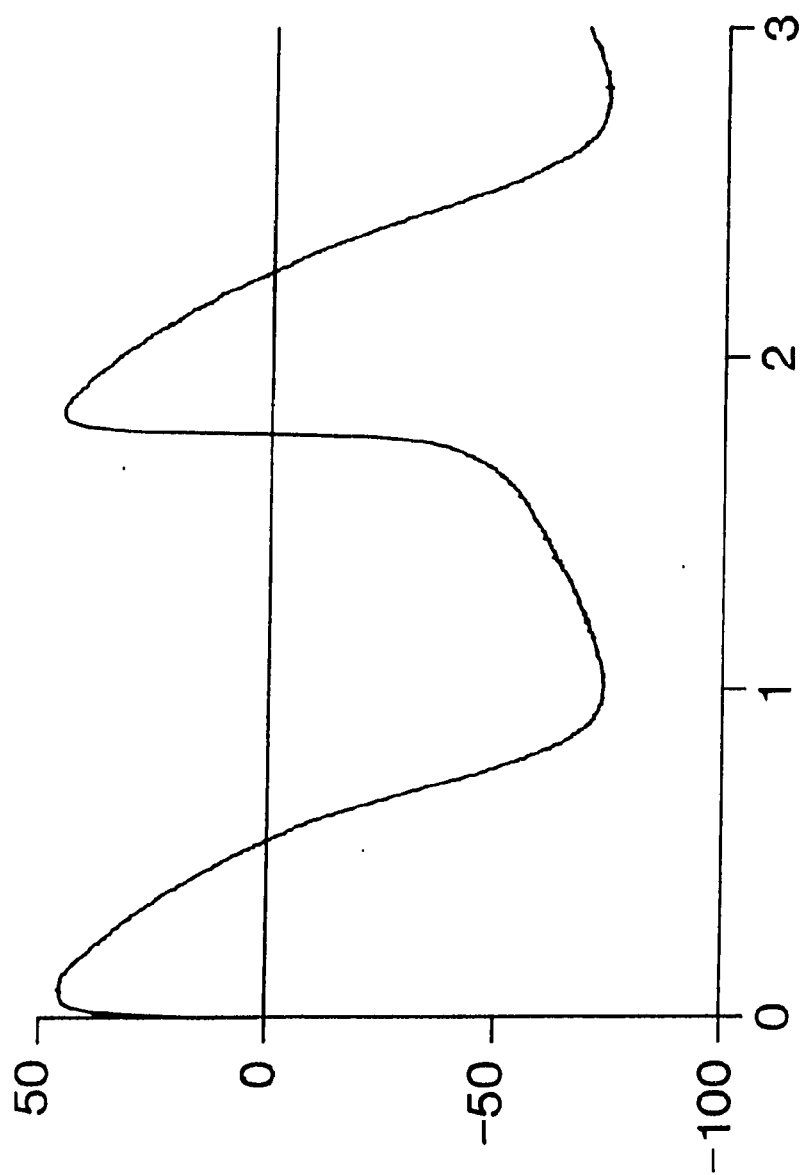


Figure 3.15

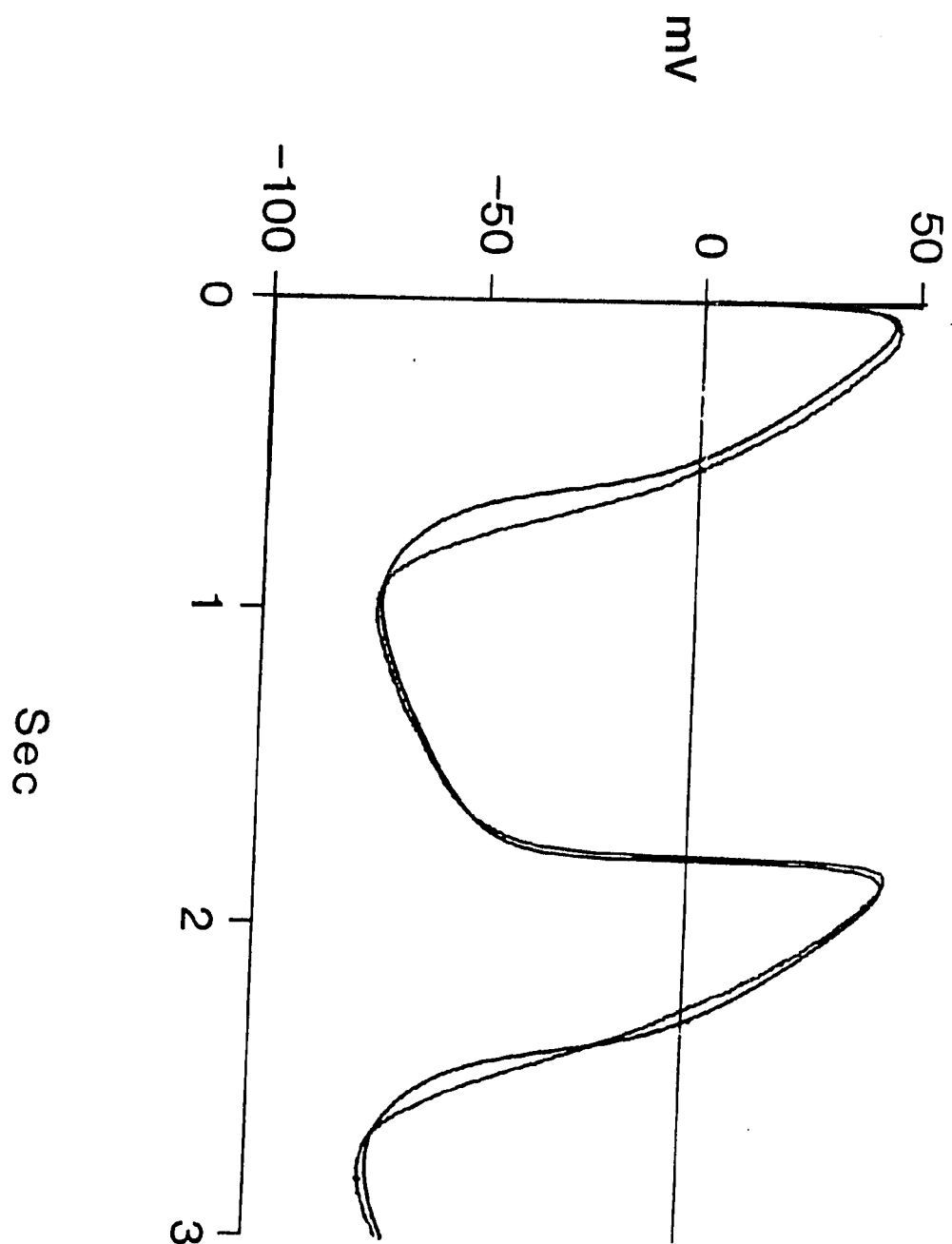
A typical action potential observed in single isolated bullfrog sinus-venosus cells.



Sec

Figure 3.16

Model and experimental action potentials after adjustment of the model parameters. This match was achieved by increasing  $I_{Ca}$  by 20% and by increasing  $I_{Background}$  by 23% over the standard values given in table 3.1.



the magnitude of various currents to obtain a reasonably good fit to the experimental waveform. In this case two current systems were changed relative to the standard values given in Table 3.1 .

The ability to reproduce experimentally observed action potentials by small adjustments of the magnitudes of the underlying membrane currents is an important measure of the adequacy of this model.

### III.3.1 Background Currents.

It has been noted previously that sinus venosus cells lack an inward rectifier current, and that the current-voltage relation for background currents is approx. linear (Shibata and Giles, 1984; Giles and Shibata, 1985). The experimental data illustrating the background current in sinus venosus cells was obtained by blocking  $I_{Ca}$  and measuring the instantaneous change in current resulting from a clamp step. These are shown in Figure 3.17, Panel A. An analogous 'protocol' in the sinus venosus model gives the result in Figure 3.17, Panel B. They are very similar in magnitude and slope.

### III.3.2 The Transient Calcium current.

The leading edge of the sinus venosus action potential is generated by activation of  $I_{Ca}$ . In addition, the last part of the diastolic depolarization as well as the upstroke of the action potential is thought to be influenced by  $I_{Ca}$  (Brown, Giles, Noble, 1977; Giles and Shibata, 1985). Consequently, an initial test of

Figure 3.17

A description of the background currents in Bullfrog sinus-venosus.

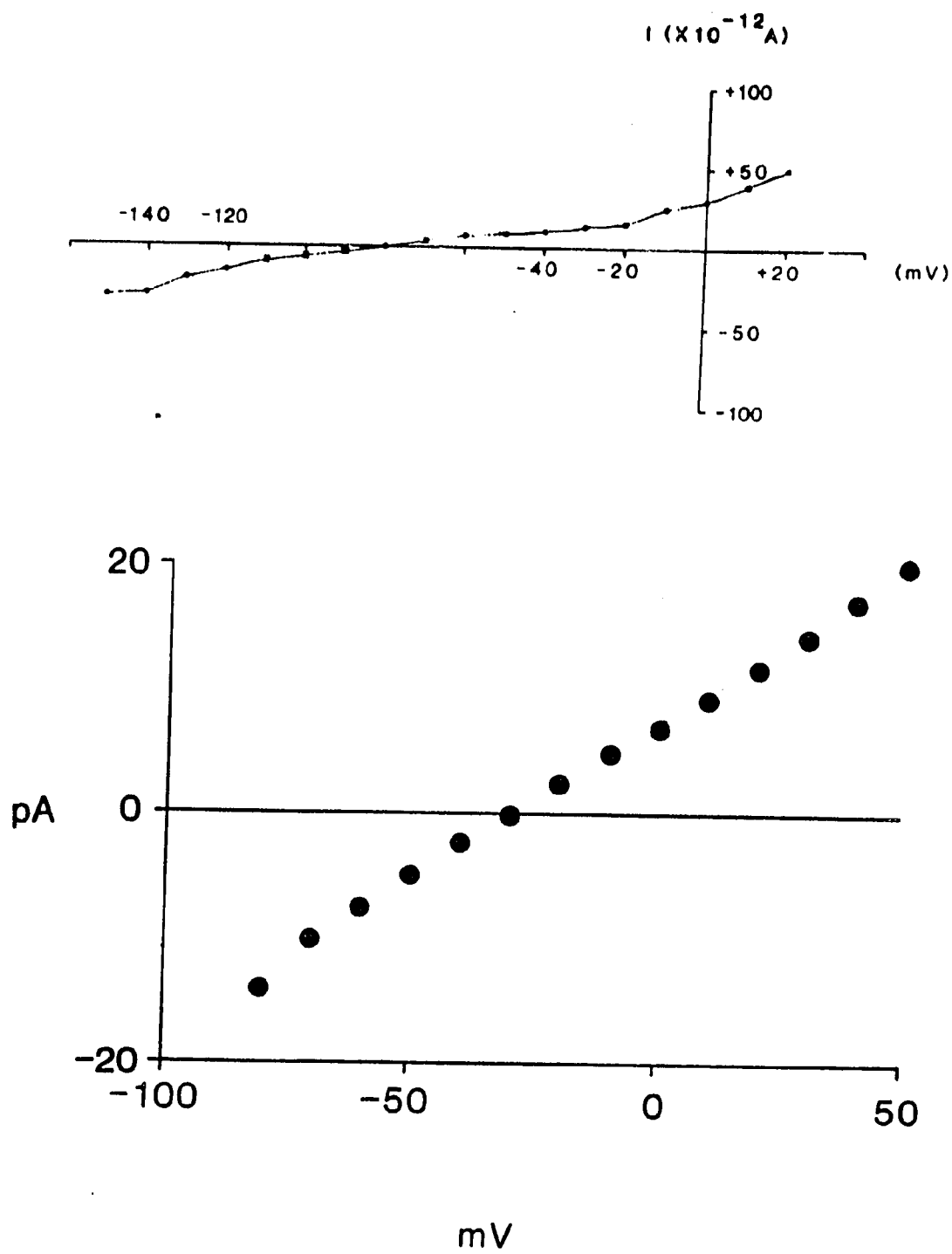
Panel A

The background currents as measured experimentally.

Panel B

The background current as reproduced by the sinus-venosus model.





the  $I_{Ca}$  characterization might ask is the maximum  $dV/dt$  comparable to experimentally observed values and does the onset of the rapid upstroke in the model occur in the same range of potential as is experimentally observed? Table 3.3 answers the question concerning comparable maximum  $dV/dt$  in the affirmative, while inspection of Figure 3.16 will show that the onset of rapid upstroke does occur in a similar range of potentials.

$I_{Ca}$  recorded from sinus venosus are shown in Figure 3.18, Panel A (taken from Shibata, 1983). The analogous model results in Panel B. Following the capacitive transients (which are not modelled) the model and experimental traces are very comparable.

In a more quantitative check, Figure 3.19 shows the experimental results of the peak of these inward currents recorded during a calcium voltage clamp protocol superimposed upon the model generated result. Over most of the physiologic range of potentials the agreement is quite close, with values usually falling within or near the standard error of measurement of the experimental data. There is some disagreement in the range of potentials near where  $I_{Ca}$  is activated. The activation of  $I_{Ca}$  seems to occur in a slightly higher range of potentials than the model result would indicated; this discrepancy is minimal when one considers the small relative magnitude of currents in this range and the uncertainty of the measured resting (maximum diastolic)

Figure 3.18

Calcium currents during voltage clamp in the Bullfrog sinus-venosus for three different clamp potentials.

Panel A

Experimental measurements. Holding potential  $-80$  and clamp pulse as indicated. (Shibata, 1983).

Panel B

Model results.

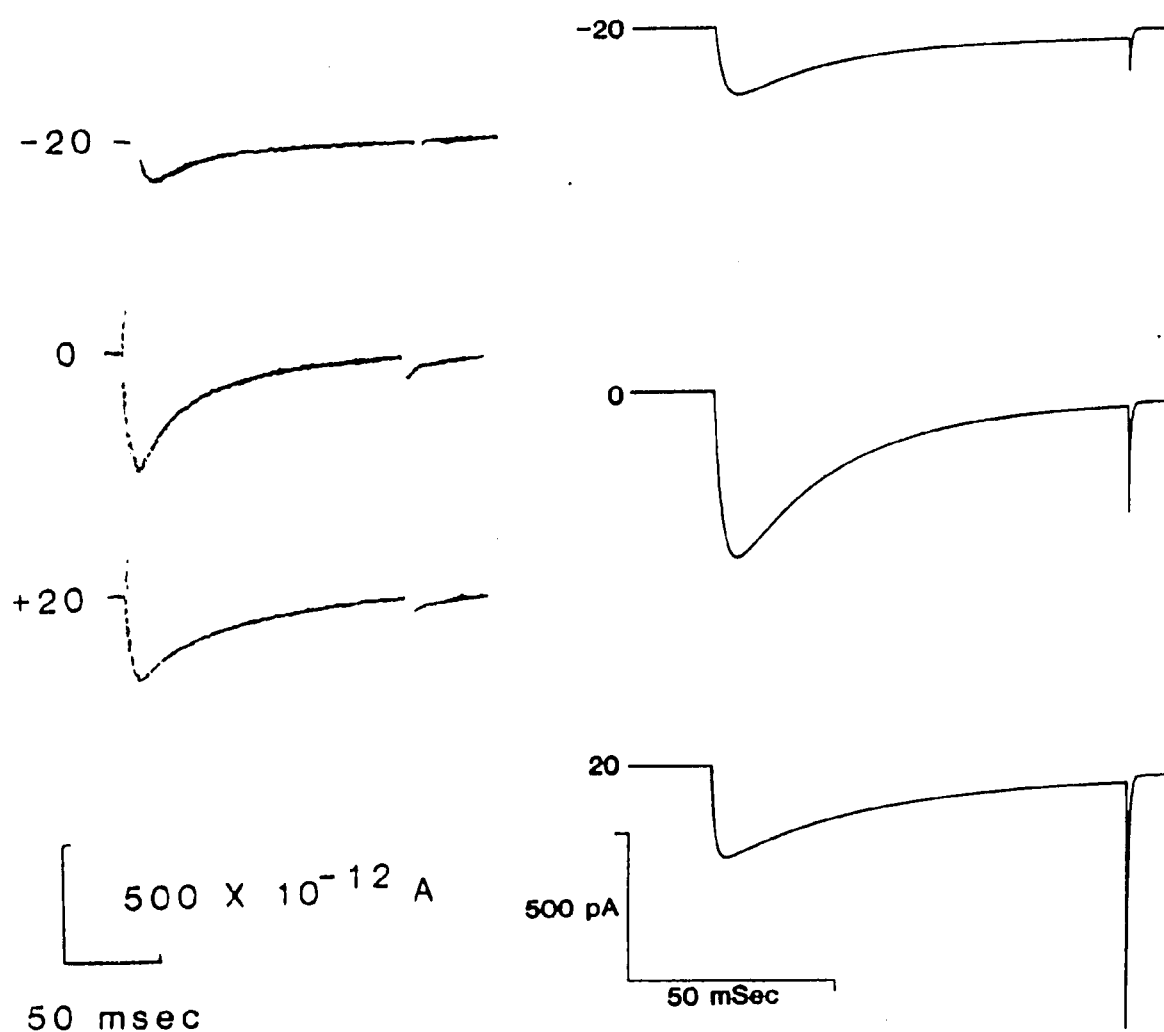
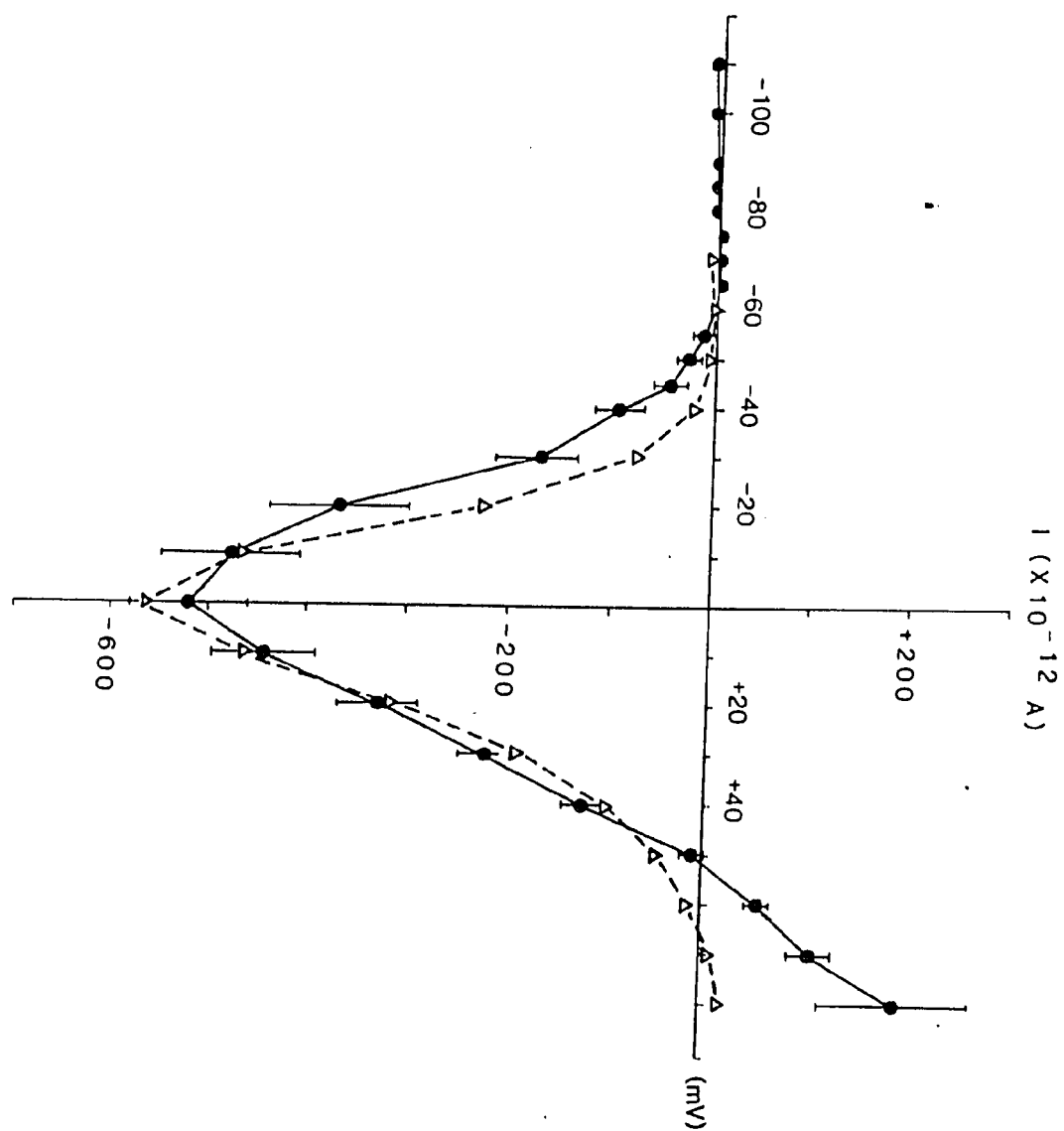


Figure 3.19

Peak inward currents during voltage clamp of sinus-venosus cells. Dots with standard error bars are experimentally observed values while the triangles are the model generated values.



potential. This may vary by as much as 5 mV (Hume and Giles, 1981) due to electrode tip potential.

### III.3.3 The Delayed Rectifier.

The experimental results indicate that the delayed rectifier current in both sinus venosus and in atrium have very similar magnitudes and kinetics (Hume et. al. (1985), Shibata and Giles (1985)). Although testing the model results for this current may seem redundant, a similar protocol to that used to illustrate the potassium kinetics and magnitude in atrium are reproduced here for the sinus venosus, in the interest of completeness. Figure 3.20 shows a side by side comparison of experimental records (Panel A) of the delayed rectifier current and the analogous model results (Panel B). These results are very comparable. As in the atrial delayed rectifier modelling, in this simulation the internal potassium and internal calcium concentrations were held constant.

### III.3.4 Extracellular Compartment.

The effects of the restricted extracellular space on sinus venosus pacing cells is, in light of the extremely slow  $dV/dt$  and hence small net current a perhaps less important issue than accumulation and depletion for a single beat as in an atrial action potential. For this reason and also due to the absence of sinus venosus accumulation/depletion data, the problems concerning accumulation/depletion in the sinus venosus model are deferred to the Results (Chapter 4).

Figure 3.20

Delayed outward currents in Bullfrog sinus-venosus. Panel A experimentally observed currents (Giles and Shibata, 1985), Panel B model generated currents.



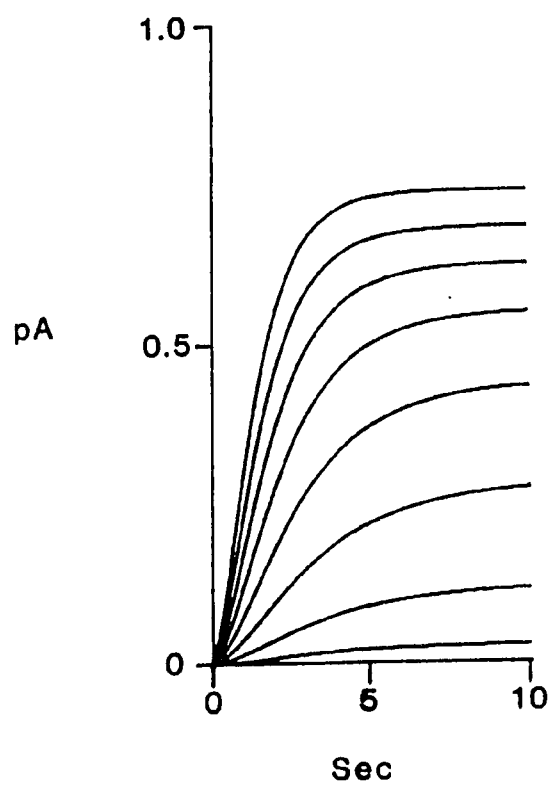
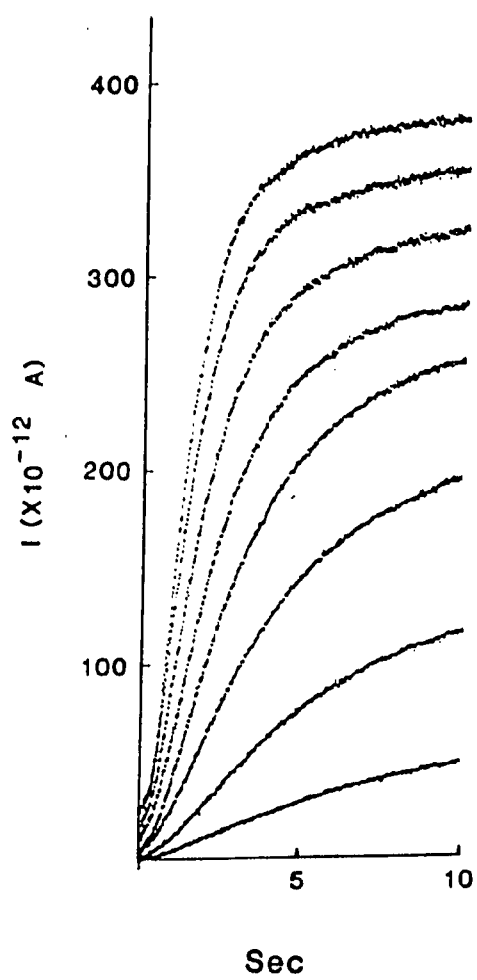


Figure 3.21

Internal concentrations and occupancy during the sinus-venous action potential.

Panel A

The sinus-venous model action potentials.

Panel B

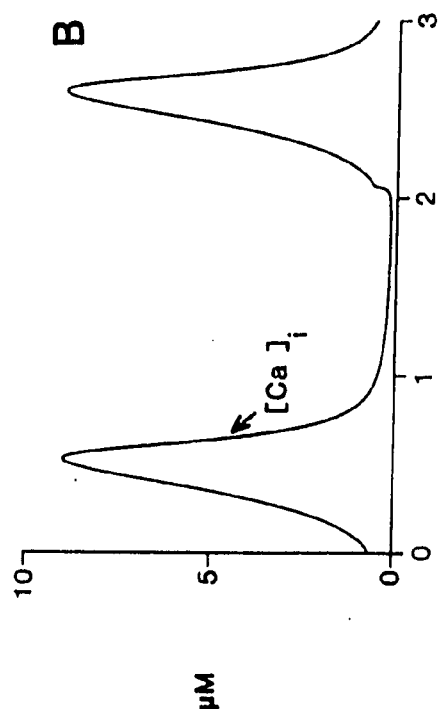
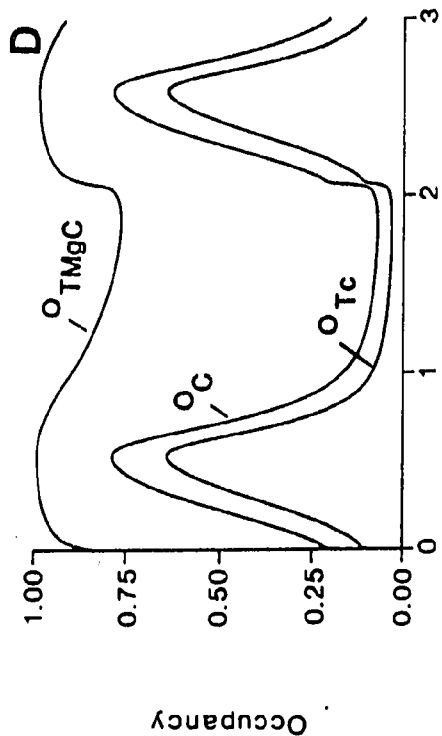
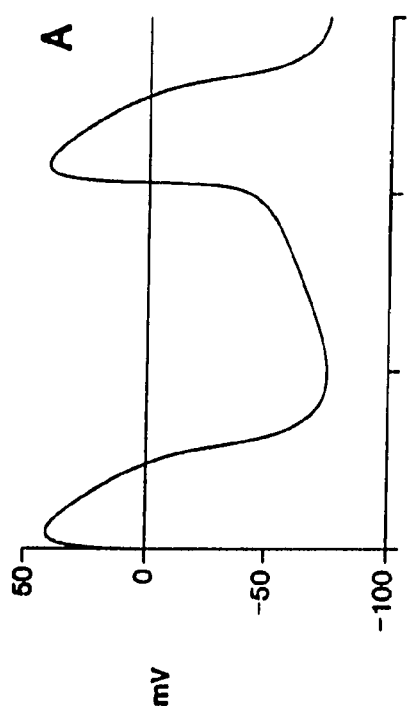
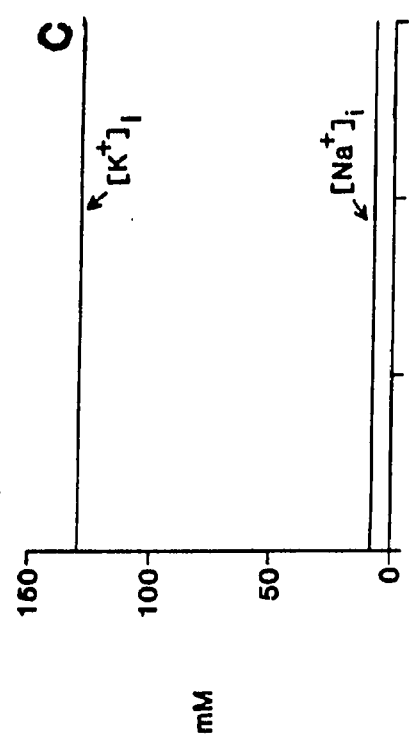
Sodium and potassium concentrations during the action potentials.

Panel C

Calcium activity during the action potentials.

Panel D

Fractional occupancy of three different types of binding sites by  $\text{Ca}^{++}$ .



Sec

Sec

The internal concentrations of three major ionic species can be continuously monitored in this sinus venosus model. Of these it is generally accepted that  $[K^+]_i$  remains fairly constant in a normally beating cell while calcium undergoes substantial variation during spontaneous activity. Figure 3.21, Panel A shows two spontaneous action potentials and panel B shown the modelled internal sodium and potassium concentrations during these beats. Note that there is no substantial variation during normal sinus venosus activity.

As expected, internal calcium concentration does not remain constant during normal sinus activity. Figure 3.21, Panel C shows the substantial variation during the time course of normal sinus venosus activity. In spite of the substantially larger calcium current (both observed and modelled, Giles and Shibata, 1985) than in atrium, the range of variation in internal calcium concentration is within the generally accepted values  $10^{-7}$  to  $10^{-6}$  M (Noble, 1979). Internal calcium binds to various intracellular proteins. The time course of  $Ca^{2+}$  occupancy of these binding sites is shown in Figure 3.21, Panel D. The sites of most interest are the calcium specific sites on troponin. Their occupancy controls the contraction of the fibre; it is therefore important to ensure that enough calcium binds to this site to account for the tension observed in intact tissue. The occupancy developed, 63% of the total number of sites, seems sufficient to account for

the strong regular contractions of the isolated sinus venosus cells.

#### III.4 SUMMARY:

This chapter has outlined the computational methods used in solving model equations and has presented the initial tests of the model and comparisons with some basic experimental observations. Both atrial and primary pacemaker activity can be simulated, and the models yielding this activity can also simulate voltage-clamp results. Hence, there is some foundation for believing that the model current densities are appropriate; and, therefore, can be used to predict accumulation/depletion results as well as model more complex experimental situations.

## CHAPTER IV

## MODEL RESULTS

IV.0 Introduction

The two previous chapters presented a mathematical model of cardiac activity, reviewed the experimental results upon which it was based and tested it against a series of experimental observations. This chapter will describe the interaction of transmembrane currents, concentration changes and buffer occupancies that underly the electrical activity of the frog atrial cell and the frog sinus-venous cell.

By simply reviewing the currents computed for the model action potential (Fig 4.1) a number of observations can be made:

- 1) When the atrial cell is at rest, or quiescent,  $I_{K1}$ ,  $I_{Background}$  and  $I_{NaK}$  are the dominant currents.
- 2) Following a depolarizing stimulus,  $I_{Na}$  becomes the dominant current and is responsible for the initial rapid depolarization.  $I_{Na}$  then inactivates quickly and plays no further role in the action potential until

Figure 4.1

A summary of the transmembrane ionic currents during repolarization.

Panel A

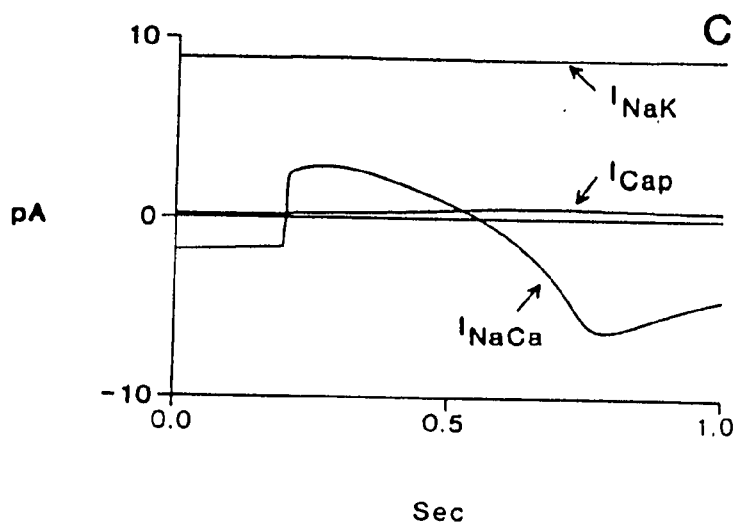
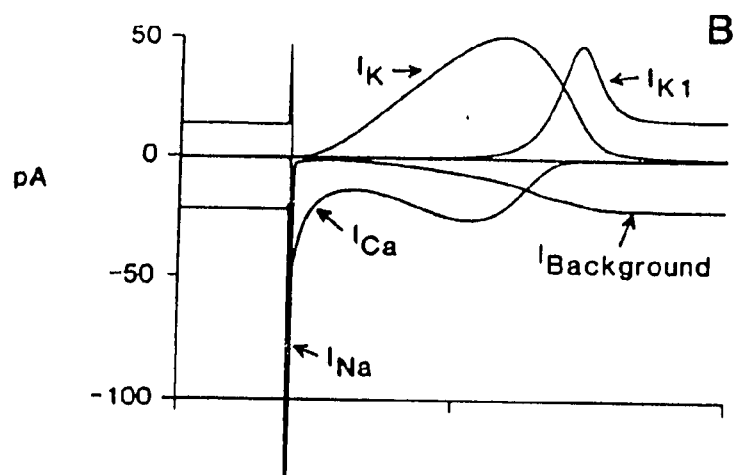
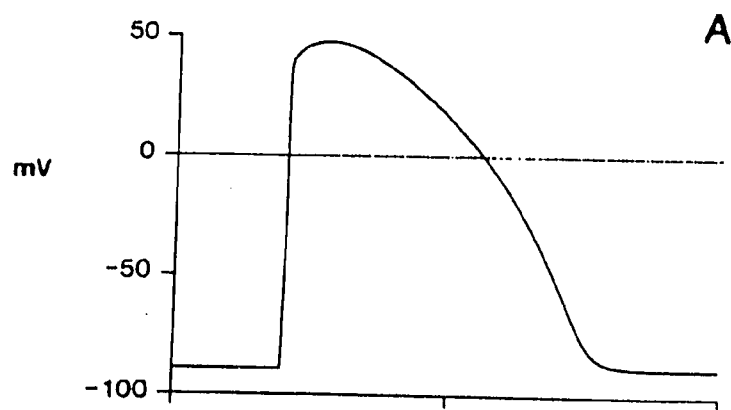
The Atrial Action potential

Panel B

The channel currents

Panel C

The pump and exchanger currents.





the cell membrane repolarizes and it resets, becoming ready for the next stimulus.

- 3)  $I_{Ca}$  is the next current to become active, it provides an inward current which generates the slow secondary portion of the action potential upstroke. In addition, it provides inward current needed to maintain the amplitude and duration of the plateau of the action potential.
- 4)  $I_K$  activates more slowly than the inward currents but grows steadily during the time when the action potential is at depolarized potentials; initiating repolarization by "overpowering"  $I_{Ca}$ .
- 5)  $I_{K1}$  becomes important in late repolarization as  $I_{Ca}$  becomes inactivated and  $I_K$  approaches its reversal potential.
- 6) The changes in the pump and exchanger currents are relatively small in comparison to the active channel currents, and the pump and exchanger currents turn on with considerable delay and are slow relative to the active channel currents.

The period in which the membrane is returning to its resting potential from peak depolarization involves the interaction of two gated currents and possibly background and pump currents. Repolarization has been recognized as a very important electrophysiologic phenomenon in the heart: it controls the refractory period, and is an important determinant of the T wave.

#### IV. 1 The Mechanism of Repolarization

The long slow repolarization phase of the cardiac action potential has been the subject of previous modelling studies. The pioneering work of Noble (1962), done largely in the absence of experimental data, used two mechanisms to prolong the plateau and delay the repolarization phase of the cardiac action potential. The first was a  $K^+$  selective channel with very slow kinetics and the second was a maintained inward current active during the plateau portion of the action potential. Subsequent experimental work revealed a  $K^+$  conductance in cardiac preparations which had slow (relative to squid axon) kinetics and which increased during the course of the action potential (Vassalle 1965, Noble and Tsien 1969b). At about the same time a second inward current carried by calcium ions was discovered, (Reuter

1967). It had a magnitude and kinetics appropriate for supporting the plateau phase of the cardiac action potential.

The idea of inward and outward currents balancing during the plateau phase has been a feature of all subsequent models of cardiac electrical activity. This raises the question "What initiates repolarization?" It may be the "turn off" of an inward current or the "turn on" of an outward current. Goldman and Morad (1977) proposed that repolarization in frog ventricle was governed by a decrease in  $\text{Na}^+$  conductance and a concurrent increase in  $\text{K}^+$  conductance. Later Drouhard and Roberge (1982) proposed that "action potential repolarization [in frog ventricle] is controlled solely by the inactivation parameter  $t$ ." ( $t$  inactivates a potassium current). Most recently the work of DiFrancesco and Noble (1985), while not a direct effort to address the initiation of repolarization, implies that the sodium calcium exchange process provides the sustained inward current necessary to maintain the plateau phase of the mammalian Purkinje fibre action potential and may therefore be importantly involved in repolarization. This idea was first suggested by Mullins (1979, 1981). Although the mammalian Purkinje fibre is quite different from the frog atrium; this new idea concerning repolarization deserves consideration in cardiac models which include  $\text{Na}^+/\text{Ca}^{++}$  exchange currents.

How then, is repolarization initiated in the frog atrium? Considering each of the individual model generated currents underlying the action potential (Fig. 4.1) provide a possible answer:

- a)  $I_{\text{Background}}$  is an increasing inward current at all times after peak depolarization, and is therefore unsuitable as a mechanism for initiating repolarization.
- b)  $I_{K1}$  is virtually zero until late repolarization and consequently has no effect on the initiation of repolarization.
- c)  $I_{Na}$  is active only during the initial depolarization and does not play a role in repolarization.
- d)  $I_{Ca \text{ Pump}}$  is too small in magnitude to be important.
- e)  $I_{NaK}$  does not change significantly during an action potential.
- f)  $I_{NaCa}$  is a small decreasing net outward current during the early stages of repolarization and eventually becomes net inward (depolarizing) in later repolarization. This means it changes in a manner that opposes rather than propels repolarization.

- g)  $I_{Ca}$  is active during the time-course of repolarization of the bullfrog atrial action potential. As can be seen from the simulated  $I_{Ca}$  traces, it exhibits an initial inward 'spike' which occurs late during the action potential upstroke; it then rapidly turns-off to a partially inactivated state, but exhibits a slow increase during the early stages of repolarization, thus the theory that repolarization is initiated by a turn off of an inward (carried by  $Na^+$  in Morad and Goldman (1977)) current is inconsistent with this model. In late repolarization, deactivation of  $I_{Ca}$  plays an important role by eliminating an inward current at the same time as  $I_K$  decreases when the action potential nears  $E_K$ .
- h)  $I_K$  slowly and steadily increases during the action potential. It is net outward and is increasing in the proper direction to initiate and control early repolarization. In this model of frog atrial activity,  $I_K$  initiates repolarization.

Thus, through direct inspection of the underlying ionic currents  $I_K$  has been tentatively identified as the mechanism initiating repolarization and dominating early repolarization.

Thus, through direct inspection of the underlying ionic currents  $I_K$  has been tentatively identified as the mechanism initiating repolarization and dominating early repolarization. Repolarization has been studied experimentally and a comparison of the model results with experimental results is necessary in evaluating whether the conclusions concerning repolarization are well founded.

#### IV. 1.1 Interval Duration Experiments.

Experimentally, if a second action potential is initiated soon after the first, it is found to be considerably shorter in duration. The relationship of the interval between two action potentials and the duration of the second one is known as the interval-duration relation. There are thought to be two effects contributing to the measured interval duration relation; the inactivation of the  $Ca^{++}$  current and the activation of the  $K^+$  current (Noble 1979; Carmeliet, 1977). After an action potential these processes will return to their resting values at the membrane resting potential. If an action potential is elicited before these processes can return to their resting values, the duration of the subsequent action potential will be shorter than usual since less inward current may be activated and the outward current will already be partially activated.

An experiment designed to measure this shortening of the action potential might proceed as follows:

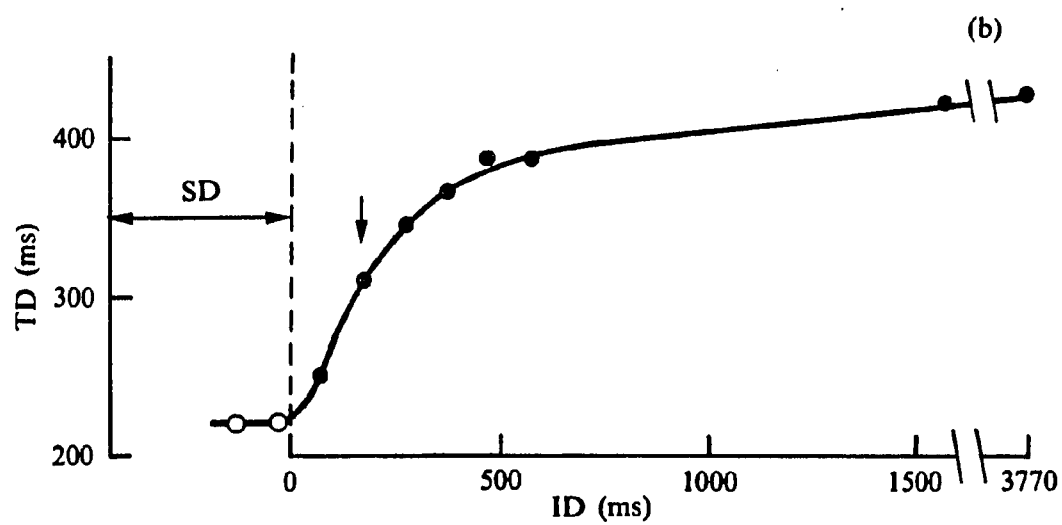
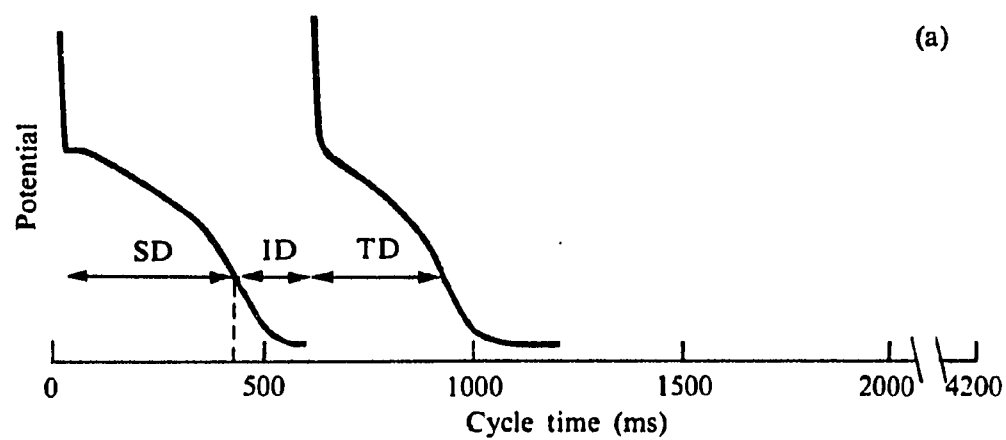
- 1) The preparation would be stimulated at a regular frequency.
- 2) At fixed intervals a single premature action potential would be inserted into the sequence.
- 3) The interval between the end of the preceding action potential and the "premature" action potential would be measured. This would be called the 'interval duration'.
- 4) The duration of the second action potential would also be measured. The duration of this action potential can be plotted against the interval duration. Sometimes the measurement of the shortened action potential may be normalized by representing it as a fraction of the duration of the unshortened action potential recorded at the normal frequency.

Demonstration of this experimental measurement is shown in Figure 4.2 for Purkinje fibre action potentials (Noble, 1979).

Figure 4.2

The interval duration measurement in purkinje fibre. (a) Example of an experimental record. The first action potential was initiated and its duration was about 450 mseconds. The second action potential was initiated after an interval (ID) and its duration (TD) is plotted in (b) against the interval duration. (Noble, 1979).





Recently, experiments of this sort have been performed using isolated bullfrog atrial cells. Figure 4.3 a shows the results of such an experiment. Model results from a similar protocol are shown in Figure 4.3 b, the action potentials are different in shape due to the natural variability of atrial action potential waveforms (described previously) but the changes in action potential duration with interval duration appear similar.

Normalizing both the model and experimental action potential durations as a fraction of their respective control durations yields the plots in Figure 4.4. There is acceptable agreement. The two main currents thought to influence the duration of the action potential ( $I_{Ca}$  and  $I_K$ ) are as predicted by the model are shown in Figure 4.5. Inspection of the changes in the underlying currents when the interval is shortened, and the action potential duration decreases; the  $I_K$  current is activated with less delay (due to the residual activation from the previous action potential), while the  $I_{Ca}$  shows no decrease in amplitude. This result seems consistent with the idea that the turn on of  $I_K$  initiates repolarization.

#### IV. 1.2 All-or-None Repolarization.

Experimentalists interested in determining which ionic currents are changing during the repolarizing phase of cardiac action

Figure 4.3

Interval duration experiments in isolated bullfrog Atrial cells.

Panel A

experimental observations

Panel B

model results

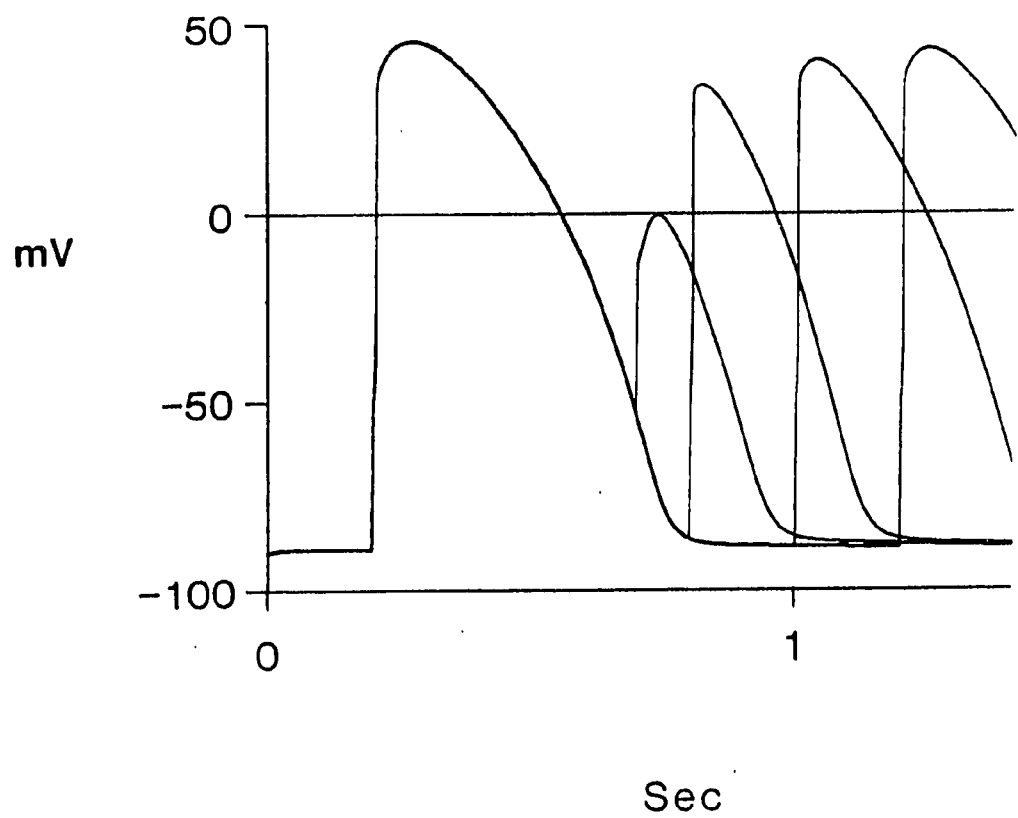
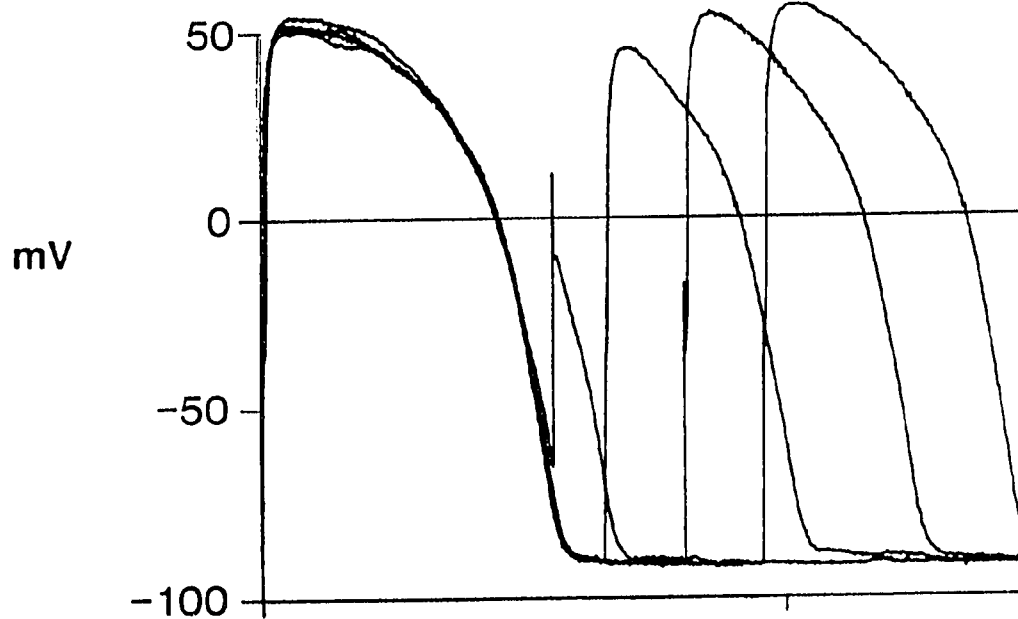


Figure 4.4

Normalized interval duration plots for experimental and model atrial action potentials. Panel A shows an experimentally observed relation while Panel B shows the model result.

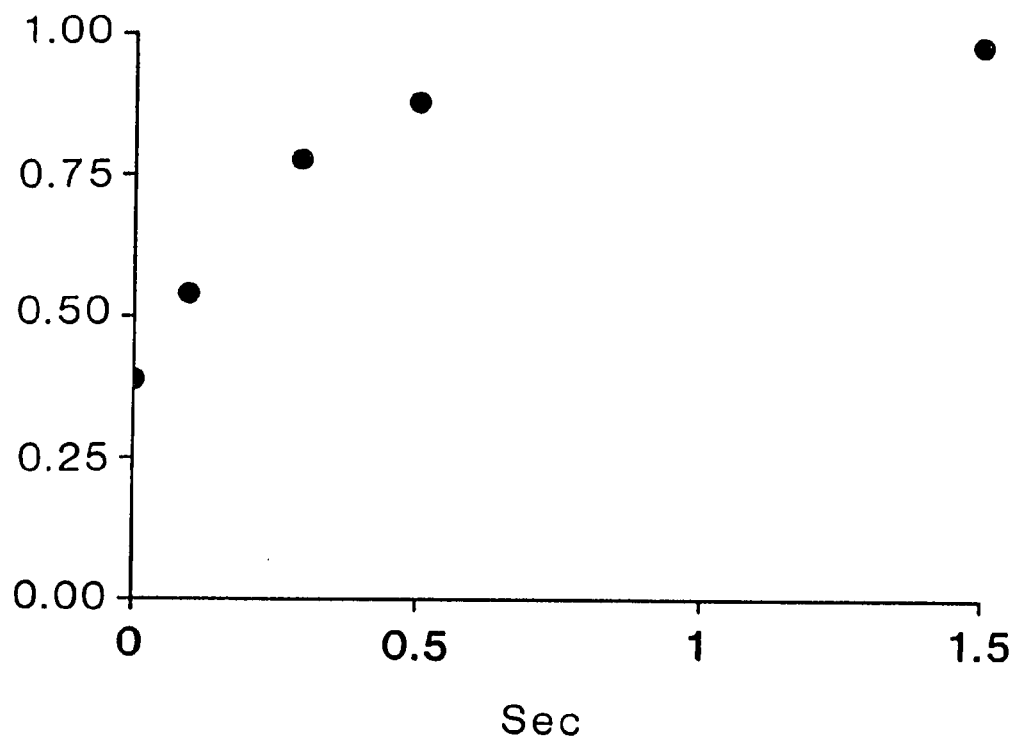
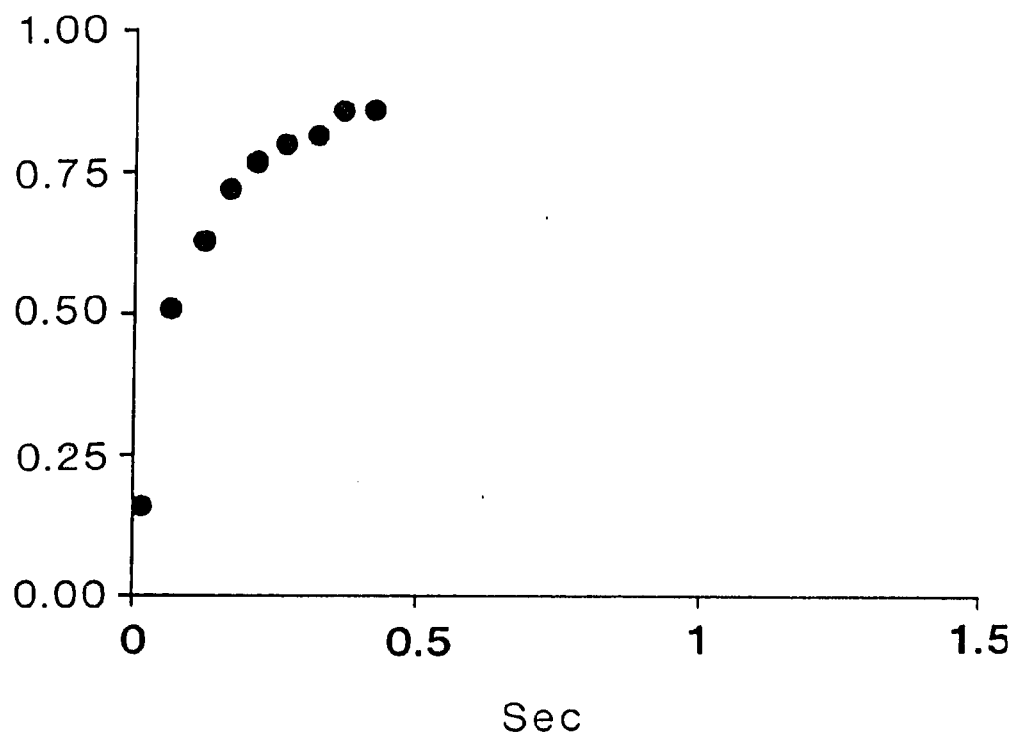
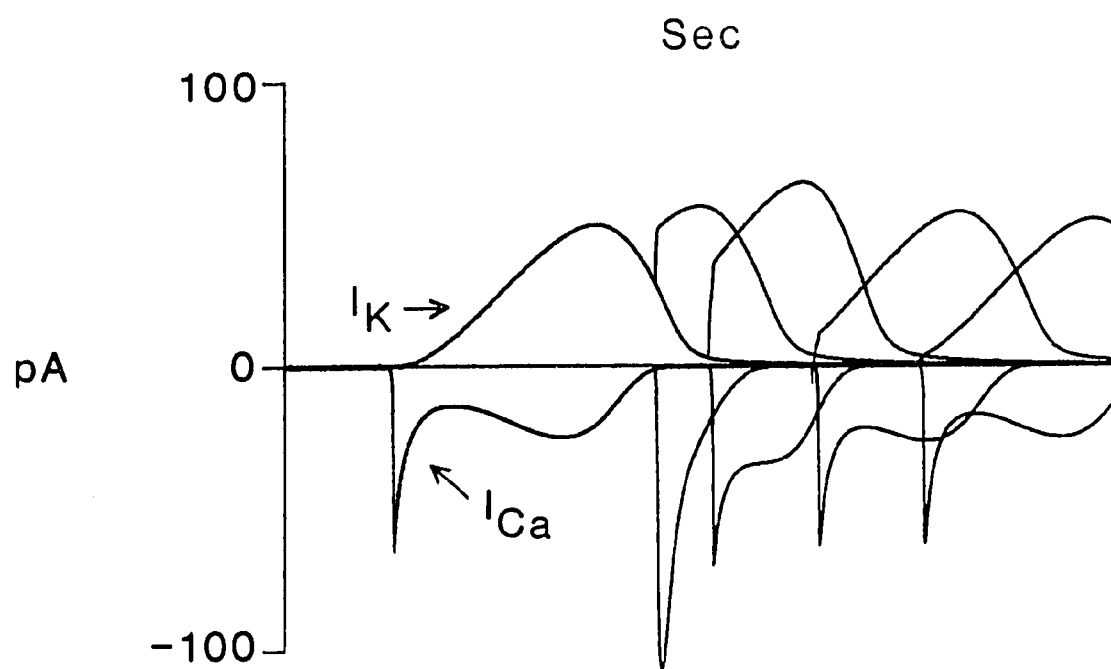
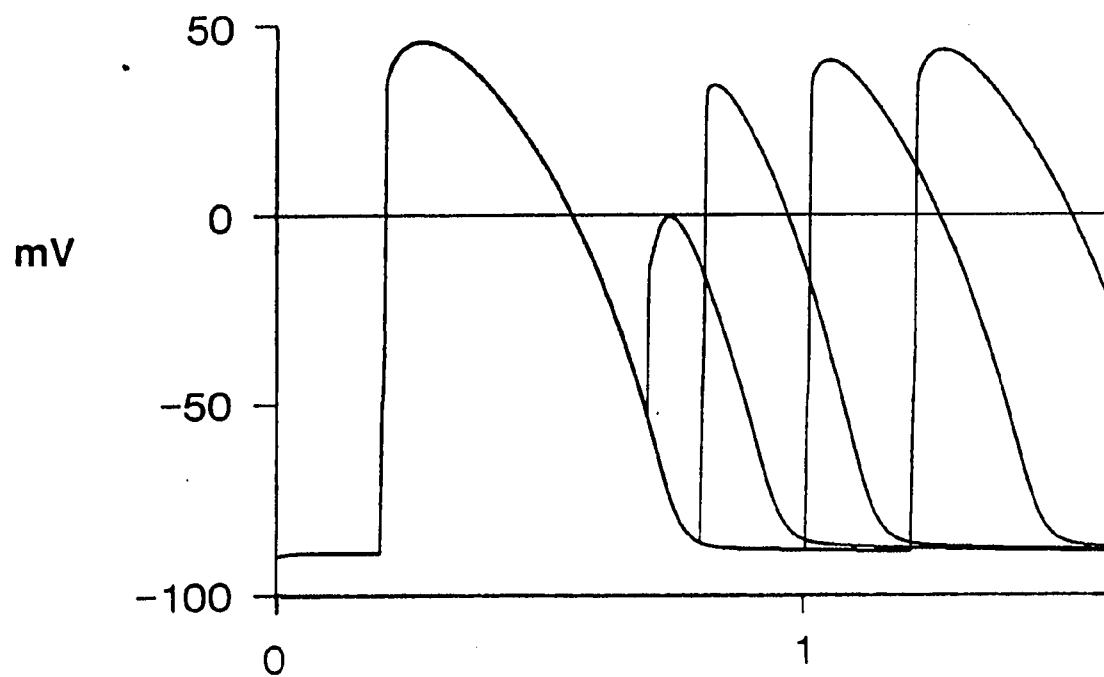


Figure 4.5

Interval duration results and the underlying  $\text{Ca}^{++}$  and  $\text{K}^+$  currents.





potentials have attempted to manipulate them by quickly changing the voltage during the action potential. Vassalle (1966) used pulses of current during the plateau of multicellular mammalian Purkinje fibre preparations to displace the membrane potential progressively closer to the maximum diastolic potential at selected times after the rapid upstroke. He found that for a given time delay after the leading edge of the action potential there was a well defined potential level negative to which the membrane potential failed to return to the plateau. This potential is called the all-or-nothing threshold for repolarization. When this procedure is repeated at different times during the plateau; the all-or-nothing repolarization threshold potential can be shown to be time-dependent potential. It is similar to a change of the "abolition threshold" in the course of the squid giant axon after treatment with tetraethylammonium chloride. (Tasaki and Hagiwara ;1957).

The phenomena of all-or-none repolarization was studied by Goldman and Morad (1977) in frog ventricle. They found that application of brief (30-150 mSec) anodal voltage clamp pulses during the plateau of the action potential revealed a threshold potential for immediate repolarization, but the response was not all-or-none but graded. They also concluded that instantaneous conductances in the frog ventricle are linear over a very broad range of potentials during repolarization, and that the plateau is

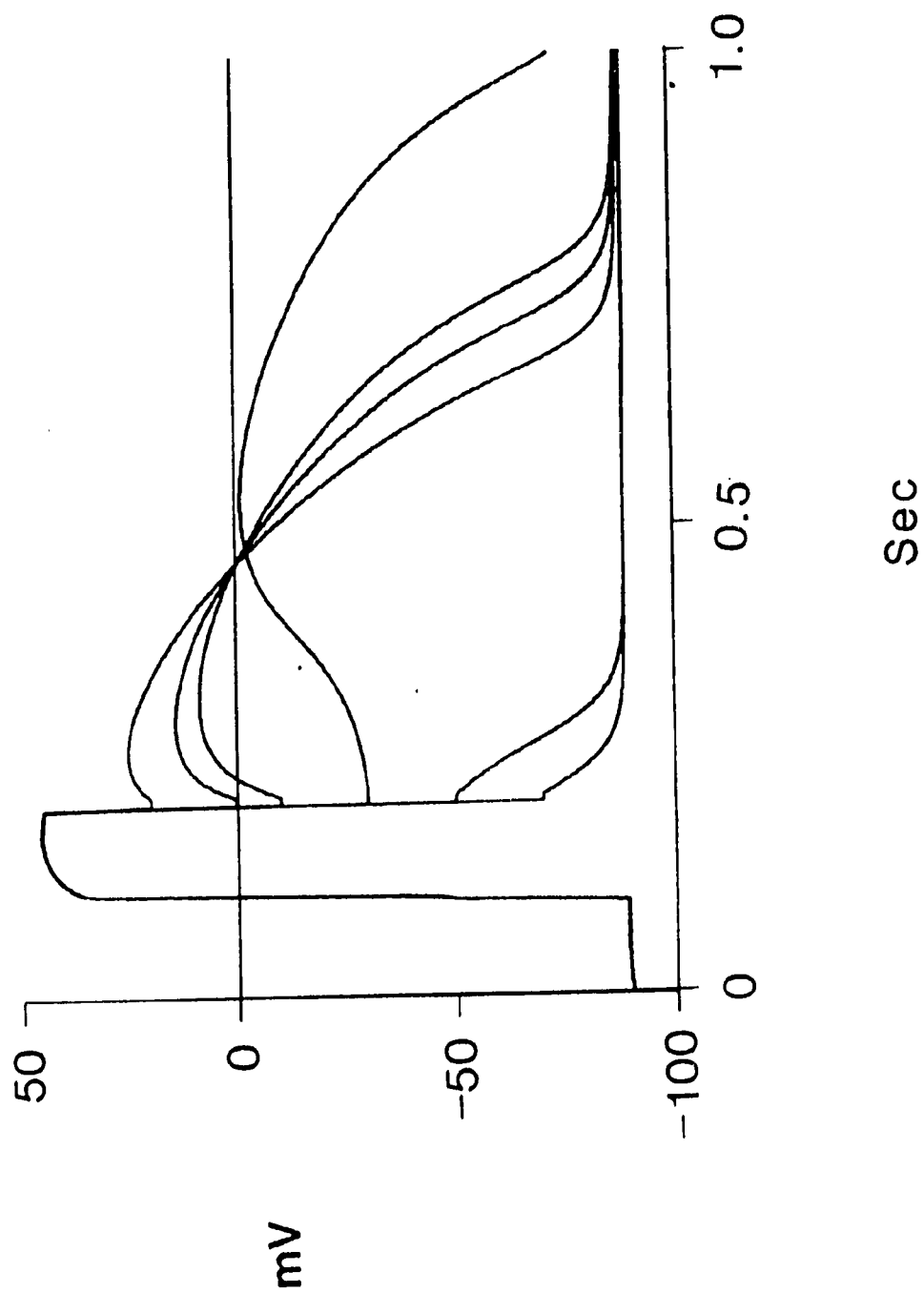
maintained by a fine balance of a  $\text{Na}^+$  inward current and a  $\text{K}^+$  outward current. These conclusions are so inconsistent with the model and experimental measurements on frog atrium that the possibility that these two tissues are very different in terms of their underlying current mechanisms needs to be considered. However, recent studies on isolated single cells of frog ventricle, Tung and Morad (1985) indicated that the currents measured are qualitatively similar to those previously described in single frog atrial cells. This includes a non-linear inward rectifier background (instantaneous) current; which is in direct contradiction to the linear instantaneous current-voltage relation measured by Goldman and Morad (1977) in multicellular preparations. This sort of inconsistency may be due to inadequate voltage clamp control of the multicellular preparation. (see Kootsey ;1975 for a review of how inadequate clamp control in multicellular preparations may seriously affect all-or-none repolarization measurements)

In the absence of reliable data on closely related tissue types the all-or-none repolarization protocol results for the atrial model are given in figure 4.6, without comparison to experimental results.

#### IV. 1.3 Buffering, Na/Ca Exchange and Repolarization.

Figure 4.6

A simulation of "all or none" repolarization in bullfrog atrium. The action potential was interrupted after 100 mSec to clamp potentials of -70, -50, -30, -10, 0 and 20 mV for 10 msec and then released from clamp.



In the Beeler and Reuter (1977) model of the mammalian ventricle action potential it was noted that if one computes the influx of calcium from voltage clamp experiments, or from a model, the influx is sufficient to raise intracellular calcium ion concentration significantly. This shift in calcium ion concentration will influence all currents dependent on calcium. It will result in a reduction of the potential at which the slow inward (calcium) current reverses, and will increase the potential at which the  $\text{Na}^+/\text{Ca}^{++}$  exchanger reverses.

Subsequent modelling studies have investigated the effects of the changes in internal calcium upon cardiac membrane currents. In the DiFrancesco and Noble (1985) model of mammalian Purkinje fibre, the  $\text{Na}^+/\text{Ca}^{++}$  exchange mechanism is a very important current source. It provides the inward current balancing the outward current of the delayed rectifier ( $I_K$ ) and is crucial in maintaining the plateau phase of repolarization. This is clearly not the role of the  $\text{Na}^+/\text{Ca}^{++}$  current in our model of frog atrial membrane. The difference in the role of  $\text{Na}^+/\text{Ca}^{++}$  in the frog model and the mammalian DiFrancesco and Noble (1985) model arises from the very different ways in which internal calcium concentrations are computed and the physical differences in the frog atrial and mammalian Purkinje fibre which dictate the computations. Changes in  $[\text{Ca}^{++}]_i$  in frog atrium is thought to be produced by only  $I_{\text{Ca}}$ , while in mammalian cardiac cells there is substantial release of

calcium from internal stores (e.g. the sarcoplasmic reticulum). The details of the mechanism(s) of internal calcium regulation can very strongly influence the size of the  $\text{Na}^+/\text{Ca}^{++}$  exchanger currents.

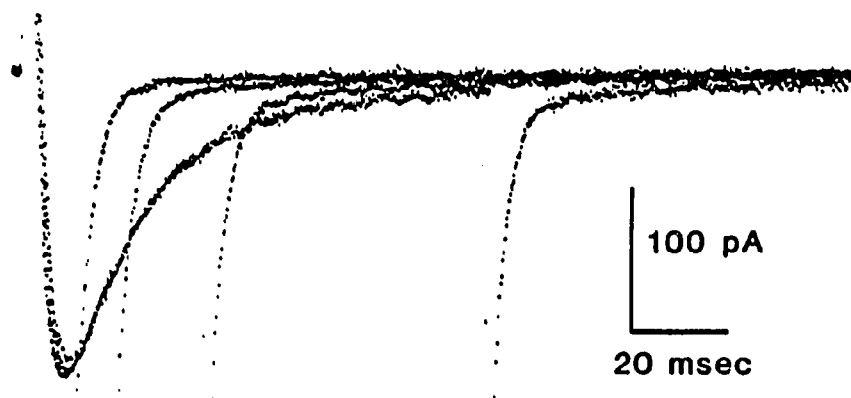
Campbell (1985) modelled the effects of calcium influx via the calcium on the calcium current and  $\text{Na}^+/\text{Ca}^{++}$  exchange current in frog atrium. In this model he incorporated a component of intracellular regulation not included in the DiFrancesco and Noble (1985) model, binding of  $\text{Ca}^{++}$  by intracellular proteins. Campbell (1985) showed that the  $\text{Na}^+/\text{Ca}^{++}$  exchanger could account for the "slow tails" observed during experiments designed to measure the  $\text{Ca}^{++}$  inward current figure 4.7 and that internal buffering could influence the time course of the  $\text{Na}^+/\text{Ca}^{++}$  current. The "slow tails" are an inward current measured upon return to the holding potential after a clamp pulse designed to activate a calcium current. The time course of decay of this outward current is much slower than that of the gating variable, hence the descriptive term "slow tails". They are not "tails" in the traditional sense of deactivation of a current by a gating variable and are dependent upon calcium entry during the clamp pulse. (Campbell;1985)

The formulation for binding of  $\text{Ca}^{++}$  by intracellular proteins used in this model is the same as that used by Campbell (1985). The effect of buffering on the  $\text{Na}^+/\text{Ca}^{++}$  exchanger current

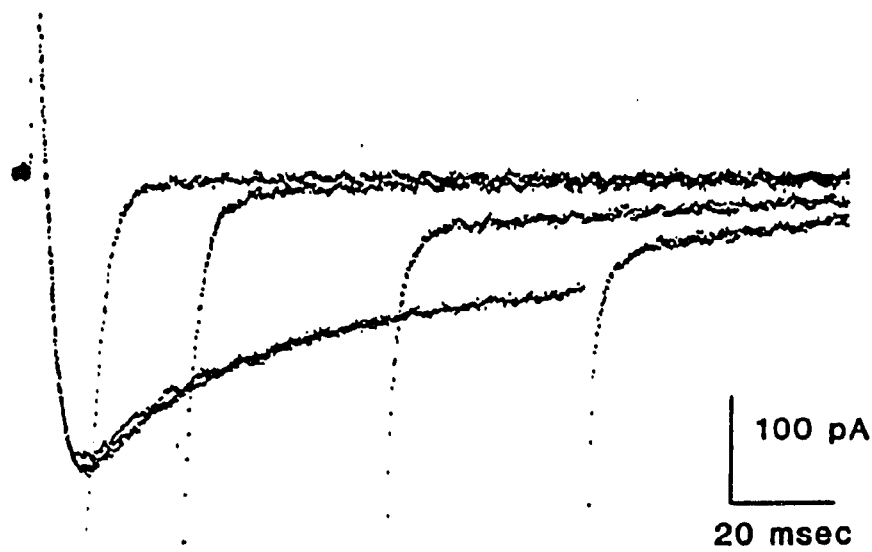
Figure 4.7

"Slow tails" observed during voltage clamp experiments designed to measure the calcium channel current. (Campbell 1985).

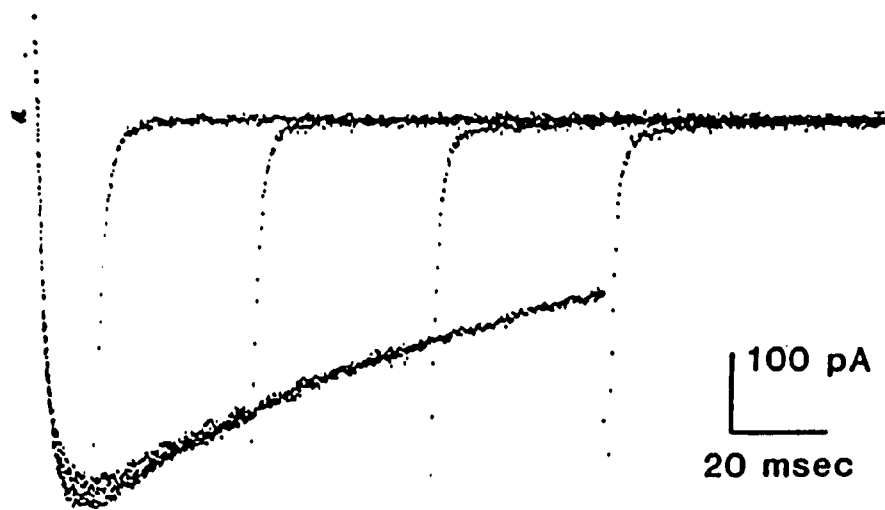
(i) 2.5 Ca



(ii) 2.5 Sr



(iii) 2.5 Ba





can thus be viewed during the time-course of the atrial action potential.

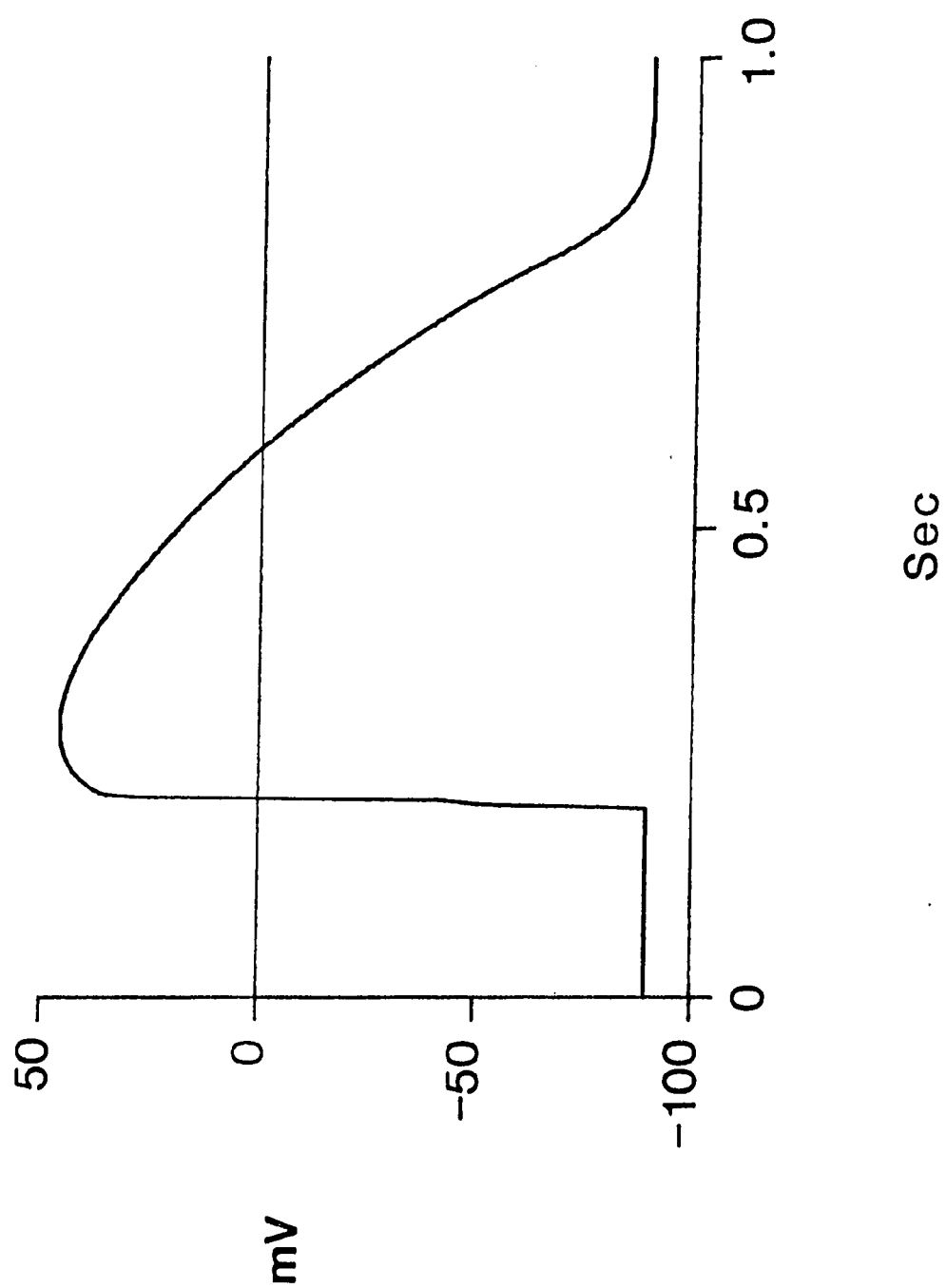
Figure 4.1 previously showed the model action potential and underlying currents in the presence of internal calcium buffering. Figure 4.8 shows the frog atrial model in the absence of internal calcium buffering. The shape of the action potential looks only slightly different. Underlying the action potential there are some differences the internal  $\text{Ca}^{++}$  concentration; the transient peak occurs earlier and is larger. Consequently a larger  $\text{Na}^+/\text{Ca}^{++}$  peak current is generated.

#### IV. 1.4 The Resting Potential and Late Repolarization.

In the voltage range near the resting potential,  $I_{K1}$  is the largest steady state conductance in frog atrial cells (Hume and Giles, 1983). The reversal potential is not solely determined by the efflux of  $\text{K}^+$  since the resting potentials are significantly positive to the equilibrium potential ( $E_K$ ) (Lüttgau and Niedegerke, 1958; Walker and Ladle, 1973). This suggests some steady inward current contributes to the resting potential. Hence, the resting membrane potential does not behave as an ideal  $\text{K}^+$  electrode; but it is close to  $E_K$  and is also a good indicator of changes in  $E_K$ . In isolated bullfrog atrial cells,

Figure 4.8

The model action potential generated when intracellular buffering is "turned off". The action potential looks very similar to the normal model action potential except that the last 30 mV of repolarization are not as abrupt due to the accented sodium calcium exchange current.



Hume and Giles(1981) found that a 46 mV change in resting potential occurred for every factor of 10 change in external  $K^+$  concentration. This is similar to the slope of 48 mV/decade change in  $K^+$  found in intact frog atrium (Hume and Giles; 1981).

It has been known for some time that ventricular muscle gradually depolarizes during rapid heart-rates (Niedegerke and Orkand, 1966). They suggested that this depolarization could be due to accumulation of extracellular  $K^+$ . More recent experimental evidence (obtained using  $K^+$  sensitive microelectrode impalements) exists suggesting that a net efflux of  $K^+$  occurs during the plateau, and the rapid repolarization phase in frog ventricle; this has been correlated with sustained accumulation and slow depolarization in frog ventricle (Morad, 1980; Kline and Morad (1976)).

Morad (1980) speculates that accumulation of  $K^+$  in the paracellular spaces plays an important role in the regulation of action potential duration. On his hypothesis regulation of the duration of the action potential was brought about by a shift in the reversal potential and the I-V for the inward rectifier ( $I_{K1}$ ) along the voltage axis, so that for higher  $K^+$  concentrations there is more outward current at plateau levels. Given the similarity between the currents found in frog atrium and frog ventricle it is of interest to examine the behavior of the model in presence of a restricted extracellular space.

Figure 4.9 shows two trains of model action potentials - panel A is in the absence of a restricted extracellular space while panel B is in the presence of a restricted extracellular space. Note that in Panel A (no restricted space) there is no shift in resting potential, while the restricted case shows a resting potential depolarization which relates to the shift in extracellular  $K^+$  ( $[K]_o$ ). This agrees with the experimental data (Morad, 1980).

The shift in the model  $I_{K1}$  I-V relation is, as expected, positive to nearly the same degree as the change in resting potential. Figure 4.10 shows the model  $I_{K1}$  at normal (2.5 mM)  $K^+$  concentrations and at the peak concentration shift in figure 4.9. This shift can effect late repolarization but is clearly too small in the potential ranges positive to 0mV to have much of an effect in early repolarization. There are several differences between the frog atrial model and the experimental set-up of Morad (1980) that could be responsible for the differences in conclusions concerning repolarization. Morad's (1980) preparations were bathed in a higher concentration of  $[K^+]$  (3.0mM as opposed to the 2.5mM used here) which causes the membrane to rest at more depolarized potentials and increases the magnitude and shifts in the depolarized direction the current to voltage relation of the instantaneous rectifier. More importantly, Morad's (1980) experiments were conducted in a low calcium solution (0.2 mM or less) which results

Figure 4.9

Effects of repetitive activity in the absence and presence of a restricted extracellular space.

Panel A

Repetitive stimulation of the atrial model in the absence of a restricted extracellular space.

Panel B

Repetitive stimulation of the atrial model in the presence of the three compartment model.

Panel C

$[K^+]_{\text{cleft}}$  concentration during repetitive stimulation of the atrial model in the presence of the three compartment model.

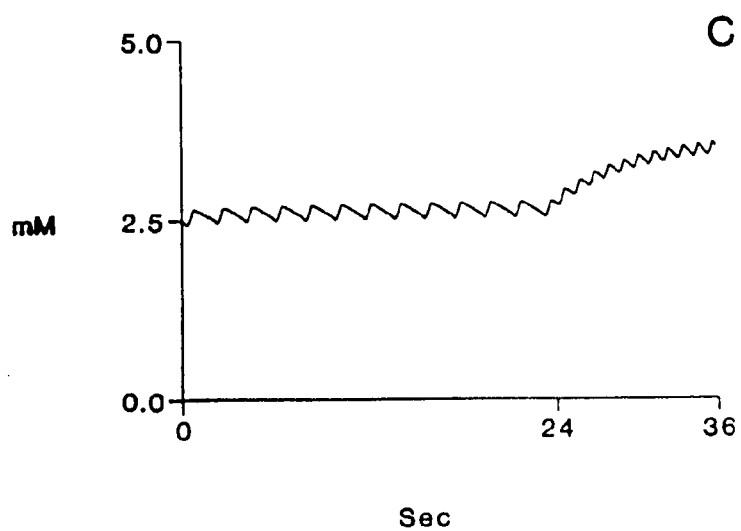
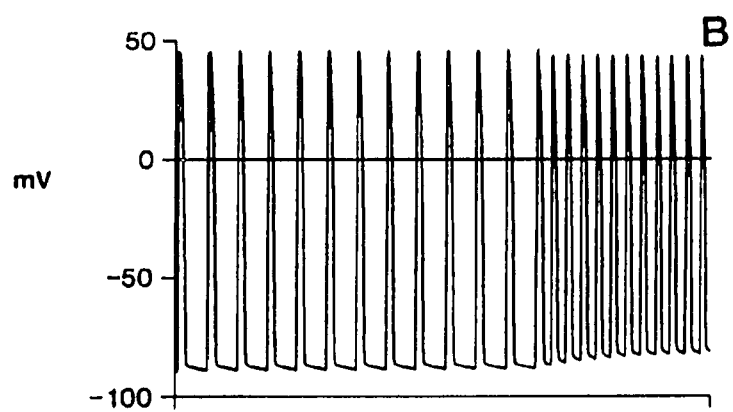
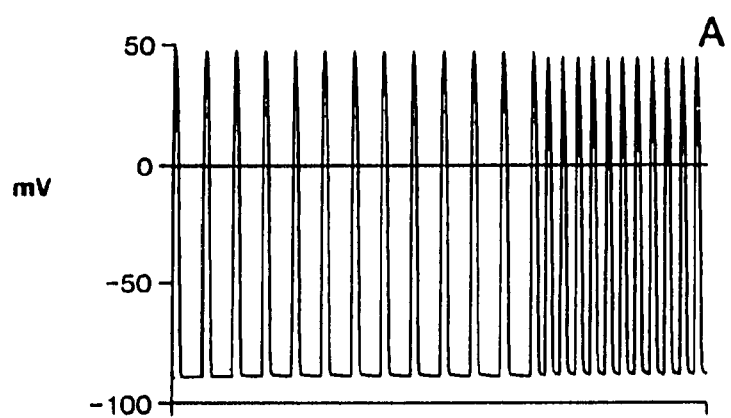
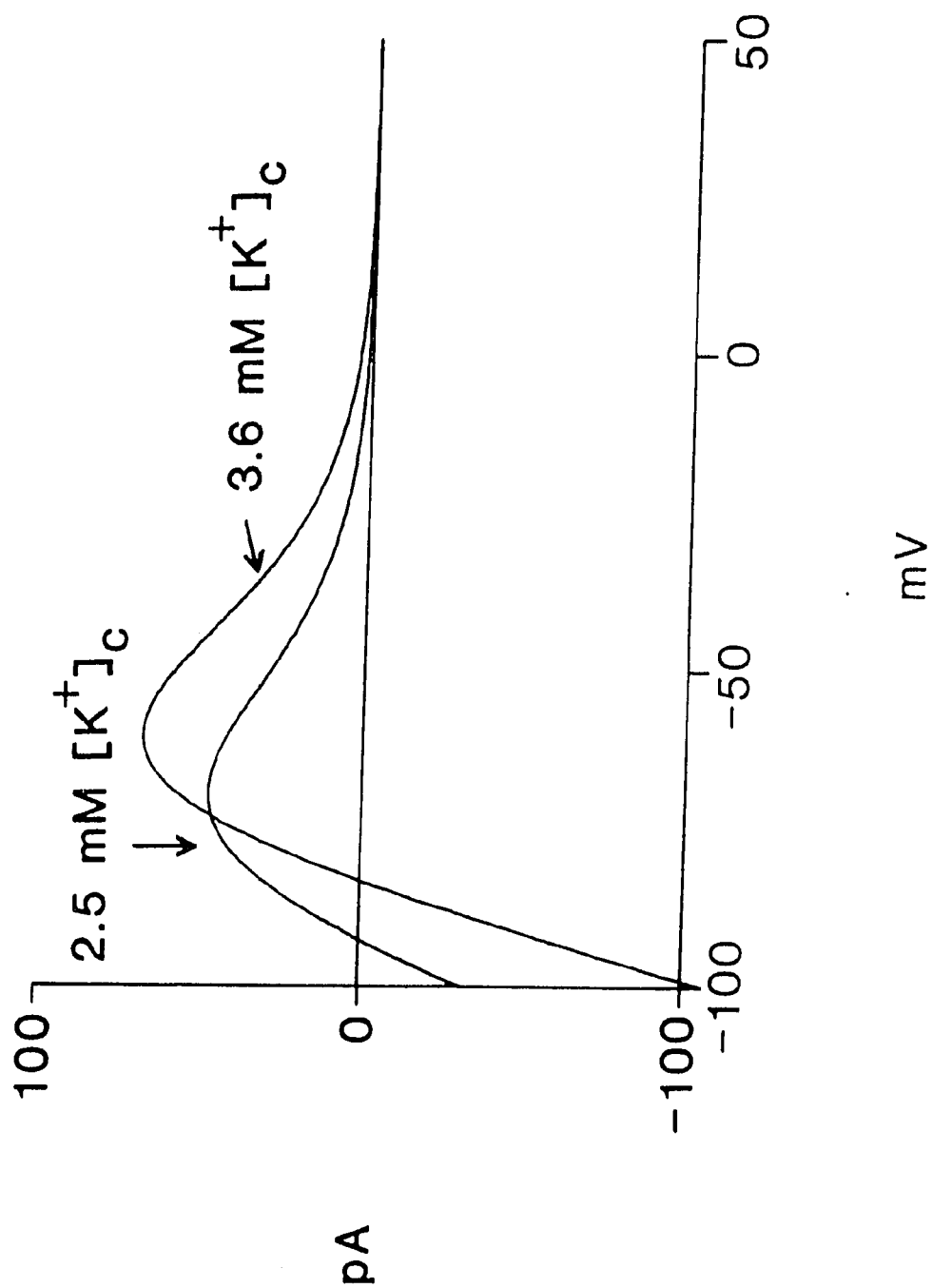


Figure 4.10

A plot of the model  $I_{K1}$  relationship for a 2.5 mM  $K^+$  cleft concentration and the maximum accumulation (3.6 mM) achieved by the model in the previous figure. (see text).





in a much lower plateau and much broader action potential, hence the events underlying repolarization may have been altered. Note that  $I_{K1}$  will contribute a significant net outward current much earlier in the time course of the action potential if the peak depolarization is much lower (e.g. +20 mV in Morad (1980) vs. 40 mV in Hume and Giles, (1983)). The 3.0 mM  $K^+$  perfusion concentration used by Morad (1980) shifts the  $I_{K1}$  I-V relation to more depolarized potentials prior to accumulation where it may have more of an effect on repolarization.

The role of  $I_{K1}$  on rest and late repolarization has also been studied using pharmacological blocking agents, e.g.  $Ba^{++}$  which, in low concentrations is very selective for this channel. (Hermsmeyer and Sperelakis (1970); Argibay, et. al (1983); Shibata and Giles(1985)). The addition of  $Ba^{++}$  has also been found to produce automaticity in frog atrium. (Shibata and Giles;1985).

The atrial model can mimic the effects of  $Ba^{++}$  block by adjustment of the  $I_{K1}$  conductance. Figure 4.11 a shows the effect of applying a Ringers solution containing  $Ba^{++}$  (100\_M) in an isolated atrial cell. As  $I_{K1}$  becomes blocked the "foot" of the action potential begins to "kick out", this is in precisely the range of potentials predicted by the model. Figure 4.11 b shows the same effect mimiced by lowering the conductance of the  $I_{K1}$  channel. If all of the  $I_{K1}$  conductance is eliminated then the

Figure 4.11

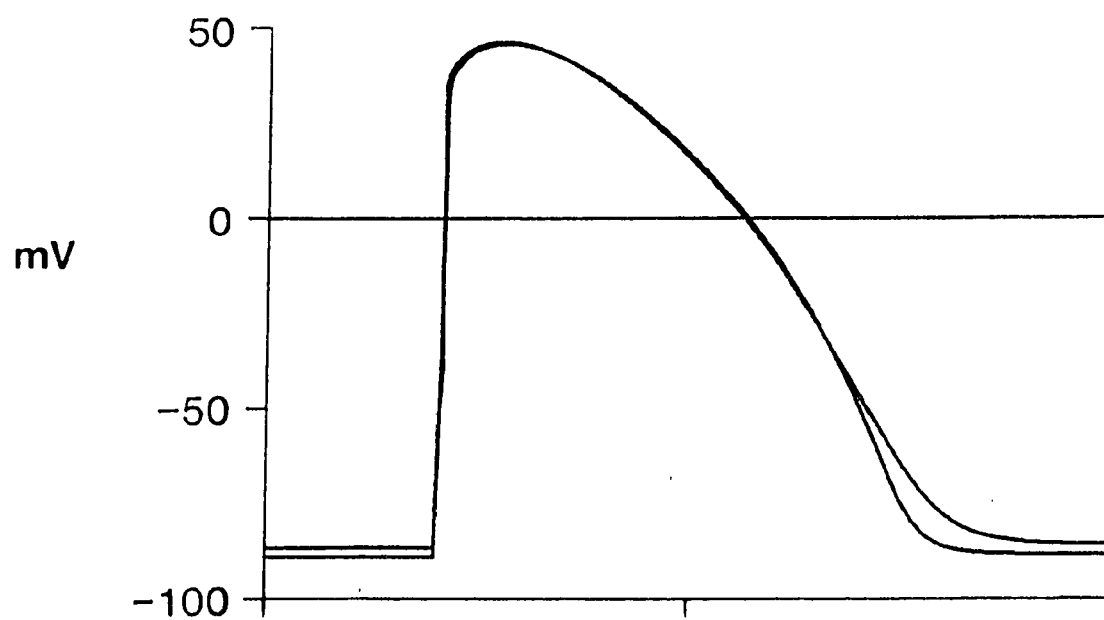
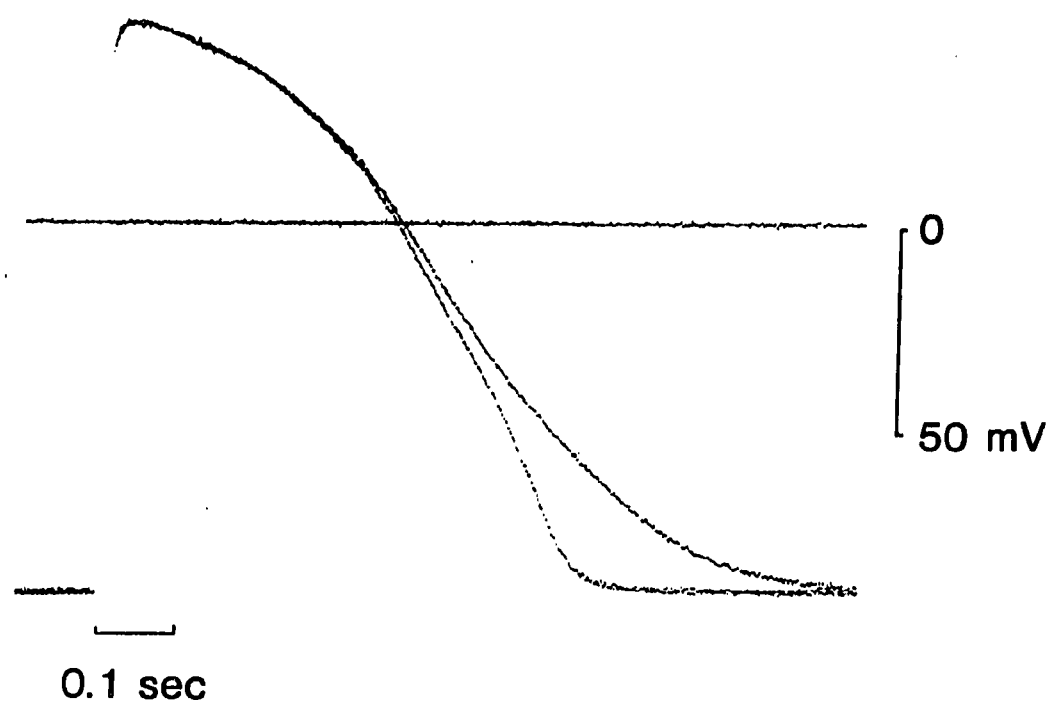
Effects of the application of  $\text{Ba}^{++}$  (50  $\mu\text{m}$ ) on the atrial action potential. Note that which lengthens the action potential.

Panel A

experimental result

Panel B

model simulation



model shows spontaneous pacing (Figure 4.12). Unfortunately the upstroke of the model action potential is much slower than that observed in an actual atrial cell undergoing  $Ba^{++}$  induced pacing. This may be due to some deficiency in the model formulation of one or both of the transient inward currents or may be due to some additional effect of  $Ba^{++}$ .

#### IV.2 Frequency Dependent Effects on $[Ca^{++}]$ in Atrial Cells.

##### IV.2.1 Intracellular Calcium and Frequency.

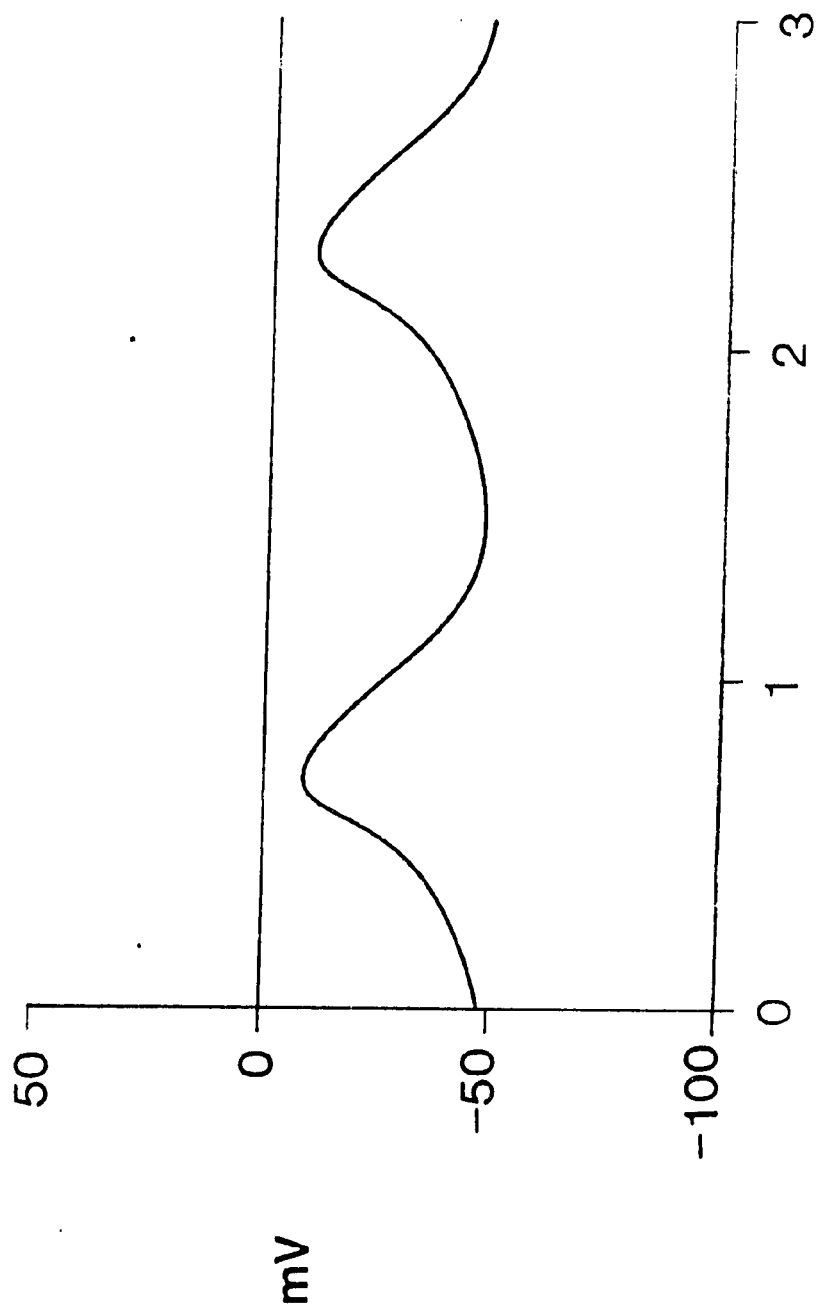
The amount of tension developed during an action potential cannot be related simply to the  $Ca^{++}$  entering the cell during that action potential. When a series of action potentials occur, it has been long known (c.f. Dale (1930), Bowditch (1871)) that peak tension is developed only after several action potentials. This phenomenon is the 'staircase' effect (Niedergerke 1956 ; Orkand 1968). It suggests that the  $Ca^{++}$  entering during all of the preceeding action potentials is also an important determinant of the strength of contraction.

In mammalian heart there is evidence that entry of  $Ca^{++}$  via  $I_{Ca}$  during each action potential is responsible for releasing  $Ca^{++}$

Figure 4.12

Simulation of induced pacing in the atrium by removing the  $I_{K1}$  current. The pacing achieved is very weak and the membrane is very depolarized this pacing more resembles that due to a depolarizing constant current pulse (Noble, S.

1976) than the pacing due to Ba application.



from the intracellular stores of  $\text{Ca}^{++}$  in the sarcoplasmic reticulum. The model of frog atrial cells presented here does not include such internal stores of  $\text{Ca}^{++}$  in the sarcoplasmic reticulum (see Chapter II p. 64-65.). However, the staircase phenomenon is found in frog ventricle (Niedergerke (1956)). When an excised frog ventricle is stimulated periodically after a sufficiently long period of quiescence, the first contractions are small, and succeeding responses gradually increase; the small initial contractions are accompanied by full sized action potentials. (Niedergerke (1956)).

If the  $\text{Ca}^{++}$  specific sites were "alone" inside of the atrial cell it would be expected that the change in occupancy during an action potential would be roughly proportional to the amount of  $\text{Ca}^{++}$  entering the cell during that beat. Further, the change in occupancy would be the largest and quickest when nearly all the sites were vacant (i.e. when  $K_{\text{on}}$  would be at its fastest). One way to account for the increasing occupancy expected for the  $\text{Ca}^{++}$  specific site would be an increase in calcium influx during the action potential. Figure 4.13 shows modelling results intended to illustrate this effect. The atrial membrane model was allowed to remain quiescent for a "long time" (i.e. 120 seconds). It was then stimulated at a rate of 0.5 Hz (figure 4.13 a) and the internal  $\text{Ca}^{++}$  buffer occupancies (Panel b) were monitored. All action potentials are full sized and the net  $\text{Ca}^{++}$  influx due to



Figure 4.13

The staircase effect in the frog atrial model. The membrane was allowed to rest for 120 seconds and was then stimulated at a rate of 0.5 hz for 24 seconds and then at 1.0 hz for 12 seconds.

Panel A

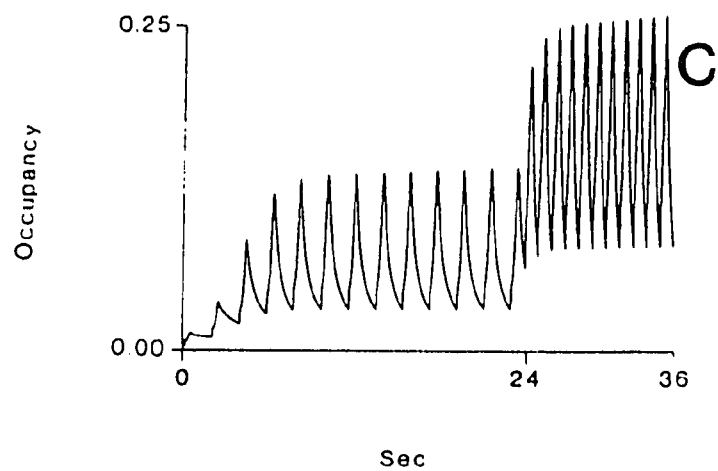
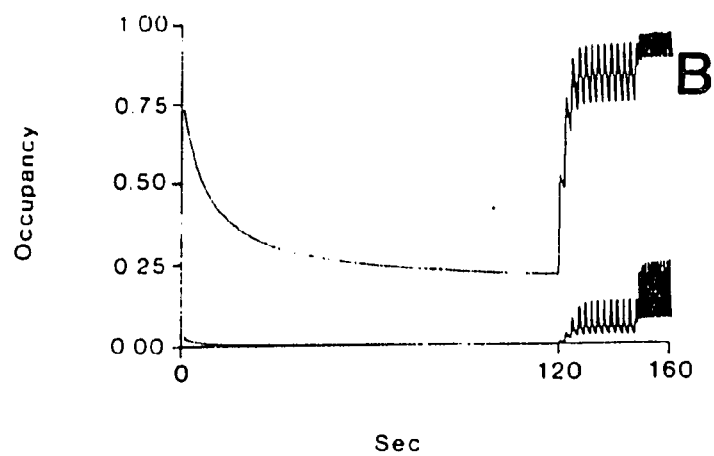
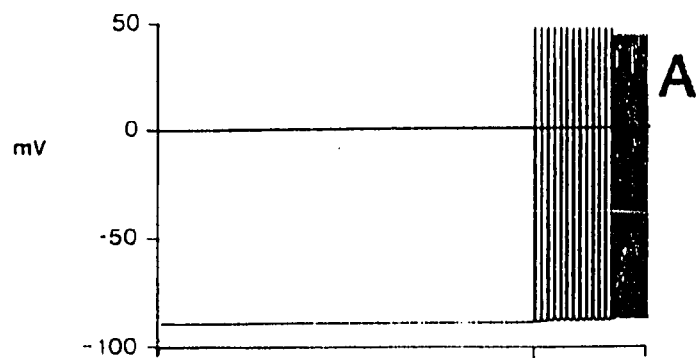
The membrane potential

Panel B

The internal occupancy of the  $Mg^{++}/Ca^{++}$  competitive site by  $Ca^{++}$  (top trace) and of the  $Ca^{++}$  specific site by  $Ca^{++}$  (bottom trace).

Panel C

The occupancy of the  $Ca^{++}$  specific site by  $Ca^{++}$  "blown up" for better visualization.



$I_{Ca}$  is nearly the same for all the action potentials, and does not increase during each successive action potential. The extrusion mechanisms begin to extrude more calcium with each cycle. Therefore this atrial model does not relate the increase in transient  $Ca^{++}$  occupancy on the  $Ca^{++}$  specific sites on Troponin to an increased calcium influx during each successive action potential.

Occupancy of the  $Ca^{++}$  specific sites on troponin does increase with each successive action potential following a long period of quiescence. The internal free  $Ca^{++}$  concentration transient also increases with each successive action potential (Panel D). The mechanism for this is evident from figure 4.13 b; a slow build up of  $Ca^{++}$  bound to the  $Mg^{++}/Ca^{++}$  competitive site on troponin is occurring with each successive beat. The  $Mg^{++}/Ca^{++}$  sites had lost most of their  $Ca^{++}$  during the quiescent period due to the relatively low resting internal  $Ca^{++}$  concentration. Calcium entering the cell is more readily bound to these sites than to the  $Ca^{++}$  specific sites, and since it is released from these sites only very slowly the  $Ca^{++}$  bound to them builds up until the occupancy is very near that of the occupancy for the average  $Ca^{++}$  concentration during the subsequent interval. It is the competition by the  $Ca^{++}/Mg^{++}$  competitive site with the  $Ca^{++}$  specific site that causes the slow buildup in peak occupancy of the  $Ca^{++}$  specific site.

This mechanism is very similar to the mechanism proposed by Chapman and Niedergerke (1970a,b) to explain the staircase phenomena in the frog heart. They suggested that their experimental results "could be explained if the contraction of the frog heart is brought about by the action of two different calcium compounds,  $Ca_1$  and  $Ca_2$ , which both vary with the external calcium concentration but respond at characteristically different rates to a change in this concentration. Compound  $Ca_1$  appears to initiate the contractile process, whereas  $Ca_2$  modifies its strength."(Chapman and Niedergerke;1970b)

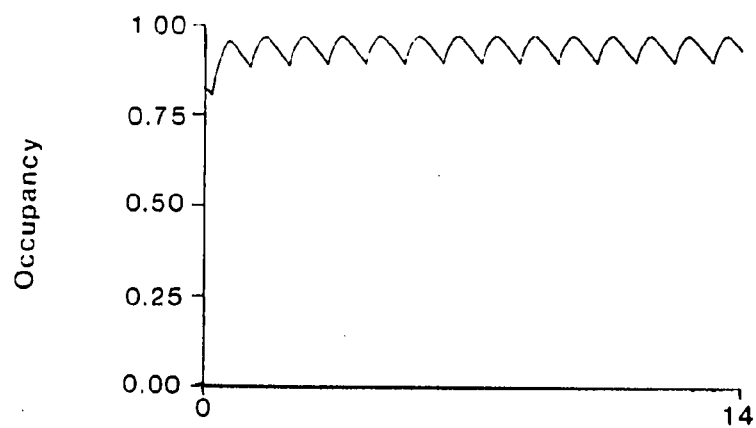
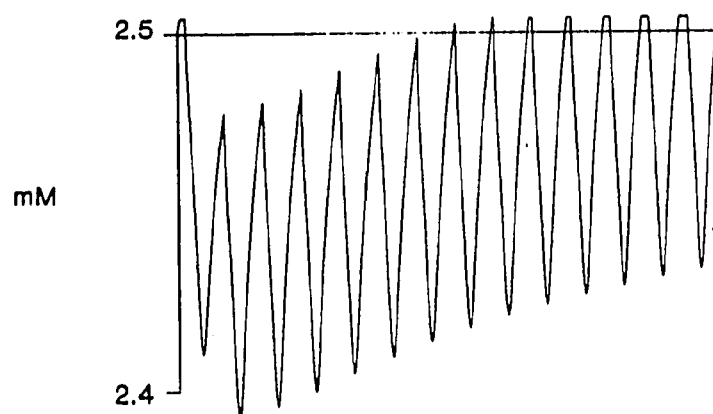
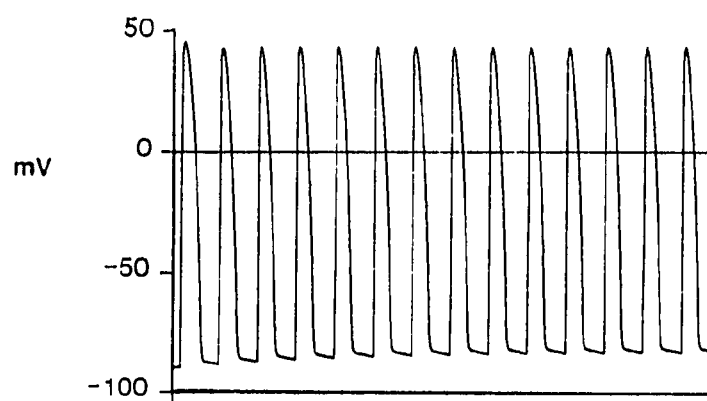
#### IV.2.2 External Calcium and Frequency

As mentioned in chapter III there is a net  $Ca^{+}$  influx across the cell membrane into the intracellular compartment during a typical action potential. This may cause a small depletion of cleft  $Ca^{++}$  (Morad(1980), Cleeman et. al. (1984)). Does a rapid series of action potentials show an increasing depletion of cleft  $Ca^{++}$  in a fashion similar to the accumulation of cleft  $K^{+}$  during rapid stimulation?( Dresdener and Kline(1985))

Figure 4.14 a shows an action potential train elicited at a frequency of 1 Hz after a period of normal (0.5 Hz) stimulation under simulation conditions including a restricted extracellular

Figure 4.14

The effect of a change in rate upon the extracellular  $\text{Ca}^{++}$  concentration. The figure shows a train of action potentials at 1.0 Hz after a period of stimulation at 0.5 Hz. The train starts with the first "premature" action potential. Panel B shows the cleft  $\text{Ca}^{++}$  concentration and panel C shows the occupancy of the  $\text{Mg}^{++}$  competitive site. Note that the change (depletion) in average cleft  $\text{Ca}^{++}$  concentration is both small and rapid, occurring within the first two beats.



space. Panel B shows the time course of extracellular  $\text{Ca}^{++}$  concentration and Panel C shows the fractional occupancy of the  $\text{Ca}^{++}/\text{Mg}^{++}$  competitive site by  $\text{Ca}^{++}$ . Obviously cumulative  $\text{Ca}^{++}$  depletion can occur under some circumstances but its time-course is much faster than the analogous cleft  $\text{K}^{+}$  accumulation. The reasons for this are apparent: The processes regulating internal  $\text{Ca}^{++}$  are much quicker to react and consequently the  $\text{Ca}^{++}$  depletion is entirely due to a change in the equilibrium amounts of  $\text{Ca}^{++}$  bound to the internal buffer proteins rather than by a slow change in internal concentration. The depletion which the model predicts has not yet been measured in frog heart, since both optical and  $\text{Ca}^{++}$  sensitive microelectrode measurement of cleft  $\text{Ca}^{++}$  activity involve suppression of contraction by reduced extracellular  $\text{Ca}^{++}$  concentration in order to minimize measurement artifacts (Cleemen et. al, 1984; Dredener and Kline(198?)).

#### IV.3 Frequency and Intracellular $\text{Na}^{+}$ .

Intracellular sodium concentration plays an important role in modulating or controlling a number of transmembrane currents. It is crucial in determining the behavior of the  $\text{Na}^{+}/\text{Ca}^{++}$  exchanger, the magnitude of the  $\text{Na}^{+}/\text{K}^{+}$  pump current, as well as the reversal potential of the  $I_{\text{Na}}$ . Because of its relatively high internal concentration (7.5 mM) within the cell, relative changes of

sodium concentration within the cell may be expected to occur with a much slower time course than analogous accumulation/depletion effects for  $K^+$  and  $Ca^+$  in the extra-cellular space.

Figure 4.15 shows the internal  $Na^+$  concentration during a period of quiescence and then during stimulation at (i) 0.5 Hz for 12 beats and (ii) at 1.0 Hz for an additional 12 beats. It is apparent that internal  $[Na^+]_i$  concentration can be effected by stimulus rate but that such changes occur very slowly, taking minutes to change between steady states that differ by millimolar amounts. This indicates that internal sodium concentration is not significant over periods of a minute but may be during protocols lasting many minutes (e.g. during measurements on contraction of hypodynamic frog heart Chapman and Niedergierke (1970a,b)). With present computing facilities, however, simulations of protocols lasting over several minutes are prohibitive.

#### IV.4 Pacing in the Bullfrog Sinus-Venous

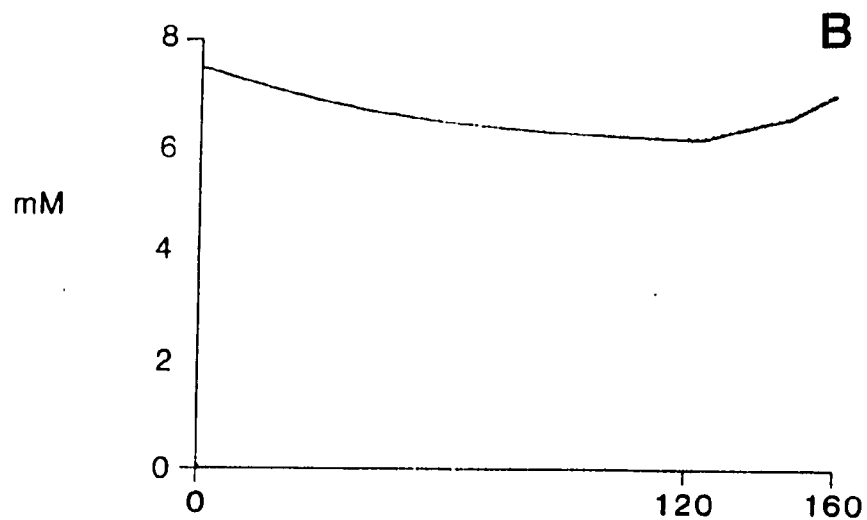
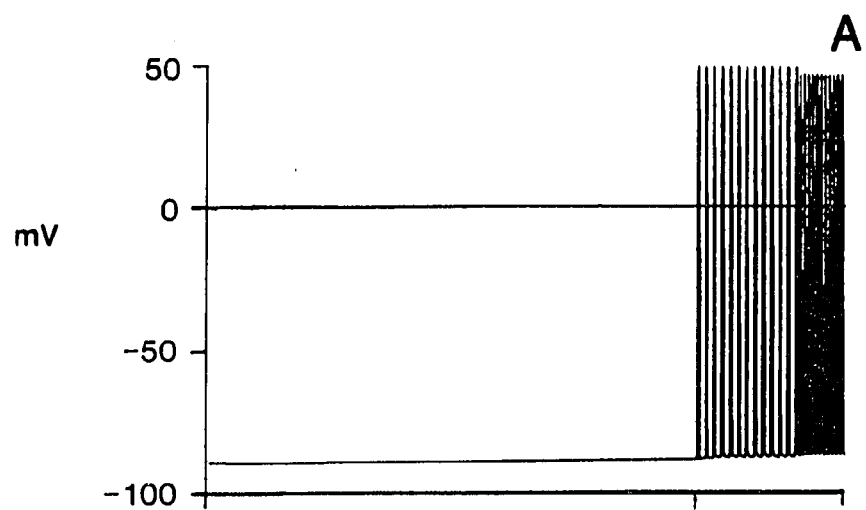
##### IV.4.0 Introduction

In the Hodgkin-Huxley (1952d) model of the squid giant axon it was noted that a nerve fibre whose membrane was described by these equations would gradually run down. Since potassium leaves the cell continuously, some additional process in the living



Figure 4.15

The effect of a change in rate upon the intracellular  $\text{Na}^+$  concentration. The figure shows a train of action potentials at 0.5 Hz and 1.0 Hz after a quiescent period. Panel B shows the internal  $\text{Na}^+$  concentration. Note that the change in intracellular  $\text{Na}^+$  concentration is very slow taking minutes to effect millimolar changes.



animal maintains the ionic gradients which are the immediate source of energy used in action potential generation. The early models of cardiac electrical activity also failed to include mechanisms that maintain the ionic gradients across the cell membranes (Noble (1962), McAllister, Noble and Tsien (1975), Beeler and Reuter (1977), Yanagihara, Noma, Irisawa (1980) Bristow and Clark (1982)). Beeler and Reuter (1977) were concerned enough with changes in internal calcium concentration to provide for some mechanism of calcium sequestration but the effects of this mechanism were only evident in reversal potential changes for  $E_{Ca}$ , and not e.g. in  $Ca^{2+}$  extrusion.

Improvements in experimental technique and the corresponding increase in the knowledge concerning sarcolemmal transport mechanisms has resulted in a second generation of cardiac models in which the contributions of these mechanisms are considered to be integral parts of the electrical activity of the cell. In both the DiFrancesco and Noble (1985), and Noble and Noble (1984) models there are substantial effects on the shape of the action potential due to the  $Na^+/Ca^{++}$  exchange current. In the Noble and Noble (1984) model of sinus activity, the  $Na^+/K^+$  pump current is sufficiently large to be important in the determination of  $dv/dt$  during the diastolic interval and can even suppress pacemaker activity in the presence of increased internal sodium concentration.

#### IV.4.1 Pacing in the Absence of Pump and Exchanger Currents.

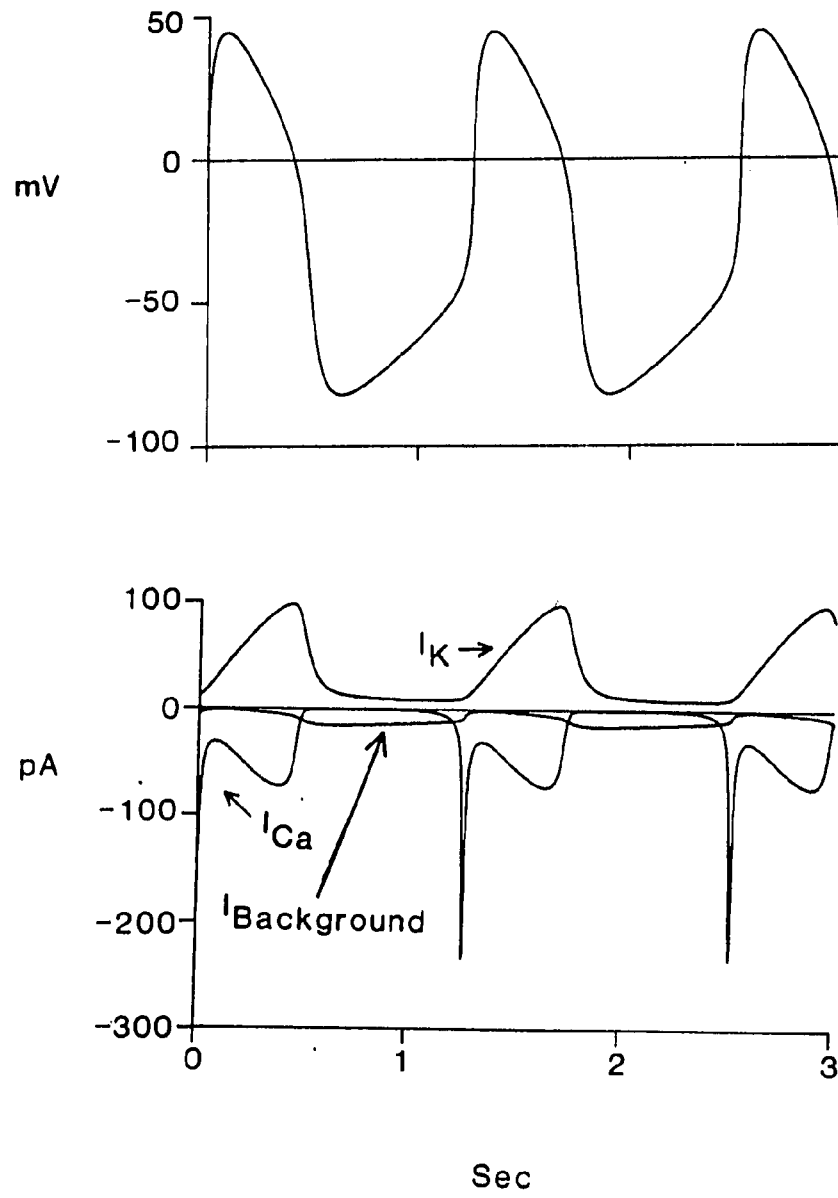
The bullfrog sinus-venosus is distinct from mammalian pacemaker cells in that it does not have the  $I_f$  or "pacemaker" current (Giles and Shibata, 1985). Hence, spontaneous pacing does occur in these cells; and it arises from an interaction of the currents that underly the action potential. The sinus-venosus model results from the interaction of six current systems ( $I_{Ca}$ ,  $I_K$ ,  $I_{Background}$ ,  $I_{NACA}$ ,  $I_{NAK}$  and  $I_{Ca Pump}$ ). In order to obtain a clearer picture of the role of each of these currents during the diastolic interval a subset of the model equations can be utilized.

Figure 4.16 shows the model waveform generated when  $I_{NACA}$ ,  $I_{NAK}$  and  $I_{Ca Pump}$  are removed and internal concentrations are held constant. The action potential waveshape looks very similar to that of the model with pumps, currents and ionic concentration changes incorporated. The main difference appears to be an increase in the frequency of oscillation which could be compensated for by increasing  $I_{Background}$ .

Detailed inspection of the ionic current changes underlying the 'simplified' model action potential suggests a role for each of the transmembrane ionic currents:

Figure 4.16

Simulation using only a subset of the Sinus-Venosus model parameters. Sinus venosus action potentials are simulated using only three membrane currents and assuming constant intracellular and extracellular concentrations. The results produce normal, although rapid, pacing.



(1)  $I_K$  is activated during the time-course of a normal action potential and slowly deactivates during the time course of the diastolic interval. The deactivation of  $I_K$  is important during the diastolic interval; particularly in the early portion of the interval. This conclusion is consistent with similar modelling studies in mammalian pacemaker cells (Brown et al. 1984a,b and Noble and Noble 1984).

(2)  $I_{Ca}$  begins to activate during the last 100 milliseconds of the diastolic interval. The activation of this current indicates that  $I_{Ca}$  provides small amounts of inward current during the last 1/3 to 1/5 of the diastolic depolarization. This is consistent with the findings of Giles and Shibata (1985) in frog sinus-venosus and Brown et al. (1984) in rabbit Sino-Atrial node.

(3)  $I_{Background}$  provides an inward current which decreases slightly as depolarization proceeds. This provides most of the inward current generating diastolic depolarization in the simplified model; and hence it serves the same role as  $I_{Na,b}$  does in the Noble and Noble (1984) model of rabbit S-A model pacing.

In summary, the pacemaker potential is supported by a steady inward current from  $I_{Background}$ , is initially modulated by the

slow decay of  $I_K$  during the first half of diastolic depolarization, and is accelerated by activation of  $I_{Ca}$  just prior to the upstroke of the action potential.

#### IV.4.2 Pacing in the Presence of Pump and Exchanger Currents.

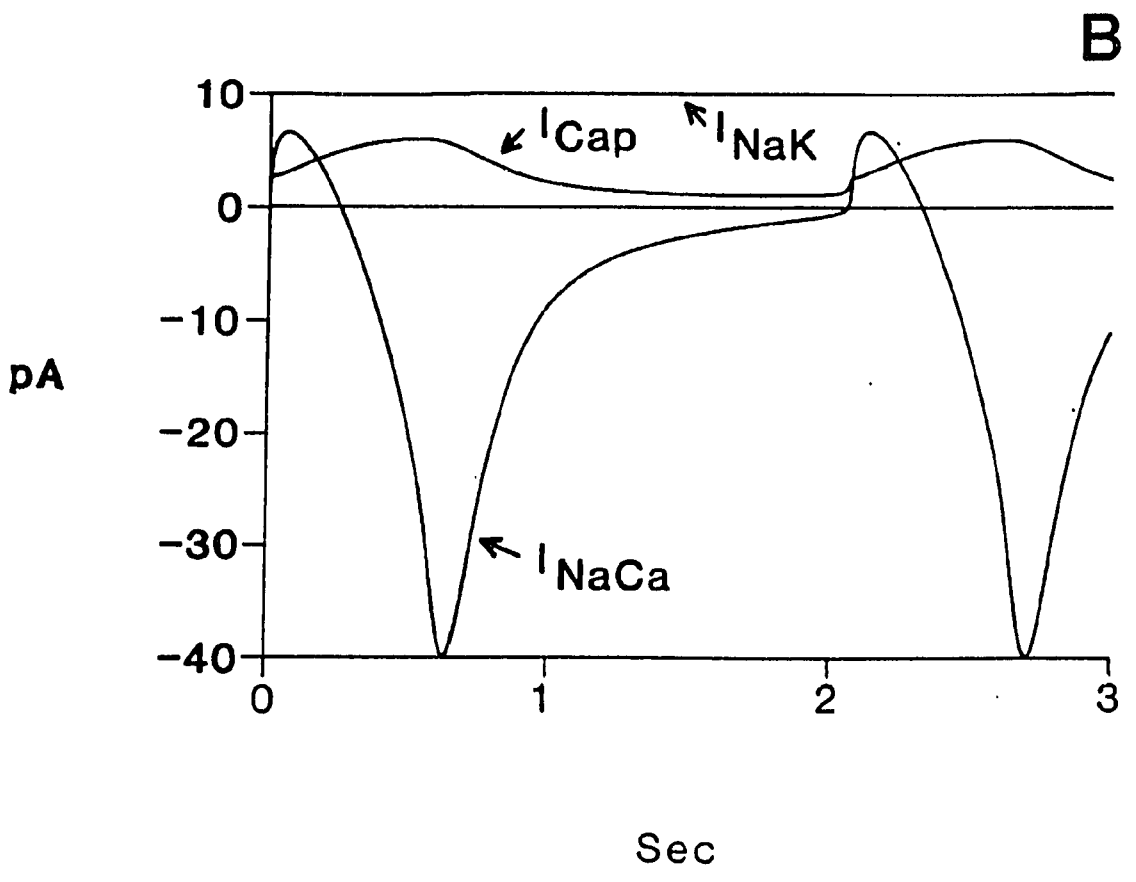
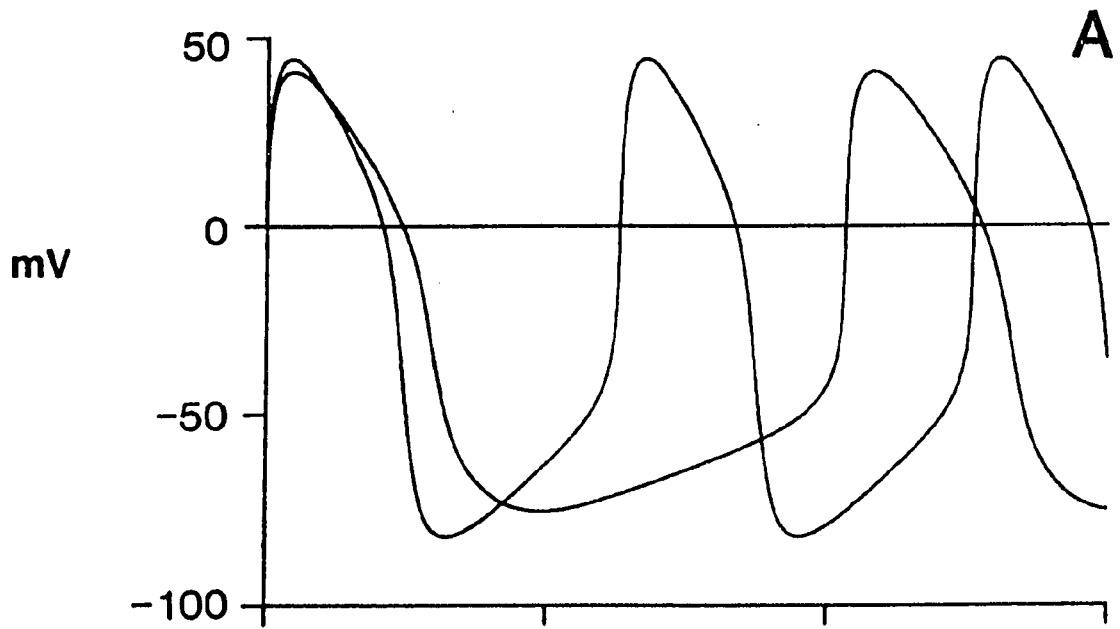
In the previous section the relative roles of the various ionic channel currents were evaluated by comparing the model output in the absence of pump and exchange currents and concentration changes. By comparing these simplified results with the model results incorporating ionic pumps and exchange currents as well as concentration changes, the relative roles of the ionic pump and exchange mechanisms during pacemaking activity can also be evaluated.

Figure 4.17 a shows the action potential from the "simplified" simulation superimposed upon the action potential from the model incorporating ionic pump and exchange currents and concentration changes. The most noticeable difference is that repolarization proceeds more slowly with the incorporation of pump and exchange currents and repolarization brings the potential to a less negative maximum diastolic value. This is due to the inclusion of  $I_{NaCa}$  which becomes progressively more inward during repolarization and peaks near the maximum diastolic potential.



Figure 4.17

A comparison of pacing in the presence and absence of pump and exchange currents. Panel A shows the two action potential waveforms. The more rapid action potential is generated in the absence of pump and exchange currents. Panel B shows the pump and exchange currents that are responsible for the difference.



$I_{NaCa}$  has a much greater influence during late repolarization in sinus-venosus than in atrium for two reasons: 1) There is no  $I_{K1}$  in sinus-venosus to 'dominate' this portion of the cycle. 2) There is a much larger influx of  $Ca^{++}$  in sinus-venosus, resulting in a much larger  $Na^+/Ca^{2+}$  exchanger current. This result suggests that this current may play a role in determining maximum diastolic potential and in the rate of diastolic depolarization. This role is contrary to the role predicted by the model of H. Brown et al. (1984b) for mammalian S-A node.

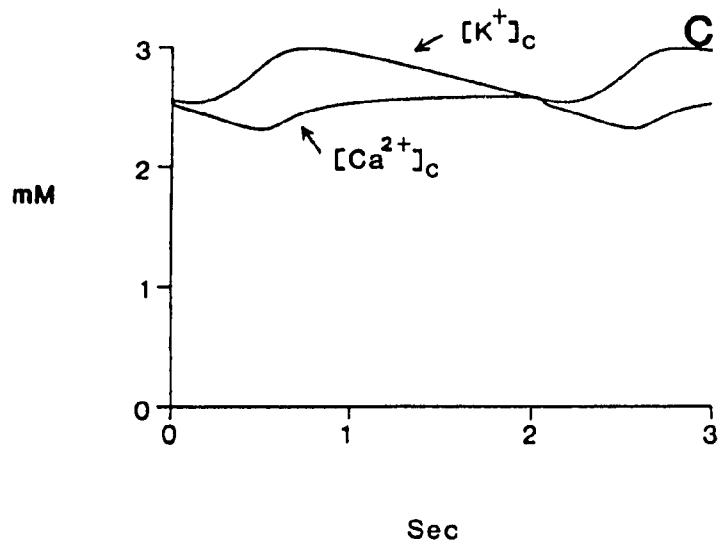
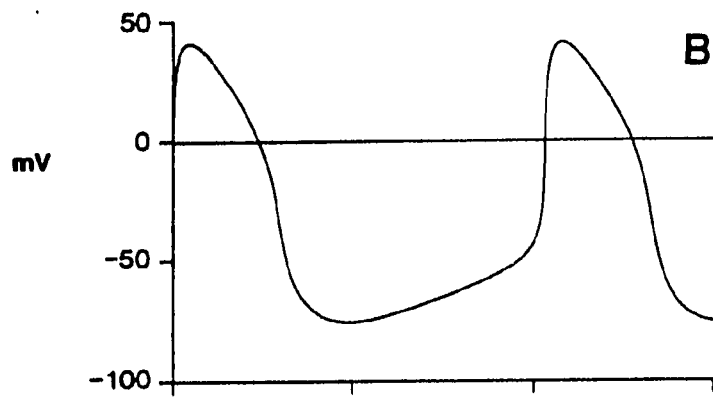
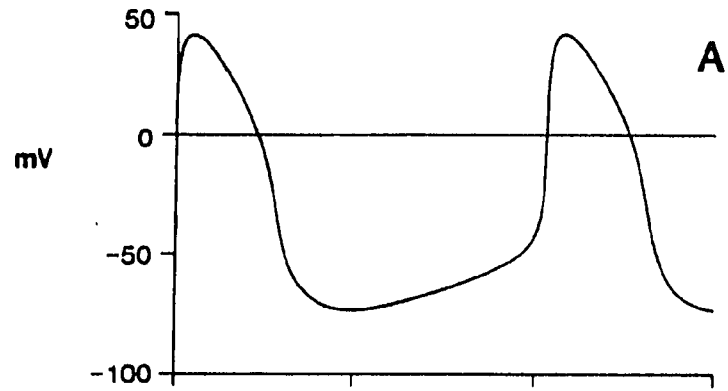
The diastolic interval in the absence of ionic pump and exchange mechanisms is greatly shortened. This is due to the lack of a  $Na^+/K^+$  pump current in the "simplified" simulation. The  $Na^+/K^+$  current provides a current in the hyperpolarizing direction which is substantial when considering the very small net currents needed to produce the diastolic depolarization. As mentioned in Chapter II the  $Na^+/K^+$  pump is thought to be voltage insensitive and must be sufficient to extrude all  $Na^+$  entering during one cycle. Therefore the magnitude of the model current during diastolic depolarization is likely to provide a good estimate of the contribution of the  $Na^+/K^+$  pump to the diastolic depolarization. These results are consistent with the mechanisms proposed by Noma and Irisawa (1975) and Noble and Noble (1984) concerning the effects of  $Na^+/K^+$  output on spontaneous activity.

#### IV.4.3 Pacing in the Presence of a restricted extracellular space.

An examination of the action potentials presented in Figure 4.18a,b shows that there is no discernible difference between the membrane action potential and the action potential in the presence of a restricted extracellular space. It is safe to assume then that in normal pacing accumulation/depletion phenomena have no significant role. It should however be noted that due to the much larger  $\text{Ca}^{++}$  current in sinus-venosus the model predicts a fluctuation in cleft concentration of  $\text{Ca}^{++}$  of  $\sim 0.3$  mM and of approximately 0.5 mM for  $\text{K}^{+}$  during each cycle (Fig. 4.18c). This is larger than the transients predicted for atrial tissue in the atrial model. These results are steady-state results in that the model potential waveform was taken after 30 seconds so that start-up effects would be minimized and concentration changes due to perfusion from the bulk medium would have stabilized ( $T_p = 10$  seconds).

Figure 4.18

A comparison of pacing in the presence and absence of a restricted extracellular space. Panel A shows the standard potential waveform. Panel B shows the action potential generated in the presence of a restricted extracellular space. Panel C shows the amount of accumulation and depletion occurring. Note that the action potential appear identical.



Chapter VDISCUSSION

The major goal of this work has been to mathematically reconstruct the action potential and the pacemaker potential in atrium and in sinus venosus of the bullfrog heart. Where possible the mathematical formulations for the ionic currents have been based on data which is available from experimental measurements of the equivalent circuit and of the transmembrane currents. The details of the mathematical formulation of the model and of the experimental results have been discussed previously in Chapters III and IV. This chapter will summarize the apparent strengths and weaknesses of this model, and will relate these computer simulations to previous mathematical reconstructions of the action potential and pacemaker potential in frog and mammalian cardiac muscle.

V.1 Previous work

Within the past fifteen years a number of attempts have been made to mathematically simulate the electrophysiological activity in bullfrog atrium, but no simulations of pacemaker activity from bullfrog sinus venosus have been reported. As noted previously,

Besseau (1972) developed a model of the frog atrial action potential based upon some data from double sucrose gap experiments; and Drouhard and Roberge (1982) attempted to simulate the repolarization process in bullfrog ventricle. In the latter work no attempt was made to match the model parameters to experimental data; and in fact, much of the directly relevant cardiac literature seems to have been ignored (see below).

The most direct precedent for the present results is the Masters thesis of Robinson, (1984). In this modelling, thesis preliminary data from single cells derived from bullfrog atrium was used to simulate the atrial action potential. Although the waveform of the atrial action potential was reconstructed quite successfully, and some (e.g. see calcium and potassium currents) of the transmembrane ionic currents could be quantitatively reproduced; nevertheless, this model failed to reproduce many of the frequency-dependent phenomena seen in bullfrog atrium. Robinson noted that this may have been due to the lack of accurate experimental data describing e.g. the kinetics of the sodium current.

The present work represents a significant extension of the Robinson study. Thus, a model for frog sinus pacemaker activity has been developed and the possible contributions of pump currents (sodium-potassium pump and calcium-pump), exchanger currents (the sodium-calcium exchanger), and intracellular buffering of calcium



ions have been included. The resulting model (presented in this thesis) represents the most complete description of the electrophysiological phenomena in frog heart, which is available at present. Moreover, it includes each of the important parameters which the most complete model of the mammalian cell (DiFrancesco and Noble, 1984) have emphasized should be involved in quantitative models of cardiac electrophysiological activity. In fact, the DiFrancesco and Noble (1984) model fails to account for intracellular calcium buffering; a phenomenon which we have shown is of considerable importance in accounting for calcium homeostasis in atrial and sinus cells and in predicting the size and time course of the sodium-calcium exchanger current and hence determining its physiological role.

V.2 Usefullness of this model in determining the physiological role of ionic, pump, or exchanger currents in normal electrophysiological activity in the heart:

The extent to which these simulations or any computer modelling is useful or successful in electrophysiology depends critically upon its ability to quantitatively reproduce experimentally observed phenomena and its predictive value. In the present work considerable effort has been expended to determine to what extent this model can simulate basic electrophysiological

phenomena: e.g. the waveshape of the action potential, the appropriate rates of depolarization and/or repolarization, frequency dependent phenomena (I-D relation), and all-or-none repolarization. In the case of the atrium model, each of these phenomena can be reproduced quite satisfactorily. As expected, the transmembrane currents which underly the action potentials can also be quantitatively reproduced using the existing model equations. However, a number of important shortcomings in this regard were noted.

1. The model fails to reproduce the rapid upstroke velocity experimentally observed during pacing induced by  $Ba^{++}$  block of  $I_{k1}$ .

2. The activation of the peak  $I_{Ca}$  during voltage clamp conditions occurs at a more depolarized potential in the model when compared to experimental observations.

3. Reconstruction of the transient sodium current is only semi-quantitative and is based on a steady state inactivation relation observed at reduced temperatures which may effect this measurement.

4. The assumption of completely selective permeabilities for computing the membrane currents does not describe the ion transfer process at extreme ranges of transmembrane potential. (e.g.  $I_{Ca}$  does not carry net outward current at potentials positive to 50 mV )

Similarly, the sinus venosus model quite accurately simulates the waveform of both the pacemaker and the action potential of the frog heart. In addition, (although this model may appear to be simply a reduced atrial model) this mathematical reconstruction work drew our attention to some significant differences in the current densities and kinetics in these two tissues. For example: 1) The calcium current in the sinus tissue is approximately two times larger than that in atrium. 2) Neither the fast transient inward ( $I_{Na}$ ) nor the instantaneous inward rectifier is present in sinus venosus. 3) Calcium extrusion capacity sinus cells must be larger than in atrium.

Having developed adequate mathematical reconstructions of the atrial action potential as well as the pacemaker potential and the action potential in the sinusvenosus cells provided a means of assessing ionic mechanism(s) for the generation of various portions or phases of the action potential. Two phases were studied in some detail: 1. The mechanism of development of the pacemaker potential and 2. the ionic basis for repolarization of the action

potential in sinus tissue and in atrium. In the case of the sinus pacemaker response perhaps the most interesting questions concern whether it is possible for the same potassium current,  $I_K$ , to be involved in repolarization of the action potential and also modulate or partially control the initial portion of the pacemaker potential. Existing experimental evidence (Giles and Shibata, 1985; Shibata and Giles, 1985) suggests that this is the case and also draws attention to the importance of activation of a calcium current in the last one-third of the pacemaker potential just prior to the initiation of the action potential. The mathematical model presented here is in agreement with these experimental findings and provides a further, more quantitative basis for understanding the ionic mechanism of the pacemaker potential. Moreover, in sinus tissue our simulations of the action potential and the pacemaker potential strongly suggests that the same potassium current  $I_K$ , can indeed initiate repolarization and control pacing. Finally, this experimental and theoretical work provides a clear-cut example of cardiac pacemaker activity that can occur in the absence of the  $I_F$  current which appears to be important in generation of pacemaker activity in the mammalian sinoatrial node.

The strength and the uses of these models can in this thesis best be illustrated by considering of the mechanism(s) of repolarization of the atrial action potential. It may be useful

to first briefly summarize the conflicting views which exist concerning the mechanism(s) repolarization in frog heart. Brown, Clark and Noble (1969), following on the work of Noble and Tsien (1969), suggested that a time- and voltage-dependent outward current,  $I_X$  slow, initiated and controlled repolarization in frog atrium. In contrast, Horackova and Vassort (1976) concluded that the decline of a calcium current was the major factor initiating and controlling repolarization. As noted earlier, the work of Goldman and Morad (1977) suggested that repolarization in frog ventricle occurs by a decrease in  $Na^+$  conductance and a simultaneous increase in  $K^+$  conductance. Because addition of  $Ca^{++}$  to their  $Ca^{++}$  free Ringers solution shortened action potential duration without changing their measurements of the 'instantaneous' total ionic conductance of the membrane, they suggested that  $Ca^{++}$  influences the kinetics of the ion transport systems without altering the magnitude of their conductances. Recently the theoretical work of Drouhard and Roberge (1982) modified the model of Beeler and Reuter to simulate repolarization in frog ventricle by including some of the mechanisms suggested by Goldman and Morad (1977). In order to reproduce the lower  $K^+$  conductance found during the plateau they introduced an inactivating potassium channel, but in contrast to Goldman and Morad (1977) they found that repolarization was determined mainly by the interplay of  $I_{Si}$  (a Calcium current) and  $I_K$ ; the sodium component was not thought to

be importantly involved. Drouhard and Roberge (1982) felt that action potential repolarization is controlled by the inactivation gating variable governing the time dependent  $K^+$  channel.

V.3 The physiological significance of the sodium and potassium pump currents and sodium calcium exchange currents in bullfrog heart.

The mathematical reconstruction of frog atrial and sinus membrane electrical activity incorporates a  $Na^+/K^+$  pump and a  $Na^+/Ca^{++}$  exchange mechanism as an integral part of the model. These currents are important in maintaining the internal concentration gradients in a healthy cell and hence are of very real importance to the electrical activity of the membrane. The contribution of these mechanisms as currents interacting with the channel currents in producing the resting potential, the action potential plateau and repolarization, pacemaker potential is much less clear. The modelling results presented here indicate that for frog atrium and sinus:

1. The resting potential is slightly sensitive to the  $Na^+/K^+$  pump since it provides a current roughly half the size of  $I_{NaK}$  could be added into  $I_{Background}$  as a

constant current source without affecting the accuracy of the results.

2. The resting potential is slightly sensitive to  $I_{NaCa}$  immediately after an action potential (particularly during rapid stimulation) and may account for the slight after depolarization seen in single isolated atrial cells (Hume and Giles, 1983).
3. The contributions of the extrusion mechanisms play little role in the plateau and repolarization processes.
4. The pacemaker potential can be affected by the currents generated by the extrusion mechanisms. In the case of  $I_{NaK}$  this could be modelled by addition of a constant current to  $I_{Background}$  without affecting the results.  $I_{NaCa}$  is large enough in sinus venosus to modify the diastolic depolarization process but the changes it introduces might be overlooked when one considers the natural variability of the sinus-venosus potential waveform.

The role of these currents seems to be secondary to the roles played by the dominant channel currents in frog sinus-venosus. Their effect is only noticeable during periods of small net current or after concentration changes (either due to stimulation or perfusion). This is in direct contrast to the model of DiFrancesco and Noble (1985) which is critically dependent upon internal  $\text{Ca}^{++}$  concentration, and hence upon the calculation of internal  $\text{Ca}^{++}$ . It is important to note that the internal binding sites for  $\text{Ca}^{++}$  reduce the size of the internal  $\text{Ca}^{++}$  transient and hence modulate the size and the time of onset of the  $\text{Na}^+/\text{Ca}^{++}$  exchange current. In the model of bullfrog atrial activity the presence or absence of internal  $\text{Ca}^{++}$  buffering which produced significant attenuation of the  $\text{Ca}^{++}$  transient in the DiFrancesco and Noble (1985) model would have tremendous effect upon the repolarization phase of the action potential.

#### V.4 Future development and uses of these mathematical models:

Successful mathematical reconstruction of the action potential in the atrium and the sinus venosus of the bullfrog heart provides the basis for a number of important extensions of this work. Examples include: 1. It will be possible to study propagation of the action potential. Theoretical studies of propagation phenomena are much needed and will allow tests of



working hypotheses concerning mechanisms of conduction. It is not known to what extent the capacitance or resistance of the intracellular junction (the nexus) influences conduction speed and/or propagation velocities between cardiac cells. In addition, so-called anisotropic conduction is not well-understood, although there is some experimental evidence in favor of it. Extensions of the present models to include conduction of the action potential in one and two dimensional networks may provide new insights into these phenomena. 2. Secondly it will be possible to gain further insight into the mechanism of action of the autonomic transmitters, and possibly of other pharmacologic agents. As an example, although the current which acetylcholine activates in the atrium and sinus venosus has been identified many of its features appear very difficult to measure directly. With the existing models of the atrium and the sinus venosus, it may be possible for example to test various shapes of current voltage relationship for the ACH induced current and thus gain important mechanistic insights which have so far not been able to be obtained experimentally. 3. Finally, since the model that has been developed is Fortran based and somewhat modular, it should be possible to use it as a framework for developing entirely new models for other parts of the heart or for other excitable tissues e.g. smooth muscle cells.

## REFERENCES

- Adrian, R.H. (1969). Rectification in muscle membrane. Prog. Biophys., 19:339-369.
- Armstrong, C.M. and Bezanilla, F. (1977). Inactivation of the sodium channel. II. Gating current experiments. J. Gen. Physiol., 70:567-590.
- Argibay, J., Ildefonse, M., Ojeda, C., Rougier, O., and Tourneur, Y. (1983). Inhibition by Ba of background current and of its modifications by carbachol in frog atrium. J. Mol. Cell. Cardiol., 15:785-788.
- Attwell, D., Eisner, D., and Cohen, I. (1979). Voltage clamp and tracer flux data: effects of a restricted extra-cellular space. Quarterly Rev. of Biophysics, 12:213-261.
- Barry, P.H., and Adrian, R. (1973). Slow conductance changes due to potassium depletion in the transverse tubules of frog muscle fibres during hyperpolarizing pulses. J. Membrane Biol., 14:243-292.
- Bassinhwaighe, J.B. and Reuter (1972). Calcium movements and excitation-contraction coupling in cardiac cells. Electrical Phenomena in the Heart. DeMellow, W.C. (ed.), Academic Press, N.Y.

- Bayerdörffer, E., Eckhardt, L., Haase, W., and Schulz, I. (1985).  
Electrogenic calcium transport in plasma membrane of rat  
pancreatic acinar cells. J. Memb. Biol., 84:45-60.
- Baylor, S.M., Chandler, W.K., and Marshall, M.W. (1983).  
Sarcoplasmic reticulum calcium release in frog skeletal  
muscle fibres estimated from arsenazo III calcium  
transients. J. Physiol., 344:625-666.
- Beeler, G.W. and Reuter, H. (1970a). Voltage clamp experiments on  
ventricular myocardium fibres. J. Physiol., 207:165-190.
- Beeler, G.W. and Reuter, H. (1977). Reconstruction of the action  
potential of ventricular myocardial fibres. J. Physiol.  
(London), 268:177-210.
- Besseai, A. (1972). Analyse, selon le modele de Hodgkin-Huxley,  
des conductances membranaires du myocarde de grenouille. J.  
Physiol. (Paris), 64:647-670.
- Bevington, P.R. (1969). Data Reduction and Error Analysis for the  
Physical Sciences. McGraw-Hill: New York. pp. 204-246.
- Borle, A.B. (1981). Control, modulation, and regulation of cell  
calcium. Rev. Physiol. Biochem. Pharmacol., 90:14-153.
- Bowditch, H.P. (1932). Ludwig's Arbeiten. 139.
- Bozler, E. (1977). The Initiation of Impulses in Cardiac Muscle.  
A. Rev. Physiol. 26:341-56.
- Bristow, D., and Clark, J.W. (1982). A mathematical model of  
primary pacemaking cell in SA node of the heart. Am. J.  
Physiol., 243:H207-H218.

- Brown, H. and Noble, S. (1969). Membrane currents underlying delayed rectification and pacemaker activity in frog atrial muscle. J. Physiol. (London), 204:717-736.
- Brown, H.F. and Noble, S. (1969). A quantitative analysis of the slow component of delayed rectification in frog atrium. J. Physiol. (London), 204:737-747.
- Brown, H.F., Clark, A. and Noble, S. (1975). Identification of the pacemaker current in frog atrium. J. Physiol. (London), 258:521-545.
- Brown, H.F., Giles, W. and Noble, S. (1977). Membrane currents underlying activity in frog sinus venosus. J. Physiol. (London), 271:783-816.
- Brown, H.F., Kimura, J., Noble, D., Noble, S. and Tanpignon, A. (1984a). The slow inward current,  $i_{si}$  in the rabbit sino-atrial node investigated by voltage clamp and computer simulation. Proc. Roy. Soc. Lond. B222:305-328.
- Brown, H.F., Kimura, J., Noble, D., Noble, S. and Tanpignon, A. (1984b). The ionic currents underlying pacemaker activity in rabbit sino-atrial node: experimental results and computer simulations. Proc. Roy. Soc. Lond. B222:329-347.
- Brown, A.M., Lee, K.S., and Powell, T. (1981). Sodium current of single rat heart muscle cells. J. Physiol. (London), 318:479-500.

- Burden, R.L. and Faires, J.D. (1985). Numerical Analysis, 3rd Edition, Prindle, Weber and Schmidt, Boston.
- Campbell, D.L. (1985). Calcium Current and Homeostasis in Bullfrog Atrial Myocytes. Ph.D. Thesis., U. of Texas, Galveston.
- Cannel, M.B. and Allen, D.G. (1984). Model of calcium movements during activation in the sarcomere of frog skeletal muscle. Biophys. J., 45:913-925.
- Carmeliet, E. (1977). Repolarization and Frequency in Cardiac Cells. J. Physiol. (Paris). 73:903-23.
- Caroni, P., Zurini, M., Clark, A., and Carafoli, E. (1983). Further characterization and reconstitution of the purified  $\text{Ca}^{2+}$ -pumping ATPase of heart sarcolemma. J. Biol. Chem., 258:7305-7310.
- Chapman, J.B., Johnson, E.A. and Kootsey, J.M. (1983). Electrical and Biochemical Properties of an Enzyme Model of the Sodium Pump. J. Membrane Biol. 74: 139-153.
- Chapman, R.A. and Niedergierke, R. (1970a). Effects of calcium on the contraction of the hypodynamic frog heart. J. Physiol. (London), 211:489-421.
- Chapman, R.A. and Niedergierke, R. (1970b). Interaction between heart rate and calcium concentration in the control of contractile strength of the frog heart. J. Physiol. (London), 211:423-443.

- Chapman, R.A. and Miller, D.J. (1974a). The effects of caffeine on the contraction of the frog heart. J. Physiol., 242:589-613.
- Chapman, R.A. (1978). The effects of changes of the tonicity of the bathing fluid upon the tension generated by atrial trabeculae isolated from the heart of the frog, Rana pipiens. Quart. J. Exp. Physiol., 63:291-304.
- Chapman, R.A. (1979). Excitation-contraction coupling in cardiac muscle. Prog. Biophys. Molec. Biol., 35:1-52.
- Cleemann, L., Pizarro, G., and Morad, M. (1984). Optical measurements of extracellular calcium depletion during a single heartbeat. Science, 226:174-177.
- Cohen, I., and Kline, R. (1982).  $K^+$  fluctuations in the extracellular spaces of cardiac muscle. Circ. Res. 50:1-16.
- Cole, K.S. (1949). Dynamic Electrical Characteristics of the Squid Axon Membrane. Archs. Sci. Physiol. 3:253-8.
- Coulombe, A., and Coraboeuf, E., (1983). Simulation of potassium accumulation in clefts of Purkinje fibres: Effect on membrane electrical activity. J. Theor. Biol., 104:211-229.
- Cranefield, P. (1975). The Conduction of the Cardiac Impulse. Futura, Kisco, N.Y.
- Crank, J. (1975). The Mathematics of Diffusion. Clarendon Press. Oxford, 414pp.

- Dale, A.S. (1932). The staircase phenomenon in ventricular muscle. J. Physiol. (London), 75:1-16.
- Desmedt, J.E. (1953). Electrical activity and intracellular sodium concentration in frog muscle. J. Physiol., 121:191-205.
- DiFrancesco, D., and Noble, D. (1985). Model of cardiac electrical activity incorporating ionic pumps and concentration changes. Phil. Trans. R. Soc. Lond. B, 307:353-398.
- DiPolo, R. and Beauge, L. (1983). The calcium pump and sodium-calcium exchange in squid axons. Ann. Rev. Physiol., 45:313-324.
- Dresdner, K.P. and Kline, R.P. (1985). Extracellular calcium ion depletion in frog ventricular muscle. Biophys. J., 48:33-46.
- Drouhard, J-P., and Roberge, F. (1982). A simulation study of the ventricular myocardial action potential. IEEE TRANS., Biomedical Eng. BME-29:494-502.
- Ebihara, L. and Johnson, E. (1980). Fast sodium current in cardiac muscle. A quantitative description. Biophys. J., 32:779-790.
- Eisner, D.A. and Lederer, W.J. (1985). Na-Ca exchange: stoichiometry and electrogenicity. Am. J. Physiol., 248:C198-C202.

- Endo, M. (1977). Calcium release from the sarcoplasmic reticulum. Physiol. Rev., 57:71-108.
- Fabiato, A. (1982). Calcium release in skinned cardiac cells: variations with species, tissues, and development. Fed. Proc., 41:2238-2244.
- Fabiato, A. and Fabiato, F. (1978). Calcium-induced release of calcium from the sarcoplasmic reticulum of skinned cells from adult human, dog, cat, rabbit, rat and frog hearts and from foetal hearts and newborn rat ventricles. Ann. N. Y. Acad. Sci., 307:491-522.
- Fozzard, H., January, C., and Makielski, J. (19 ). New studies of the excitatory sodium currents in heart muscle. Circ. Res., 57:475-485.
- Frankenhauser, B. and Hodgkin, A.L. (1957). The action of calcium on the electrical properties of squid axons. J. Physiol., 299:289-307.
- Frankenhausen, B. (1962). Instantaneous potassium currents in myelinated nerve fibres of *Xenopus Laevis* investigated with voltage clamp technique. J. Physiol., 160:40-45.
- Gadsby, D.C. (1980). Activation of electrogenic  $\text{Na}^+/\text{K}^+$  exchange by extracellular  $\text{K}^+$  in canine cardiac Purkinje fibres. Proc. Natl. Acad. Sci. U.S.A., 77:4035-4039.
- Gadsby, D.C. (1984). The Na/K pump of cardiac cells. Ann. Rev. Biophys. Bioeng., 13:373-398.



- Gadsby, D.C., Kimura, J. and Noma A. (1985). Voltage dependence of Na/K pump current in isolated heart cells. Nature (London), 315:63-65.
- Gaskell, W.H. (1884). On the Innervation of the Heart with Special Reference to the Heart of the Tortoise. J. Physiol. (London). 4:43.
- Gaskell, W.H. (1887). On the Action of Muscarin Upon the Heart, and on the Electrical Changes in the Non-Beating Cardiac Muscle Brought About by Stimulation of the Inhibitory and Augmentor Nerves. J. Physiol. (Lond.). 8:404-15.
- Giles, W.R. and Shibata, E.F. (1985). Voltage clamp of bull-frog cardiac pace-maker cells: a quantitative analysis of potassium currents. J. Physiol. (London), 368:265-292.
- Gillespie, W.F. and Meves, H. (1980). The time course of sodium inactivation in squid giant axons. J. Physiol., 137:218-244.
- Goldman, Y., and Morad, M. (1977). Ionic membrane conductance during the time course of the cardiac action potential. J. Physiol. (Lond.), 268:655-695.
- Goldman, Y. and Morad, m. (1977). Regenerative repolarization of the frog ventricular action potential: a time- and voltage-dependent phenomenon. J. Physiol., (London), 268:575-611.
- Haas, H.G., Meyer, R., Einwöchter, H., and Stockem, W. (1983). Intracellular coupling in frog heart muscle,

- electrophysiological and morphological aspects. Pflügers Arch. 399:321-335.
- Haas, H.G., Kern, R., Einwachter, H.M. and Tarr, M. (1971). Kinetics of Na inactivation in frog atria. Pflügers Arch. ges. Physiol., 323:141-157.
- Hagiwara, S., and Jaffe, L.A. (1979). Electrical properties of egg cell membranes. Ann. Rev. Biophys. Bioeng., 8:385-416.
- Hagiwara, S. and Takahashi, K. (1974). The Anomalous Rectification and Cation Selectivity of the Membrane of a Starfish Egg Cell. J. Membrane Biol. 18:61-80.
- Hasselbach, W. and Oetliker, H. (1983). Energetics and electrogenicity of the sarcoplasmic reticulum calcium pump. Ann. Rev. Physiol. 45:325-339.
- Hasuo, H. and Koketsu, K. (1985). Potential dependency of the electrogenic  $\text{Na}^+$ -pump current in bullfrog atrial muscles. Jap. J. Physiol., 35:89-100.
- Hess, P. and Tsien, R.W. (1984). Mechanism of Ion Permeation through Calcium Channels. Nature, 309:453d-456.
- Hermesmyer, K. and Sperelakis, N. (1970). Decrease in  $\text{K}^+$  conductance and depolarization of frog cardiac muscle produced by  $\text{Ba}^{++}$ . Am. J. Physiol., 219:1108-1114.
- Hille, B., Woodhull, A.M., and Shapiro, B.I. (1975). Negative surface charge near sodium channels of nerve: Divalent

- ions, monovalent ions, and pH. Phil. Trans. Roy. Soc. Lond. B, 270:301-318.
- Hille, B., and Schwarz, W. (1978). Potassium channels as multi-ion single-file pores. J. Gen. Physiol., 72:409-442.
- Hiraoka, M., Ikeda, K., and Sano, T. (1980). The mechanism of barium-induced automaticity in ventricular muscle fibres. Adv. in Myocardiology, 1:255-266.
- Hodgkin, A.L. and Keynes, H. (1957). Movements of labelled calcium in giant squid axons. J. Physiol. (Lond.), 138:253-281.
- Hodgkin, A.L., and Huxley, A.F. (1952a). Currents carried by sodium and potassium ions through the membrane of the giant axon of *Loligo*. J. Physiol. (London), 116:449-472.
- Hodgkin, A.L., and Huxley, A.F. (1952b). The components of membrane conductance in the giant axon of *Loligo*. J. Physiol. (London), 116:473-496.
- Hodgkin, A.L., and Huxley, A.F. (1952c). The dual effect of membrane potential on sodium conductance in the giant axon of *Loligo*. J. Physiol. (London), 116:497-506.
- Hodgkin, A.L., and Huxley, A.F. (1952d). A quantitative description of membrane current and its application to conduction and excitation in nerve. J. Physiol. (London), 117:500-544.
- Hodgkin, A.L., and Katz, B. (1949). The effect of sodium ions on the electrical activity of the giant axon of the squid. J. Physiol. (London), 108:37-77.

- Holroyde, M.J., Robertson, S.P., Johnson, J.D., Solaro, R.J., and Potter, J.D. (1980). The calcium and magnesium binding sites on cardiac troponin and their role in the regulation of myofibrillar adenosine triphosphatase. J. Biol. Chem., 255:11668-11693.
- Horackova, M. and Vassort, G. (1976). Calcium conductance in relation to contractility in frog myocardium. J. Physiol. (London), 259:597-616.
- Hume, J.R., and Giles, W. (1981). Active and passive electrical properties of single bullfrog atrial cells. J. Gen. Physiol., 78:19-42.
- Hume, J.R., and Giles, W. (1983). Ionic currents in single isolated bullfrog atrial cells. J. Gen. Physiol., 81:153-194.
- Jack, J.J.B., Noble, D., and Tsien, R.W. (1975). Electric current flow in excitable cells. Oxford, Clarendon Press.
- Johnson, J.D., Collins, J.H., Robertson, S.P. and Potter, J.D. (1980). A fluorescence probe study of  $\text{Ca}^{2+}$  binding to the  $\text{Ca}^{2+}$  specific sites of cardiac troponin and troponin C. J. Biol. Chem., 255:9635-9640.
- Keenan, M.J., and Niedergierke, R. (1967). Intracellular sodium concentration and resting sodium fluxes of the frog heart ventricle. J. Physiol., 188:235-260.

- Kline, R., and Cohen, I. (1984). Extracellular  $[K^+]$  fluctuations in voltage-clamped canine cardiac Purkinje fibres. Biophys. J., 46:663-668.
- Kline, R., and Morad, M. (1976). Potassium efflux and accumulation in heart muscle, evidence from  $K^+$  electrode experiments. Biophys. J., 16:367-372.
- Klitzner, T., and Morad, M. (1983). Excitation contraction coupling in frog ventricle possible  $Ca^{++}$  transport mechanisms. Pflügers Archiv, 398:274-283.
- Keynes, R.D., and Swan, R.C. (1959). The effect of external sodium concentration on the sodium fluxes in frog skeletal muscle. J. Physiol. (London), 147:591-625.
- Kootsey, J.M. (1975). Voltage clamp simulation. Fed. Proc., 34:1343-1349.
- Kracke, G.R., and DeWeer, P. (1982). The rate co-efficient of sodium efflux from giant squid axon. Biophys. J., 37:220a.
- Kushmeric, M.J and Podolsky, R.J. (1969). Ionic Mobility in Muscle Cells. Science 166:1297-1298.
- Luttgan, H.C. and Niedegerke, R. (1958). The antagonism between Ca and Na ions on the frog's heart. J. Physiol. (London), 143:486-505.
- Marmont, G. (1949). Studies on the Axon Membrane. I. A New Method. J. Cell. Comp. Physiol. 34:351-82.

- McAllister, R.E., Noble, D., and Tsien, R.W. (1975).  
Reconstruction of the electrical activity of cardiac  
Purkinje fibres. J. Physiol. (London), 251:1-59.
- Meves, H. (1978). Inactivation of the sodium permeability in  
squid axon giant nerve fibres. Proq. Biophys. Molec. Biol.,  
33:207-230.
- Meyer, R., Stockem, W., Schmitz, M., and Haas, H.G. (1982).  
Histochemical demonstration of an ATP-dependent  $\text{Ca}^{2+}$ -pump in  
bullfrog myocardial cells. Z. Naturforsch., 37c:489-501.
- Mobley, B.A. and Eisenberg, B.R. (1975). Sizes of components in  
frog skeletal muscle measured by methods of stereology. J.  
Gen. Physiol., 66:31-45.
- Moore, J.W. and Romon, F. (1974). On numerical integration of  
the Hodgkin and Huxley equations for a membrane action  
potential. J. Theor. Biol., 45:249-273.
- Moore, L.E., Schmid, A. and Isenberg, G. (1984). Linear electri-  
cal properties of isolated cardiac cells. J. Membrane  
Biol., 81:29-40.
- Moore, L.E., Clark, R.B., Shibata, E.F. and Giles, W.R. (1986).  
Comparison of steady-state electrophysiological properties  
of isolated cells from bullfrog atrium and sinus venosus.  
J. Membrane Biol., 89:131-138.
- Morad, M. and Goldman, Y. (1973). Excitation-contraction coupling  
in heart muscle: Membrane control of development of  
tension. Prog. Biophys. Mol. Biol., 27:259-313.

- Morad, M. (1980). Physiological implications of K accumulation in heart muscle. Fed. Proc. 39:1533-1539.
- Morad, M., Goldman, Y.E., and Trentham, D.R. (1983). Rapid photochemical inactivation of  $\text{Ca}^{2+}$  antagonists shows that  $\text{Ca}^{2+}$  entry directly activates contraction in frog heart. Nature, 304:635-638.
- Morcos, N.C. (1981). Isolation of frog heart sarcolemma possessing  $[\text{Ca}^{2+} + \text{Mg}^{2+}]$ -ATPase and  $\text{Ca}^{2+}$  pump activities. Biochim. Biophys. Acta., 643:55-62.
- Mullins, L.J., and Frumento, A.S. (1963). The concentration dependence of sodium efflux from muscle. J. Gen. Physiol., 46:629-654.
- Mullins, L.J. (1977). A mechanism for Na/Ca transport. J. Gen. Physiol., 70:681-695.
- Mullins, L.J. (1981). Ion Transport In Heart. Raven Press, N.Y.
- Nakayama, T. and Irisawa, H. (1985). Transient outward current carried by potassium and sodium in quiescent atrioventricular node cells of rabbits. Circ. Res., 57:65-73.
- Nasi, E. and Tillotson, D. (1985). The rate of diffusion of  $\text{Ca}^{++}$  and  $\text{Ba}^{++}$  in a nerve cell body. Biophys. J. 47:735-738.
- Nelson, M.T. and Blaustein, M.P. (1980). Properties of sodium pumps in internally perfused barnacle muscle fibres. J. Gen. Physiol., 75:183-206.

- Niedergerke, R. (1956). The 'staircase' phenomenon and the action of calcium on the heart. J. Physiol., 134:569-583.
- Niedergerke, R. (1963). Movements of Ca in frog heart ventricles at rest and during contractions. J. Physiol., 167:515-550.
- Niedergerke, R. and Orkand, R.K. (1966). The dual effect of calcium on the action potential of the frog's heart. J. Physiol. (London), 184:291-311.
- Niedergerke, R., Page, S., and Talbot, M.S. (1969a). Determination of calcium movements in heart ventricles of the frog. J. Physiol., 202:58P-60P.
- Niedergerke, R., Page, S., and Talbot, M.S. (1969b). Calcium fluxes in frog heart ventricles, Pflügers Archiv., 306:357-360.
- Noble, D. (1962). A modification of the Hodgkin-Huxley equations applicable to Purkinje fibre action and pacemaker potentials. J. Physiol. (London), 160:317-352.
- Noble, D. (1972). Conductance Mechanisms in Excitable Cells. In Biomembranes 3 (ed. F. Kreuzer and J.F.G. Slegers), pp. 427-447. New York. Plenum Press.
- Noble, D., and Tsien, R.W. (1968). The kinetics and rectifier properties of the slow potassium current in cardiac Purkinje fibres. J. Physiol. (London), 195:185-214.



- Noble, D., and Tsien, R.W. (1969a). Outward membrane currents activated in the plateau range of potentials in cardiac Purkinje fibres. J. Physiol. (London), 200:205-231.
- Noble, D., and Tsien, R.W. (1969b). Reconstruction of the repolarization process in cardiac Purkinje fibres based on voltage clamp measurements of membrane current. J. Physiol. (London), 200:233-254.
- Noble, S.J. (1976). Potassium accumulation and depletion in frog atrial muscle. J. Physiol. (London), 258:579-613.
- Noble, D. (1979). The Initiation of the Heartbeat, end ed. Clarendon Press, Oxford, 12pp.
- Noble, D., and Noble, S. (1984). A model of sino-atrial node electrical activity based on a modification of the DiFrancesco-Noble (1984) equations. Proc. Roy. Soc. Lond., B222:295-304.
- Noma, A. and Irisawa, H. (1975). Effects of  $\text{Na}^+$  and  $\text{K}^+$  on the resting membrane potential of the rabbit sinoatrial node cell. Jap. J. Physiol., 25:287-302.
- Ojeda, C., and Rougier, O. (1974). Kinetic analysis of the delayed outward currents in frog atrium. Existence of two types of preparation. J. Physiol. (London), 239:51-73.
- Orkand, R.K. (1968). Facilitation of heart muscle contraction and its dependence on external calcium and sodium. J. Physiol. (London), 196:311-325.

- Page, S.R., and Niedergerke, R. (1972). Structures of physiological interest in the frog heart ventricle. J. Cell. Sci., 11:179-203.
- Pizarro, G., Cleemann, L., and Morad, M. (1985). Optical measurement of voltage-dependent  $\text{Ca}^{2+}$  influx in frog heart. Proc. Natl. Acad. Sci., 82:1864-1868.
- Potter, J.D., and Zot, H.G. (1982). The role of actin in modulating  $\text{Ca}^{2+}$  binding to troponin. Biophys. J., 37:43a.
- Provencher, S. (1976). A fourier method for the analysis of exponential decay curves. Biophys. J., 16:27-41.
- Reid, A. and Hecht, H. (1967). Barium-induced automaticity in right ventricular muscle in the dog. Circ. Res., 21:849-856.
- Reuter, H. (1967). The dependence of slow inward current in Purkinje fibres on the extracellular calcium concentration. J. Physiol. (London), 192:479-492.
- Reuter, H. and Seitz, N. (1968). The dependence of calcium efflux from cardiac muscle on temperature and external ion concentration. J. Physiol. (London), 195:451-470.
- Robertson, S., Johnson, D., and Potter, J. (1981). The time-course of  $\text{Ca}^{2+}$  exchange with calmodulin, troponin, parvalbumin, and myosin in response to transient increases in  $\text{Ca}^{2+}$ . Biophys. J., 34:559-569.

- Robinson, K. (1983). A mathematical reconstruction of the frog atrial action potential based on voltage clamp data. Master's Thesis, Rice U., Houston.
- Rougier, O., Vassort, G., and Stämpfli, R. (1968). Voltage clamp experiments on frog atrial muscle fibres with the sucrose gap technique. Pflügers Archiv. ges. Physiol., 301:91-108.
- Sachs, J.R. (1970). Sodium movements in the human red blood cells. J. Gen. Physiol., 56:322-341.
- Sachs, J.R., and Welt, L.G. (1967). The concentration dependence of active potassium transport in the human red blood cell. J. Clinical Invest., 46:65-77.
- Schatzmann, H.J. (1983). The red cell calcium pump. Ann. Rev. Physiol., 45:303-312.
- Shibata, E.F. (1983). Ionic currents in isolated cardiac pacemaker cells. Ph.D. Thesis, U. of Texas, Galveston.
- Shibata, E.F., and Giles, W. (1984). Cardiac pacemaker cells from bullfrog sinus venosus lack an inwardly rectifying background  $K^+$  current. Biophys. J., 45:136A.
- Shibata, E., Momose, Y., and Giles, W. (1984). An electrogenic  $Na^+/K^+$  pump current in individual bullfrog atrial myocytes. Biophys. J., 45:136A.
- Singer, S.J. and Nicholson, G. (1972). The fluid mosaic model of the structure of cell membranes. Science, 175:720-730.

- Sordahl, L.A. (1974). Effects of magnesium, Ruthenium Red, and the antibiotic ionophore A23187 on initial rates of calcium uptake and release by heart mitochondria. Archs. Biochem. Biophys., 167:104-115.
- Standen, N.B., and Stanfield, P.R. (1982). A binding site model for calcium channel inactivation that depends on calcium entry. Proc. R. Soc. (London), B217:101-110.
- Tasaki, I. and Hagiwara, S. (1957). Demonstration of two stable potential states in the squid giant axon under tetraethylammonium chloride. J. Gen. Physiol., 40:859-885.
- Tourneur, Y., Mitra, R., and Morad, M. (1984). Activation of the inwardly rectifying  $K^+$  current in guinea pig isolated atrial and ventricular cells. Biophys. J., 45:136A.
- Tung, L. and Morad, M. (1985). A comparative electrophysiological study of enzymatically isolated single cells and strips of frog ventricle. Pflugers Arch., 405:274-284.
- Unwin, N. and Henderson, R. (1984). The structure of proteins in biological membranes. Science, 250:78-95.
- Vassalle, M., Johannes, K. and Hoffman, B. (1962). Toxic effects of ouabain on Purkinje fibres and ventricular muscle fibres. Am. J. Physiol., 203:433-439.
- Vassalle, M. (1965). Cardiac pacemaker potentials at different extra- and intracellular K concentrations. Am. J. Physiol., 208:770-775.

- Vassalle, M. (1966). Analysis of cardiac pacemaker potential using a "voltage clamp" technique. Am. J. Physiol., 210:1335-1341.
- Walker, J.L., and Ladle, R.O. (1973). Frog heart intracellular potassium activities measured with potassium microelectrodes. Am. J. Physiol., 225:263-267.
- Wallinga-de Jonge, W., Boom, H., Heijink, R., and van der Vliet, G. (1981). Calcium model for mammalian skeletal muscle. Med. & Biol. Eng. & Computing, 19:734-748.
- Wolff, D.J., Poirier, P.G., Brostrom, C.O. and Brostrom, M.A. (1977). Divalent Cation Binding Properties of Bovine Brain  $\text{Ca}^{++}$ -dependent Regulator Protein. J. Biol. Chem. 252:4108-4117.
- Yanagihara, K., Noma, A. and Irisawa, H. (1980). Reconstruction of Sino-Atrial Node Pacemaker Potential Based on the Voltage Clamp Experiments. Jap. J. Physiol. 30:841-857.